WÜRZBURGER GEOGRAPHISCHE ARBEITEN

Mitteilungen der Geographischen Gesellschaft Würzburg

Herausgeber:
R. Baumhauer - B. Hahn - H. Job - H. Paeth - J. Rauh - B. Terhorst

Heft 103

Jens Brauneck

LATE QUATERNARY CLIMATE CHANGES IN THE CENTRAL SAHARA
-
New evidence from palaeoenvironmental research in NE-Niger

2010

Im Selbstverlag des Instituts für Geographie der Julius-Maximilians-Universität Würzburg
in Verbindung mit der Geographischen Gesellschaft Würzburg

Jens Brauneck

LATE QUATERNARY CLIMATE CHANGES IN THE CENTRAL SAHARA

-

New evidence from palaeoenvironmental research in NE-Niger

WÜRZBURGER GEOGRAPHISCHE ARBEITEN

Herausgegeben vom Institut für Geographie der Universität Würzburg in Verbindung mit der Geographischen Gesellschaft Würzburg

Herausgeber: R. Baumhauer – B. Hahn – H. Job

Schriftleitung: B. Sponholz

WÜRZBURGER GEOGRAPHISCHE ARBEITEN
Mitteilungen der Geographischen Gesellschaft Würzburg

Herausgeber: R. Baumhauer – B. Hahn – H. Job

Heft 103

LATE QUATERNARY CLIMATE CHANGES IN THE CENTRAL SAHARA

Jens Brauneck

2010

Im Selbstverlag des Instituts für Geographie der Julius-Maximilians-Universität Würzburg
in Verbindung mit der Geographischen Gesellschaft Würzburg

Computersatz:
Jens Brauneck, Institut für Geographie der Julius-Maximilians-Universität Würzburg

Druck:

Bezug über den Buchhandel oder direkt bei:
Institut für Geographie der Julius-Maximilians-Universität Würzburg
– Würzburger Geographische Arbeiten –
Am Hubland
D-97074 Würzburg
E-Mail: geographie@uni-wuerzburg.de
URL: http://www.geographie.uni-wuerzburg.de/vortraege_schriftenreihen/wuerzburger_geographische_arbeiten/

Zuschriften:
Geographische Gesellschaft Würzburg
c/o Institut für Geographie der Julius-Maximilians-Universität Würzburg
Am Hubland
D-97074 Würzburg

ISSN ???????

CONTENTS

List of figures……..VI
List of tables……..…V
Preface……..…VII
Abstract……..…VIII
Zusammenfassung……..X

1 Introduction 1
2 Geographical setting of the study area 2

2.1 Geomorphology 2
2.2 The geological framework 4
2.3 Vegetation 5
2.4 Present climatic dynamics of Northern Africa 6
2.5 Geographical setting of the study sites 10
2.5.1 Seggedim 10
2.5.2 Fabérgé depression 11
2.5.3 Enneri Achelouma / Seeterrassental 13
2.5.4 Yoo Ango 15

3 Sedimentary deposits as tools for environmental reconstruction 17

3.1 Physical sediment features 18
3.1.1 Visual description 19
3.1.2 Grain size 20
3.1.3 Magnetic susceptibility 21
3.2 Sediment chemistry 21
3.2.1 Organic carbon 21
3.2.2 Silicon and aluminium 22
3.2.3 Iron and manganese 23
3.2.4 Alkali and alkaline earth metals 23
3.3 Mineralogy 23
3.3.1 Carbonates 24
3.3.2 Evaporitic Minerals 25
3.3.3 Silicate minerals 26
3.4 Biological Indicators 26
3.5 Archaeological findings 27
3.6 Age determination 28
3.6.1 Radiocarbon dating 28
3.6.2 Optically stimulated luminescence (OSL) dating 29

4 Palaeoenvironmental research on North African climate changes 30

4.1 Palaeoenvironmental reconstruction by proxy data 30
4.2 Review of palaeoenvironmental evidence from the central Sahara 36
4.2.1 Seggedim 37
4.2.2 Falaise de Kaouar 37
4.2.3 Fachi 38
4.2.4 Zoo Baba 38
4.2.5 Adrar Bous 39
4.2.6 Ténéré 39

4.3 The issue of the Middle Terrace 40
4.4 Computer-model-based investigations 41
4.5 Summary 44

5 Materials and Methods 46

5.1 Fieldwork 46
5.2 Laboratory methods 47
5.2.1 Core handling and sample pre-treatment 47
5.2.2 Physical Methods 48
5.2.2.1 Sediment texture/grain-size analysis 48
5.2.2.2 Magnetic susceptibility 49

5.2.3 Geochemistry 49
5.2.3.1 ICP-OES 49
5.2.3.2 X-ray fluorescence spectrometry (XRF) 50
5.2.3.3 Fuse tablets (XRF) 50
5.2.3.4 Geoscanner (XRF) 51
5.2.3.5 Carbon analysis 51
5.2.3.6 pH measurement 52

5.2.4 Mineralogy 52
5.2.4.1 XRD 52
5.2.4.2 Thin sections 53

5.2.5 Biological Indicators 53
5.2.5.1 Microfossils 53
5.2.5.2 Palynology 54

5.3 Age determination 54
5.4 Data evaluation and quality 54
5.4.1 Normative stoichiometric calculation 54
5.4.2 Normalization 55

6 Coring record from Seggedim 56

6.1 Results 56
6.1.1 Magnetic susceptibility 56
6.1.2 Stratigraphic units 57
6.1.3 Mineralogy 60
6.1.4 Geochemistry 61
6.1.4.1 ICP-OES 61
6.1.4.2 Geoscanner (XRF) 62

6.1.5 Biological Indicators 65
6.1.5.1 Estimation of biogenic silica (BSi) 65
6.1.5.2 Diatoms 67
6.1.5.3 Pollen spectra 68

6.1.6 Radiocarbon dating 69
6.1.7 OSL dating 69
6.1.8 Determination of the main lake stages 70
6.1.9 Determinations of geochemical mean values 71

6.2 Discussion 73
6.2.2 Conditions of the initial lake phase 76
6.2.3 Sedimentation and environmental conditions of the subsequent phases 77
6.2.4 Carbonates – distribution and origin 78
6.3 Conclusion 80

7 Supplementary study sites Results 82

7.1 Fabérgé 82
7.1.1 Profile 1 82
7.1.2 Profile 3 85
7.1.3 Profile 4 90
7.1.4 OSL-dating 94
7.1.5 Summary 94
7.2 Enneri Achelouma 95
7.2.1 Profile 8 95
7.2.2 Profile 10 100
7.2.3 Profile 11 105
7.2.4 Summary 110
7.3 Yoo Ango 111
7.3.1 Profile 12 111
7.3.2 Profile 13 116
7.3.3 Summary 122
7.4 Discussion 123
7.4.1 Evaluation of the supplementary study sites and data quality 123
7.4.2 Environmental settings 125
7.5 Conclusion 129

8 Synthesis 131

8.1 Synopsis of palaeoenvironmental reconstruction 131
8.2 Model of Late Quaternary environmental progression in NE Niger 135
8.3 Conclusion 141

9 References 143
10 Appendix 154

LIST OF FIGURES

Figure 1 Map of north-eastern Niger (Baumhauer et al., 2009a) 3
Figure 2 Pattern of low level winds (at ground level) and pressure over Africa (Gasse & Roberts, 2004) 7
Figure 3 Cross section of ITCZ (July-August) along the zero meridian (Gasse & Roberts, 2004) 8
Figure 4 Model of rainfall distribution over Northern Africa (Gasse & Roberts, 2004) 9
Figure 5 Cross section of the Seggedim depression (modified from Baumhauer 1988) 11
Figure 6 Geomorphological map of the Fabérgé study site (by J. Krause) 12
Figure 7 Geomorphological map of the Seeterrassental (Krause & Schuett, 2009) 14
Figure 8 Geomorphological map of Yoo Ango 15
Figure 9 Ternary diagram for textural classification of sediments (Flemming, 2000) 20
Figure 10 Northern hemisphere summer insolation (from Berger & Loutre, 1991) compared to records obtained from the 658C core (deMenocal et al., 2000) 36
Figure 11 Location of the study sites 46
Figure 12 The operation of a Kullenberg Piston Corer (U.S.G.S., 2001) 47
Figure 13 Laboratory work schedule for the Seggedim core 48
Figure 14 Results of magnetic susceptibility measurement 57
Figure 15 Main properties of the 2005 core (5-15 m depth) 59
Figure 16 Distribution of carbonates and mole ratios of determining chemical features 60
Figure 17 $SiO_2 + Al_2O_3$ distribution, mole ratios 61
Figure 18 Selected results from the Geoscanner analysis 62
Figure 19 Main results obtained from a XRF scan of the 782-790 cm section 63
Figure 20 Main results obtained from a XRF scan of the 1401-1409 cm section 64
Figure 21 Comparison of XRF images, analysed elements appear bright (high reflectance) 65
Figure 22 BSi estimations based on aluminium and titanium 66
Figure 23 Diatom assemblage of the Seggedim coring (BAUMHAUER 1991, modified) 67
Figure 24 Mean lake stage values and standard deviations of selected oxides 70
Figure 25 Comparison of point wise (ICP) and total (Geoscanner) chemical analysis 72
Figure 26 Calibrated radiocarbon dates of the 2005 coring compared to dates from 1984 73
Figure 27 Radiocarbon dates from the bottom core section 75
Figure 28 Radiocarbon dates from the mid core section 75
Figure 29 Lake stages and corresponding radiocarbon dating 80
Figure 30 Palaeoenvironmental progression within the Seggedim basin 81
Figure 31 Selected geochemical features of profile 1 82
Figure 32 Mineralogical features of profile 1 84
Figure 33 Main mole ratios of profile 1, CIA values derived from oxides 85
Figure 34 Selected geochemical features of profile 3 86
Figure 35 Mineralogical features of profile 3 87
Figure 36 Grain size distribution of profile 3 88
Figure 37 Main mole ratios of profile 3, CIA values derived from oxides 89
Figure 38 Normative balancing of main minerals in profile 3 89
Figure 39 Selected geochemical features of profile 4 90
Figure 40 Mineralogical features of profile 4 92
Figure 41 Grain size distribution of profile 4 92
Figure 42 Main mole ratios of profile 4, CIA values derived from oxides 93
Figure 43 Normative balancing of main minerals in profile 4 93
Figure 44 Selected geochemical features of profile 8 95

Figure 45 Mineralogical features of profile 8 97
Figure 46 Grain size distribution of profile 8 98
Figure 47 Main mole ratios of profile 8, CIA values derived from oxides 99
Figure 48 Normative balancing of main minerals in profile 8 100
Figure 49 Selected geochemical features of profile 10 101
Figure 50 Mineralogical features of profile 10 102
Figure 51 Grain size distribution of profile 10 103
Figure 52 Main mole ratios of profile 10, CIA values derived from oxides 104
Figure 53 Normative balancing of main minerals in profile 10 105
Figure 54 Selected geochemical features of profile 11 106
Figure 55 Mineralogical features of profile 11 107
Figure 56 Grain size distribution of profile 11 108
Figure 57 Main mole ratios of profile 11, CIA values derived from oxides 109
Figure 58 Normative balancing of main minerals in profile 11 110
Figure 59 Selected geochemical features of profile 12 112
Figure 60 Mineralogical features of profile 12 113
Figure 61 Grain size distribution of profile 12 114
Figure 62 Main mole ratios of profile 12, CIA values derived from oxides 115
Figure 63 Normative balancing of main minerals in profile 12 116
Figure 64 Selected geochemical features of profile 13 117
Figure 65 Mineralogical features of profile 13 118
Figure 66 Grain size distribution of profile 13 119
Figure 67 Main mole ratios of profile 13, CIA values derived from oxides 120
Figure 68 Normative balancing of main minerals in profile 13 121
Figure 69 Potential source of error for alternating radiocarbon dates of profile 12 124
Figure 70 Literature analysis of Holocene palaeoenvironmental research in the Central Sahara (modified from SCHUETT & KRAUSE, 2009) 132
Figure 71 Regional palaeoenvironmental progression throughout the Holocene 135
Figure 72 Comparison of local results with insolation values (30°N) and terrigenous dust records from a deep sea coring. Original dust record (deMENOCAL et al., 2000), Insolation values (BERGER & LOUTRE, 1991) 140

LIST OF TABLES

Table 1 Basic and derived attributes of sediments (Last, 2001b, p42).....18
Table 2 Magnetic behaviors, sources and states (Dearing, 1994).....21
Table 3 Climatic development of Niger and Northern Chad (Servant, 1973/1983).....31
Table 4 Climatic development of Adrar Bous (Williams et al., 1987).....39
Table 5 Mineralogy interpretation scheme.....53
Table 6 Diatom assemblage of the basal section 1440-1470 cm.....68
Table 7 Diatom assemblage of the upper section 1300-1440.....68
Table 8 Radiocarbon dates from the 2005 Seggedim coring.....69
Table 9 Mineralogical composition of rock fragments.....79
Table 10 Main geochemical statistics of profile 1.....83
Table 11 Correlation matrix of profile 1.....83
Table 12 Main geochemical statistics of profile 3.....86
Table 13 Correlation matrix of profile 3.....87
Table 14 Main geochemical statistics of profile 4.....91
Table 15 Correlation matrix of profile 4.....91
Table 16 Main geochemical statistics of profile 8.....96
Table 17 Correlation matrix of profile 8.....96
Table 18 Main geochemical statistics of profile 10.....101
Table 19 Correlation matrix of profile 10.....102
Table 20 Main geochemical statistics of profile 11.....106
Table 21 Correlation matrix of profile 11.....107
Table 22 Main geochemical statistics of profile 12.....112
Table 23 Correlation matrix of profile 12.....113
Table 24 Main geochemical statistics of profile 13.....117
Table 25 Correlation matrix of profile 13.....118
Table 26 Contrasting properties of palaeoenvironmental archives.....135

PREFACE

This thesis is based upon studies carried out within the multidisciplinary project “Late Quaternary environmental change in the Central Sahara (NE-Niger)” between June 2005 and July 2008. The project has been funded by the German Research Foundation (Deutsche Forschungsgemeinschaft – DFG). As this work originates in an interdisciplinary research project, a multitude of people participated in realizing it.

First, I have to thank Prof. Dr. Roland Baumhauer and Prof. Dr. Britta Schütt for enabling me to join the project as well as providing helpful scientific advice and for being the reviewers of my dissertation. I also thank Prof. Dr. Peter Felix-Henningsen for submitting the results of the OSL dating and all other members of the LIMNOSAHARA expedition team for their cooperation.

Furthermore, thanks to Dr. Phillip Hoelzmann for being an excellent advisor in laboratory methods and techniques as well as Manuela Dermici-Scholz for her support at the geoscience laboratories of the Freie Universität Berlin. Emmi Krings from the same institution provided unstinting support concerning the mineralogy measurements and introduction to the analysis software, although occasionally being bugged by unsatisfactory sample preparation. Besides accommodating me on several occasions, Jan Krause and Nicole Marquardt provided the geomorphological maps of largely unknown areas and were a motivating source of conversations and ideas.

Prof. Dr. H. Frimmel and Dr. U. Schüßler from the department of Geodynamics and Geomaterial Sciences at the Institute of Geography at Würzburg University provided the opportunity to use the RFA analysis facilities. Dr. Erhard Schulz executed the pollen analysis and supplied helpful assistance in many ways (Multumesc!). Tomasz Goslar of the Poznan Radiocarbon Laboratory executed multiple swift examinations for radiocarbon dating and supported it by helpful recommendations on the overall procedure. Dr. Dieter Rammlmair of the Federal Institute for Geosciences and Natural Resources (BGR) in Hannover is thanked for introducing me to the Itrax Core scanner and for constantly refining the method. Dr. Gerhard Daut of the Department of Geography at Jena University facilitated the susceptibility measurements of the split cores. Dr. Reinhard Bierl of the hydrology department at the Institute of Geography at Trier University coordinated the grain size analysis.

Certainly, I have to express my gratitude to Tanja Rölker and Naomi Hallan for proofreading this work so rapidly yet precisely. Finally, I thank my wife for providing constant support and encouragement all the way through this study and for setting up the ultimate deadline.

ABSTRACT

Surveys by the Universities of Wuerzburg and Berlin, starting in the 1970´s have revealed the existence of palaeolakes in remote areas in Niger. Initial research has shown that the sediments found are suitable for reconstructing its late quaternary palaeoenvironment. Although a high number of investigations focused on the succession of climatological conditions in the Central Sahara, some uncertainties still exist as the results show discontinuities and mostly are of low temporal and spatial resolution.

Two expeditions in 2005 and 2006 headed to the northeastern parts of Niger to investigate the known remains of palaeolakes and search some new and undetected ones. Samples were taken at several study sites in order to receive a complete picture of the Late Quaternary environmental settings and to produce high-resolution proxies for palaeoclimate modelling.

The most valuable and best-investigated study site is the sebkha of Seggedim, where a core of 15 meters length could be extracted which revealed a composition of high-resolution sections. Stratigraphical, structural and geochemical investigations as well as the analysis of thin sections allow the characterization of different environmental conditions from Early to Mid Holocene. Driven by climate and hydrogeological influence, the water body developed from a water pond of several metres depth within a stable, grass and shrub vegetated landscape, to an alternating freshwater lake in a more dynamic environmental setting. Radiocarbon dates set the beginning of the stage at about 10.6 ka cal BP, with an exceptionally stable regime to 6.6 ka cal BP (at 12.6 metres' depth), when a major change in the sedimentation regime of the basin is recorded in the core. Increased erosion, likely due to decreased vegetation cover within the basin, led to the siltation/filling of the lake within a few hundred years and the subsequent development of a sebkha/salt pan due to massive evaporation. Due to the lack of dateable material in the upper core section, the termination of the lake stage and the onset of the subsequent sebkha stage cannot be determined precisely but can be narrowed to a period around 6 ka BP.

The results obtained from the core are compared with those from terrestrial and lacustrine sediments from outside the depression, situated a few hundred kilometres further to the north. These supplementary study sites are required to validate the information obtained from the coring. Within the plateau landscape of Djado, Mangueni and Tchigai, two depressions and a valley containing lacustrine deposits, were investigated for palaeoenvironmental reconstruction. Depending on modifying local factors, these sediment archives were of shorter existence than IX the lake, but reveal additional information about the landscape dynamics from Early to Mid Holocene.

A damming situation within a small tributary at Enneri Achelouma led to lacustrine sedimentation conditions at Early Holocene in the upper reaches of the valley. The remnants of the lacustrine accumulations show distinct changes in the environmental conditions within the small catchment, as the archive immediately responded to local climate-induced changes of precipitation. Radiocarbon dating of the deposited sediments revealed ages from 8780 ± 260 cal a BP to 9480 ± 80 cal a BP.

The sites of Yoo Ango and Fabérgé show a completely different sedimentation milieu as they consist of basins within the foothills of the Tchigai. The study sites show increased catchment sizes, probably extending towards the Tchigai massif and are most likely influenced by groundwater charge. The widespread occurrence of wind shaped relicts and the limited amount of lacustrine remnants indicate a generally high aeolian activity in both areas. Only in wind sheltered spots, parts of the lacustrine sequences were preserved, that show ages spanning from Early to Mid Holocene (9440 ± 140 cal a BP – 6810 ±140 cal a BP) and give additional evidence of fires from pre-LGM periods. Although intensively weathered, all profiles indicate distinct changes in the sedimentation conditions by alternating geochemical values and the mineralogical composition.

The information obtained from the records investigated in this work confirms the heterogeneity of reconstructed environmental succession in the Central Sahara. The Mid Holocene rapid (within decades) and uniform development from more humid to extremely arid environmental conditions cannot be confirmed for the Central Sahara. In addition, a division of Early and Mid Holocene wet periods cannot be confirmed, either. Actually, the evidences obtained from the palaeoenvironmental reconstructions revealed major variations in the timing and extend of lacustrine and aeolian periods. Evidently, a transitional time has existed between 7 to 5 ka BP where alternating influences prevailed. This is indicated by the varying sedimentation conditions in the Seggedim depression as well as the evidence of soil properties on a fossil dune, with a time of deposition dated to 6200 ± 400 cal a BP and the removal of lacustrine Sediments at the Seeterrassental at Mid Holocene. In respect to provide a complete picture of landscape succession and to avoid misinterpretation, the investigation of several dissimilar spots within a designated study area is prerequisite for further investigations.

ZUSAMMENFASSUNG

Bereits seit den 1970er Jahren sind Vorkommen von Paläoseen im Nordosten Nigers bekannt und waren Gegenstand einer Vielzahl von Untersuchungen über die Paläoumweltbedingungen der Zentralen Sahara des Spätquartärs. Trotz der großen Anzahl an Analysen bestehen noch immer Unsicherheiten in Bezug auf das zeitliche Ausmaß feuchter und trockener Phasen in diesem Gebiet, da angrenzende Areale deutlich unterschiedliche Entwicklungen aufweisen können. Im Zuge zweier Expeditionen in den Jahren 2005 und 2006 in den äußersten Nordosten Nigers, wurden an bereits untersuchten und erstmalig entdeckten Standorten Proben genommen, um ein komplettes Bild über die spätquartären Umweltbedingungen in diesem Gegend zu erlangen und um die Aussagekraft verschiedener Sedimentarchive zu überprüfen.

Der wertvollste und am intensivsten untersuchte Standort ist die Sebkha von Seggedim, wo ein Bohrkern von 15 Meter Länge gewonnen werden konnte, welcher hochauflösende Sedimente einer ununterbrochenen Sequenz vom Frühen bis Mittleren Holozän aufweist. Untersuchungen zur Stratigraphie, Sedimentstruktur, Geochemie und Mineralogie ermöglichen die Unterscheidung mehrerer Stadien der Seeentwicklung und der damit verbundenen Umweltbedingungen. Durch klimatische und hydrogeologische Einflüsse geprägt, entwickelte sich der Wasserkörper zunächst zu einem wenige Meter tiefem, jedoch biologisch sehr produktivem Gewässer innerhalb einer stabilen Gras- und Strauchlandschaft. Datierungen belegen den Beginn dieser außerordentlich stabilen Phase vor ca. 10.600 Jahren und einer Dauer bis 6.600 Jahre vor heute. Ab 12,6 Meter Tiefe zeigt sich ein deutlicher Wechsel im Sedimentationsverhalten des Sees. Verstärkter Sedimenteintrag, höchstwahrscheinlich ausgelöst durch reduzierte Vegetationsbedeckung und Variationen in der Saisonalität der Niederschläge innerhalb des Einzugsgebietes, führte zur Verlandung des Sees binnen weniger Jahrhunderte und der anschließenden Entwicklung einer Sebkha (Salz-Ton-Pfanne) durch verstärkte Evaporation. Durch das Fehlen datierbaren Materials in den oberen Abschnitten des Kerns kann die Endphase des Sees und der nachfolgende Beginn der Sebkhaphase nicht exakt bestimmt werden, allerdings kann dieser Bereich auf eine Zeit um 5500 bis 6000 Jahre vor heute eingegrenzt werden.

Die Ergebnisse der Bohrkernuntersuchungen sind im Folgenden mit weiteren Ergebnissen von lakustrinen Sedimenten außerhalb der Depression verknüpft worden. Diese zusätzlichen Untersuchungen dienen zur Validierung der Bohrkerndaten und zur Überprüfung potentieller überregionaler klimatischer Zusammenhänge. Einige hundert Kilometer nordwärts, inmitten der Plateaus von Djado, Mangueni und Tchigai wurden Standorte auf deren Entwicklung im Spätquartär untersucht. Aufgrund der unterschiedlichen, durch die Geographie bedingten, lokalen Faktoren weisen diese lakustrinen Sedimentarchive deutlich kürzere Lebensdauer auf, jedoch ermöglichen sie teilweise einen genaueren Einblick in die vorherrschende Dynamik innerhalb dieser Landschaften.

Durch die Blockade eines tributären Tals im Enneri Achelouma wurden für einen kurzen Abschnitt im Frühholozän Seesedimente in dessen Oberlauf akkumuliert, welche kurzzeitige, aber deutliche Änderungen der Umweltbedingungen dokumentieren. Datierungen zeigen die Existenz dieser Seebecken oder Seeterrassen von 9480 ± 80 cal a BP bis 8780 ± 260 cal a BP. Durch Veränderungen im Niederschlagsregime kam es anschließend zu einer Zerschneidung und teilweisen Ausräumung des abgelagerten Materials.

Die Standorte Yoo Ango und Fabérgé weisen ein komplett anderes Sedimentationsmilieu auf, da sie aus Becken innerhalb der Ausläufer des Tchigai Plateaus bestehen und deutlich größere Einzugsgebiete aufweisen. Zusätzlich sind beide Standorte grundwasserbeeinflusst und stark durch die sehr hohe äolische Aktivität in diesem Gebiet geprägt, sichtbar an dem weitverbreiteten äolischen Formenschatz sowie der geringen Anzahl erhaltener Seesedimente. Nur in wenigen windgeschützten Lokalitäten wurden lakustrine Sedimentpakete erhalten, die ebenfalls früh- bis mittelholozäne Alter

aufweisen. Trotz der intensiven Verwitterung die sämtliche untersuchten Sedimente betrifft, weisen nahezu alle Profile eindeutige Veränderungen auf, sowohl in Bezug auf die geochemischen Werte als auch die mineralogische Zusammensetzung.

Aus den untersuchten Profilen wird eine feuchtere Phase zu Beginn des Holozäns ersichtlich, die jedoch starken Schwankungen unterlegen war, wie in den Profilen von Achelouma zu sehen ist. In einer Phase des Übergangs im Mittelholozän endete zunächst die lakustrine Sedimentation in Achelouma, dann in der Fabérgé-Senke. Die erhöhte Niederschlagsvariabilität führte in Achelouma zur teilweisen Ausräumung der Seesedimente, während in der Fabérgé- Senke Dünen aktiv waren. Die Ergebnisse von Seggedim zeigen ebenfalls starke Veränderungen der Umweltbedingungen an, jedoch zeitlich versetzt zu den Ergebnissen aus den anderen Gebieten.

Insgesamt weisen die Ergebnisse der Paläoumweltrekonstruktionen große zeitliche Unterschiede bezüglich des Endes der lakustrinen Phasen auf. Die Untersuchungen zeigen deutlich, dass lokale geographische Faktoren eine klimatische Interpretation von Klimaarchiven erschweren können. Insbesondere dann, wenn wie im Falle Seggedim, ein überregionaler Aquifer die Existenz eines Wasserkörpers in einem ansonsten ariden Gebiet verlängert und klimatische Einflussfaktoren zeitweise ausgeklammert werden. Um Fehlinterpretationen zu vermeiden und ein Gesamtbild der landschaftlichen Entwicklung eines Raumes zu erhalten, sind Informationen aus mehreren grundverschiedenen Paläoumweltarchiven erforderlich.

1 INTRODUCTION

Although a number of palaeoenvironmental investigations have been realized in Northern Africa over the last four centuries, reliable continuous data on Late Quaternary climatic and landscape changes in the Central Sahara is limited in quantity as well as in quality. Due to the diverse sources of palaeoenvironmental data, depending as it does on the nature and condition of the available archives, the information that can be deduced is frequently of low temporal and spatial resolution. When these fractions of evidence from different sources, also referred to as proxies, are assembled, inconsistent and incompatible data make it difficult to form a complete picture of the progression of the landscape.

The research project "Late Quaternary Environmental Change in the Central Sahara (NE Niger)", known as LIMNOSAHARA, is funded by the German Research Foundation (DFG). The aim of this interdisciplinary project is to review existing evidence and to complete missing segments of the Holocene palaeoenvironmental history of the central Sahara. To achieve this, physical geographers, palaeopedologists, palaeobotanists and archaeologists, from the Universities of Wuerzburg, Berlin, Gießen, Frankfurt and Niamey, are working on different subprojects and with different emphases.

The foundations of this project were two expeditions to the central Sahara, in 2005 and 2006. Because of the need for a variety of bulky equipment, these field trips were made by road, starting in Germany. Because of ongoing political disputes between Niger and Libya, the intended border crossing in Southern Libya was not accessible and the route originally planned was abandoned. The alternative route involved a detour of several thousand kilometres via West Africa, passing through France, Spain, Morocco, Western Sahara, Mauritania, Mali and Burkina Faso. The destination of both trips was the far northeastern area of Niger, as previous research had shown that palaeolimnic sediments and palaeosoils - regularly distributed in the central Sahara - are suitable for reconstructing its Late Quaternary palaeoenvironment (e.g. BAUMHAUER 1986). These deposits show a great range of diversity in both their genesis and the prevailing environmental setting. The essential information about the environmental setting of Niger is available thanks to considerable earlier geomorphological fieldwork, largely by the Wuerzburg Desert Research Group. The group, founded by Horst Hagedorn, realized more than 10 expeditions to the southern central Sahara between 1977 and 1991. However the parts of the central Sahara which lie inside Niger were not accessible from 1992 to 2000, due to civil war, riots and unrest.

During the most recent field trips, made by the LIMNOSAHARA project in 2005 and 2006, numerous soil and sediment samples were collected. Most importantly, a continuous 63 mm core of lake sediment, extending to the bottom of the sandstone depression at 15 metres depth, was extracted from underneath a saltpan at the oasis of Seggedim. Lakes or lacustrine sediments are considered to contain the most valuable climate archives (Wright, 1991). However, depending on the size of the investigated lakes, the influence of climate signals can be overlaid by local factors, such as the water table, the geology, or anthropogenic influences. Distinctions need to be made between sediment changes in a core which are due to local and regional factors in the surrounding landscape ecology, and those which can be attributed to Late Quaternary climate change. To achieve this, a number of less complete soil and sediment samples were taken in areas with an identified palaeoenvironmental record as well as at new sites at the Plateau de Djado, the Plateau de Mangueni and in the foothills of the Plateau de Tchigai (App. figure 1). The analysis of these samples provides the necessary spatial information about quaternary climate change, which is required to extend the highly localized information obtained from the core and other palaeolake sediments to the entire region and to complete the determination of palaeoenvironmental dynamics in the central part of the Sahara.

2 GEOGRAPHICAL SETTING OF THE STUDY AREA

2.1 Geomorphology

Niger is located in western Africa (Figure 1). Two thirds of its land surface is fully arid desert, within the Sahara. Only in the south, where the Sahel begins, does vegetation cover increase and the landscape begins to change into savannah. The eponymous Niger River flows just in the southwestern part of the country, generating the most fertile areas surrounding the capital city Niamey.

The study area is concentrated in the south central part of the Sahara, between 17° - 23°N and 11° - 15° E, in the far north east of Niger. The major part of this area is covered by the Ténéré sand plain, which is located between the Air Massif in the west and the Plateau de Djado and the Kaouar in the east (Figure 1). It has a north-south extension from the Algerian border into the Erg (sand sea/dune sea) de Ténéré in the southeastern part of Niger. The Erg de Ténéré, the predominant element of the landscape of central Niger, merges towards the east into the Erg de Fachi-Bilma and the Grand Erg de Bilma and ends in Chad. These Ergs are typically dominated by huge longitudinal dunes, which are aligned NE-SW along the direction of the predominant wind, the Harmattan.

Towards the northeast, these dune seas are broken up by latitudinally oriented escarpments, with endorheic basins in the western front of the cuesta. The escarpments are mostly dissected and have been partly removed, leaving small inselbergs and plateau fragments in the plains. Typically, the endorheic basins contain lakes or lacustrine remnants, suitable for palaeoenvironmental investigation.

The endorheic basin of Kaouar (also referred to as Kawar) runs within the foreland depression of the scarp of Bilma, which itself follows a north-south-running tectonic structure which, according to BAUMHAUER (1991), most likely extends further north to the western border of the Murzuk basin. The Kaouar runs from north to south with a total length of 80 km and a mean width of 6 km. The depression extends to approximately 80 m below the surrounding plain. The Kaouar escarpment stretches about 150 km from north to south. Along the scarp foot, a depression has developed with several inhabited oasis towns, such as Bilma and Dirkou. The southern part contains four saline lakes of the Na-CO_3-SO_4-Cl brine type, which have persisted to the present day. The lakes are shallow, fed by artesian groundwater, and bordered by belts of salt marsh. The total area of the lakes varies throughout the year, from 0.5 to 200 ha, with lengths of 2-3 km and widths of 100-200 m (BAUMHAUER 1986, 1991). The highest point of the escarpment is Pic Zoumri, a Zeugenberg at the northern end of the Kaouar, close to the village of Seggedim (also called Seguedine), where the southernmost study site of this work is located.

The cuesta of Zoo Baba is situated 70 km south of the Erg de Bilma and consists of sandstones, most likely from the Cretaceous or Palaeocene, of clayey to silty texture/nature, and in places rich in carbonate (BAUMHAUER, 1987). The western rim forms a steep slope, of which the middle and lower parts are covered by deeply -dissected fossil landslides. The pediment's basal zone is dissected in the same way, but lacks any signs of landslides. An endorheic depression is situated west of the cuesta, which elevates to 578 m asl (above sea level). The western frame of the depression is formed by the terraced slopes of the large Bilma dune field (GRUNERT et al., 1991).

The endorheic depression of Fachi stretches over a length of 25 km along a 150 m high escarpment and is situated within the Erg de Ténéré, some 150 km W-SW of Bilma. Quaternary deposits of lacustrine origin cover the base of the depression and salines (salt pans) are the only sign of water (SERVANT, 1983).

Moving further north, the predominating landscape units are the plateaus of Djado, Mangueni and Tchigai, indicating the southern margin of the Murzuk basin, located in the south of Libya. The plateaus of Djado and Mangueni are located in the northern edge of Niger, flanking the basin of Madama to the west, whereas the plateau of Tchigai flanks the eastern side of the Madama basin. The whole area has an elevation of/rises about 400-500 metres asl, whereas the relative height of the escarpments ranges from a few to several hundred metres. The Mangueni plateau consists of an extensive and coherent upland area that is only dissected by short valleys at its extreme fringes and is inclined at about 0.5 ° to the Murzuk basin (GRUNERT, 1983).

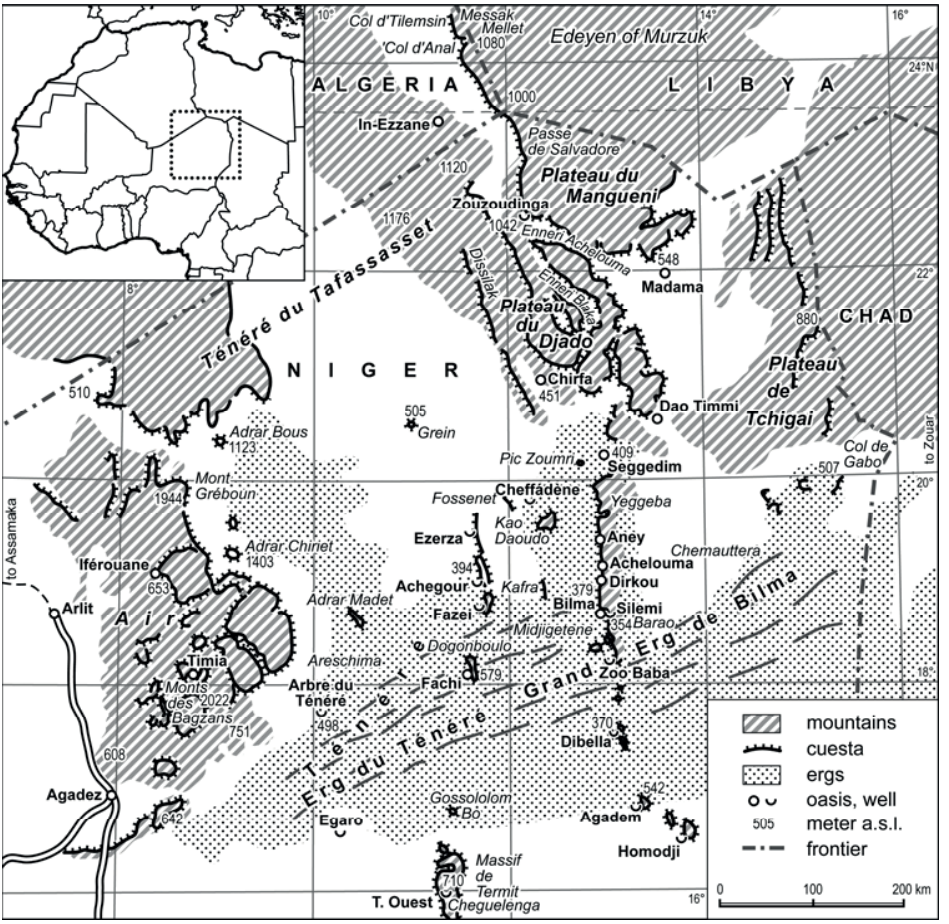

Figure 1 Map of north-eastern Niger (Baumhauer et al., 2009a)

Regular and continuous block slides are found at the eastern margins of the Plateau de Djado, the blocks very frequently having distorted shapes and outlines. The blocks largely cover the slope, and are assumed to increase in age from top to bottom (GRUNERT, 1983). At the southern margin of the Plateau de Mangueni and in the western parts of the Plateau de Djado, towards Enneri Blaka, the slides are of the mudflow type, showing a rather chaotic pattern and a distinct fluvial drainage pattern.

Towards the south, the signs of the aeolian dynamics which shape the landscape are increasingly visible (GRUNERT, 1983).

In contrast to this, the Plateau de Djado is dissected by valley systems which strike NW-SE. These valley systems represent palaeo-drainage systems which are only partially drained in present times. One of the biggest wadis is Enneri Blaka, which marks the border between the fully-carved plateau areas in the west and the more complete plateau area in the northeast (GRUNERT, 1983). The plateaus are separated by a large valley, Enneri (wadi) Achelouma, with a maximum width of about 20 km at its opening. It is situated within the subsequent zone of the plateau edges, and has developed a consistent and continuous slope (GRUNERT, 1983).

The present amount of groundwater recharge (if there is any) can be neglected for northeastern Niger; only in the far southwestern areas of Niger has aquifer recharge been demonstrated, using measurement of electrical conductivity (MASSUEL et al., 2006). Thus, any groundwater occurrence must be related to fossil recharge. Water-bearing wells are known to exist in the plateau area at Zouzoudinga, Achelouma and Blaka Kallia, with a water table at approximately 10 metres depth (GRUNERT, 1983).

2.2 The geological framework

This chapter provides a short summary of the geological setting of the investigated areas. Details of more comprehensive and elaborate examinations can be found in the publications mentioned below. Basic exploration of the geological situation in northeastern Niger was substantially completed by two researchers in the 1960s: FAURE (1966), who investigated Niger's eastern areas towards the Plateau de Djado, and PIRARD (1962), who focused on the hydrogeology of eastern Niger. Virtually all subsequent works on geology in this region refer to these publications. Generally, the central Sahara's main structures are plateaus and plains from the Palaeozoic, Mesozoic and Tertiary periods (Appendix Figure I). The underlying basement consists of an etchplain of Precambrian metamorphic and crystalline rocks. A slight inclination of the deposited sediments due to tectonic activity has caused massive erosion and thus shaped the characteristic scarplands of the central Sahara (BAUMHAUER et al., 2009a; FAURE, 1966).

Mesozoic formations found in Niger (in particular those from the Triassic to the Lower Cretaceous) lack for the most part sufficient fossils to determine any subdivisions. Consequently, these facies were summarized in the past as Nubian sandstone. The sandstone facies is found at the rim of the Murzuk basin, builds up most of the Plateau de Mangueni and the eastern parts of the Plateau de Djado and is present in the Bilma and Emi Bao formations of the Bilma basin. Investigating the geology of both basins, BAUMHAUER (1986) concluded that these formations are coherent. According to GRUNERT (1983), a two-fold division can be set up. The northern compartment consists of the bottom Tilemsin layers and the overlying Messak sandstones, its southern equivalent being the Nubian sandstone (KALLENBACH, 1972). The Messak sandstone, also referred to as "Grés de Nubie", mainly contains kaolinitic clays and marks the end of Mesozoic sedimentation in the Murzuk area (BUSCHE, 1998). The Tilemsin layers are of special interest as they contain large amounts of illite, a clay mineral with an increased ability (compared to kaolinite) to incorporate water and subsequently to swell, which is therefore considered to be one of the main causes for the extensive landslides in the central Sahara (BUSCHE, 2001). GRUNERT (1983) emphasizes that the Tilemsin layers are the main cause of the mudflow-like slides at the southern fringes of the Plateau de Mangueni, compared to the block slides at the Djebel Messak.

The onset of post-sedimentary landform development began after the deposition and diagenesis of the Messak (or Nubian) sandstone (PACHUR & ALTMANN, 2006). The "Continental Intercalaire"

(or Continental Intercalary) is a North African rock stratum of the Lower Cretaceous and consists mainly of diverse sandstones and clays, predominantly deposited as continental sediments (BUSCHE, 1998; LEFRANC & GUIRAUD, 1990). It is common knowledge that this formation incorporates North Africa's largest water reservoirs, with an extent of more than 600,000 km² and an estimated water volume of 50,000 km³ underneath the northern Sahara (GASSE, 2002). The best-studied water-bearing formation within the Continental Intercalaire is the Nubian sandstone aquifer. The aquifer emerges in several areas in northern Africa, establishing permanent bodies of water in otherwise arid areas; for instance, in the Kaouar region, Lake Yao/Chad (KROEPELIN et al., 2008), or at the numerous oases within the Murzuk basin, which are situated along artesian outcrops of the Nubian sandstone (PACHUR & ALTMANN, 2006).

During tertiary times, a moist and hot tropical climate predominated, corresponding to Niger's geographical position near the equator. The residual products of the intense chemical as well as physical weathering are referred to as "Continental Terminal" (PACHUR & Altmann, 2006), as they mark the termination phase of the most recent terrestrial sedimentation (BUSCHE, 1998).

Throughout the Kanemian (20-12 ka BP/LGM) the entire eastern parts of the Sahara and Chad basins were subject to massive deflation and aeolian accumulation, comparable to the present dynamics (PACHUR & Altmann, 2006), and associated with a complete desiccation of Lake Chad (THIEMEYER, 2000). As a result, major parts of Niger are covered with sand dunes of quaternary origin.

The northern and eastern parts of the Plateau de Djado consist of Nubian sandstone, equivalent to the top layer of the Plateau de Mangueni. The remaining parts of the Djado plateau consist of a NNE-SSW-striking series of predominantly sandstone sediments of palaeozoic age (Cambrian - Ordovician) that have been largely disintegrated by erosion (GRUNERT, 1983). The Plateau de Mangueni consists of mud- and sandstone sediments from the Cretaceous and Tertiary, which belong to both the Continental Intercalaire and the Continental Terminal (BUSCHE, 1998; GRUNERT, 1983)

Little is known of the geology of the Plateau de Tchigai, which forms the southwestern foothills of the Tibesti Massif. According to PIRARD, (1962), the basin of Madama consists mainly of clay-mudstones and clayey sandstones from the Carboniferous. Following the slope up the Tchigai Massif, the bedrock changes to predominately clayey sandstones and groundwater-bearing sandstone, which drains subterraneously into the basin.

2.3 Vegetation

The African continent extends altogether from 40°N to 40°S, incorporating a range of climatic and ecological zones, from fully arid deserts to fully humid tropical rainforests. Since the number of weather stations in the desert areas of northern Africa is rather low, the transition of the ecozones from Sahel to Sahara, which involves a distinct increase in precipitation, is best visualized by the changing vegetation (Appendix Figure II). The central Sahara extends from approx 32°N to 16°N, with a transition to the Sahel zone (≈16°N to 13° N), which is then followed by the Sudanian belt (≈13°N to 10°N). The flora of the central Sahara has to tolerate mean annual precipitation of 50-100 mm, with a high variability (erratic rainfall) and intermissions of several years. It is mainly made up of *Acacia Panicum* and *Tamarix Stipagrostis,* but survives in hyperarid areas only in wadis and depressions where the water table is accessible or the sparse precipitation can accumulate (SCHULZ, 1991). The ephemeral vegetation of the desert, short-lived therophyte taxa (SCHULZ, 1991), also called Achab vegetation, is commonly found after erratic rainfall that occurs randomly on a local scale.

Moving southward, into a region with a mean precipitation of approximately 200-250 mm/a, the Sahel steppe commences. The transition is marked in the landscape by the more extensive appearance of *Acacia Panicum* (SCHULZ, 1991). The Sudanian belt consists mainly of dry forest and savannah-type vegetation, requiring an annual precipitation of 500 to 1500 mm (GASSE & ROBERTS, 2004). This progression and the distinct seasonality of the rainfall in northern African latitudes correspond to the displacement of the Intertropical Convergence Zone (ITCZ) and the associated Hadley cell over the year. Across the longitudinal direction of the Sahara, the climate is determined by its continentality, creating a general decrease of rainfall from west to east, with small modifications due to the Saharan mountains, which increase the precipitation at a local scale (GASSE & ROBERTS, 2004). A shift of the existing margins would cause major changes in the ecological conditions of the area in between. Such changes have occurred numerous times in the past, particularly during the transition from glacial to non-glacial periods. Palaeoenvironmental research on marine and terrestrial sediment records has provided detailed information of Holocene variations in the monsoon circulation, causing major climate changes in the lower latitudes, which have been most comprehensive studied in Africa and central Asia (e.g. KROEPELIN & PETIT-MAIRE, 2000).

A more comprehensive description of the vegetation of Niger can be found for instance in SCHULZ (e.g. 1991) and for the eastern Sahara in RITCHIE and HAYNES (1987).

2.4 Present climatic dynamics of Northern Africa

As indicated by the vegetation map (Appendix Figure II), northern and western areas of Africa are mainly characterized by the explicit latitudinal course of zonal boarders, determined by the distribution of precipitation. A very large number of investigations have confirmed the seasonal migration of the Intertropical Convergence Zone (ITCZ) as the key influence on northern African climate (e.g. COHMAP Members, 1988). The ITCZ is a low pressure belt where the air masses from north and south of the equator (trade winds) converge and tend to rise, supported by increased surface temperatures (MCGREGOR & NIEUWOLT, 1998; NICHOLSON, submitted 2007).

The ITCZ, also referred to as the meteorological equator, moves according to the displacement of maximum solar heating throughout the year (MCGREGOR & NIEUWOLT, 1998). The gradient of land surface temperature in North Africa is also considered to be the driving force for the migrating position of the ITCZ (BRACONNOT et al., 2000). In addition, the ITCZ movement is also controlled by other compartments of the general atmospheric circulation, since teleconnections exist between the tropical and mid latitude atmosphere (MCGREGOR & NIEUWOLT, 1998; NICHOLSON, 2001). This movement of the ITCZ creates the humid tropical zone at the equator and the adjacent monsoonal climate zones (GASSE & ROBERTS, 2004). The south of Niger benefits from the West African monsoon, which causes rainfall during the northern-hemisphere summer but barely reaches into the central parts of the Sahara. Figure 2 shows the typical maximum positions of the ITCZ in the boreal or northern-hemisphere summer (July-August) and the boreal winter (January).

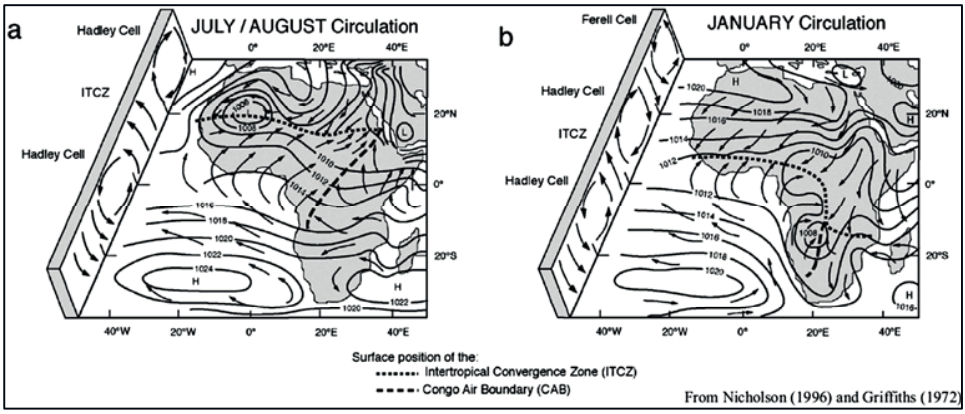

Figure 2 Pattern of low level winds (at ground level) and pressure over Africa (Gasse & Roberts, 2004)

In the northern-hemisphere summer the typical climatic setting is determined by the northward migration of the ITCZ to about 18° to 20° N. Simultaneously, an intense low pressure area (a "heat low") becomes established above the Western Sahara and the Arabian Peninsula, while high pressure predominates over Central Africa (GASSE, 2002). The northern hemisphere summer is characterized by massive tropical rainfall in low latitudes, below 20° N.

Figure 3 shows a cross section of the ITCZ at its northward position along the zero meridian. The area of summer rainfall can be divided into 3 sections: the equatorward area of continuous monsoon precipitation, a zone of squall-line storms and showers, and the northernmost area of exceptional storms, up to 20°N. The northernmost component of this system is the northeast-southwest running trade wind regime also referred to as the Harmattan (GASSE, 2002). The Harmattan is the ground component of the African continental trade wind system and is considered to be the driving force of aeolian dust export from the Bodelé depression to southern West Africa (SCHWANGHART & SCHUETT, 2008), which is believed to be the largest source of atmospheric dust (BRISTOW et al., 2009).

It is the surface compartment of this slope, referred to here as the ITCZ but also known as the Intertropical Front (ITF) or Intertropical Discontinuity Front (ITD), which is the main reason for these variations in nomenclature. Depending on the characteristics being investigated (low pressure, convergence of air masses, cloud and precipitation maximum) definitions of the ITCZ's maximum longitudinal positions may vary (MCGREGOR & NIEUWOLT, 1998; NICHOLSON, submitted 2007), as the origin of these characteristics depends on different subsystems and their positions are not consistent (Figure 3). Nevertheless, the surface position of the ITCZ controls the summer rainfall distribution in the southern central Sahara and northern Sahel from approximately 23°N to 15°N (NICHOLSON, submitted 2007).

According to Nicholson (2007), rainfall in Western Africa is generally more dependent on features of the upper-level circulation than on surface features and moisture sources from continental evaporation are more important for the monsoon than those from the Atlantic. The precipitation in the area of continuous monsoon rains (also referred to as the tropical rain belt) largely depends on the position and the ascent of the African Easterly Jet and the Tropical Easterly Jet (Nicholson, submitted 2007).

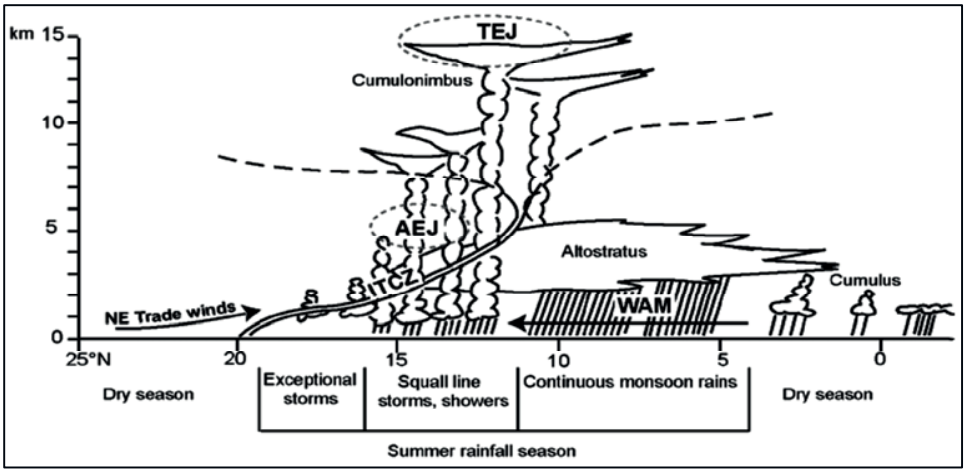

Figure 3 Cross section of ITCZ (July-August) along the zero meridian (Gasse & Roberts, 2004)

The African Easterly Jet (AEJ) is the zone of maximum easterly winds (BURPEE, 1972), which results from the thermal and moisture gradients between the hot Sahara and the colder Gulf of Guinea and is located in the mid-troposphere (GASSE & ROBERTS, 2004). These gradients are predominantly influenced by the sea-surface temperatures (SST) of the southeastern tropical Atlantic (SSTA), which determine the amount of precipitation in West Africa (VIZY & COOK, 2001). Dry conditions in the Sahel may be associated with higher SSTA, due to a smaller land-ocean thermal gradient, causing weakened monsoon activity and consequently reduced precipitation in the Sahel (ELTAHIR & GONG, 1996; VIZY & COOK, 2001).

In the Sahel zone, the squall lines are considered to be the main source of the convective rainfall during the northern-hemisphere summer (e.g. PETERS & TETZLAFF, 1988; ROWELL & MILFORD, 1993). Squall lines are westward moving cells of moist convective air masses, which persist for several hours and show a broad range of precipitation intensities (ROWELL & MILFORD, 1993). They are intensified by topography and increased surface moisture as well as by increased surface temperatures (ROWELL & MILFORD, 1993). The squall lines are part of the West African monsoon, but are initiated by the upper level jets, the African Easterly Jet and the Tropical Easterly Jet (GASSE & ROBERTS, 2004). The African Easterly Jet (AEJ) itself is not the main/usual source of precipitation in West Africa, but may contribute a certain amount of rain by transporting reworked humid air from central Africa (GALLAIRE et al., 1995, originally from CADET & NNOLI, 1987). African Easterly Waves are wavelike compensation turbulences in the mid-troposphere, which form over the eastern parts of central Africa, south of the AEJ (BURPEE, 1972) and modify the rainfall distribution of the squall lines (NICHOLSON, submitted 2007).

In the northern-hemisphere winter, the ITCZ shifts southward to about 3° or 4°N and high pressure becomes established over the Arabian Peninsula (Arabian High) and North Africa. A low-pressure area dominates the central and eastern Mediterranean, and is associated with the shift of the mid-latitude Westerlies towards the equator. At this time of year the mediterranean parts of North Africa receive the majority of their annual precipitation (GASSE, 2002).

The northern fringes of the Sahara (above 24° N) also receive some of this winter rainfall and are therefore associated with the mediterranean precipitation regime. Figure 4 illustrates the high impact

of boreal summer precipitation on the annual precipitation in the area below 20°N latitude. Virtually the complete annual rainfall occurs during a 3-month period from June to August (JJA), indicating the influence of a monsoonal regime (GASSE & ROBERTS, 2004). The extratropical rainfall distribution shows the minor contribution of northern-hemisphere summer precipitation to the total annual amount, evidently because of the winter rainfall regime. The figure reveals the exceptional position of the central parts of the Sahara in the overlap of the disparate precipitation systems. In addition, cyclonic perturbations of Atlantic, Mediterranean or Saharan origin can provide very large amounts of local rainfall. Even the Saharan mountains in the north can be affected by winter rainfall, despite the fact that the predominant origin of rain-bearing air masses is the summer monsoon (GASSE, 2002). For instance, GRUNERT (1983) refers to a precipitation event as Madama rain, which occurred in June 1943 and brought 41.1 millimetres of rain in one day.

A recent investigation of the precipitation dynamics at the Air Massif evidences the high impact of topography on the local rainfall regime (GALLAIRE et al., 1995). Originating in the Guinea monsoon (also referred to as the West African Monsoon), the air masses approaching from the southwest contain just small residual amounts of moisture at this latitude. With increasing altitude, precipitation amounts in the south-western parts of the Air Massif rise to an annual mean of 125.3 mm, with more than 170 mm/a in the highest parts of the Air Massif (GASSE, 2002). Adrar Bous, located in the north-eastern part of the Air, receives only 4.8 mm/a because of the rain shadow effect (GALLAIRE et al., 1995). There are very few weather stations in the central parts of the Sahara. The closest station to the study sites is located in Bilma, in the Kaouar valley. The mean annual rainfall is about 10 mm, with a potential annual evaporation rate of approximately 2700 mm (BAUMHAUER et al., 2009a).

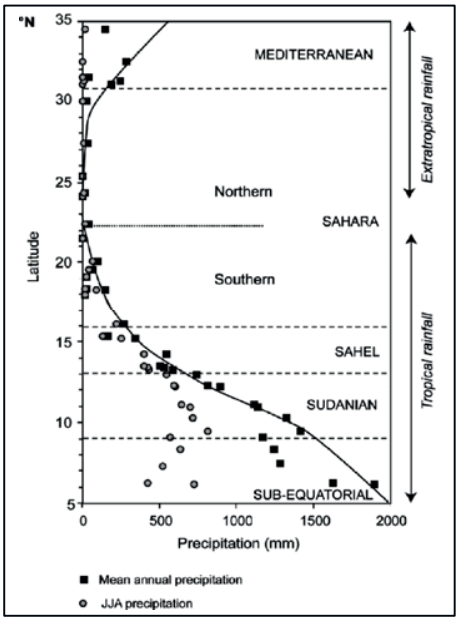

Figure 4 Model of rainfall distribution over Northern Africa (Gasse & Roberts, 2004)

In the eastern Sahara, south of 20°N, the sources of precipitation are in the Atlantic Ocean and, in contrast to the western and central Sahara, in the Indian Ocean, as the monsoon flow converges with the Indian monsoon winds over the Ethiopian plateau, causing heavy summer rains (GASSE & ROBERTS, 2004).

2.5 Geographical setting of the study sites

2.5.1 Seggedim

The central study site of this work, Seggedim (20°24´N / 12°48´E), is located in north-eastern Niger, east of the Ténéré desert and south of the Djado plateau, and marks the northern end of the Kaouar (Figure 1). The eponymous oasis lies inside an endorheic depression that stretches for about 9 km in an E-W direction in front of a cuesta, and has a mean width of 2.5 km. The highest point of the cuesta is the formation of Emi Bao with a height above sea level (asl) of 639 metres and an elevation of about 220 m above the surrounding area. At the south-western fringe of the depression, Pic Zoumri, a Zeugenberg with an absolute height of 567 m, constitutes the northernmost point of the Kaouar escarpment (e.g. Baumhauer 1991). Within the depression and situated between Emi Bao and Pic Zoumri, a sebkha has developed, due to available groundwater at several metres depth (Figure 5). The groundwater provides the basis for both the well-known saltpans and the adjacent freshwater wells.

The depression belongs to the geologic Lake Chad basin and the cuesta consists of marine sand and siltstones from the Late Cretaceous (Turonian, 93-89 Ma, to Maastrichtian, 70-65 Ma). The ambient plain is in fact a serir (gravel desert plain), consisting of eroded gravels from conglomeratic layers of the cuesta, whereas most of the depression is covered by sand (Baumhauer and Schulz 1984).

Due to the courageous ascent of the Emi Bao by Dr. Barbara SPONHOLZ, lithology samples from several layers of the escarpment were obtained during the excursion in 2006. In addition, samples from the Pic Zoumri base debris were collected in order to gain a basic understanding of the mineralogical background of the depression. For reasons of comparison, a piece of swamp iron ore was analysed to estimate the iron content. Although not considered completely representative, the results show an unambiguous dominance of the quartz compartments (Appendix Table I), even in the designated swamp iron ore. Goethite and hematite show minor fractions, ranging between 1 and 28 percent. Kaolinite appears only randomly in the investigated samples.

As the hydrological situation is not well known, estimates for the annual recharge of groundwater do not exist. Precipitation for the area has been measured in Bilma, about 150 km south of Seggedim but can be applied to Seggedim, as no great divergence is likely. The mean annual precipitation amounts to about 10 millimetres, while the potential evaporation lies at 2700 mm/a (BAUMHAUER et al., 2009). As groundwater is available, the vegetation units are oriented along the geologic and geomorphologic structures that affect water availability. Halophytes such as *Tamarix canariensis* and *Juncus maritimus* are grow around the saltpans and at water points. The sporadic colonies of trees include *Acacia raddiana* and *A. ehrenbergiana* as well as the doum palm (*Hyphaene thebaica*), beside the more frequent and harvested date palms (*Phoenix dactylifera*), which grow in the surrounding of the sebkha on the sand dunes. The occurrence of the diverse grasses depends on the surface, for instance the Desert Grass (*Panicum turgidum*) grows on coarser sand and gravels, whereas other taxa, such as *Imperata cylindrica*, *Desmostachya bipinnata* and *Sporobolus spicatus*, are found on dune sands (BAUMHAUER et al., 2004).

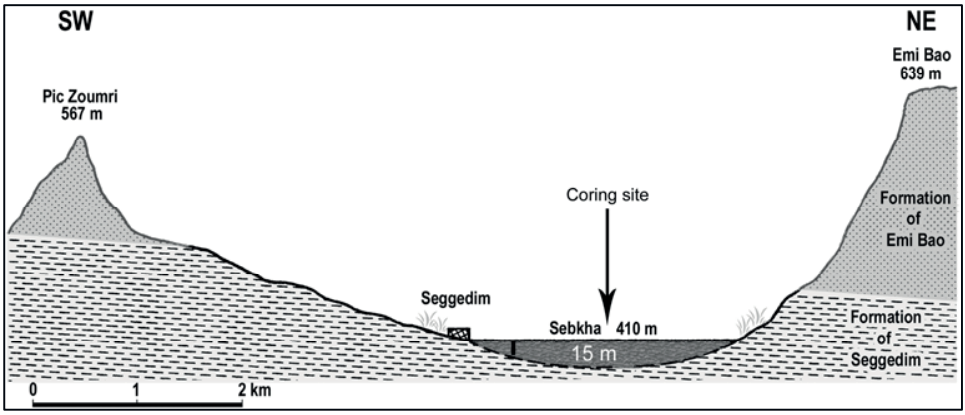

Figure 5 Cross section of the Seggedim depression (modified from Baumhauer 1988)

Previous investigations have revealed the presence of Late Quaternary lacustrine sediments underneath the saltpan sediments, indicating a climate-induced transition from a freshwater lake to the present sebkha (BAUMHAUER et al., 2004). The first corings, performed in 1989 and 1990, reached down to 8 metres and revealed a three-way development of the sebkha (BAUMHAUER et al., 2004):

UNIT 1 790-640 cm depth:	freshwater milieu;
UNIT 2 640-550 cm depth:	decreasing lake levels;
UNIT 3 550-0 cm depth:	sebkha sedimentation.

Two radiocarbon dates were obtained from the core, at 790 cm depth, showing an age of 7905 ± 275 a BP (Calendric Age calBP: 8816 ± 327) and at 590 cm depth with an age of 6850 ± 345 a BP (Calendric Age calBP: 7716 ± 315). Both datings were executed on bulk organic matter. Archaeological sites near the sebkha have been dated to 2090 ± 105 a BP (Calendric Age calBP: 2097 ± 145) and 8890 ± 365 a BP (Calendric Age calBP: 10028 ± 449) (BAUMHAUER and SCHULZ 1984).

2.5.2 Fabérgé depression

The site referred to as Fabérgé (21°02’18’’ N/13°42’00’’E) is actually a nameless spot inside the geologic Djado basin, situated north-east of the Djado plateau. It was named Fabérgé because of certain archaeological finds in the basin, highly specific tools of Neolithic age. It consists of a depression of 20 m depth inside a NE-striking planar stratum of heavily weathered, carbonate siltstones. The depression is partly covered by diatomitic and sand-to-silty limnic sediments, probably from the Middle Holocene. Nevertheless, large areas have been dismantled by deflation. The depression itself shows several tectonic features. The geomorphological map (Figure 6) shows a number of lineaments and their right angle connections, some joint striking and several spring mounds, both inside the basin and on top of the surrounding hills. The basin of Fabérgé is embedded in a plain that discharges in a northeastern direction, although the depression itself discharges towards

the southeast. A few drains in the northern parts of the depression are connected with the plain through headward erosion. Grabenstructures in the western and southwestern areas determine the pattern of incoming wadis. A massive alluvial fan has developed in the southern part.

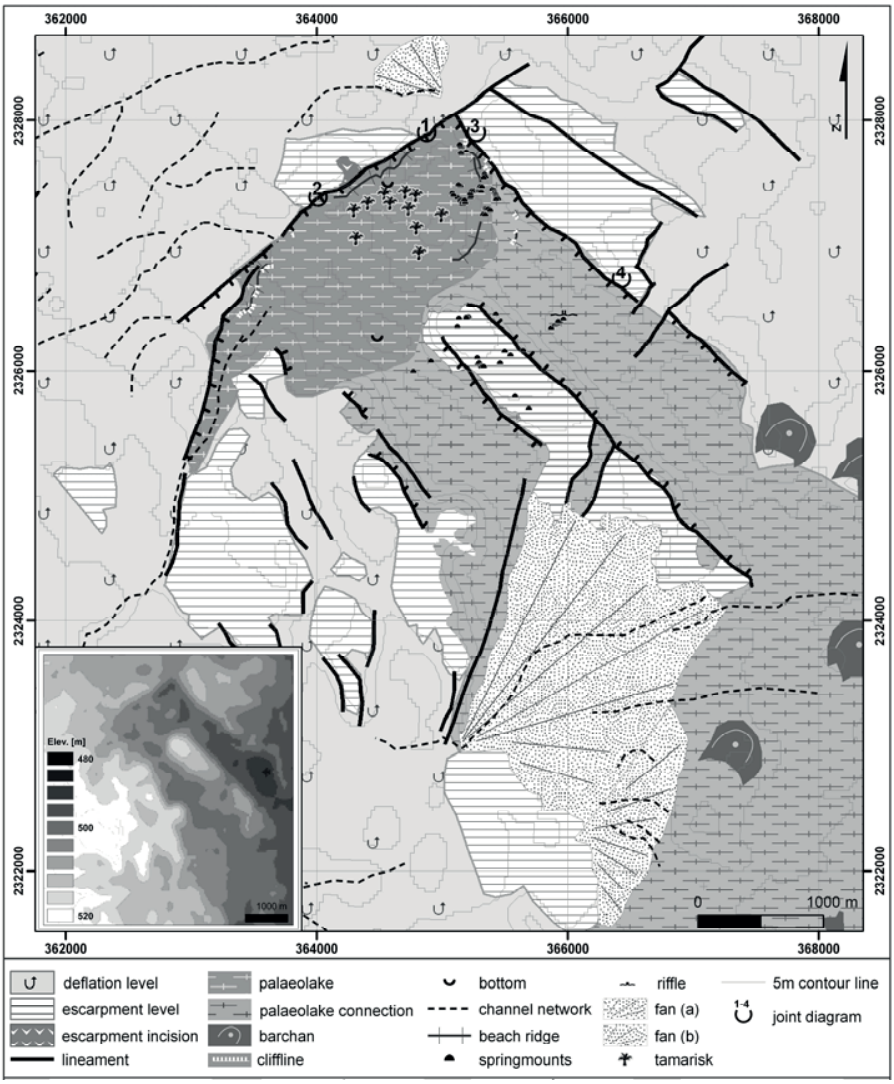

Figure 6 Geomorphological map of the Fabérgé study site (Krause, J.& Marquardt, N)

Hummocks of up to 15 metres height inside the depression, overgrown with tamarisks (*Tamarix africana*), and yardangs, give evidence of the powerful aeolian dynamics. The basal parts of the hummocks are intermeshed with the lacustrine sediments. Tamarisks are halophytes and show a layered structure due to salt excretion (glandular secretion of absorbed salt). Windblown sand and

(diatomitic) dust is trapped on the surface of the tamarisks, which leads to the growth and stabilisation of the tamarisk hills. The captured sands inside the tamarisk hummocks show obvious signs of weathering and soil development, indicating the former humid character of the basin. Excavations at the base of the hummocks indicate that the onset of development of the tamarisks was on fossil dunes after the lake desiccated.

Large diatomitic banks are associated with silificated and carbonate-rich reed tubes and molluscs, indicators of the previous existence of periodic to perennial shallow waters. Further indicators for the past presence of a lake are skeletal remains of a huge mammal inside the basin, as well as a very large number (> 140) of tumuli (burial mounds) and Neolithic artefacts. Until now, this area has not been studied in detail; consequently, no comprehensive information is available.

2.5.3 Enneri Achelouma / Seeterrassental

At the front side of the northwest-southeast striking scarp of the Plateau du Mangueni, a large number of obsequent valleys discharge into the Achelouma Valley (Enneri Achelouma). The Enneri Achelouma (22°20'N/12°40'E) is a SE-striking valley system that runs along a graben structure separating the Plateau de Djado (SW) from the Plateau de Mangueni (NE) (KRAUSE & SCHUETT, 2009).

The plateau de Mangueni consists of mud- and sandstones from the Cretaceous-Carboniferous Continental Intercalaire and the Tertiary Continental Terminal; the surface of the plateau inclines N-NE. The bedrock of the plateau de Djado is mainly made up of Palaeozoic sediments (Ordovician-Cambrian) with the surface inclined towards the south (PACHUR & ALTMANN, 2006).

BUSCHE et al. (1979) and GRUNERT (1983) investigated this area and discovered a tributary to the Achelouma valley; GRUNERT refers to it as the "Seeterrassental", meaning the valley of Lake Terraces. This tributary is incised north-eastwards into the SW-headed escarpment of the Plateau de Mangueni, creating a dry valley of about 15 kilometres length and a maximum width of 2 kilometres, with a total catchment area of 31.3 km².

Extensive landslides at the plateau's edges built up several natural dams inside the valley, probably in the Early to Middle Quaternary (BUSCHE, 2001). Subsequently, terraces of small water-filled basins developed inside the valley and lacustrine sediments were deposited over many centuries. Results from ostracod analysis indicate freshwater conditions in a somewhat wetter and cooler climate than at present (GRUNERT, 1983). Due to massive erosion by substantial fluvial dynamics, most likely initiated by a lake outburst, the remnants of these deposits are only partially preserved.

The geomorphological map (Figure 7) is derived from remote sensing data and field investigations in 2006 (KRAUSE & SCHUETT, 2009) and shows the main features of the Seeterrassental. Massive landslides at the plateau's edges, in combination with fluvial incisions, have led to lateral erosion. The present channel bed is incised into the bottom of the former streams, indicated by parallel-running fluvial terraces at different heights on both sides, and is most likely the result of present-day rainfall. The hill slopes flanking the valley bottom on both sides are heavily slump-affected (KRAUSE & SCHUETT, 2009).

Beside the lacustrine sediments, palaeosoils on lee dunes are located in sheltered sites along the entire valley, with a maximum occurrence in its upper course. In order to validate and supplement previous results with up-to-date analyses, this valley was a designated study site. Three sediment profiles were investigated in the upper reaches of the valley, where fluvial dynamics were not too forceful and parts of the sediments remained preserved.

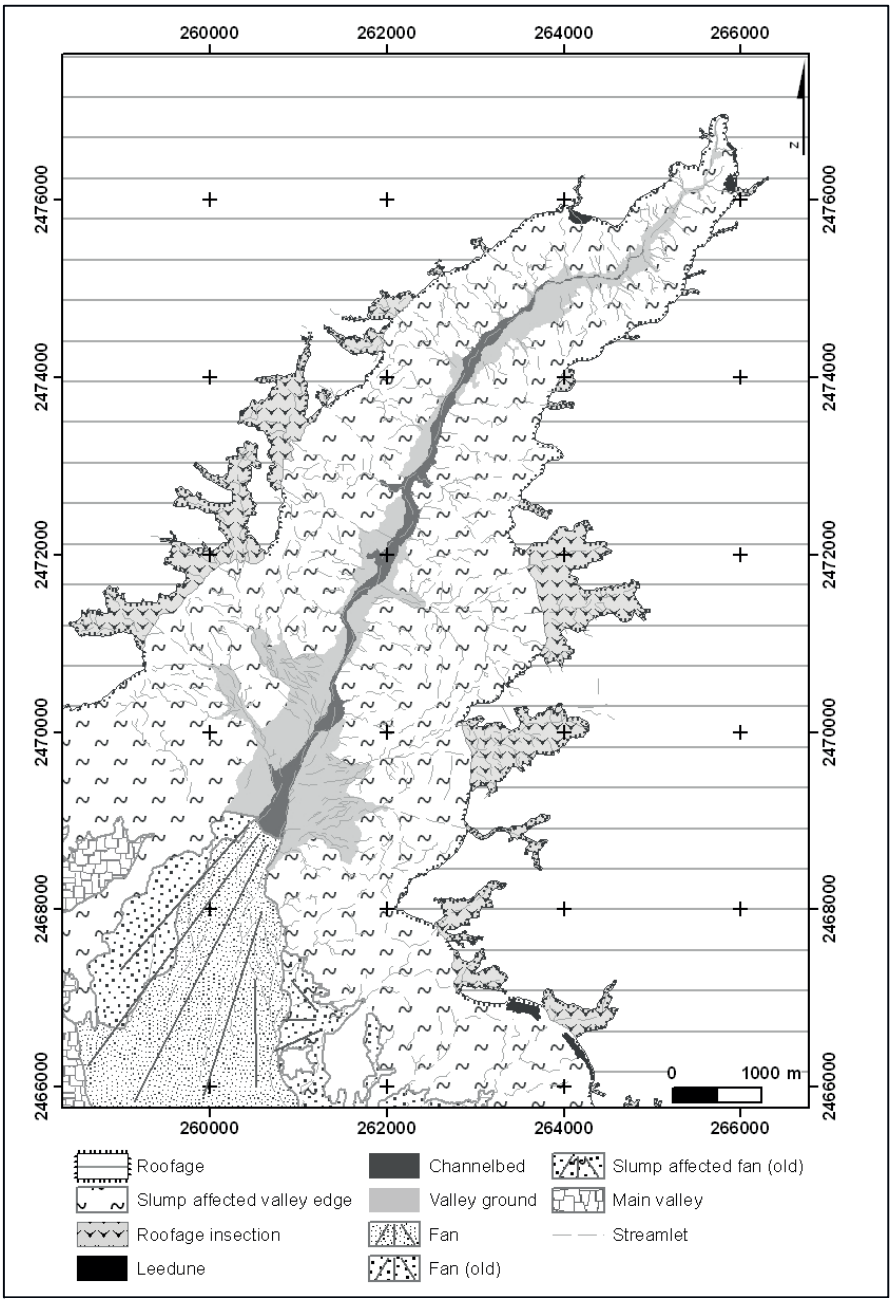

Figure 7 Geomorphological map of the Seeterrassental (Krause & Schuett, 2009)

2.5.4 Yoo Ango

The site referred to as Yoo Ango (21°47`N, 14°21`E, 487 m asl) is a small depression in the eastern part of the Madama basin (Plaine de Madama), some kilometres north-eastern of Emi Fezzane, the highest point in this area. The landscape consists of a chaotic system of small basins and ridges among alternating claystones, water bearing sandstones and clayey sandstones (Pirard, 1962).

Yoo Ango is located in the western foothills of the Plateau de Tchigai, in front of the Tchigai massif. The geomorphological map of the area (Figure 8) shows the depression, which is located in a heavily incised plateau. At the north to north-western edge, the basin is separated from the plateau by a small scarp overlain by NW-SE striking alluvial fans, which originate in the plateau fringes.

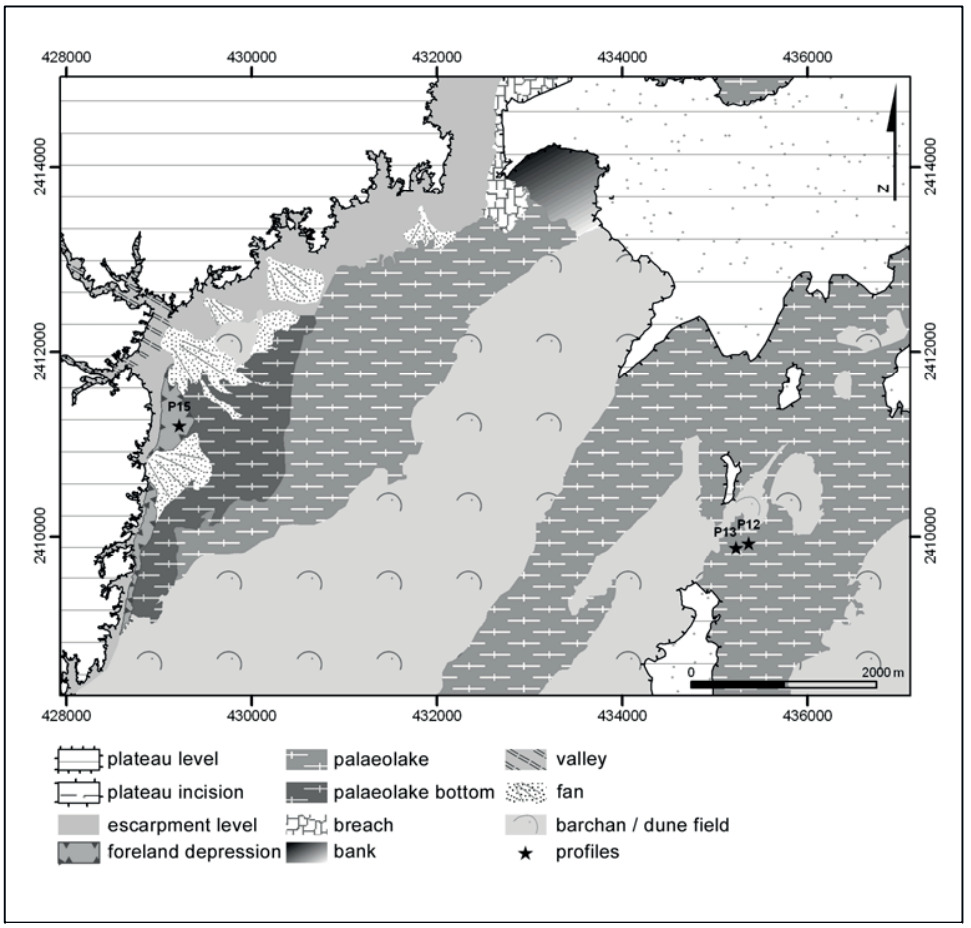

Figure 8 Geomorphological map of Yoo Ango (Krause, J.& Marquardt, N)

The interior of the depression is determined by massive deflation. One of the dominating features within the basin is the occurrence of NE-SW moving barchans, which follow the main wind direction. Similar to the Fabérgé site, large diatomitic banks with molluscs on top are found, indicators of the previous existence of periodic to perennial shallow waters. A very large number of fireplaces and Neolithic artefacts are present all over the area.

Due to the massive deflation, lacustrine sediments are primarily preserved in small depressions. In these the soil surface shows alternating features, from aggregated siltic material to sand and gravel-dominated layers, containing numerous Neolithic tools, which are found in restricted areas. The profiles which were investigated were located in the south-eastern part of the depression. Two sediment profiles were sampled for geochemical analysis and an adjacent fireplace was sampled to estimate the time of human settlement. Up to now this area has not been studied in detail; consequently, no comprehensive information is available.

3 SEDIMENTARY DEPOSITS AS TOOLS FOR ENVIRONMENTAL RECONSTRUCTION

The fact that sedimentation processes inside lakes occur comparatively undisturbed over long periods makes them ideal material for palaeoenvironmental and palaeoclimatological reconstructions. Palaeoenvironmental information derived from different sources, also referred to as proxy data, characterizes the environmental conditions of a given drainage basin, which are principally determined by climate, endogenic dynamics and anthropogenic influence (SCHUETT, 2004).

"[…] in many terrestrial environments lake sediments provide virtually the only available stratigraphic sequences of microfossils or chemical materials amenable to paleoclimatic interpretation - and often the only organic matter useful for radiocarbon dating –[…]" (WRIGHT, 1991,p. 37)

As mentioned previously, lakes remain the best source of palaeoenvironmental data, especially in continental areas, although the influence of climate signals can be overlaid by local factors (FONTES & GASSE, 1991), such as the water table [or: groundwater levels] (KELTS & K.J.HSUE, 1978), geology (RYNER et al., 2007) or anthropogenic influences (CHALIE & GASSE, 2002). Nevertheless, lake sediments from within a small catchment area are especially important local climate archives as they react immediately to environmental changes (FICKEN et al., 1998).

With respect to these local factors, three major categories of proxies must be distinguished when investigating palaeoenvironmental information from sediment deposits (SCHUETT & KRAUSE, 2009):

- proxies indicating synsedimentary environmental information, which preserve the environmental situation of the time of deposition (type and origin of deposited carbonates, pollen, diatom and ostracod taxa);
- proxies showing presedimentary environmental information, which represent developments previous to the sedimentation (soil sediments, translocated sediments and organic matter);
- proxies indicating postsedimentary information, which provide information about changes after the sediment was deposited (efflorescence of evaporation minerals within deposited sediment, contamination of saline groundwater).

For these reasons, interpretations of palaeoenvironmental records must be made with appropriate care and the main characteristic features of the records obtained need to be investigated and interpreted individually, with a focus on their diverse origins/sources/attributes. However, only a combination of such multiproxy data provides the required information for a comprehensive environmental analysis.

Table 1 shows the main sediment characteristics and their classification by basic attributes. As not all features can be examined in a project that is limited both by time and financial resources, a selection of properties that is both sufficient and significant must be identified.

Table 1 Basic and derived attributes of sediments (Last, 2001b, p42)

SELECTED PHYSICAL CHARACTERISTICS AND PROPERTIES	INTERNAL	TEXTURE	SIZE	AVERAGE SIZE
				RANGE OF SIZES
				SORTING
			SHAPE	ROUNDNESS
				SPHERICITY
				SURFACE TEXTURE
			ARRANGEMENT/FABRIC	PACKING
				ORIENTATION
		SEDIMENTARY STRUCTURES		BEDDING
				INTERBEDDING
				DIRECTIONAL FEATURES
				POST-DEPOSITIONAL FEATURES
	EXTERNAL	EXTERNAL FORM/GEOMETRY		SIZE (THICKNESS, WIDTH, LENGTH)
				CONFIGURATION/SHAPE
				NATURE OF BOUNDARIES
		RELATION TO BASIN FRAMEWORK		POSITION IN STRATIGRAPHIC SEQUENCE /CYCLE
				OVERALL VERTICAL TREND
				OVERALL LATERAL TREND
SELECTED COMPOSITIONAL PROPERTIES AND CHARACTERISTICS		MINERALOGY AND GEOCHEMISTRY		DETRITAL COMPONENTS
				ENDOGENIC COMPONENTS
				AUTHIGENIC COMPONENTS
				MAJOR + MINOR ELEMENTS
				TRACE ELEMENTS + CONTAMINANTS
				ISOTOPIC
				ORGANIC
			BIOLOGICAL	
SELECTED DERIVED MASS PROPERTIES		POROSITY	PORE SIZE	PERMEABILITY
		HARDNESS	ACOUSTIC VELOCITY	STRENGTH
		DENSITY	COLOUR	MAGNETIC PROPERTIES

3.1 Physical sediment features

The physical properties of sediments include a variety of characteristics, such as the size, shape and texture/composition of the grains of deposited material. The main goal of investigations into these physical properties is to gather information about the sources, the transport mechanisms and the past physical and chemical properties within the basin being investigated. In this way, information about the palaeoenvironmental conditions within the investigated area can be obtained from its sedimentary features (LAST, 2001b).

Because sediments are composites of different types of material, a scheme of classification is necessary to permit further interpretation. The most intuitive classification relates to the particles' sources (BOYLE, 2001):

- authigenic particles (trans-)formed within the lake, of biological and/or inorganic origin
- biogenic : from biological sources;
- allogenic: the source is located outside the lake, detrital;
- aeolian: windblown allogenic particles;
- minerogenic/lithogenic: from mineral source within the catchment area, bedrock;
- diagenetic (authigenic): post-burial modification/transformation of deposited material.

The major problem with this classification is the very frequent appearance of mixed particles, where a single source cannot be explicitly determined, but this method is nevertheless preferable to compositional or fraction-based classifications because of its comprehensive applicability (BOYLE, 2001).

3.1.1 Visual description

When investigating sedimentary deposits containing palaeoenvironmental records, the initial step is the description of the visual properties of the record, in most cases in combination with photography for further study (preservation of original appearance) (KEMP et al., 2001).

Stratigraphic description is performed, to obtain information on recurring phases and events and to give a broad estimate of the bedding characteristics within a deposit (KEMP et al., 2001). Changes in the sedimentation rate may be evidence of changes in the accumulation processes or in the status of the water level (FRITZ, 2008).

Throughout this work, the nomenclature for the description of the bedding properties of the core sediments being investigated is based on SCHNURRENBERGER et al. (2003). As a result, only those beds with less than 1 centimetre thickness are referred to as laminations or laminae; with additional proof of annual deposition rates by (radiocarbon) dating they are called varves.

Homogenous sequences need to be handled with special care, due to possible fine structures not visible to the human eye. High-resolution images or microscopy of thin sections can provide valuable information. Where no laminations are present in sediment cores, the investigated sections must be examined as to whether they have occurred as a result of bioturbation or massive inflow by clastic input (KEMP et al., 2001).

In most cases distinct colour changes in a sediment record indicate changes in the environmental conditions. In the majority of palaeoenvironmental investigations, soil and sediment colours are determined by Munsell colour charts, with the disadvantage that this is time-consuming and counter-intuitive (KEMP et al., 2001). Another method is to use the selected Munsell colours to derive numerical values (redness ratio) in the case of iron accumulations (FELIX-HENNINGSEN, 2000), as hematite and goethite show distinct colour variations, from red to yellowish brown and metallic grey (BIGHAM et al., 2002).

3.1.2 Grain size

Grain size analysis gives evidence of the transport mechanisms (aeolian, fluvial, glacial) which led to the deposition of the investigated material. This is especially important in extremely variable environments like the central Sahara, where humid phases have alternated rapidly with arid to hyperarid phases (c.f. chapter 4). For fluvial transportation of sediments (surface wash), sufficient amounts of water must be available, whereas aeolian transportation of sediment requires a sufficient amount of wind energy and a reduction of the stabilizing vegetation cover. Grain size analysis can therefore provide at least a broad idea of environmental conditions and the amount of existing water in a particular drainage basin at a given time. Changes in the sedimentation rate may be evidence of changes either in the accumulation processes or in the status of the water level (FRITZ, 2008). As lacustrine sediment differs from soils in its chemical and physical structure, its texture analysis requires a different classification system (FLEMMING, 2000).

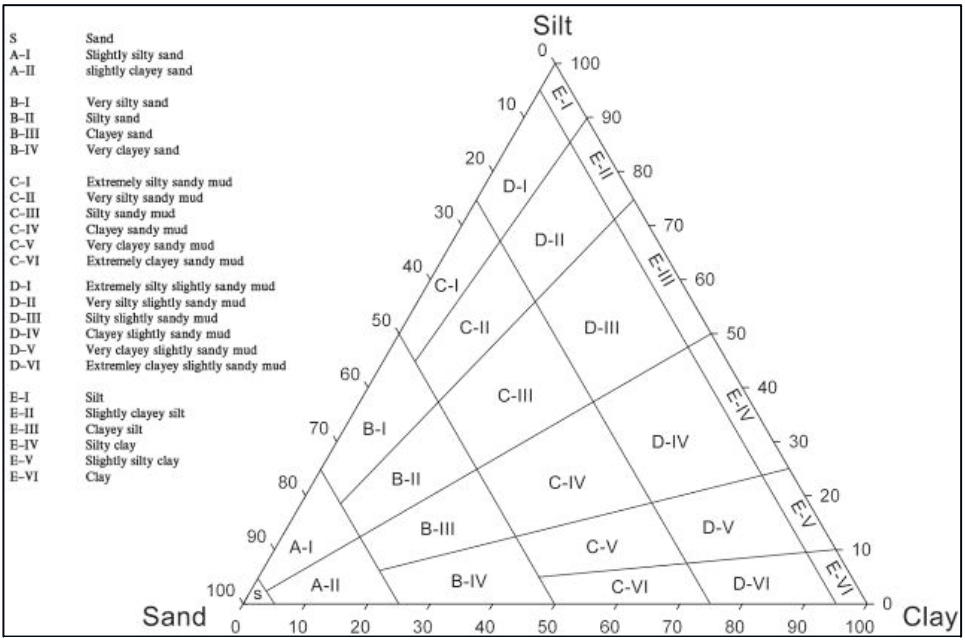

Figure 9 Ternary diagram for textural classification of sediments (Flemming, 2000)

According to the German classification of grain fractions, the soil separates are classified into the following ranges: clay (< 2 µm), fine silt (2 – 6.3 µm), medium silt (6.3 – 20 µm), coarse silt (20 – 63 µm), fine sand (63 – 200 µm), medium sand (200 – 630 m) and coarse sand (630 – 200 µm/0.63 – 2.0 mm).

Associated with the determination of the size of a particle is its shape and spherical geometry. Particles assigned to one range of sizes may show major variations in the regularity and the symmetry of their shapes (LAST, 2001b).Great care is therefore necessary when determining the size of deposited sediments.

3.1.3 Magnetic susceptibility

The magnetic susceptibility describes the ability of a material to be magnetized ("magnetisability"), which is most common in minerals containing iron (Fe). Five kinds of magnetic behaviour exist (c.f. Table 2) and the magnetic susceptibility of natural substances is the sum of all these. When measuring susceptibility with a Bartington sensor, a magnetic field is created and magnetisation within the field is detected (DEARING, 1994). The susceptibility of materials can be detected on split cores, whole cores or small bulk samples.

The most intense signals of magnetic susceptibility originate in pure iron, which is unlikely to be found in natural systems. Strong signals in sediments are related to ferrimagnetism, which originates either in primary minerals, such as magnetite, or in secondary minerals formed by fires, soil formation, bacterial activity or the development of iron sulphides within a lake (DEARING, 1994).

Table 2 Magnetic behaviors, sources and states (Dearing, 1994)

State of magnetism	Magnetic behaviour	Material
Remain magnetised in absence of magnetic fields	Ferromagnetism	Pure iron
	Ferrimagnetism	Iron minerals, e.g. Magnetite, greigite
	Canted antiferromagnetism	Iron minerals, e.g. Haematite, goethite
Magnetic only in presence of magnetic fields	Paramagnetism	Fe-bearing minerals, e.g. Biotite, pyrite
	Diamagnetism	Non fe-minerals, water, organic matter

3.2 Sediment chemistry

The use of the chemical features of terrestrial and lacustrine sediment profiles to investigate and reconstruct palaeoenvironments and palaeoclimate in arid regions is a very common method and is regularly applied (BAUMHAUER, 1986; BAUMHAUER, 1988; BAUMHAUER, 1991; BAUMHAUER & SCHULZ, 1984; BAUMHAUER et al., 2004; GASSE, 2000; GASSE et al., 1987; GASSE & ROBERTS, 2004; GASSE et al., 1990; GOSCHIN, 1988; HOELZMANN et al., 2004; HOELZMANN et al., 1998; HOELZMANN et al., 2000; SCHUETT, 1998a; SCHUETT, 1998b; SCHUETT, 2004; SCHUETT & BAUMHAUER, 1999). As the palaeoenvironmental records show major variations in their composition and conservation status, a wide range of methods is available to investigate the chemical properties of sediments.

3.2.1 Organic carbon

Despite it is generally being present in small quantities, organic carbon is a major factor when analysing lacustrine deposits, because it contains the information necessary to reconstruct the environmental conditions of lakes and their drainage basins (MEYERS & TERANES, 2001). The amount is usually specified in total organic carbon percentage (TOC), or loss on ignition (LOI), which determines the organic matter in a sample and is generally about twice the level of TOC (DEAN, 1999; MEYERS & LALLIER-VERGÉS, 1999; MEYERS & TERANES, 2001). However,

because of the instability and varying levels of non-carbon sediments, TOC measurement is preferable to LOI analysis when quantifying organic matter content (MEYERS & TERANES, 2001).

Organic matter within lacustrine sediments consists of a wide variety of biochemical remnants from the flora and fauna which existed in the lake. For the most part the organic matter originates from plants (MEYERS & LALLIER-VERGÉS, 1999) and can be referred to as an accumulation of "geochemical fossils" (MEYERS & TERANES, 2001). Organic matter in sediment records can easily be demineralised and consumed by organisms. In stable, stratified lakes where layers of different density become established, either due to saline (halocline) or thermal (thermocline) causes, the undermost layer, the hypolimnion, remains anoxic throughout the year, and the organic matter will be preserved (Collinson, 1982).

The bulk of the organic carbon contained in a sediment record depends as much on the prevailing biomass production of the lake before sedimentation as on the extent of decay and demineralisation after sedimentation (MEYERS & LALLIER-VERGÉS, 1999). Particularly in tropical areas, where many lakes develop thermal stratification, those with only low productivity rates of biomass can still preserve large/measurable/substantial amounts of organic matter, because of their reducing and anoxic hypolimnia (COLLINSON, 1982). However, according to KRAUSKOPF and BIRD (1995) it is not the anoxic conditions which preserve organic matter, but rather the organic matter which is the cause of the reducing and anoxic conditions. Thus, a measured/recorded level of TOC can provide information of postsedimentary processes and degrees of conservation (MEYERS & LALLIER-VERGÉS, 1999), because it represents that part of the organic matter which, for diverse reasons, has not been mineralised after deposition. The resulting TOC concentrations supply information about the sources and types of organic substances, the processes of deposition and the degree of preservation (MEYERS & TERANES, 2001).

Decreasing lake levels can not only cause reduced TOC amounts, due to decreased algal production, but also increased TOC amounts, as the relocation of high organic sediments from the lake shorelines into the deeper areas is a common process (MEYERS & LALLIER-VERGÉS, 1999). The wide ranges of processes which lead to a given TOC concentration, in combination with their interactions, are the major reasons for fluctuations in the organic matter distribution of lakes. The fact that TOC values are specified by weight/weight ratios makes them susceptible to substantial variations, due to changing sediment composition (MEYERS & TERANES, 2001). KRAUSKOPF & BIRD (1995) refer to sediments rich in both organic matter and pyrite minerals as "sapropels" and organic-rich sediments without pyrite as "gyttja"

3.2.2 Silicon and aluminium

Silicon (Si) and aluminium (Al) are, following oxygen, the two most abundant minerals, according to Clarkes' account of the mineralogical composition of the earth's crust (OKRUSCH, 2005), and are a focus in many environmental studies. In lacustrine sediments, the major contribution of silica is provided by quartz sand (JONES & BOWSER, 1978); silicon is the essential element of the mineral quartz (SiO_2) as well as of silicates such as clays, feldspars and mica. Aluminium is also a major component of clays (aluminium phyllosilicates) as well as participating in the composition of numerous other minerals.

Elemental concentrations provide information about environmental changes, surface wash and weathering processes within an investigated basin. The Si/Al (as well as the Ti/Si) ratio can provide information on the quantity of diatoms and the level of biogenic silica, titanium or aluminium having a constant value in detritus input (PEINERUD et al., 2001). If a strong positive correlation of silica and aluminium exists for several depths and if the ratio of Si to Al remains at a fairly constant level,

the elements may reflect the external (clastic or allogenic) components in the deposited sediment and only small amounts, if any, may be contributed by endogenic or authigenic processes (JONES & BOWSER, 1978). Biogenic silica (BSi) is incorporated by diatoms, using solute silicic acid from the lake water. Especially in (hyper-)saline playa lakes, the diatom populations can build up to extremely high levels, leading to a large/measurable/significant increase in biogenic silica.

3.2.3 Iron and manganese

According to MACKERETH (1966), changes in the sources of iron (Fe) and manganese (Mn) can be determined using a comparison of Fe to the Fe/Mn ratio. Where maximum concentrations (maxima) of Fe coincide with minima of the Fe/Mn ratio, reducing conditions are most likely. In contrast, maximum Fe concentrations together with maximum Fe/Mn values are evidence for changes in the catchment area (BOYLE, 2001). Since the ratio of iron to manganese (Fe/Mn) shows a rather wide range in lacustrine deposits (JONES & BOWSER, 1978), it must be interpreted carefully.

An overall description of the complex and varied processes in lakes which involve iron and manganese is given by DAVISON (1993). The formation of Fe and Mn oxides in lakes is predominantly driven by redox processes, but they do not form exclusively in anoxic waters. The prevailing conditions of their formation are modified by the oxidation states of the Fe and Mn oxides, organic matter levels, photochemical reactions and the general status of the lake (DAVISON, 1993).

3.2.4 Alkali and alkaline earth metals

Alkali and alkaline earth metals are among the principal/most important elements in geochemistry. The most investigated alkali metals are sodium (Na) and potassium (K). The principally investigated alkaline earth metals are magnesium (Mg), calcium (Ca) and strontium (Sr). A main feature of these elements is their very high solubility, alkali metals being more soluble than alkaline earth metals, due to their low ionization potential and low electronegativity. Clastic sediments contain their alkali and alkaline earth metals bound to the crystal structure of minerals such as feldspars and carbonates (cf. the following chapter: Mineralogy).

3.3 Mineralogy

Minerals are crystalline substances of natural origin and consist of inorganic compounds or elements, organic matter excluded. The mineralogical analysis of lacustrine deposits is considered fundamental to understand the development of the sediment record, providing information about transport mechanisms and environmental conditions (limnological, hydrological and climatic) in the basin (LAST, 2001a).

The mineralogical and chemical composition of a lake system is affected by a large variety of influences, such as water chemistry, the distribution of rainfall and the climatic situation of the site being investigated (COLLINSON, 1982).

In general, the minerals deposited in lacustrine environments origin in three different sources (COLLINSON, 1982; LAST, 2001a):

1 Allogenic minerals are detritus: their origin lies outside the lake system;
2 Authigenic minerals originate in postsedimentary processes (after the sediment has been deposited);
3 Endogenic minerals are built up or transformed within the body of water.

Whenever possible, distinctions should be made as to the origin of the investigated material, so as to form an idea of the processes that have led to the accumulation of the sediment. Nevertheless, many lacustrine deposits consist of a combination of materials from all mineral sources and indeed the variety of lacustrine sediments is greater than of those of marine or any other continental sediments (LAST, 2001a).

Allogenic or detrital minerals are determined mainly by the geology of the area and possible soil-forming processes (COLLINSON, 1982) as well as the processes that led to their deposition (e.g. aeolian or fluvial) (LAST, 2001a).

Authigenic minerals are important when investigating environmental changes within a basin (LAST, 2001a), especially when neo-tectonic activity/movement has occurred/is occurring, but their interpretation must be linked to chronological information.

Endogenic minerals are soluble minerals that precipitate out of solution due to super-saturation and thus build up solid primary minerals (COLLINSON, 1982). They contain the most valuable information about palaeolimnology and palaeohydrology, because their formation is linked to particular conditions within the water body (LAST, 2001a). In many lakes, carbonates are a key component of the endogenic minerals. Particularly in arid environments, evaporites (including carbonates) are valuable indicators of water chemistry (LAST, 2001a).

3.3.1 Carbonates

Carbonate minerals usually make a large contribution to lacustrine deposits, providing a wide range of fractions from all mineral sources (allogenic, authigenic and endogenic) (JONES & BOWSER, 1978). The solubility of $CaCO_3$ in water is mostly determined by the pH of the water body and the solubility of CO_2. Temperature is only of minor importance, mainly because higher water temperatures decrease the solubility of CO_2 and carbonate will precipitate as a reaction to this. KRAUSKOPF and BIRD (1995) give the following equations to describe the relationships between carbonate, carbon dioxide, carbonic acid and pH:

A strong acid (low-pH environment) will dissolve calcite, as in the following equation:

a) $CaCO_3 + 2H+ \rightarrow Ca^{2+} + H_2O + CO_2$

With higher pH values, the equation must be changed to:

b) $CaCO_3 + H+ \rightarrow Ca^{2+} + HCO^{3-}$

When calcium carbonate dissolves in carbonic acid (H_2CO_3), the reaction may be summarized as:

c) $CaCO_3 + H_2CO_3 \rightarrow Ca^{2+} + 2HCO^{3-}$

The effect of pH on solubility is shown in the following equilibrium equation:

d) $H_2O + CO_2 \rightarrow H_2CO_3$

Equation d) implies that the more CO_2 is dissolved in the water, the higher the amount of carbonic acid will be; any factor decreasing the amount of carbon dioxide will consequently cause the precipitation of $CaCO_3$ (KRAUSKOPF & BIRD, 1995). Additionally, non-stoichiometric calcium carbonates may develop through the incorporation of magnesium or strontium in solutions containing increased concentrations of Mg (due to gypsum formation or the consumption of CO_2 by aquatic plants), which may lead to the formation of measurable amounts of dolomite. The ratio of magnesium to calcium determines the nomenclature, from low-Mg-calcite (Mg/Ca < 2) to high-Mg-calcite (Mg/Ca > 7) to aragonite (Mg/Ca > 12) (PACHUR & ALTMANN, 2006).

When investigating carbonates in lacustrine deposits, primary and secondary carbonate minerals must be distinguished (MUELLER et al., 1972). Both primary carbonate minerals (calcite, high-Mg-calcite, aragonite, hydrous Mg carbonates) and secondary carbonates, such as dolomite, huntite or magnesite, developed under diagenetic conditions (postsedimentary). Secondary carbonates can only develop in sediments containing a quantity of high-Mg calcite and a ratio of magnesium to calcium (Mg/Ca) above 7 (MUELLER et al., 1972).

The predominant carbonate mineral and primary endogenic phase in lakes is calcite ($CaCO_3$), whereas dolomite ($CaMg(CO_3)_2$) development is relatively unusual (JONES & BOWSER, 1978). Aragonite is unstable under normal environmental conditions and will most likely change into calcite (KRAUSKOPF & BIRD, 1995).

3.3.2 Evaporitic Minerals

When studying lacustrine systems in arid to hyperarid areas, evaporitic minerals are of special interest, because they are direct indicators of the palaeolimnological conditions inside a body of water (LAST, 2001a). The precipitation of these minerals is a direct result of conditions in the water and therefore responds to even small modifications in temperature or composition (SONNENFELD, 1984).

The development of evaporites requires two basic conditions (EUGSTER, 1980):

1. a basin/depression where evaporation is greater than inflow;
2. an adequate supply of soluble minerals.

A high variability in the mineralogical composition is a typical feature of continental evaporitic deposits and brines; even adjacent basins can show extremely large variations in their chemical and mineralogical attributes. Nevertheless, most continental evaporites consist of only a few anions and cations (Na, K, Ca, Mg, C, SO_4, and HCO_3-CO_3) (EUGSTER, 1980).

One feature used to differentiate evaporites is their manner of accumulation. For instance, gypsum, halite and thenardite are most likely to precipitate in bedded units in ephemeral or perennial (salt) lakes, whereas glauberite and bloedite are considered to form authigenically in interstitials (intrasediment precipitates) or after they have been deposited (EUGSTER, 1980).

Surface crusts of evaporitic material develop through the evaporation of groundwater and the efflorescence of evaporitic minerals on top of the sediment body (EUGSTER, 1980). The development of secondary gypsum crusts is especially linked to the upward movement of groundwater inside the sediment profile due to evaporation. This process, also referred to as “per ascensum”, leads to the development of secondary hydromorphic gypsum (ECKARDT et al., 2001).

Because of their high solubility, evaporitic minerals are liable to postsedimentary alteration, resulting in a wide variety of authigenic minerals (EUGSTER, 1980), although some minerals are

ubiquitous. For example, a frequent constituent of evaporitic deposits is NaCl (halite) (KRAUSKOPF & BIRD, 1995), as it can easily be soluted and relocated with percolating water.

The development of some evaporites is limited by the amount of available components. For instance, the prerequisite for the formation of gypsum ($CaSO_4 * 2H_2O$) is the presence of sulphur. Consequently, the course of the geochemical sulphur cycle is vital for the genesis of gypsum (ECKARDT et al., 2001).

3.3.3 Silicate minerals

Silicate minerals originate exclusively in the weathering of their parent rocks and their grains are mostly of sand to silt size (SPOSITO, 1998). They are the major constituent of the Earth's crust and make up about 90% of its mineral composition, with feldspars being the most abundant of the primary silicate minerals.

Feldspars can be found in many sedimentary, metamorphic and igneous rocks and vary as much in their chemical composition as in their crystal structures (KRAUSKOPF & BIRD, 1995). The basic composition of feldspars consists of silicon, aluminium, oxygen and, depending on the crystal alignment, either monovalent Na^+ and K^+ or bivalent $Ca^{2+,}$ for charge balance (SPOSITO, 1998). Alkaline feldspars ($KAlSi_3O_8$) or K-feldspars are a category of minerals with similar composition (orthoclase, microcline etc.), formed both during the diagenesis and metamorphism of numerous types of rock and through the crystallisation of magma (KRAUSKOPF & BIRD, 1995). Mica is also a primary silicate mineral and is predominantly represented by muscovite and biotite, the basic compositon of K, Si, Al and O being modified by the incorporation of either additional Al (muscovite) or Mg and Fe (biotite) (SPOSITO, 1998).

Kaolinite is a clay or secondary aluminosilicate mineral, as it results from the weathering and conversion of other aluminosilicates (KRAUSKOPF & BIRD, 1995) and, together with gibbsite, is one of the final products of feldspar weathering (SPOSITO, 1998).

3.4 Biological Indicators

Biological indicators, also referred to as palaeoecological data, are derived from biological remnants within sediments, such as diatoms (silica algae) or pollen. Diatoms are found in water bodies all over the world and as their explicit structures (cell walls or shells, also referred to as frustules) are mainly composed of silica, which is very robust, their fossils can attest to past populations (BATTERED et al., 2001). In contrast, pollen consists of cellulose and sporopollenin, a polymer that can be easily oxidized, but is nevertheless extremely resistant to most physical and chemical decomposition. Furthermore, the shape and other features of the grains can be used to identify the taxonomic unit of the originating plant (BENNET & WILLIS, 2001). Both types of indicators can be well preserved in lacustrine sediments and a variety of information can be derived from the overall numbers in a defined mass or volume and from a taxonomic classification of the individuals detected. Additional palaeoenvironmental information can be derived from green algae (charophytes), which are considered to provide fossil evidence exclusively of the benthic flora (SOULIÉ-MÄRSCHE, 1991).

Diatoms are suitable indicators for a wide range of limnological parameters, such as lake depth, the salinity and trophic status of the water, and the temperature of Quaternary lakes (SERVANT-VILDARY, 1977). This is because the variety of diatoms in an aquatic system is determined by the

basin characteristics (shape and geometry), which influence the different available habitats. Planktonic diatom taxa drift in the open water zone (pelagic zone), whereas benthic taxa live on top of or underneath the sediment surface. In addition, such habitats are influenced by the physical, chemical and biological properties of a given body of water (BATTERBEE et al., 2001). Consequently, the diversity of diatoms can be used to reconstruct synsedimentary conditions, by comparing the diatom populations of recent and ancient lakes. This makes predictions about palaeohydrochemistry possible, since climatic changes influence the overall volume of lakes as well as their chemical composition (GASSE et al., 1997).

Pollen provides information about the vegetation surrounding the lake, but also, depending on the prevailing winds, in remote areas. Although different plants vary in the quantity of pollen they produce, in their location (with respect to the place of deposition) and the degree of preservation of their pollen grains, palynology (the science of pollen, spores etc.) remains a useful tool for palaeoenvironmental reconstruction (BENNET & WILLIS, 2001).

The combination of biological proxies can give proof of major changes in the hydrological composition of a lake system, especially during transitional climate stages, as has been exemplarily demonstrated in a multidisciplinary investigation of a sediment record from northern Tanzania (RYNER et al., 2007). The focus of this investigation was on microfossil assemblages, combined with pollen and isotopic nitrogen data. The combination of the pollen analysis, which reflects the surrounding areas, and information about the hydrologic features within the basin has revealed interesting results, such as the simultaneous occurrence of spreading arid vegetation, turbidites and high lake levels from 13 to 10.3 ka BP. This leads to a conclusion that there was increased runoff, due to the amplified seasonality of precipitation.

The appearance of rhizome-concretions, mainly consisting of goethite accretion, is evidence of the presence of shallow ponds with vegetation on their banks within ancient dune areas (FELIX-HENNINGSEN, 2004). These concretions also referred to as swamp iron ores, can be considered as indirect biological indicators for humid periods within the central Sahara.

3.5 Archaeological findings

Massive and rapid environmental changes in Northern Africa are considered to be motivating and controlling factors for the cultural development of north African civilisations, as migration routes have been determined by the environmental setting (e.g., KUPER & KROEPELIN, 2006; NICOLL, 2001). Thus archaeological finds can provide substantial information about the environmental conditions in an area. The presence of prehistoric human settlements is usually taken to imply the presence of fresh water or food. This is especially true when investigating the now fully arid regions of the Sahara, with their limited supply of water. The reconstruction of ancient vegetation from charcoal remains (e.g. NEUMANN, 1989) and the chronological classification of Palaeolithic tools (e.g. TILLET, 1985) support and extend the palaeoenvironmental evidence obtained from sedimentary deposits.

3.6 Age determination

Achieving a reliable chronology is a crucial step in palaeoenvironmental reconstruction. In accordance with the recommendations made by the INQUA Dryland Dating Subcommission (KNOTT & OWEN, 2007), three major rules should be borne in mind when dating quaternary deposits in drylands:

1. multiple dating methods should be used if possible;
2. if just one dating method can be applied several samples from each stratigraphic sequence should be analysed;
3. key sites within the study area must be used to evaluate several dating techniques and to confirm the applicability and the reliability of each method.

As a source of inferential evidence lacustrine deposits are of central importance, because they frequently contain the only remnants of organic matter in deserts (WRIGHT, 1991) and because their variable composition sometimes allows the use of multiple dating techniques to validate the results (e.g. FONTES & GASSE, 1991; SZABO et al., 1995).

3.6.1 Radiocarbon dating

Radiocarbon dating is the most commonly applied technique for geochronological dating, as it was among the earliest methods invented. It can be applied to a range of materials and covers a period of time from about 150 years to a maximum of 60,000 years BP (LIAN & ROBERTS, 2006). The basis for radiocarbon dating is the radioactive decay of elements. The rate of decay itself cannot be altered by any factors in the geologic surroundings and can therefore be utilised for the evaluation of elapsed time (KRAUSKOPF & BIRD, 1995). Neutrons of cosmic origin (i.e. the sun) collide with ^{14}N atoms in the atmosphere, which are subsequently transformed to the ^{14}C isotope of carbon, through neutron capture. These are oxidized to CO_2. ^{14}C shows radioactive decay with a half-life of 5730 years, whereas ^{12}C, the most common isotope stage of carbon, remains stable, as does ^{13}C. The constant absorption of CO_2 by living organisms, through photosynthesis, solution in water, or consumption of plant material, leads to the constant deposition of ^{14}C in the structure of the organisms. As soon as absorption stops, on the death of the consuming organism, the incorporation of ^{14}C stops as well. The radioactive decay of the isotope leads to a subsequent decline in the amount of ^{14}C in the structure. The ratio of the unstable to the stable isotope can consequently be used to determine the date of death of the organism (KRAUSKOPF & BIRD, 1995).

In most cases, radiocarbon dating deals with organic material from a variety of sources, both flora (wood, charcoal, mud,) and fauna (shells, bones, organic mud/debris). Contamination by translocated organic material, mainly charcoal, occasionally occurs (BUBENZER et al., 2007b; SNYDER et al., 1994) and alternative supplementary dating material must be tested.

When dating biogenic carbonates by the radiocarbon method, shifting of dates must be taken into account, whether caused by contamination from carbon-containing groundwater (hard water effect) or by carbonate bedrock (carbon reservoir effect) (FONTES & GASSE, 1989; SNYDER et al., 1994; ZHOU et al., 1999). However, detailed studies on gastropods have revealed the reliability of various gastropod taxa for radiocarbon data (FRITZ & POPLAWSKI, 1974), especially those terrestrial snails

which incorporate aragonite in their shells (BRENNAN & QUADE, 1997; PIGATI et al., 2004; ZHOU et al., 1999). The reliability of this type of data is due to the fact that these shell carbonates incorporate atmospheric carbon and the $^{12}C/^{14}C$ ratio thus reflects the point in time of their construction (FONTES & GASSE, 1989).

In addition, radiocarbon dating of inorganic carbonates is also possible, but very susceptible to error, due the dilution effect (FONTES & GASSE, 1989), as comparative studies of organic and inorganic radiocarbon dating of lacustrine sediments have shown, indicating the need to validate such results in order to construct an adequate dating scheme (GASSE et al., 1990).

Variations in the sun's activity and the intensity of incoming cosmic rays make it necessary to calibrate radiocarbon dates. Such a calibration can be achieved using known variations of solar activity (KRAUSKOPF & BIRD, 1995) and results in a scale of calibrated calendar years (cal a BP). For the northern hemisphere, terrestrial sediments can be calibrated using the IntCal04 calibration curve (BLACKWELL et al., 2006).

3.6.2 Optically stimulated luminescence (OSL) dating

The optically stimulated luminescence of quartz grains is a dating technique which can be used to determine the point in time of the burial of sediment (WINTLE & MURRAY, 1997), or at least of its last contact with sunlight (LIAN & ROBERTS, 2006). This method is based on the emission of luminescence when radiation in the green and blue spectral range (optical energy) is directed at quartz grains (WINTLE, 1997; WINTLE & MURRAY, 1997). A major refinement of this method has made it possible to use it on single grains of quartz or feldspars (DULLER et al., 2003), although larger quantities are essential to obtain statistically adequate data, especially for younger sediments (WINTLE, 1997).

Depending on the material to be dated, the range of the OSL dating method extends from a few years to several hundreds of thousand years BP, providing a direct output in calendar years (LIAN & ROBERTS, 2006). Results obtained from OSL dating techniques have the proven potential to enhance chronologies that were set up by radiocarbon dating (BUBENZER et al., 2007a) and are of unique significance for areas of discontinuous environmental settings.

4 PALAEOENVIRONMENTAL RESEARCH ON NORTH AFRICAN CLIMATE CHANGES

Reconnaissance surveys in northeastern Niger since 1977 have revealed the existence of palaeolakes in the Central Sahara from such evidence as diatomite-lined depressions. Initial research has shown that the sediments found are suitable for reconstructing the Late Quaternary palaeoenvironment in northeastern Niger. As the focus of the present work is on environmental changes in the central Sahara, from the Late Pleistocene/Early Holocene to the present, this chapter covers research on climatic development in northern Africa, starting at the Late Glacial Maximum (LGM) and extending to recent hyperarid conditions. The first step of palaeoenvironmental reconstruction is to gather information on environmental changes by proxy data (cf. Chapter 3: Sedimentary deposits as tools for environmental reconstruction). As the information from sedimentary deposits is limited to the regional scale, a closer look at the regional differences and the environmental setting of major lacustrine sites is required. To show evidence of major climatic changes on the continental scale and to investigate their causes, it is necessary to use computer-based investigations and to model a hindcast, using proxies from palaeoenvironmental reconstructions as the primary data base.

4.1 Palaeoenvironmental reconstruction by proxy data

The Last Glacial Maximum (LGM) is distinguished by a maximum of continental aridity, low worldwide temperatures and sea levels, as well as, obviously, the maximum extent of the continental ice shields (ROGNON & WILLIAMS, 1977). However, not all areas necessarily reached the peak of glaciality at the same time (ADAMS & FAURE, 1997). Periods of maximum aridity show different time extents in different areas of Africa. An extended time-range is therefore used to determine the LGM, but usually an examination of the period between 18 and 21 ka BP is sufficient to determine the maximum (glacial) extent. The LGM marks a major turning point in global climate change: the time prior to it is an era of expanding ice sheets; the subsequent era is characterised by the retreat and disappearance of continental ice shields (NICHOLSON & FLOHN, 1980).

Continental aridity is recorded more or less all over Africa at the LGM. For instance, Lake Victoria is thought to have twice become completely desiccated (15.9 – 14.2 ka BP and 18 – 17 ka BP) during this period (STAGER et al., 2002) and at most low water levels are indicated for Lake Chad (ADAMS & TETZLAFF, 1984). The numerous studies of Lake Chad and the many palaeoclimatological interpretations derived from them overlook the fact that the waterbearing source areas are very varied and not located in the same region, e.g. some are located in the Cameroon tropics (NICHOLSON & FLOHN, 1980). Consequently, palaeoenvironmental studies of Lake Chad will mostly be excluded hereafter.

SERVANT (1973/1983) was among the first to systematically investigate Quaternary lacustrine deposits in the central Sahara, primarily in the eastern areas of Niger (Air Massif etc.) and northern Chad. He gives a detailed description of the area's climatic development over the last 40,000 years (since the Pleistocene) and distinguishes several phases of quaternary climate development/change based on his investigations of the environmental history of the Cainozoic. Of these phases, the Chadian can additionally be separated into Chadian I (from 9500 to 7500 a BP, Early Holocene) and Chadian II (7000 to 5000 a BP, Mid Holocene), following SERVANT's assumption of the occurrence

of an arid phase from 7500 to 7000 BP. The Kanemian is identical to the Ogolian in Western Africa (MICHEL, 1973).

Table 3 Climatic development of Niger and Northern Chad (Servant, 1973/1983)

Years Before Present	Climate	Episode/Stage
> 40.000	Extremely Arid	-
40.000-20.000	Moderately Humid	Ghazalian
20.000-12.000/14.0000	Extremely Arid	Kanemian (*Ogolian Michel*)
13.000-10.500	Moderately Humid	Upper Pleistocene
10.500-9.500	Moderately Arid	Pleistocene /Holocene
9.500-5.000	Extremely Humid	Tchadien (Early-Mid Holocene)
5.000-3-500	Arid Phase	Nouakchottien
3.500-2.500	Moderately Humid	
2.500-Present	Arid	Present

In addition to the general climatic framework provided by SERVANT and MICHEL, essential information is available about the geomorphology of the central Sahara, thanks to considerable earlier geomorphological fieldwork in northeastern Niger, largely by the Wuerzburg Desert Research Group. The group was instituted by Horst Hagedorn and from 1977 to 1991 it realized more than 10 expeditions into the southern Central Sahara, with a variety of participants. A large number of palaeoenvironmental records have been investigated in the Nigrian areas of the central Sahara, but only a few of the sites have yielded long-duration sediment profiles, with evidence of the climate history of the region from the Holocene and parts of the Pleistocene. These lacustrine deposits are considered the most valuable for palaeoenvironmental reconstruction. Depending on the relief, the remnants of the palaeolakes are best preserved in endorrheic foreland depressions, which are generally situated along the escarpment and plateau relicts (cf. chapter 4.2). In the following chapter, the most informative sedimentary records are reviewed, to obtain a basic understanding of the local conditions which influenced them.

DAMNATI (2000b), has provided a collection of Holocene lake records from northern Africa, derived from a compilation of lake and pollen data, to give an overview of the climatological succession (JOLLY et al., 1998a). He concludes that:

- there was a major period of medium to high lake levels between 10000 and 6000 BP;
- lakes closest to the equator show the first signals of high lake levels (The peak in lake levels is thought to have occurred between 9 and 8 ka BP. The lake records referred to originate from Mauritania, Niger, Mali and Sudan),
- there was an unstable transition phase between 7 and 6 ka BP , indicated by lake level fluctuations and records of aeolian activity;
- after 6 ka BP the majority of the lakes show decreasing levels, which indicate an increasingly dry climate.

Lacustrine sediment records provide excellent evidence of humid periods but usually lack evidence of arid periods. On a first examination the occurrence of hiatus and increasing aeolian input may indicate increasing arid conditions, but absolute dating of the arid periods remains a crucial point in the case of palaeosoils on fossil dunes. Due to the lack of datable organic material in aeolian

accumulations and the insufficient information from the relative dating of bordering layers, the recently developed technique of OSL-dating has provided essential information about the temporal pattern of aeolian dynamics (BUBENZER et al., 2007a). In the acquisition of complete information on past arid stages in the Sahara, dunes have been shown to have a high potential for palaeoenvironmental reconstruction, although such dunes are frequently discontinuous (ROGNON & COUDÉ-GAUSSEN, 1996).

A compilation of palaeoclimatic data by SWEZEY focuses on aeolian dynamics, mainly during the Holocene (SWEZEY, 2001). Although the author emphasizes the fragmentary nature of the records, the joint data show a pattern of aeolian sediment mobilisation and stabilisation across northern Africa. The main period of sediment stabilisation is recorded from 11 to 5 ka BP. Aeolian sediment mobilisation was predominant before 11 ka and after 5 ka BP. Referring to SERVANT (1973/1983) and MICHEL (1973), VOELKEL (1988) set up a classification of three different dune generations, which can be differentiated by their weathering stages and locations. The dunes of the first generation are considered to have developed in the Kanemian (20 to 12 ka BP), a phase of extreme aridity and increased dune mobility. After a time of enhanced humid conditions (also referred to as the Chadian), arid conditions predominated from the Middle Holocene (Nouakchottian) up to the present, only interrupted by a short period of slightly increased humidity. Widespread dry conditions during the Late Pleistocene have been confirmed by a very large number of investigations in the central Sahara, some of which will be reviewed in chapter 4.2.

In contrast to the prevailing arid conditions in southwestern Africa, a complete set of groundwater examinations in northern Africa (EDMUNDS et al., 2004) has given evidence of a massive recharge of the aquifers and the presence of a colder climate (approx. 7° C colder than at present) for the period of the LGM. The authors propose a southward shift of the rain-bearing westerlies into the area of the Sahara during that time. This shift involved a decrease of monsoonal precipitation at the Sahara-Sahel border. The investigation of groundwater tables in the basin of Murzuk has revealed a rather wide age range, from 20 ka to 40 ka BP (KLITZSCH et al., 1976). The authors conclude that the water table was from the Pleistocene, with only minor recharge in the present time. Another study, of stable isotopes in North African groundwater (ZUPPI & SACCHI, 2004), investigates the main causes and timing of a massive recharge of the water tables. The authors assume three main humid periods in the Pleistocene and one in the Middle Holocene (from 7 to 4.5 ka BP).

A compilation of palaeohydrological records from northern Africa shows increased lake levels during the late Pleistocene for a record from Algeria, although arid conditions prevailed there (GASSE & ROBERTS, 2004; HOELZMANN et al., 2004). A further increase of lake levels began in the region at approximately 11 ka BP. This arid-to-humid transition (AHT) is considered as a time of decreasing arid conditions, which ended at approximately 9.3 ka BP, with the onset of generally humid conditions (GASSE et al., 1990). For a different site in the Sahel zone of Niger, the authors note the onset of freshwater conditions at approximately 9.7 ka BP and a return to more arid conditions at around 7 ka BP, associated with major hydrological fluctuations. Large hydrological fluctuations of the river Niger are also recorded in a core from the Gulf of Guinea, indicating several major climatic events within the Niger drainage area during the Late Pleistocene and the Early Holocene (LEZINE et al., 2005). A gradual increase of precipitation during the last transition from the glacial to the interglacial has been observed, as well as evidence for major instabilities of the hydrological cycle during that time. Four dry phases can be observed during the transition, which lasted from 14.5 ka to 9.8 ka BP, where at least three of them correlate to the Younger Dryas. A coring in Tanzania investigates pollen and magnetic susceptibility records and focuses on major environmental changes since 45 ka BP, especially those related to the African monsoon regime (GARCIN et al., 2007). The distinct southward migration of the ITCZ during the Younger Dryas is considered to have caused reduced precipitation in those areas currently affected by the monsoon.

African monsoon activity subsequently intensified, in correlation with a more distinct latitudinal movement pattern of the ITCZ during the Early to Middle Holocene.

In a compilation of different palaeoenvironmental results, NICHOLSON and FLOHN (1980) investigate and compare lacustrine records from northern Africa. The authors conclude that a three-phase climatic development took place in the Late Quaternary, with the periods between the major stages considered to be transitional: arid conditions from 20 ka to 12 ka BP, humid conditions from 10 to 8 ka BP and again humid conditions from 6.5 to 4.5 ka BP.

A more recent compilation of lake status data from northern Africa (DAMNATI, 2000a) reveals generally increased lake levels between 10 and 6 ka BP, beginning in the eastern Sahara. Aridisation is considered to have started at about 6 ka BP, reaching its full extend at 4 ka BP.

The comparison of radiocarbon dates indicating fresh water conditions from the Sahara with those from Chinese palaeosoils and lakes (GUO et al., 2000) reveals significant evidence of humid conditions at 9.5 ka BP and the development of arid conditions in the central Sahara after 5 ka BP. The spatial distribution across latitude shows a deficit of dates between 24° and 30° N compared to those below 23°N and above 30°N. This remarkable aspect is likely to have arisen because of the different rainfall regimes over the southern central Sahara (monsoon) and the northern Sahara (Mediterranean), which are dominant up to the present day. The authors hypothesize that changes in the insolation of the northern Hemisphere are the controlling force for changes in monsoon dynamics.

For far north-western Africa, palaeoenvironmental reconstructions based on pollen sequences reveal a drier and warmer climate in Morocco from the Early to Middle Holocene (10 ka to 6.5 ka BP) than at present (CHEDDADI et al., 1998). The records indicate a transitional phase, lasting about 1000 years and leading to greater precipitation and cooler conditions, at approximately 6.5 ka BP. A sequence of high-resolution terrigenous records, from a core taken west of the Moroccan coast, confirms the frequent occurrence of dry conditions in northwest Africa during the Early and Middle Holocene (HOLZ et al., 2007). The authors assume a strong influence by the westerlies on the northwest African climate throughout the Holocene, since precipitation seems to occur predominantly in winter.

For East Africa, KUPER and KROEPELIN (2006) provide a comprehensive collection of radiocarbon data from the BOS-Project (Occupation History of the Eastern Sahara), which lasted from 1980 to 1992, and from the Collaborative Research Centre (Sonderforschungsbereich – SFB) project 389 (“ACACIA”: Arid Climate, Adaptation and Cultural Innovation in Africa), which lasted from 1995 to 2007. Both projects investigated the dynamics and external factors controlling the prehistoric occupation of the eastern Sahara, with an additional focus on the reconstruction of climatic and environmental conditions in the Holocene. The data reveal the beginning of humid conditions at about 10.5 ka BP (8500 BCE), caused by a northward shift of the monsoonal precipitation regime. This regime then remained stable and caused semi-humid conditions in the southern fringes of the eastern Sahara, while the centre remained semi-arid. At around 7.3 ka BP (5300 BCE) a southward retreat of the monsoonal system set in, causing a latitudinal gradient of desiccation which probably persisted for several centuries.

A study of submerged lake sediments from NW Sudan reveals the occurrence of humid conditions in the eastern Sahara during the Middle Holocene (RITCHIE et al., 1985). The main humid period is observed/recorded between 8.5 and 6.1 ka BP, followed by a steady decrease of precipitation after 6 ka BP and the subsequent desiccation of the lake at approx. 4.5 ka BP. Evidence from the Selima Oasis in the north of Sudan indicates that the main pluvial period extended from 9.5 to 4.5 ka BP (RITCHIE & HAYNES, 1987). The reconstruction of the palaeoenvironment is mainly based on pollen analysis, which indicates a northward movement of four degrees for the present vegetation zonation. Additionally, the actual precipitation gradient showed a northward shift of the same extent from the Early to the Middle Holocene. Studies of the isotopic composition of molluscs from four

lakes located in NW Sudan reveal a northward shift of the present monsoonal precipitation regime of 800 km during the Early and Middle Holocene (ABELL & HOELZMANN, 2000). The shift caused enhanced precipitation up to 21°N, with the most humid period lasting from 9 ka to approximately 5.6 ka BP. An overview of palaeoecological research in the eastern parts of the Sahara suggests a northward migration of the Sahara-Sahel transition of approx. 600 km (KUPER & KROEPELIN, 2006).

In Western Africa, a reconstruction of palaeoenvironmental conditions from lacustrine sediments confirms a northward shift of the Sahelian boundary of an estimated 3 to 4°. The study site, located in Mali at 20°30' N- 21° N , 0° - 1°W, shows a maximum of lacustrine conditions between 6130 ± 180 BP and 7520 ± 70 BP (PETIT-MAIRE & RISER, 1981). An estimation of precipitation in the area suggests a level of 500-600 mm/a in Early Holocene, without determining whether the rainfall originated in Mediterranean winter or monsoonal summer rains (ADAMS & TETZLAFF, 1989).

A compilation of results obtained from soils which had developed on fossil Pleistocene dunes in Niger confirms a gradient of humidity from SW to NE. The gradient most probably developed due to a regular decline of precipitation, caused by the northward shift of the monsoon, between 9 ka and 7.5 ka BP and from 4.5 ka to 3 ka BP (FELIX-HENNINGSEN, 2000).

South of the Tropic of Cancer precipitation increased towards the south during the Early and Middle Holocene, because of a monsoonal precipitation gradient, while a gradient of decreasing precipitation existed north of the Tropic of Cancer, running west to east (PACHUR & ALTMANN, 2006). According to these authors, freshwater lakes persisted in the west and ephemeral rivers built up fine-grained (pelitic) sediments, by fluvial accumulation, in the east. A compilation of palaeoenvironmental data for the eastern Sahara confirms the existence of humid conditions during the Early and Middle Holocene, extending from 9.3 to 4.5 ka BP (PACHUR & HOELZMANN, 2000). The dataset reveals a rapid beginning of humid conditions at 9.3 ka BP, but a decelerated ending due to the buffering effect of replenished aquifers in the area. Furthermore, diminishing precipitation gradients were detected, running west to east and south to north, suggesting significant influence from squall lines originating in the SW-NW-running monsoon.

In an isotope investigation from the West Nubian palaeolake basin in NW Sudan, Early Holocene precipitation estimates for 16° to 20°N suggest levels ranging from more than 300 up to 500 mm/a (HOELZMANN et al., 2000). The significant decrease of oxygen isotope values leads to a presumption of intense monsoonal precipitation in combination with thunderstorms during the uninterrupted lake stage, ranging from approximately 9.5 to 4 ka BP. The continuous sediment record is considered to indicate stable climatic conditions during the Early Holocene, as no signs of desiccation or droughts are found, in contrast to the palaeoenvironmental records from adjacent areas. Low levels of clastic input are considered to be proof of decreased surface runoff due to widespread vegetation cover.

An analysis of shells from Wadi Howar (NW Sudan) revealed the existence of a strong seasonality in the eastern Sahara during the Middle Holocene. Two rainy seasons of different lengths were active at approximately 7 ka BP, both originating in the northward shift of the ITCZ (RODRIGUES et al., 2000). An investigation with a focus on the reasons for variations in Holocene precipitation in the southwest area of Egypt (LINSTAEDTER & KROEPELIN, 2004) reveals increased monsoonal rainfall during the period between 9.3 and 5.4 ka BP and confirms additional winter rains in the final stage of the Holocene humid phase (5.4 to 4.5 ka BP). A combination of regional factors - altitude, geomorphology and climatic boundaries - modified the overall climate so that, in addition to the rapid and intense monsoonal precipitation system, a second system of continuous winter rains developed during the Middle Holocene.

A study of stable isotopes derived from mollusc shells in NW Sudan indicates a recharge of the Sudan's deep aquifers by increased monsoonal precipitation between 9000 and 6000 a BP. A

precipitation gradient of decreasing rainfall, running south to north, can be derived from palaeolake investigations. The northern lakes (slightly above 20°N) received less precipitation and evaporation took place over extended periods. Early Holocene rainfall is considered to be of seasonal character (summer precipitation), the monsoonal rainfall diminished after the climatic optimum (about 6 ka BP) and evaporation periods extended. The termination of the Holocene climate optimum is not recorded, due to massive deflation, but the authors suggest 4500 a BP in the north (21°N) and 4000 a BP in the south (17°N), indicating a retreat of the monsoonal precipitation regime, which had originated in the south (ABELL & HOELZMANN, 2000).

Indications of the Early Holocene greening of the Sahara are recorded in numerous pollen studies, although many study sites are insufficiently conserved to provide evidence for the complete Holocene succession (e.g. GARCIN et al., 2007; LEZINE et al., 2005; RITCHIE et al., 1985; RITCHIE & HAYNES, 1987). A compilation of several hundred pollen records from Africa and the Arabian Peninsula shows systematic changes in ecosystems over the last 6000 years, as they respond directly to the climatic settings (JOLLY et al., 1998b). The regions north of 15°N in particular show massive changes in vegetation, which are associated with a northward expansion of monsoon activity and a simultaneous southward expansion of the Mediterranean winter precipitation regime.

Pollen data from Egypt indicates at least a slight amplification of rainfall, which in combination with lower temperatures led to low evaporation rates and consequently to the establishment of perennial lakes (NEUMANN, 1989). The data suggests similar flora to today during the Early Holocene, but with a more extensive distribution. For Sudan, the pollen records suggest a northward migration of the vegetation zones of approximately 500-600 km in the Early to Middle Holocene. Consequently, two separate/distinct ecological landscape belts developed in the Eastern Sahara. Egypt showed a desert landscape with a somewhat denser vegetation cover, with annual precipitation of approximately 50-100 mm. In Sudan, south of 22°N, tropical savannah prevailed, due to a distinct increase in annual precipitation.

To determine the dimension of the Mid Holocene climatic optimum a multi-proxy analysis of a marine sediment record from the Ocean Drilling Program (ODP), near the shore of Mauretania, West Africa was carried out (Figure 10). It focused on terrigenous (aeolian) sediment input, oxygen isotopes, biogenic opal concentrations, Ca-carbonates and bulk density (deMENOCAL et al., 2000; deMENOCAL, 2001).

The record obtained shows several abrupt changes in sediment composition, which were dated to 14.8 cal ka BP, 12.3 cal ka BP and 5.5 cal ka BP. The authors state that the values at the beginning and end of the so-called “African Humid Period“(AHP) were very similar at approximately 470 W/m², only 4.2% greater than the present-day level of 451 W/m². Thus, the crossing of this value in the Late Pleistocene and the Mid Holocene defines the beginning and the end of the AHP. Figure 10 shows the movement of the summer insolation values and the terrigenous output, which run contrary to one another. During the period of the AHP, the landscapes of the central Sahara are thought to have been stabilized by an effectively closed vegetation cover, probably due to increased precipitation. The stages outside this period were presumably dominated by aeolian activity, as indicated by the distinct increase of terrigenous dust export.

Aeolian sediment mobilisation across Northern Africa is clearly recorded after 5 ka BP in lacustrine sediment archives by the frequent occurrence of hiatus, increasing aeolian input and evaporites (SWEZEY, 2001). However, due to the lack of datable organic material and the rather limited information from dating of bordering layers, the temporal pattern of aeolian dynamics is still a major point of discussion.

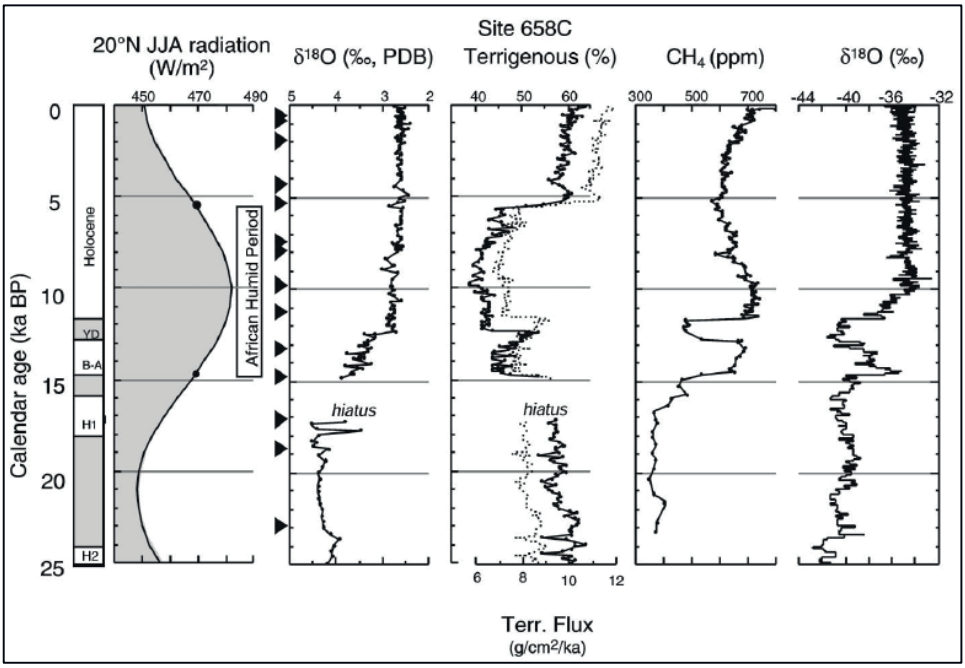

Figure 10 Northern hemisphere summer insolation (from Berger & Loutre, 1991) compared to records obtained from the 658C core (deMenocal et al., 2000)

In addition, the definition of the Late Pleistocene/Early Holocene to Mid Holocene humid period is rather vague, as the suggested timing patterns show great dissimilarities. They extend from 14.8 to 5.5 cal ka BP (deMENOCAL et al., 2000), 11 to 4 ka BP (THOMPSON et al., 2002), or 9 to 6 ka BP (RENSSEN et al., 2003; RIAL et al., 2004), depending on the nature and position of the palaeoenvironmental records which were investigated. As several arid interruptions are visible in many of the records obtained, the term "African Humid Period" seems to be an inappropriate term for the several humid stages that occurred from the Late Pleistocene to the Middle Holocene. Other frequently-used terms are Early Holocene Wet Phase (ABELL & HOELZMANN, 2000) and Holocene Climate Optimum (9 to 6 ka BP) (CLAUSSEN et al., 2003; RIAL et al., 2004).

4.2 Review of palaeoenvironmental evidence from the central Sahara

As several continental-scale palaeoclimatic reconstructions have revealed, major differences exist in the timing and the extent of humid and arid phases. A regional focus can provide further information about the process of Late Quaternary climate changes in the central Sahara/Niger. To achieve this, palaeoenvironmental information from significant study sites within the central Sahara has been compiled.

4.2.1 Seggedim

Previous investigations had revealed the presence of Late Quaternary lacustrine sediments underneath the saltpan sediments, indicating a climate-induced transition from a freshwater lake to the present sebkha (BAUMHAUER et al., 2004). The first corings, in 1989 and 1990, reached down to a maximum of 8 metres and revealed a three-way development of the sebkha (BAUMHAUER et al., 2004):

> UNIT 1: 790-640 cm: clays of different colours, organic content 0.8 to 2.4 %, consisting of charcoal material. Biological indicators (algae) show a freshwater milieu, the pollen spectrum shows open vegetation similar to the present although more extensive – freshwater milieu;
> UNIT 2: 640-550 cm: clays with increasing amount of sand towards the top of the sequence, high detrital content, layers of increased calcite content > 24 % at 640 cm, changing environmental conditions – decreasing lake levels;
> UNIT 3: 550-0 cm: evaporite-rich sand, low content of fine material, above 550 cm no appreciable pollen content, probably due to oxidation and destruction of the pollen, salt crust on top 25 cm thick – sebkha sedimentation.

Two radiocarbon dates were obtained from the core: at 790 cm depth, showing an age of 7905 ± 275 a BP (Calendric Age cal BP: 8816 ± 327), and at 590 cm depth with an age of 6850 ± 345 a BP (Calendric Age cal BP: 7716 ± 315). Both radiocarbon dates were obtained from bulk organic matter. Archaeological sites near the sebkha were dated to 2090 ± 105 a BP (Calendric Age cal BP: 2097 ± 145) and 8890 ± 365 a BP (Calendric Age cal BP: 10028 ± 449) (BAUMHAUER & SCHULZ 1984). Further palynological investigations have led to the conclusion that there was Saharan savannah vegetation throughout the Early Holocene, with a distinct change towards Saharan vegetation at about 6.5 ka BP (BAUMHAUER et al., 2004; SCHULZ, 1991).

4.2.2 Falaise de Kaouar

The southern part of the Kaouar depression contains four saline lakes of the Na-CO_3-SO_4-Cl brine type, which still exist at the present day. The lakes are shallow, fed by artesian groundwater, and with belts of salt marsh bordering them. The total area of the lakes varies throughout the year, from 0.5 to 200 ha, with lengths of 2-3 km and widths of 100-200 m (BAUMHAUER 1986, 1991). Over a period of several years more than 40 stratigraphic profiles showing Holocene lacustrine sedimentation were investigated for their lithology, sedimentology and diatom assemblages (SERVANT 1983, BAUMHAUER 1986). The 36 profiles analysed by BAUMHAUER (1986) show the following climatic development:

- a phase of aeolian activity, lasting at least from 20,000 to 9300 a BP;
- probably two phases of Holocene lacustrine sedimentation, from 9300 to 7500 and 6500 to 5000 a BP. The aeolian phase which presumably intervened is only apparent at the littoral zone of the palaeolake; the centre contains a continuous record. The maximum lake level is thought to have occurred at about 8000 a BP (cal BP about 8900), at 25 m above ground;
- a regression phase starting at 5000 a BP.

4.2.3 Fachi

The endorheic depression of Fachi stretches over a length of 25 km along a 150 m high escarpment and is situated inside the Erg de Ténéré, some 150 km W-SW of Bilma. Quaternary deposits of lacustrine origin cover the base of the depression and salines remain the only sign of water (SERVANT, 1983). SERVANT investigated two sites: Fachi and Dogonboulo (20 km north of Fachi). He concludes that four stratigraphic units can be distinguished:

1. an initial lake phase, consisting of small ponds, due to increased groundwater levels and dated by gastropod shells to 10,620 ± 390 BP;
2. a lake transgression phase, with several metres of diatomitic and siltic mud, with one sample dated to 8770 ± 170 BP. The lake level of this phase is thought to have risen more than 20 metres above today's ground level;
3. a layer showing lake regression, together with the occurrence of aeolian sands and pottery; archaeological findings suggest Neolithic settlement;
4. a transgression phase, indicated by a layer several metres thick, dated from 7655 ± 225 to 6850 ± 250 a BP, and consisting of alternating layers of diatomite and of mud made up of silt and clay.

Charcoal pieces in the fourth unit reveal the presence of Sudanian savannah to woodland vegetation (NEUMANN, 1989).

4.2.4 Zoo Baba

The cuesta of Zoo Baba is situated 70 km south of the Erg de Bilma and consists of Cretaceous to Palaeocene, clayey to silty, partly carbonaceous-rich sandstones (BAUMHAUER 1987). Investigations have revealed a freshwater lake, which existed from the Early to the Middle Holocene, presumably connected to the Bilma/Kaouar aquifer. The western rim of the cuesta forms a steep slope, its middle and lower parts being covered by fossil landslides, which are deeply dissected by small channels. The channels contain relics of two accumulation terraces and of lacustrine diatoms. A so-called middle terrace, consisting of sandy and gravelly material, is connected with landslide debris above (410 m) and with a thick diatomite below (395 m), which has been deposited in the partly eroded channel. The coarse gravel lower terrace has no connection with the landslide and lacustrine material (GRUNERT et al., 1991). The terraces were investigated for diatomite profiles and pluvial lake levels. Two radiocarbon dates were obtained from the profiles and revealed ages of 5370 ± 100 (organic matter, cal BP: 6144 ± 116) and 6725 ± 85 a BP (carbonate material, cal BP: 7589 ± 68). The latter is thought to be influenced by hardwater effects and has been corrected to 6000 ± 85 a BP (calBP: 6856 ± 104). The investigation of the diatomites has revealed the following environmental succession (BAUMHAUER 1988, GRUNERT et al 1991, BAUMHAUER 1992):

- lake level maximum at about 6800 to 6000 a BP;
- lower levels before 6800 a BP and from 6000 to 5400 a BP;
- from 5400 a BP up to the present no further data is available.

4.2.5 Adrar Bous

At the location of Adrar Bous fluviatile, lacustrine and aeolian sediments of the Late Quaternary age are present at different levels, as well as Neolithic findings (WILLIAMS et al., 1987). Adrar Bous is located 65 km ENE of the highest mountain of the Air Massif, and consists of a granite massif which rises 300 metres above the surrounding plains. According to PACHUR and ALTMANN (2006), the Air Massif is an area of increased precipitation. Sporadic local storms at the Air result in flash floods, although the climate is generally fully arid and only randomly influenced by the Monsoon precipitation (in June, July and August). The present mean annual rainfall in the Air Massif shows variations from only 100 mm at the SW to 170 mm in elevated regions, and down to less than 5 mm in the mountain's rain shadow, at the north-eastern fringes where the study site is located (GALLAIRE, 1995). Evidently, any increase of precipitation must have originated in the Mediterranean precipitation regime. WILLIAMS et al. (1987) have published a model for the climatic development of Adrar Bous, generated from previous and localized investigations.

Table 4 Climatic development of Adrar Bous (Williams et al., 1987)

Age (a BP)	**Environmental setting**	**Climate**
> 40.000 to < 150.000	Extensive lakes. Major period of swamp soil formation	Humid
> 12.000	Prolonged deflation, minor slopewash, weak iron segregation, carbonate precipitation	Arid
> 8.000	Upper lake. Swamp soils formed.	Humid/cool
c. 7.500	Dune migrations, deflation, carbonate precipitation	Arid
4.000-6.000 +	Weak pedogenesis, then iron segregation. Lower lake.	Sub-humid
1.500-2.500	Minor vertical erosion; slopewash	Semi-arid
0-1.500	Modern wind action, minor slopewash and gullying	Arid and hot

4.2.6 Ténéré

Remnants of Holocene palaeolakes are widespread throughout the dune depressions of the Sahara, especially in the sandy deserts of the Ténéré (FELIX-HENNINGSEN, 2000; FELIX-HENNINGSEN, 2004) and in the eastern Sahara (PACHUR & Altmann, 2006). Wherever found, these lacustrine profiles show similar attributes, such as gleyic features or bleached horizons, indicating comparable development. According to PACHUR and ALTMANN (2006) the accumulation of limnic sediments on dune sands follows a distinct order of development, visible in the stratigraphic profile:

- in the interstices of deposited sand, deposits of organic material, iron hydroxides and calcite accumulate; the composite is characterized as lacustrine sand;
- subsequently, the sedimentation of Mg-calcite commences, followed by predominantly layered calcite ($CaCO_3$> 90 % = autochthonous calcite = Seekreide); the integrated minerogenic detritus is considered to be of aeolian origin;

- decreasing water depth leads to flourishing algae mats and increased reducing conditions; the bacterial reduction of organic material and the associated increase in magnesium levels lead to the predominant development of aragonite;
- the terminal stage is characterized by the development of evaporites from the sulphate group (halite & sodium carbonate minerals).

A special feature of lacustrine sediments on dune sands are ferric rhizome concretions, also referred to as swamp iron ores or bog iron ores. These indicate palaeolake shorelines within the central Sahara (FELIX-HENNINGSEN, 2000; FELIX-HENNINGSEN, 2004). They mainly consist of goethite and are built up around the air-filled parts (aerenchyma) of swamp vegetation, due to predominant reducing conditions within the (palaeo-)lake (FELIX-HENNINGSEN, 2004). These concretions indicate humid conditions, as their development is strictly limited to stagnant water bodies and can therefore be used to determine the pattern of palaeolake distribution. Shallow shorelines are a prerequisite for the development of swamp iron ores , and are the main reason for their widespread occurrence in the rather smooth and undulated landscape of the Ténéré and in the numerous small basins in the Plateau de Tchigai (FELIX-HENNINGSEN, 2004). The compilation of results obtained from developed soils which were formed on Pleistocene (fossil) dunes indicates the existence of two phases of increased humidity in the Holocene, which presumably lasted from about 9 ka to 7.5 ka BP and from 4.5 ka to 3 ka BP (FELIX-HENNINGSEN, 2000). A number of soil characteristics indicate a gradient of decreasing humidity from SW to NE, most likely due to a regular decline of precipitation, comparable to the present situation further in the south, which is caused by the northward shift of the monsoon.

4.3 The issue of the Middle Terrace

The appearance of lacustrine sediments in elevated areas of North Africa has been reported by several authors. For instance, SERVANT (1973) explored stratified fluvial deposits, of clayey to loamy grain size, coating valley floors in the eastern Air Massif. ROGNON (1967) dated similar deposits in the Hoggar (southern Algeria) to 11580 ±350 a BP and 8380 ± 300 a BP. At the Col d'Anai (Air Massif) lacustrine deposits within a sandy terrace have been dated to 15.8 ka BP (GRUNERT, 1983). JAEKEL investigated widespread clayey and well-stratified fluvial deposits in the Tibesti Mountains, located in Northern Chad (e.g. JAEKEL 1979). Sediments containing increased amounts of organic material were dated to 16120 ± 215 a BP (Hv 5624) and 14445 ± 180 a BP (Hv 5625) and referred to as the "Middle Terrace". Radiocarbon dates were obtained from a profile from an adjacent terrace, showing a reversed age profile, from 24045 ± 410 a BP at the bottom to 24865 ± 435 a BP at the top. The accumulation period of the Middle Terrace is believed to represent the most humid period during the Late Pleistocene, lasting to the Early or even the Middle Holocene.

The distribution of similar deposits in the area of Northern Niger has led to the assumption of a relationship with the Middle Terrace observed in the Tibesti Mountains (BUSCHE, 1979; GRUNERT, 1983). Both authors assigned the fine-grained lacustrine and fluvial deposits of the Achelouma valley and the Col d'Anai to JAEKEL's "Middle Terrace", although they show dissimilarities in their radiocarbon dates of several thousand years. These variations have been explained by separate climate developments of the northern and southern areas. The northern records are assumed to have developed under the influence of a mediterranean climate (northern hemisphere winter, precipitation driven by westerlies). The southern region, however, was influenced by the African monsoon regime, resulting in summer precipitation.

BUSCHE (1979) emphasizes the origin of the sediments from eroded soil profiles and thus their significance, not for the most humid periods but for tapering humid conditions. As the most humid periods initiated the development of the soil properties, the landscape must have been stabilized, for instance by vegetation, and soil erosion must have occurred later, when vegetation cover was removed.

According to PACHUR and ALTMANN (2006), the Tibesti Mountains enhance any climatically-induced increase of precipitation and were the source area for numerous palaeo-drainage systems during the Quaternary. From the southern and south-eastern Tibesti foothills, palaeo-rivers drained into the Chad basin in the Early Holocene, building up enormous alluvial fans. Additionally, the southwestern and western fringes of the Tibesti also generated river systems incorporating many lacustrine basins in the Early Holocene, whereas in present times perennial rivers simply flow away from the mountainous areas. The geoecological scenario of the Tibesti mountains during the Early and Middle Holocene (PACHUR & Altmann, 2006) has been reconstructed as follows:

- precipitation amounts at 2000 m asl were 4-5 times greater than at present;
- there was episodic drainage of the valleys;
- any torrential discharge was absorbed by vegetation/increased retention.

The majority of these palaeoenvironmental records have this in common, that their appearance, mainly during the LGM to Kanemian stage, does not fit in with general climatic reconstructions. MALEY (2000) has investigated similar lacustrine and fluvial deposits, especially in the mountainous areas of the central and eastern Sahara, and the concurrent formation of dunes in the lowlands, during the LGM. The author concludes that:

- the precipitation regime causing the fluvial deposits in the mountainous areas originated in tropical depressions, as the sediments show fine and well sorted stratification. As monsoonal rains are considered more dynamic, they most likely result in increased sand components and generally coarser layers;
- the maximum extent of the tropical depressions reached as far as 12° N;
- high wind velocities predominated in the lowlands, causing increased evaporation; as a result, rain did not reach the lowland surfaces;
- between about 8 and 6.5 ka BP, advancing monsoonal precipitation during summer periodically alternated with precipitation from tropical depressions (winter rain);
- a Middle Holocene erosive phase occurred at about 6 to 6.5 ka BP, due to the dominance of monsoonal precipitation and reduced occurrence of tropical depressions.
- there was a period of reviving winter rains at about 4 ka BP (in combination with a general cooling).

The question arises whether the general term ”Middle Terrace” is still appropriate for these diverse sediment archives. Although similar in their characteristics, their genesis differs to a great extent, as the inducing precipitation appears to originate in dissimilar climatic systems and temporal stages.

4.4 Computer-model-based investigations

Modelling of past climatic dynamics is based on a comparison of present climatic features with evidence from past environments, inferred from palaeoenvironmental research. Depending on the data

and the allowed interaction of different environmental subsystems, results from computer-based models may give evidence of the extent of past global climate changes at different spatial and time resolutions. Furthermore, computer hindcast may provide essential information about the causes of climate change, as varying extraterrestrial input parameters (e.g. insolation) can be simulated. Major differences exist in the climate subsystems which are integrated into different computer models. General circulation models (GCM), operational at a global scale, use a variety of different input parameters, from the atmosphere, the ocean, orvegetation, and combinations of these.

KUTZBACH and STREET-PEROTT (1985) have investigated climatic development since the last glacial maximum with a GCM, and have set up a hydrological P-E (precipitation-evaporation) model to reveal probable changes in lake levels since 18 ka BP. The study confirms the plausibility of an increase in precipitation and a rise in lake levels between about 9 ka and 6 ka BP, and a decline after that period. Another GCM, working on both global and regional scales, has identified the variations of the earth's orbit as the cause of the major climatic changes in the last 18,000 years (KUTZBACH & GUETTER, 1986), leading to the following conclusions:

1. variations in the date and the season of perihelion are the major reasons for changes in seasonal radiation; meanwhile an additional/increased axial inclination (with a maximum at approximately 9 ka BP) caused an amplification of northern hemisphere summer warming;
2. land and ocean surfaces react differently to temperature changes, so symmetrical and gradual solar radiation changes may lead to amplified climatic dynamics;
3. the simulated changes in summer precipitation are much larger than those in winter, due to nonlinear connections between temperature and vapour pressure.

Subsequently, the COHMAP (Cooperative Holocene Mapping Project) has collected a huge amount of palaeoenvironmental data and combined this with a GCM, in order to investigate the source mechanisms and reasons for Holocene climatic changes. According to the authors, variations in insolation originating in changes of orbital parameters are most likely the cause of global climatic changes (COHMAP_MEMBERS, 1988).

The migration of zonal palaeoclimatic patterns associated with a displacement of landscape belts has been confirmed by model simulations of global atmospheric circulation (GUETTER & KUTZBACH, 1990). Transferring climate information on Köppen's climate classification, the model confirms a northward shift of the Sahara-Sahel boundary of about 5 degrees between 15 and 6 ka BP, through an extension of the Sahel climate and the associated contraction of the desert areas.

The BIOME 6000 project, a synthesis of global palaeoenvironmental proxies (primarily pollen data) and computer models to determine the extent of potential feedbacks between vegetation and the atmosphere, provides palaeovegetation maps of the LGM and the Mid Holocene (PRENTICE & JOLLY, 2000). The authors show a northward migration of the ITCZ during (northern hemisphere) summer in the Mid Holocene and consequently precipitation changes in the monsoon areas of northern Africa. These changes are evidently reflected in the extended Sahel vegetation to the north and the contracted Sahara desert. Climatic conditions in Africa are generally thought to have been cooler and drier during the LGM.

Climate simulations using an ocean-atmosphere model have confirmed the influence of solar variations on climate, with increasing insolation leading to a major increase in the contrast between land and sea surface temperatures (CUBASCH et al., 1997). MONTOYA et al. (2000) have used a general circulation model (GCM) based on ocean–atmosphere relations to simulate climate conditions since the last interglacial maximum (Eemian) at about 125 ka BP. They investigated a major effect on atmospheric circulation, especially on the circulation of the African summer monsoons and the associated precipitation regime. The reasons for the modifications are the changing land-ocean

temperature gradients and consequent changes in atmospheric circulation dynamics, caused by/resulting from varying surface pressure systems.

With respect to global-scale climatic interactions, models which include the atmosphere and the ocean, as well as vegetation data, promise more realistic results. The intensification of these climate subsystems due to interactions has been confirmed for the Holocene (GANOPOLSKI et al., 1998), with a strong emphasis on synergistic effects, since they appear to be the main cause of enhanced precipitation in the Sahara. The extent of vegetation changes in the Sahara during the Holocene is presumably a result of strong local positive feedback between vegetation and the atmosphere. This has been confirmed by CLAUSSEN et al. (1999), who consider vegetation-atmosphere feedback to be the driving force for the rapid climate change from humid to arid in the central Sahara. With changes in orbital parameters occurring rather slowly, feedback between vegetation and atmosphere is considered to work as an amplifier, especially at the transition from the "green Sahara" to the desert Sahara in the Mid Holocene (ALLEY et al., 2003; FOLEY et al., 2003). A compilation of global palaeoenvironmental records emphasizes the speed of Holocene environmental changes and suggests that the high variability of the climate during the last eleven millennia may be a result of several determining factors, the most important being solar variability, with natural feedbacks amplifying and enhancing rather slow changes in insolation (MAYEWSKI et al., 2004).

However, the amplification may work in two different ways. A constant vegetation cover increases the soil's absorption of precipitation and the water storage capability of the top layers. However bare soil surfaces without vegetation cover are likely to be eroded and altered, causing an overall deterioration of soil conditions (SCHEFFER et al., 2001).

The alternation of these contrasting ecological and climatic stages is considered to have occurred more or less regularly. Climate reconstruction by process modelling of several scenarios (deMENOCAL et al., 2000) shows a strong correlation between two positive feedback processes: firstly, an albedo-vegetation feedback operating in the terrestrial range and secondly, a reaction to sea surface temperature changes that control moisture transport over the continent. Because the simulated environmental changes appear non-linear, the authors suggest a threshold summer insolation value of 470 W/m² related to the vegetation-albedo feedbacks. When summer radiation passes this threshold, changes from humid conditions to arid conditions (and vice versa) occur. These changes manifest themselves as changes in vegetation, or in shifts of the vegetation belts.

Uncertainties exist in determining the extent of the feedback processes. A transient simulation with coupled atmospheric, ocean and dynamic vegetation-change data (LIU et al., 2007) has confirmed that the abrupt environmental changes at about 5 ka BP occurred because of a collapse of the vegetation cover, which corresponded to a bioclimatic threshold. Nevertheless, the authors also mention the strong climatic variability at an annual level, which complicates the isolation of causes and effects.

Simulations of a fully-coupled atmosphere-ocean-land surface-vegetation climate model for the Mid Holocene (WANG et al., 2007) have focused on the feedback dynamics of vegetation and precipitation. According to the authors, the impact of these feedback processes decreases with increasing timescales, as the background climate becomes the key influence. Whether climatic subsystems show positive or negative feedback processes is therefore most likely dependent on the period investigated.

However, the initiating environmental setting for vegetation changes in the Sahara is driven by global climate variations, the main force being insolation. Investigations of ocean surface temperatures have given evidence of the strong connection between changes driven by variations of summer insolation and the African monsoon (KUTZBACH & LIU, 1997). An increase of 15 to 20 W/m² in solar radiation at the surface of the tropical Atlantic Ocean consequently leads to rising rainfall in the Sahel zone, in combination with a northward shift of the African monsoon. An

investigation of the extent of the African Humid Period (RENSSEN et al., 2006), with a particular focus on the western Sahara and Sahel areas, has revealed a key precipitation anomaly at 9 ka BP, which is restricted to the northern hemisphere summer months (June to August). The greatest effect of the anomaly is apparently located at 20° N, with a maximum precipitation in August of 110 mm.

Vegetation and atmospheric feedbacks are considered to influence different subsystems of the monsoon circulation, although both amplify monsoon activity and consequently the northward migration of precipitation (BRACONNOT et al., 1999). An increase of vegetation causes a local enhancement of evaporation and humidity. The driving force for the migrating ITCZ position is believed to originate in the temperature gradient in North Africa (BRACONNOT et al., 2000), but the authors state that there is no direct connection between temperature maxima and precipitation maxima (cf. the present climatic dynamics of Northern Africa).

Extensive research on the coherences operating within climatic subsystems has determined that positive and negative feedbacks are the main causes of nonlinear behaviour within the climate system. The point where negative and positive feedbacks are in balance is considered to be the natural system's threshold (RIAL et al., 2004). This is a rather hypothetical and vague concept, which has to be taken into account not only when feedback processes and corresponding threshold values are determined by computer modelling and subsequently applied to a wider area, such as the central Sahara, but also where these individual features are most appropriate, when determined on a smaller scale by fieldwork.

4.5 Summary

An immense number of investigations have revealed the occurrence in the past of several major climate variations in Northern Africa, particularly those driven by global climate changes in the Quaternary. There is general agreement that there have been humid periods over northern Africa, although some discussions are still ongoing concerning the extent and duration of climate changes, since the regional dynamics tend to overlay the climatic signals stored in the palaeoenvironmental records (GUO et al., 2000).

The climate of northern Africa is driven by the seasonal migration of the ITCZ boundaries. Changes in insolation and global glaciations were the cause of several climate alterations in the Quaternary period. Compilations of lake records have revealed the migration of zonal palaeoclimatic patterns, in combination with a displacement of landscape belts, as they directly responded to different climatic situations.

At the Last Glacial Maximum (23 to 18 ka BP) climatic conditions in the central Sahara were generally dry, but cooler than at present, because of a southward shift of the pressure and wind belts of the global circulation. A humid period, lasting from 11 ka to about 5/6 ka BP, dominated the Early to Middle Holocene. The amplified monsoonal activity originated in the concurrent increase in northern hemisphere insolation. The beginning and the end of this humidity optimum were accompanied by unstable climate transitions, with variations in the amount and seasonality of precipitation. A number of climate models have shown that a desertification process of variable/varying intensity and magnitude, driven by interacting feedback processes of varying intensities, started at about 5 ka BP, and led to the present fully arid conditions. These feedback processes consist mainly of three correlated components, which influence one another: vegetation, ocean surface temperature and the atmosphere. The most contentious issue in past climate modelling is the reliability of the various proxy data used as input data. As shown in this chapter, the palaeoenvironmental records that have been investigated show wide variations in temporal patterns as to the onset and termination of changes in climatic dynamics. The task is to establish whether the

archives investigated reflect only the local geographical setting or provide information about climatic and environmental changes over a wider area.

5 MATERIALS AND METHODS

5.1 Fieldwork

Two expeditions, in 2005 and 2006, went to the northeastern parts of Niger to investigate the known remains of palaeolakes and search for new ones. Samples were taken at several study sites, to gain a comprehensive picture of late quaternary environmental conditions. A sediment core (15 metres length) was extracted from the sebkha of the scarp-foreland depression of Seggedim, complemented by a number of more incomplete soil and sediment samples from already known palaeoenvironmental contexts as well as from newly discovered sites on the plateaus of Djado and Mangueni and the foothills of the Plateau de Tchigai ().

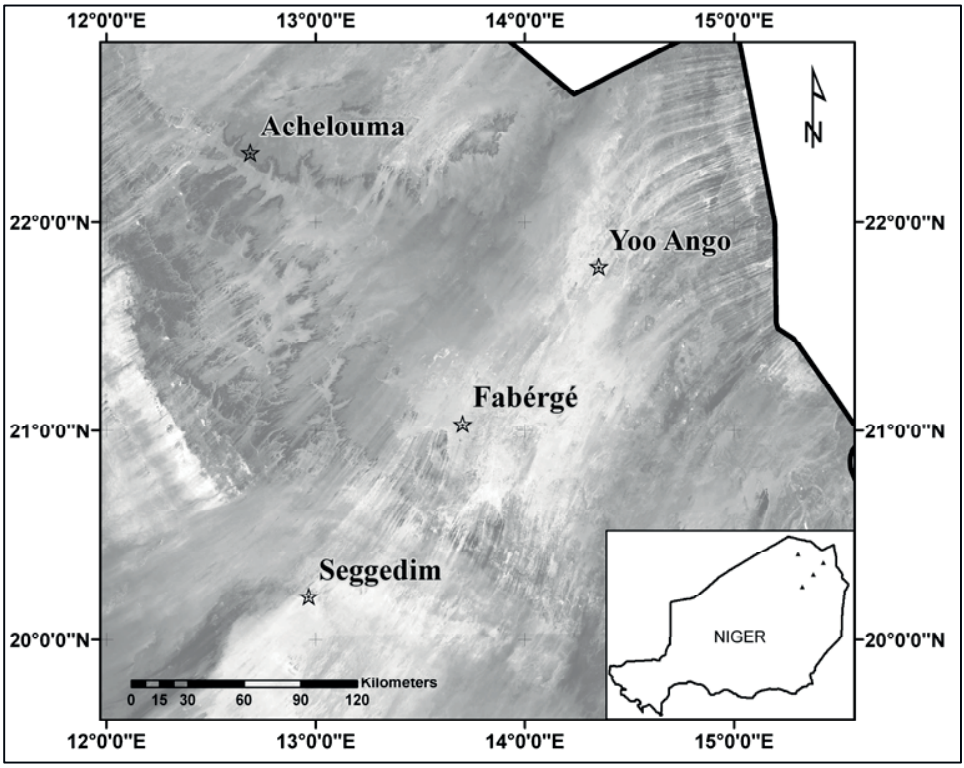

Figure 11 Location of the study sites

The coring was performed using a modified Kullenberg Piston Corer (Figure 12). A tripod frame with a pulley on top was used to lift the 20 kg striking weight and to pull out the core. Transparent inboard tubes with a diameter of 63 millimetres and a length of 2 meters were used as core barrels. Due to difficulties during the coring procedure, only one coring, going down to 15 meters, was completed in the Seggedim depression, over a two weeks period. To be transportable, the core barrels had to be cut into pieces with a maximum length of 70 centimetres. The splitting of the cores, their description and the logging of the sediment, as well as the sampling, was performed in the geomorphological laboratory at the University of Wuerzburg.

In addition to the Seggedim core, sediment profiles were sampled at sheltered sites where remains of lacustrine and colluvial sediments are protected from erosion. After preparing the profile, the main soil features (colours, beddings, horizons, and depth/height) were logged and sediment samples were taken from different horizons.

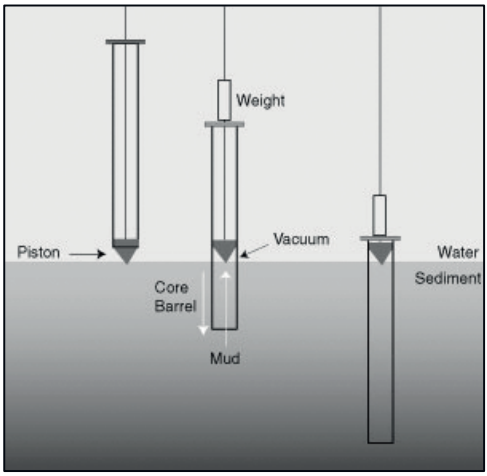

Figure 12 The operation of a Kullenberg Piston Corer (U.S.G.S., 2001)

A total of 13 profiles were investigated and sampled, but only those profiles containing suitable material for radiocarbon dating underwent further analyses. A final selection of 8 profiles of different proportions, habitus and origin were analysed for geochemistry, mineralogy and radiocarbon dating.

5.2 Laboratory methods

5.2.1 Core handling and sample pre-treatment

Due to the need for multiple analyses of the core material, a work schedule was created (Figure 13). The core sections were cut in half along the vertical axis; one half of the core was used for subsampling, the other half was archived. From the segments chosen for laboratory use (subsamples), slices of 1 centimetre thickness were taken about every 10 cm, paying attention to major

sedimentological changes. The samples that were used for geochemistry and mineralogy analyses were dried and ground in a tungsten carbide vibrating cup mill.

All investigations were performed with a focus on the non-sebkha sediment (below 5 m depth). The main lithostratigraphical features, Munsell soil colours and major changes in sedimentation were logged. High-resolution images of the split core surface were produced for each section with a modified flatbed scanner (for a complete list of the performed analyses see Appendix table 2).

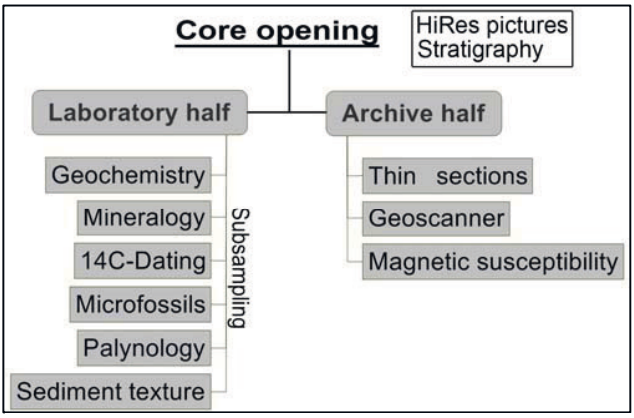

Figure 13 Laboratory work schedule for the Seggedim core

5.2.2 Physical Methods

5.2.2.1 Sediment texture/grain-size analysis

Particle Size Analysis was performed at the University of Trier Physical Geography, and Hydrology laboratory, using a Galai CIS-1 Analyzer. The main principle of the Galai CIS analyzer is the “time-of-transition” event. The investigated material is kept in solution and illuminated by a focused laser beam. Whenever a particle breaks the laser beams connection to a detector, an electrical impulse is produced. The duration of this pulse is governed by the particle size, which can therefore be calculated. By changing the size of the focused beam, a wide range of particle sizes can be detected. In addition to the size, the shape of the particles can also be established. The principal advantages of this method are its speed and the small sample size needed for the analysis. On the other hand, the small sample size raises the question of the representativeness of the sample with respect to the layer being investigated (LAST, 2001b).

An additional issue arises from the sample handling, as the measurement of the solution requires small grain sizes to achieve constant flow rates. Consequently, as a pre-treatment, the samples are sieved to a particular size and information on grain sizes above fine sand (> 150 µm) is not accessible (Dr. R. Bierl, Trier University, personal communication). The standard error of the mean (SEM) amounts to 0.7418 for all samples and sizes (n=511), the relative standard error (RSE) amounts to 0,05 %.

More detailed and elaborate descriptions of the analysis and its drawbacks can be found in LAST (2001b) and UDELHOVEN (1992). For details of the basic principle see WEBER & HERZIGER (1972).

5.2.2.2 Magnetic susceptibility

The magnetic susceptibility describes the ability of a material to be magnetized ("magnetisability"), which is most common in minerals containing iron (Fe). Five kinds of magnetic behaviour exist (c.f. Table 2) and the magnetic susceptibility of natural substances is the sum of all these. When measuring susceptibility with a Bartington sensor, a magnetic field is created and magnetisation within the field is detected (DEARING, 1994).

Magnetic volume susceptibility on the split core surface was measured in the geoecological and sedimentological laboratory of the Institute of Physical Geography of the Friedrich Schiller University, Jena. A Bartington MS2E sensor was used, measuring at 1 mm intervals. The MS2E sensor is designed for the continuous measurements of split core surfaces. However, to avoid roughness effects and contamination of the sensor, preparation of the surface is recommended. For that purpose, standard plastic wrap was used. The sensor compares the differences in permeability of free space and the sample, with adjustable high spatial resolution (active sensing region 10.5 *3.8 mm).

The obtained data was corrected for temperature effects using a two-point calibration sampling ("air value"), performed before and after each measurement operation. Because of the individual calibration that was performed for each core segment, quantitative comparisons of the results are not appropriate.

5.2.3 Geochemistry

The great heterogeneity of lake sediments, with variations in lateral distribution and stratigraphy, (BOYLE, 2001) increases the difficulty of obtaining average concentrations by appropriate sampling methods. The fact that the majority of the Earth's crust (about 99%) is a composite of 8 elements (O, Si, Al, Fe, Mg, Ca, Na, K) (KRAUSKOPF & BIRD, 1995) makes these elements especially valuable in environmental analyses.

At least two different methods are available for performing elemental analysis. The total elemental concentrations can be derived either from extracted solutions (ICP-OES), or from the solid material (XRF) (BOYLE, 2001).

5.2.3.1 ICP-OES

The bulk chemistry of the samples was measured for selected elements in aqua regia digestions, using a Perkin-Elmer OPTIMA-3000 ICP-OES (Inductively Coupled Plasma Optical Emission Spectrometry). The aqua regia digestions were produced following DIN 38414 S7.

The principle of Inductively Coupled Plasma Optical Emission Spectrometry (ICP-OES) is based on the thermal excitation of atoms and the subsequent emission of ionic radiation lines in the visible spectrum. The position of the emitted lines can be associated with certain elements and the intensity of the lines is a function of an element's concentration (BOYLE, 2001).

A major drawback of this method is the limited number of measurable elements. Aluminium and silicon cannot be determined, nor can chlorine. Because the number of ionic radiation lines produced increases with an increase in the number of electrons in the outermost electron shells, spectral interferences occur, especially with elements from the high numbered groups in the periodic table. This method is therefore most valuable for alkali and alkaline earth metals (BOYLE, 2001).

An additional critical factor is the solution of the samples in aqua regia. A microwave digestion for the total dissolution of the samples would destroy all chemical bonds and therefore provide results that are more precise, especially when large amounts of silicon are present (HORNBURG & LUEER, 2000). Nevertheless, a microwave digestion apparatus was not available.

Sulphur (S) and calcium (Ca) had to be measured in a 1:10 dilution ratio. The other elements were measured in 1:1 aqueous solutions. The standard error of the mean (SEM) amounts to 0.6904 for all samples and elements (n=1593), the relative standard error (RSE) amounts to 0,03 %.

5.2.3.2 X-ray fluorescence spectrometry (XRF)

The basic principle of all XRF methods is the photoelectric fluorescence of secondary roentgen radiation from a stimulated sample. Stimulation is produced with primary photons, whether from x-ray emitting radioisotopes (isotope source) or by accelerated electrons targeted onto the sample (tube source). Both systems produce element_specific emissions of secondary x-rays, whose emission rate is a function of the element's concentration and the sample's absorption of the x-rays. Element concentrations can be calculated via a comparison with reference samples of known composition (BOYLE, 2000; BOYLE, 2001). X-ray fluorescence spectrometry can be carried out on several different sample types, depending on the functionality of the analyzing system. For this work, XRF was measured on fuse tablets and on split core surfaces.

5.2.3.3 Fuse tablets (XRF)

The fuse tablets for XRF analysis were produced by mixing 0.6 grams of sample mass with 3.6 grams of lithium tetraborate or Spectromelt (the fusing agent) and 1 g ammonium nitrate (the oxidizing agent). By stepwise heating to 1000° C, the components are homogenized and fused in platinum melting pots and finally moulded into tablets. The tablets were analysed with a PHILIPS PW 1480 XRF spectrometer (Rh tube), the obtained data was processed using the PHILIPS X 40 software. A comparison with reference samples of known composition allows element concentrations to be calculated (BOYLE, 2000; BOYLE, 2001). The lower limits of detection of major and minor elements are shown in Appendix Table 3.

Results from the XRF analysis of fuse tablets containing high amounts of gypsum (P1, P3, P4 and P12) had to be corrected, as the method produces calculable displacements of the calcium and sulphur values. To achieve this, samples with standardized amounts of gypsum and quartz were analysed (100, 80 60 and 40 % gypsum, mixed with 0, 20 40 and 60 % of quartz). Subsequently, the measured values of calcium and sulphur were compared to the stoichiometric (calculated) results. To fit the displacements of the calcium results, a polynomial regression was used ($y=0.0242x^2+0.7343x+0.0681$), while the sulphur values could be fitted to a linear regression ($y=0.682x+0.2812$); both procedures resulted in a coefficient of correlation of $R^2= 0.99$.

The standard error of the mean (SEM) amounts to 0.4993 for all samples and elements (n=1099), the relative standard error (RSE) amounts to 0,07 %.

5.2.3.4 Geoscanner (XRF)

The Geoscanner device is a high-resolution ED-XRF (Energy dispersive X-ray spectroscopy) system developed by Cox Analytical Systems for the investigation of laminated and varved sediments. The split core surfaces were analysed at the Federal Institute for Geosciences and Natural Resources (BGR) in Hannover. Because the roughness of the sediments produced considerable distortion when measuring the entire 70 cm core segments, four representative sections of 8 cm each were individually prepared for these measurements. The capture of the secondary fluorescent x-rays is carried out using an energy dispersive detector.

The main advantages of this method are the variety of material types that can be analysed (liquids, powders and solids), the rapidity of measurement and the non-destructiveness of the analysis. The variable high resolution, with a maximum of less than 50 µm, is especially valuable for the investigation of laminated sediments, whether contained in core segments or as thin features. Detectable elements range from manganese (Mg) to uranium (U). The major disadvantages are that lighter elements than sodium (Na) cannot be detected and that the signals captured from some light elements (especially magnesium, aluminium and silicon) are weakened by absorption in air. A quantification of the elements detected is therefore not possible. In addition, interference due to crystallographic effects can occur.

The measurements result in monochrome X-ray images, which give evidence of the presence of the investigated element by reflectance and the consequent brightness of the image. Results for elements with only low reflectance may be enhanced using a graphics-editing program. The resulting brightness values are retrieved line-by-line and best represented in a scatter plot. The images themselves reveal additional information about the sedimentation dynamics, as the spatial distribution of the elements within the investigated segment can be visualized.

The apparent advantage of minimum sample preparation can be discounted when analysing core segments where inhomogeneities on the sample surface (matrix effect) regularly occur. The elaborate preparation of core cuts may lead to distortions in the analysis, which are due not to sedimentary processes but to cracks of the sediment body. Interpretations of these measurements have to be performed with considerable care.

5.2.3.5 Carbon analysis

The amount of total carbon (TC) was determined using a LECO CS-200 Carbon/Sulphur Analyzer. Exactly 1 g of dried and homogenized sample mass is heated to 850°-1100° C, which oxidizes the carbon present to carbon dioxide (MEYERS & TERANES, 2001). The CO_2 produced is measured by an infrared detector. The detection limit obtained from the literature varies between 0.02 and 0.05 weight percentage and generally depends on the respective sample size. The standard error of the mean (SEM) amounts to 0.2590 for all samples (n=178), the relative standard error (RSE) amounts to 0,08 %.

To determine the proportions of total organic (TOC) and total inorganic carbon (TIC), one of these values must additionally be determined (MEYERS & TERANES, 2001). For this work, inorganic (carbonate) carbon was measured on a Woesthoff Carmhograph analyzer. 1 to 2 g of sample mass was dispersed in H_3PO_4 (phosphoric acid). The CO_2 produced was passed through a NaOH (sodium hydroxide) solution. The changing electrical conductivity of the solution indicates the quantity of inorganic carbon. For the calibration of the test series, pure $CaCo_3$ was used.

The standard error of the mean (SEM) amounts to 0.1917 for all samples (n=178), the relative standard error (RSE) amounts to 0,11 %.

5.2.3.6 pH measurement

The pH values were determined for 30 selected core samples in $CaCl_2$ solution following ISO (International Organization for Standardization) standard number 10390. 5 mg of air-dried soil were added to 25 ml of 0.01 M $CaCl_2$ solution, giving a solid-liquid ratio of 1:5. The sample was shaken for 5 minutes and rested for 2 hours. Before the measurement with a pH electrode, the sample was stirred again. The sample was tested twice more and the measurement repeated. The mean of the three results was used. Because of the low sample size, the error of the mean and the relative standard error were not calculated.

5.2.4 Mineralogy

From the core segments chosen for laboratory use, slices of 1 centimetre thickness were taken about every 10 cm, taking account of major sedimentological changes. The samples for geochemistry and mineralogy were dried and ground in a tungsten carbide vibrating cup mill. The investigations were performed with a focus on the non-sebkha sediment (below 5 m depth).

Mineralogical investigations were executed in two parallel procedures. The primary focus was on XRD analysis, but as this does not provide information on textural or shape parameters, an additional preparation of thin sections was performed. Given the evidence that there was only one occurrence of kaolinite in the sediment samples, further investigations for clay minerals were not performed.

5.2.4.1 XRD

X-ray diffraction (XRD) is the most important and widespread method for the mineralogical analysis of lacustrine sediments. Besides being fast and fairly low-cost, this method not only provides information about the kind of minerals present (quality) but can also provide at least a semi-quantitative measure. X-rays are generated by high-energy electrons, which are targeted at a copper (Cu) metal plate. Parts of the emitted X-ray spectrum are used to produce the XRD images by pointing them at the sample surface. The sample works as a diffraction grating and scatters the x-rays, depending on the atomic distances within the crystal structure of the minerals in the sample (Last, 2001a).

Minerals were analysed by X-ray diffraction (XRD) using the Phillips X'Pert diffractometer (Model PW 1729/40) at the Institute for Geographic Sciences of the Free University, Berlin. The patterns were recorded after employing Cukα rays. The powder samples were scanned in a range of 3° (2 Θ /Theta) to 70° (2 Θ /Theta) using a step width of 0.02° (2 Θ /Theta) and a count time of 5 s per step. The semi-quantitative and qualitative identification of mineral phases is achievable using the X'Pert analysis software, the latter being more reliable. The quantity of the detected minerals can be determined in a simplified way using the following format:

Table 5 Mineralogy interpretation scheme

Imp./Sec.	Category	Coding (cf. Appendix Tables)
<50	Traces	1
50-200	Very Few	2
200-500	Few	3
500-1000	Medium	4
1000-2500	Much	5
> 2500	Very Much	6

5.2.4.2 Thin sections

The first five millimetres of the archived half-core were extracted for the manufacture of thin sections. Problems occurred during preparation due to variable salinity within the sediment. This led to a delay which prevented further investigations of this type. Information from thin sections is therefore derived from previous corings in the sebkha of Seggedim (e.g. BAUMHAUER and SCHULZ, 1984).

5.2.5 Biological Indicators

5.2.5.1 Microfossils

The diatom samples were treated according to the method described by SERVANT-VILDARY (1977). The ecological interpretation of the diatom floras followed the procedure used by GASSE & STREET (1978). The slide preparations were counted under a Leitz microscope (Diaplan) with interference-contrast equipment at a magnification of 1000x, up to the point where there was no more change in the percentages of the diatom. When counting, two valves were always taken as representative for the frustule of the respective species. Calibration was done by comparison with published data on present-day diatoms, largely from Africa. In some cases, the ecological flexibility of the dominant species made it difficult to attribute it to a specific palaeoenvironment. Suggestions as to water chemistry were only made if a sufficient number (at least 5%) of precise ecological indicators could be identified in the spectra. The same procedure was followed for the highly distinctive floral assemblages in certain samples, where the auto-ecological discrepancies either indicated meromixis, or else short-term changes in the water supply and water chemistry of the palaeolakes (personal communication, Prof. Dr. R. BAUMHAUER, 2008).

The analysis of microfossils, or diatoms, is always time-consuming and difficult for the person responsible for the analysis. Unfortunately, full information for the whole period covered by the samples could not be derived from the coring and the soil profiles within a reasonable time scale. Due to the importance and the detail obtainable from this information, future investigations will conclude this work. Basic information about the diatom populations of the upper core sections and derived information about the aquatic setting of these sequences can be found in BAUMHAUER (1988).

5.2.5.2 Palynology

For the determination of the pollen composition, samples of 1 cm³ volume were extracted from the sediment. To remove interfering sediment components such as carbonates, silica and polysaccharides, the samples must be successively processed using a number of methods, including treatment with hydrochloric acid (HCL), hydrofluoric acid (HF) and an acetolysis mixture (BENNET & WILLIS, 2001). After extracting the pollen material, the pollen spectrum was determined and the different types counted to the point of consistency in the percentages. Because this very time-consuming type of analysis could not be consistently carried out, the information about pollen distribution is very limited. Particularly the bottommost section, which probably contains the most valuable information, could not be examined in the limited time available and a detailed description will therefore be published elsewhere. As a result, the palaeoecological statements which follow are mainly based on established pollen data from previous investigations (SCHULZ, 1991; SCHULZ, 1994).

5.3 Age determination

Samples for radiocarbon dating were extracted in high organic sequences and from charcoal pieces in the bottommost part of the core. The dating procedure was performed in the Poznan Radiocarbon Laboratory using the Accelerator Mass Spectrometer (AMS) technique, which reduces the required sample size to a few grams. These dates were calibrated for 95% confidence intervals using the CalPal-2007 software (WENINGER et al., 2007), using the calibration data-set CalPal-2007Hulu (WENINGER & JOERIS, in press).

5.4 Data evaluation and quality

The measured values were tabulated and statistically tested with the Microsoft EXCEL 2003 and SPSS 15 software. Graphs were created using Sigma Plot 10.0 and Photoshop 7. A database was created and results were visualized using the SigmaPlot and LogPlot 2005 software. The interpretation of correlation matrices within this work follows this scheme:

0.00	to	0.29	very weak
0.30	to	0.49	weak
0.50	to	0.79	medium
0.80	to	0.89	strong
0.90	to	1.00	very strong

5.4.1 Normative stoichiometric calculation

Normative stoichiometric calculation was performed using the mineral components identified by the XRD analysis as the reference database for the mineralogical inventory. Stepwise computing of the geochemical results from the XRF fuse tablet analysis, using idealized stoichiometric formulae of

the confirmed minerals, gave the generalized quantitative mineral concentrations as weight percentages (BOYLE, 2001).

5.4.2 Normalization

Normalization of the geochemical results (ICP and XRF) obtained from the sediment profiles was not performed, as these showed major variations in inorganic and organic carbon content. The test-wise calculations of 40 samples from profiles 3, 4, 8, 10 and 11 included LOI balancing (TOC multiplied by 2) and CO_2 balancing (3.643 * TIC), as well as the main element values (SiO_2, TiO_2, Al_2O_3, Fe_2O_3, MgO, CaO, Na_2O, K_2O, P_2O_5, SO_3, MnO) from XRF fuse tablets. The calculated mean total weight percentage reached 95.67 % (n=40), whereas values without the added LOI and CO_2 ranged from 58 to 96 %. Although not all layers were analyzed for carbon content, the quality of the data seemed to be adequate, but no normalization of the geochemical data was performed, to prevent overestimation.

6 CORING RECORD FROM SEGGEDIM

The core sequences described in what follows were taken in 2005, using a modified Cullenberg corer with a core diameter of 63 mm. The core sequences were split, with one half of the core used for sub-sampling and the other archived. High-resolution images were produced with a modified flatbed scanner. The main lithostratigraphical features, Munsell soil colour data and major changes in sedimentation visible with the naked eye were logged. 1 cm thick slices were taken about every 10 cm, to take account of major sediment changes. These subsamples were dried and prepared for analysis of bulk chemistry, mineralogy, palynology and microfossils, with the main focus on the non-sebkha sediment (below 5 m depth). The first five millimetres of the archive half-core were cut out, to produce thin sections. The bulk chemistry of the samples was ascertained for selected elements in aqua regia digestions using an ICP-OES (Inductively Coupled Plasma Optical Emission Spectrometer). For the investigations of silicon and aluminium dynamics, additional XRF analyses on fuse tablets were performed on 30 samples. Mineralogy was measured by XRD (X-Ray Diffraction). Total inorganic carbon (TIC) and total carbon (TC) were determined using a Woesthoff Carmhograph and a carbon-sulphur analyzer. The pH values were determined in $CaCl_2$ solution following ISO 10390. Samples for radiocarbon dating were taken from highly organic parts of the sequence and from pieces of charcoal found in the bottom parts of the core. These dates were calibrated for 95% confidence intervals using the CalPal-2007 software (WENINGER et al. 2007), and the calibration data-set CalPal-2007Hulu (cf. chapter 5 Materials and Methods for details).

6.1 Results

6.1.1 Magnetic susceptibility

Figure 14 illustrates the summary results of the split-core surface measurement of magnetic susceptibility (κ – kappa) on a logarithmic scale. Five sections show increased values due to different properties. As magnetic susceptibility results are the sum of different magnetic sources (LARRASOANA et al., 2003) the compartments are hardly to determine. For a general estimation, the results are compared to the stratigraphical information obtained from the core. As the sebkha sediments (500-600 cm) and of the upper section of the unstratified clay (650-710 cm) show increased susceptibility values above 100 κ, a general high amount of magnetisable material in the catchment area can be considered.

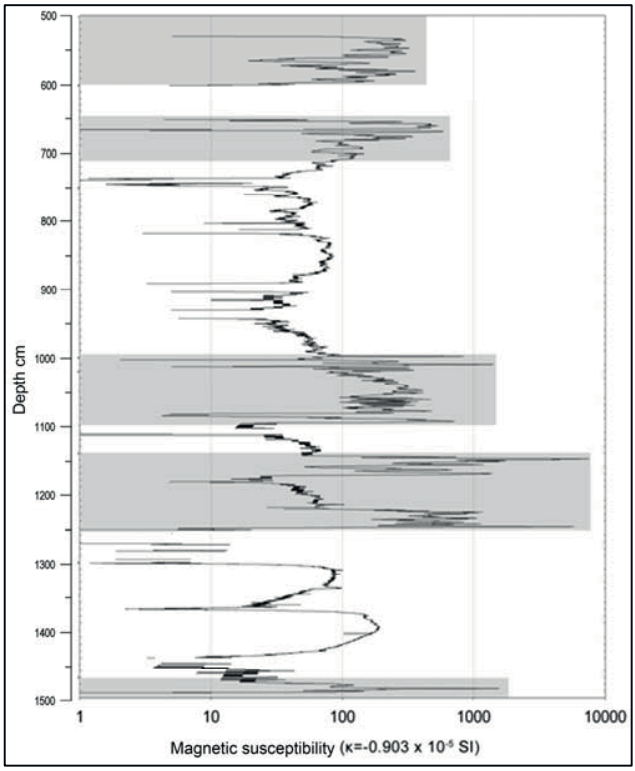

Figure 14 Results of magnetic susceptibility measurement

6.1.2 Stratigraphic units

Six distinctive stratigraphic units and several hiatus determine the stratigraphy of the core. These units are defined by major colour changes, texture and lamination properties. Some are discontinuous and appear at several depths, whereas others are located at specific depths.

Sand:

The most recent stratigraphic unit of the sebkha consists of sand and evaporitic material such as thenardite and syngenite. It extends from 0 to 600 cm depth and shows several dynamic changes of sedimentation. As the focus of this work is concentrated on the lacustrine sediments, this section is marginally investigated. A comprehensive description of the Seggedim sebkha sedimentation can be found in preceded studies (BAUMHAUER, 1986; BAUMHAUER et al., 2004).

Clay, unstratified:

This unit is located at 650 cm to 740 cm depth and shows no visible stratification of any kind. Several distinct colour changes and large rock fragments give evidence of a rather dynamic

sedimentation process. The main colours in this section range from 7,5 YR 5/8 to 10 YR 6/2 and 7,5 Y 4/2. Another homogenous unit can be located at 923 cm to 995 cm depth. Again, some sandstone fragments can be found here and no stratification is visible. The main colour is 7,5 Y 4/1. Inferred from the rock fragments deposited and the homogenous structure, these units are supposed to have originated as turbidites or from mud streams.

Clay, layered:

The main features of these units are the fine laminations that appear in regular and ground-parallel sets of bands but show variations in thickness. One major section is located at 750 cm to 780 cm depth. It consists of finely laminated clays and shows no disturbances of any kind. The dominating colour is 2,5 GY 4/1. Another set of fine laminations can be found at 1019 cm to 1055 cm. The colours range from 7,5 Y 4/1 to 3/1. One particular feature of this segment is the occurrence of fish bones at 1,032 cm that prove the existence of an ecosystem teeming with life. Another section between at 1100 cm and 1140 cm is comparable, yet with occasional white laminae. A third, very small unit between 1253 cm and 1270 cm shows variations in thickness. A few shell fragments were discovered in all three sections.

Clay, disturbed:

The units referred to as “Clay, disturbed” show laminations that are thinly bedded, heavily disturbed, undulated and partly tilted. A major amount of these units lies between 1140 cm and 1250 cm. The contact between the laminae is blurred, and there are several distinct colour changes, from 10 Y 3/1 to 7,5 Y 5/1. The disturbed bedding may be due to bioturbation during deposition. A similar segment occurs between 1270 and 1300 cm depth, with several white layers more than 2 cm thick. Two more small segments of disturbed clay appear at 995 to 1019 cm and 1055 cm to 1083 cm depth, the latter with some ferrous lenses. Their layers are also tilted, in contrast to the adjacent segments. Tilting therefore, must have taken place during sedimentation and not during the coring.

Sapropel:

This is the main unit of the bottommost part of the core, from 1300 cm to 1470 cm depth, with continuous lamination, interrupted by a few white bands. It consists of a mixture of organic material and clay distinct from the adjacent units. Aside from the white bands, its colours range from 7,5 Y 2/2 to 4/3.

Bedrock:

The small unit referred to as bedrock consists of a debris of mollusc shell fragments, heavily weathered pieces of sandstone and ferrous rocks. It comprises the section from 1470 cm to 1500 cm, marking the bottom of the core.

Gap/Disturbance:

While coring, a major gap occurred at 600 cm to 650 cm depth due to the massive changing sediment properties. Several disturbances are spread over the core due to the coring technique, which holds several difficulties such as falling sediment debris inside the borehole.

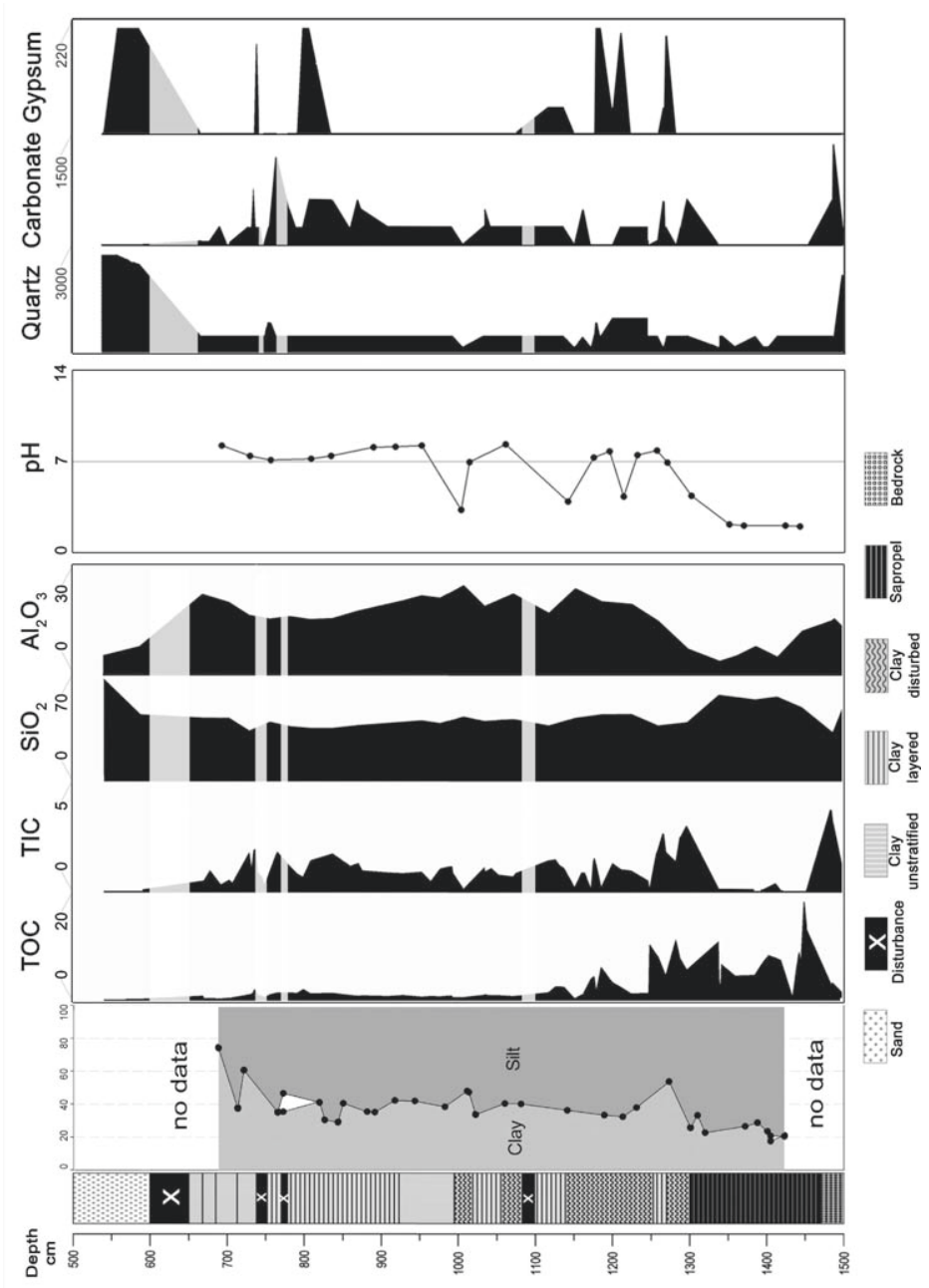

Figure 15 Main properties of the 2005 core (5-15 m depth)

6.1.3 Mineralogy

Quartz (silicon dioxide) and clay minerals (aluminium phyllosilicates), most likely kaolinite, are the essential elements of the mineralogical composition and are ubiquitously present. The amounts of quartz and clay sum up to more than 60% (semi quantitative) in mean throughout the core. Other abounding minerals, in a lesser amount, are pyrite and halite. Carbonates are widely spread throughout the core. They show a very heterogeneous composition of calcite, dolomite, aragonite and low-Mg calcite (Figure 16). This may indicate the simultaneous occurrence of allochthonous and autochthonous carbonates followed by biogenic alteration of the carbonates (cf. chapter 6.2.) The maximum concentration of carbonates can be found at depths of 764 cm (38 %) and 1280 cm to 1295 cm (>30 %). Evaporites, such as the sulphate minerals glauberite, syngenite and thenardite, show maximum values in the upper part of the core, deposited after the present hyperarid climate had set in. Gypsum occurs in several segments, with a maximum peak in the upper part, but other strong peaks at 11 to 12 m depth. Sylvine (KCl), another evaporitic mineral, is only deposited in the lowest segment, from 1300 to about 1450 cm depth. Traces of muscovite occur at various depths throughout the core.

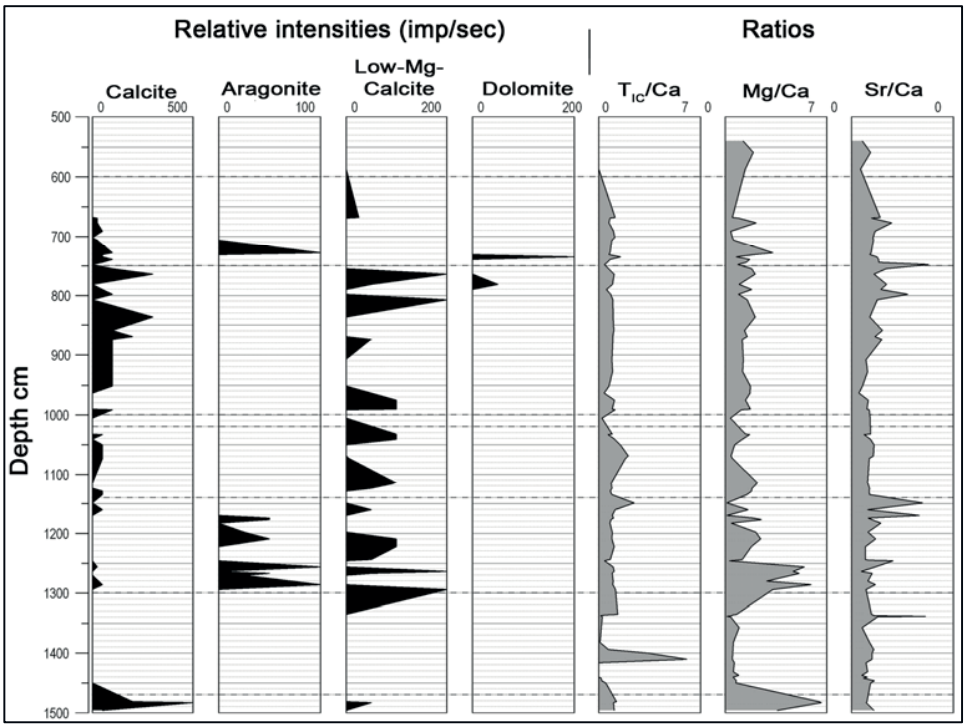

Figure 16 Distribution of carbonates and mole ratios of determining chemical features

6.1.4 Geochemistry

6.1.4.1 ICP-OES

Performing normative calculations on the ICP-OES results (BOYLE, 2002), the ascertained elements add up to about 30 % in mean. With the addition of total carbon (TC), the mean value ascends to about 34 %, leaving about 60 % unaccounted. The essential elements of the remaining part are silicon and aluminium, compared to the mineralogical analyses (quartz and clay). The results of additional XRF analyses on fuse tablets confirm the calculations. Figure 17 shows the distribution of silicon and aluminium and derived ratios in detail. SiO_2 (silicon dioxide or silica) is the major component with a mean value of 41.89 % (n=30) and a maximum of 66.34 % in the sandy unit. Al_2O_3 (aluminium oxide) shows a maximum value of 25.6 % at 1005 cm, with a mean of 15.79 % (n=30). The increase of silica in the lower parts of the core and the associated depletion of Al_2O_3 (clay) is notable. The mole ratio of Si/Al affirms the result and shows maximum values below 1300 cm as well as a very constant ratio of about 1.6. The mole ratio of Na + K/Al, also referred to as salinization ratio, shows a pattern similar to the Si/Al ratio. Potassium (K) and sodium (Na), both parts of the alkali metals, represent major evaporites in the core, halite (NaCl) and sylvine (KCl) as well as thenardite (Na_2SO_4). The ratio of Fe/Mn is a strong indicator of reducing environments (DAVISON, 1993) and shows several maximum peaks in the lower parts of the core.

The weight percentage (wt-%) maximum of sulphur amounts 31.52 % and can be found at the bottom of the core at 1496 cm, with a mean assay of 14.84 %. The maximum amount of iron is again found in the lowest segment, where some heavily weathered bedrock fragments have been discovered.

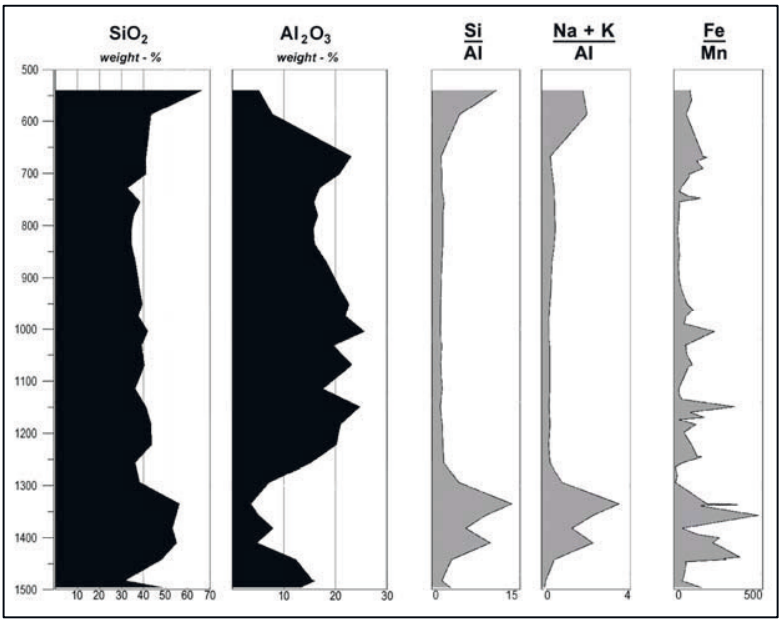

Figure 17 SiO_2 + Al_2O_3 distribution, mole ratios

The average amount of iron throughout the core is 5.7 wt-%. Calcium is spread all over the core but with differing values. Remains of gastropod shells lead to the calcium maximum of 14.74 wt-% at 1483 cm depth, immediately followed by a decline to below 1 % for the following 1.5 metres. Striking is the high correlation (0.92) of inorganic carbon (TIC) and calcium throughout the core due to the amount of carbonates, although both values show high coefficients of variation (cv-%) from 80 to 100 %.

6.1.4.2 Geoscanner (XRF)

The split core surfaces were analysed using a high resolution ED-XRF (Energy dispersive X-ray spectroscopy), also referred to as Geoscanner. The resulting data are referred to as "relative intensities", as they do not represent a comparable dimension and are valid for the analysed core section respectively. Due to the small range of detectable elements (cf. chapter 5.2.2), only a few provide convenient results. Figure 18 shows four exemplary elements, obtained from the core sections from 500 to 1500 centimetres depth, with decreasing intensities from left to right.

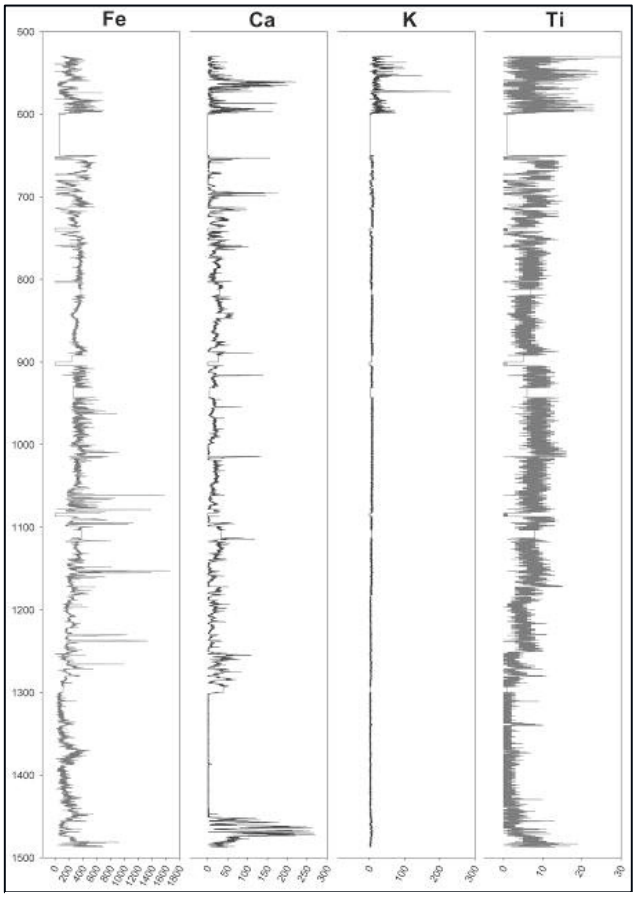

Figure 18 Selected results from the Geoscanner analysis

The results of iron, calcium, potassium and titanium show obviously dissimilar distributions patterns along the core. Iron shows rather homogeneous increased values, with only a few maxima in the mid section. According the calcium distribution, the lack of calcium in the bottom section is striking. Between 1450 and 1300 centimetres, fairly no signal of calcium is detected. Potassium shows its maximum values in the top section, due to oppressing effects by other elements as they show stronger signals in the lower sections. The signal of titanium is very weak and its pattern shows strong signals of data noise due to the topographical effects of the investigated sediment.

Due to these massive disturbances by the sediments roughness when measuring the 70 cm core segments, four representative sections of 8 cm each were individually prepared for the measurement. As two sections showed massive disturbances due to structural instabilities, only two sections are visualized for comparison. Figure 19 shows the results from 782-790 centimetres depth. The investigated elements show decreasing maximum intensities from left to right, mostly caused by their position in the periodic table of elements (cf. chapter 5.2.2). Iron and calcium show a distinct opposed distribution as local minima and maxima of both elements coincide. Titanium and manganese correlate with the iron distribution, whereas sulphur and strontium correlate with calcium.

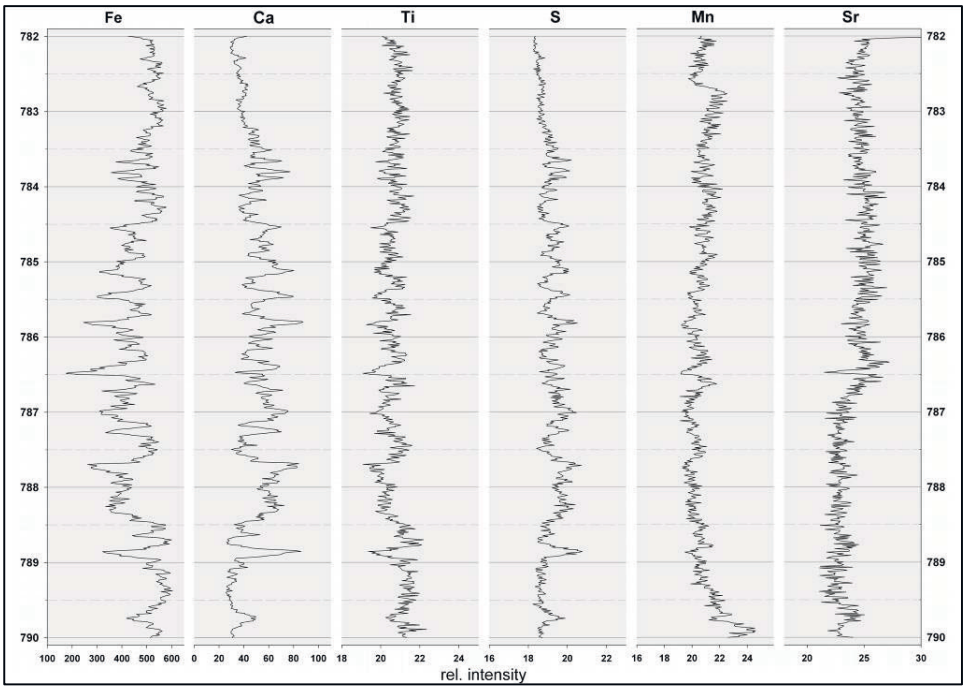

Figure 19 Main results obtained from a XRF scan of the 782-790 cm section

Figure 17 shows the results of segment 1401-1409 cm. The investigated elements show different intensities, only partly determined by atomic features. Compared to the preceding segment, iron shows doubled intensities of about 10,000 and the values of titanium and manganese are clearly increased, whereas calcium and sulphur show similar values. The most striking variation can be found

in the frequency of reoccurring minima or maxima. The distances between local maxima/minima are on a sub millimetre scale for the 1401-1409 cm section, in section 782-790 cm these distances amount to several millimetres. In addition, the contrary distribution of calcium and iron cannot be affirmed for the bottom section, as the calcium content in this depth is generally lower than above.

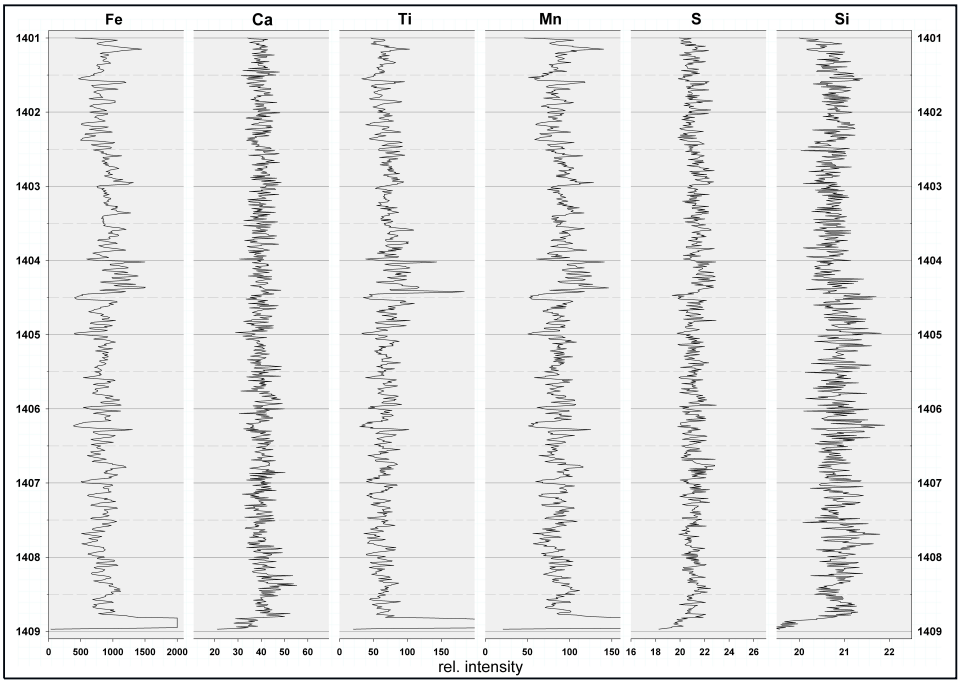

Figure 20 Main results obtained from a XRF scan of the 1401-1409 cm section

Virtually as a by-product of the XRF-Geoscanner analysis, monochrome images are produced, revealing the sedimentation pattern of the investigated elements. Figure 21 shows a compilation of images from the prepared 8-centimetres sections in three depths indicating changing sedimentation conditions. Due to the limitations of detectable elements by the analysis, only the elements representing the strongest signals are presented. The analysed elements appear bright, as they show high reflectance. The bottom part of the middle section shows a disturbance due to the elaborate preparation procedure.

Iron is an ideal element for the investigation due to its position in the periodic table of elements. At 782-790 cm and 1042-1050 cm it shows a ubiquitous appearance as it appears to be more or less regularly distributed. Within the deepest section, 1401-1409 cm, iron appears in a different distribution pattern. An apparent alternation of iron bearing layers and layers without any iron is visible. The enhancement of the other element's signals reveals the presence of sulphur within the iron layers and the widespread distribution of silicon.

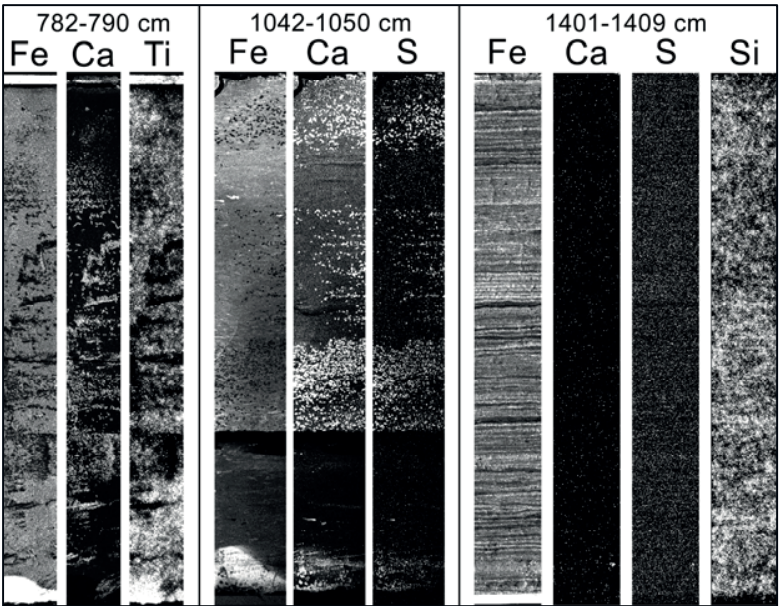

Figure 21 Comparison of XRF images, analysed elements appear bright (high reflectance)

Calcium appears at 782-790 cm and 1042-1050 cm with an irregular pattern. At 1042-1050 cm calcium is also present in larger amounts in the overall setting, indicated by the brighter background. The obvious correlation of the calcium spots with sulphur in this segment indicates the irregular appearance of gypsum. In contrast, the less intense background signal of calcium indicates a second calcium mineral, most likely calcite.

6.1.5 Biological Indicators

6.1.5.1 Estimation of biogenic silica (BSi)

Biogenic silica (BSi) is incorporated by diatoms, using soluted silicic acid from the lake water. Especially in (hyper-)saline environments, diatoms can build up huge populations, leading to an increase in biogenic silica. The ratio of Si/Al can provide information on the amount of diatoms and biogenic silica, titanium and/or aluminium work as a constant value for detritus input (PEINERUD et al., 2001). In order to perform BSi calculations on a sediment record, it is required to first obtain a

stable signal for the detritus estimation. If a high correlation of silica and aluminium exists for sufficient samples and if the ratio of Si to Al remains at a quite constant level, the elements may reflect the external (clastic or allogenic) components within the deposited sediment and only little amounts, if any, are contributed by endogenic or authigenic processes (JONES & BOWSER, 1978).

The stable ratio of silica and aluminium (Figure 17) in the section from 668 to 1256 centimetres indicates a very constant detrital input, which is consequently used as the reference segment for the background information. The mean ratio of this section is 1.68 (n=19) and as the standard deviation amounts to 0.12 a generous adjustment of 20% is performed, resulting in a factor of 1.34. To control the calculation, an additional estimation is performed based on the Si/Ti ratio.

The formulas for the performed calculations are:

based on aluminium	BSi-Al	[mol/100g] = Si [mol/100 g] – (1.34* Al [mol/100 g])
	BSi-Al	[mol/100g] *60.9 [molar mass of SiO_2] = BSi-Al [w-%]
based on titanium	BSi-Ti	[mol/100g] = Si [mol/100 g] – (54.5* Ti [mol/100 g])
	BSi-Ti	[mol/100g] *60.9 [molar mass of SiO_2] = BSi-Ti [w-%]

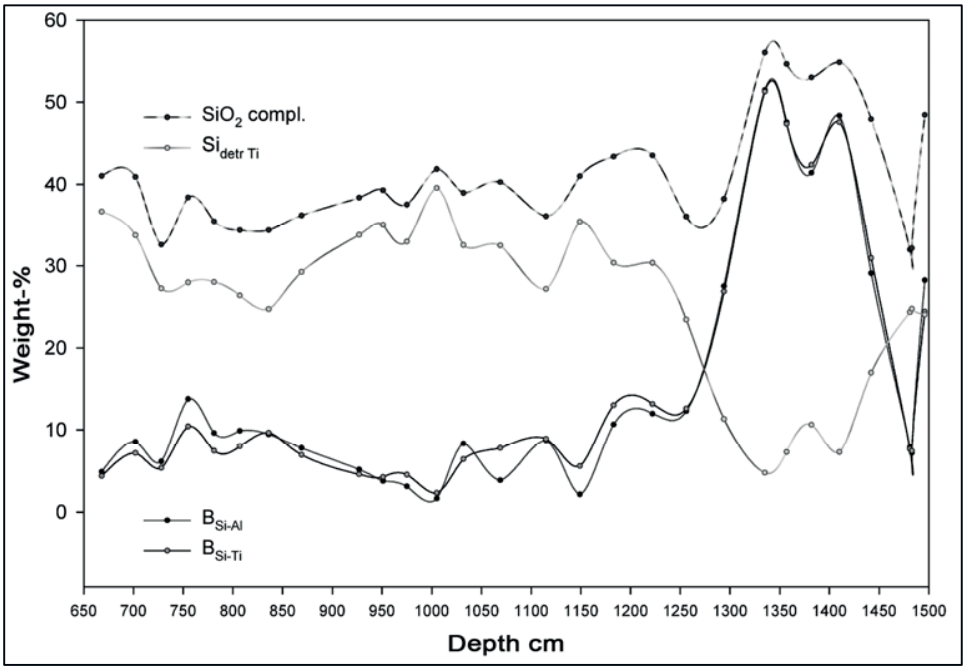

Figure 22 BSi estimations based on aluminium and titanium

The results of both estimations are very similar (Figure 22) showing only minor differences in the upper sections of the core and indicating an individual regime in the bottom section (1300-1450). The deepest parts of the core seem to contain high amounts of biogenic silica, due to the decrease in the total aluminium percentage and the associated increase of silica. The remaining (detrital)

compartments of silicon (calculated on the titanium basis = $Si_{detr\ Ti}$) show only little values of 10 % or below in the bottommost section, whereas in the upper section the values alternate about 30 %.

6.1.5.2 Diatoms

With microfossil investigations not completed yet, the results presented in this chapter originate in past publications as well as in personal communication with the processor of diatom examination, Prof. Dr. R. BAUMHAUER, Wuerzburg University. A comprehensive study on the Early to Mid Holocene microfossil succession within the Seggedim depression will be published elsewhere.

Preceded results (550-750 cm depth)

The results of the preliminary corings regarding the diatom assemblages are visualized in Figure 23. In conclusion, the investigation revealed the rapid development from a stable freshwater lake (Ca+Mg carbonate type) to a sebkha as indicated by the fundamental change of the diatom assemblage at about 670 cm. There, the increasing compartments of the oligo- to mesohaline (favouring low- to middle salinity) taxa of Campylodiscus clypeus as well as the oligohaline Epithemia zebra point out to the development of a saline (alkaline) water body (BAUMHAUER et al., 2004).

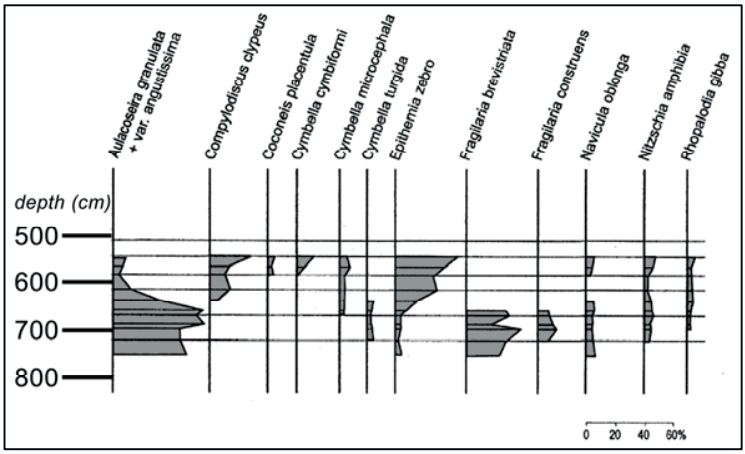

Figure 23 Diatom assemblage of the Seggedim coring (BAUMHAUER 1991, modified)

Preliminary results - Unit I (1300 – 1470 cm)

The diatom taxa of Unit I are determined by exceptionally alike spectra. Moreover, numerous valves are corroded and broken. Especially the corrosion features indicate processes of dissolving and decomposition in extreme environmental settings (BAUMHAUER, 1986; GASSE, 1987; NOËL, 1986; PAQUET, 1987). Although the investigated corrosion phenomena may influence the palaeoecological interpretation, the characteristic spectra found within the basal core section (1440-1470 cm, Table 7) indicate reconstructible palaeolimnic conditions.

Table 6 Diatom assemblage of the basal section 1440-1470 cm

> 60 %	*Rhopalodia gibberula*
2-5 %	*Anomoeoneis spaerophora*
4-6 %	*Epithemia adnata*
1-2 %	*Gomphonema constrictum*
1-5 %	*Navicula sp.*
fragments	*Campylodiscus clypeus*

Euplanktonic diatoms determine the upper core section (1300-1370 cm) of Unit I (Table 8). The absent Aulacoseira granulata var. angustissima excluded, the identical taxa appear in this section as in the underlying one (1370-1440 cm).

Table 7 Diatom assemblage of the upper section 1300-1440

> 20 %	*Aulacoseira granulata*	
> 20 %	*Aulacoseira granulata var. angustissima*	
5-20%	*Aulacoseira agassizzii, A. italica,* *Rhopalodia gibberula*	
< 5%	*Achnanthes inflata*	*Diploneis ovalis*
	Amphora ovalis	*Epithemia adnata, E. sorex*
	Anomoeooneis sphaerophora	*Fragilaria construens*
	Caloneis sp.	*Mastogloia elliptica*
	Coconeis placentula	*Navicula oblonga, N. sp.*
	Cyclotella kuetzingiana, C. meneghiniana	*Nitzschia amphibian, N. sp.*
	C. stelligera	*Pinnularia gibba*
	Cymbella cymbiformis, C. sp.	*Rhopalodia gibba*

6.1.5.3 Pollen spectra

With palynological investigations not completed yet, the results presented in this chapter originate in past publications as well as in personal communication with Dr. E. SCHULZ, Wuerzburg University. A comprehensive study on the Holocene vegetation succession within the Seggedim depression will be published elsewhere.

The vegetation inventory did not change significantly during Holocene. The transition to the present hyperarid conditions is generally marked by the tapering of the existing species and the reduction to favourable locations. In the freshwater lake phase, the slopes of the escarpment were presumably covered by an open savanna of the *Acacia-Maerua* type (BAUMHAUER et al., 2009-a). In the lake to sebkha transitional phase, the vegetation cover inside the depression altered to a desert type with predominating wadi vegetation (trees shrubs) and grasses of the *Acacia-Panicum* type. The

surrounding *Phragmite – Typha* reed belt merely appears in a reduced extent so an increasing amount of sediment accumulates within the former lake centre (BAUMHAUER et al., 2009-a).

Referring to E. SCHULZ a continuous dominance of open savannah vegetation (*Acacia-Maerua-Capparis-Panicum*) is visible throughout the core of Seggedim (personal communication, June 2008). Changing contingents of *Salvadora* and *Boscia* shrubs are present as well as local variations of *Typha-Phragmites* reeds or *Amaranthaceae* (*Chenopodiaceae; Salsola, Cormulaca*).

6.1.6 Radiocarbon dating

A total of 21 samples for radiocarbon dating (cf. Table 8) was analysed in the Poznań Radiocarbon Laboratory with accelerator mass spectrometry (AMS). The amount of dates was necessary to provide evidence of the complex sedimentation history of the record. To receive dates from other sources than organic material, radiocarbon has been measured on carbonates. The mineralogical composition revealed singular signals of aragonite at the beginning and the end of the lake phase which are interpreted as remnants of gastropod shells. Because massive contamination by carbonate bedrock could be excluded (cf. Chapter 2.5.1), five samples were analysed for inorganic radiocarbon measurement.

Depth [cm]	Uncalib age [a BP]	±	calBP (0=1950)	±	*Lab. code*	Material
660	6510	40	7420	100	*Poz-19895*	organic sediment
673	6290	40	7222	36	*Poz-24331*	tufa
678	6390	40	7340	120	*Poz-19894*	organic sediment
698	6880	50	7727	51	*Poz-24413*	organic sediment
727	5440	40	6250	80	*Poz-19913*	organic sediment
728	5310	40	6098	69	*Poz-24412*	carbonates (> 300 µm)
728	5370	40	6160	93	*Poz-24411*	carbonates (< 300 µm)
736	5770	40	6580	120	*Poz-19976*	organic sediment
763	5670	35	6460	80	*Poz-19978*	organic sediment
797	6100	40	7010	160	*Poz-19977*	organic sediment
990	6260	40	7200	80	*Poz-17470*	organic sediment
991	6300	40	7230	80	*Poz-17471*	organic sediment
1043	6360	40	7310	100	*Poz-19979*	organic sediment
1184	6170	50	7080	140	*Poz-19914*	organic sediment
1260	5840	50	6649	69	*Poz-24034*	carbonates
1261	5800	40	6600	100	*Poz-19890*	organic sediment
1300	6360	40	7310	100	*Poz-19891*	organic sediment
1375	7390	50	8240	140	*Poz-19915*	organic sediment
1455	8910	50	10050	200	*Poz-19896*	organic sediment
1482	9380	70	10608	85	*Poz-24033*	carbonates
1485	9240	50	10410	180	*Poz-17469*	organic sediment

Table 8 Radiocarbon dates from the 2005 Seggedim coring

6.1.7 OSL dating

Additional sites were sampled for the purpose of OSL-dating by the palaeosoils section within the LIMNOSAHRA project, Prof. Peter Felix-Henningsen and Peter Kornatz from Gießen University. A fossil dune was investigated, located above the scarp edge (UTM: 33Q 0291444 2239278, Lat/Long: 20°14'23,4"N 13°00'12,7,8") showing obvious characteristics of a palaeosoils (e.g. developed Bv

horizon). The profile was excavated at the middle slope section, showing a north-eastern exposition with a concave declination ranging between 5-10°. The sands show an OSL age of 11660 ± 1100 a BP (P. FELIX HENNINGSEN, personal communication, June 2008).

6.1.8 Determination of the main lake stages

Regarding the chemical, mineralogical and macroscopic sedimentological properties of the Seggedim core, six main lake stages or units (Figure 12) have been classified and statistically tested. Some of these stages are consistent with the stratigraphic units (e.g. sapropel and initial lake stage). Figure 22 shows some of the main features of five units in mean percentage with their standard deviations, compared to their total values. The results show distinct differences in their range as well as in their absolute values, used as a validation basis.

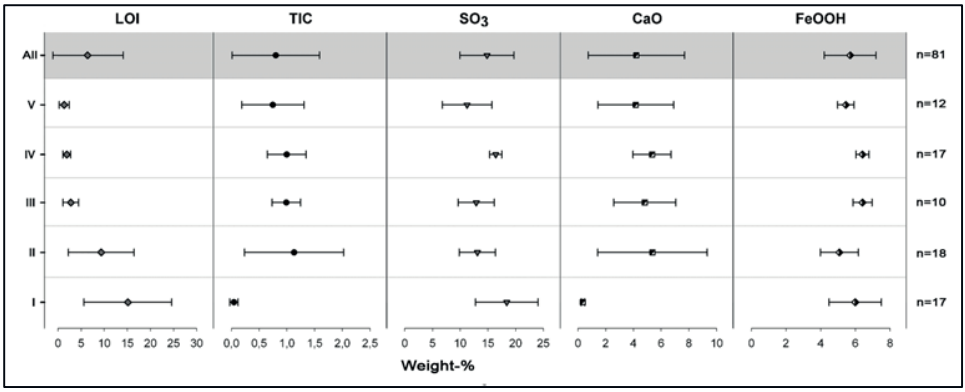

Figure 24 Mean lake stage values and standard deviations of selected oxides

Unit I – Initial Lake Phase (1470-1300 cm)

This sequence is characterized by its high organic carbon content (mean 6.87, n=17) and by its extremely low inorganic carbon content (mean 0.04, n=17). Here, TIC and calcium content are at their lowest (0.4 wt-%) compared to the mean value of the core (4.21 wt-%). The same applies to strontium, which is obviously highly correlated (0.83) with calcium throughout the whole core. Sulphur content is at its maximum (18.4 wt-%). Ph-values are very low and range from 2 (1443 cm) to 4,3 (1302 cm). Pyrite content is constantly at a high level, as is halite. Carbonates do not occur in this unit.

Unit II – Transition Phase (1300-1140 cm)

With massively decreasing LOI-values down to 1 %, the pH-values increase simultaneously. CaO and TIC show maximum values that correspond to changing carbonate peaks. Gypsum occurs in the mineralogical fraction, as well as several halite peaks. Laminated material only occurs at a small sequence from 1270 to 1253 cm. Contrary to the initial lake phase, LOI is low and TIC as well as CaO and carbonates show a maximum peak due to fragments of carbonate shells. In contrast to the

other values, FeOOH content remains stable at an average of 5.08 % (n=18): the lowest average value of iron throughout the core.

Unit III – Freshwater Lake Phase I (1140-1020 cm)

FeOOH, K_2O, MgO and Na_2O show low standard deviations and therefore low coefficients of variation at about 10 % (n=10). Gypsum occurs only in the lower parts in the sequence and vanishes at about 11 m depth, having led to diminishing amounts of CaO and SO_3 and a high positive correlation of them. Corresponding to the decrease of gypsum, pyrite shows minimum qualitative values, whereas halite shows maximum reflections. In comparison to other units, carbonates are present all over the sequence. Fish bones at 1032 cm depth are evidence of life in the lake. Magnesium shows maximum values (2.6 %) with low coefficients of variation of 6.17 %. According to this, carbonate values origin solely in dolomite. TIC and iron show a high negative correlation (-0.81), so that peaks of carbonate result in decreased iron and sulphur values and vice versa. This interrelation results in a negative correlation of CaO and FeOOH (-0.75).

Unit IV – Freshwater Lake Phase II (1000-750 cm)

Sulphur and iron show stable values throughout the sequence, with very low coefficients of variation at about 6 % (n=17). The stable values result in stable signals of pyrite and therefore a constant Fe/S mole ratio at 0.39, very close to pyrites stoichiometric mole ratio of 0.5. This difference and the weak correlation of iron and sulphur of 0.59 are evidence of a deficit of iron, respectively a surplus of sulphur, as based on the pyrite values. The surplus of sulphur increases constantly towards the top of the sequence at 750 cm. TIC and iron show a high negative correlation (-0.81), so peaks of carbonates result in decreased iron and sulphur values and vice versa. This interrelation results in a negative correlation of CaO and FeOOH (-0.75).

Unit V – Transition Phase II (750-650 cm)

All chemical values show very high coefficients of variations and the stratigraphic record is dominated by multiple distinct colour changes.

Unit VI – Sebkha (600–0 cm)

Only three subsamples of this unit have been examined, and therefore there will be no statistical interpretation. Nevertheless, the stratigraphic summary of the coring (Figure 12) shows some of the major traits, such as high content of quartz and evaporites. SO_3 and CaO correspondingly show increasing values, due to the development of sulphates (gypsum, glauberite, thenardite, syngenite). Pyrite and carbonates only appear as traces as do clay minerals. A comprehensive description of the sebkha sedimentation can be found in the preceded studies by BAUMHAUER (e.g., BAUMHAUER, 1986; BAUMHAUER et al., 2004).

6.1.9 Determinations of geochemical mean values

Figure 25 shows a comparative set of chemical data obtained from the Seggedim core. To avoid misinterpretation, the results are visualized dimensionless. Iron data at the bottom, calcium data at the top. The continuous foreground data are derived from linear XRF measurement with the Geoscanner device at the BGR Hannover. They show relative intensities of the investigated elements. As the core had to be analysed in segments and represent bulk values with huge disturbances due to topographic

effects, the maximum values are just of local relevance and cannot be used to determine the quantity of the investigated elements. The background data show the results of the point wise ICP analysis, derived from about 80 subsamples, slices of 1 cm thickness each (cf. chapter 5).

The point wise subsampling of a core is determined by certain factors, such as the sampling interval and the sample size. In this case, slices of 1 centimetres thickness were taken about every 10

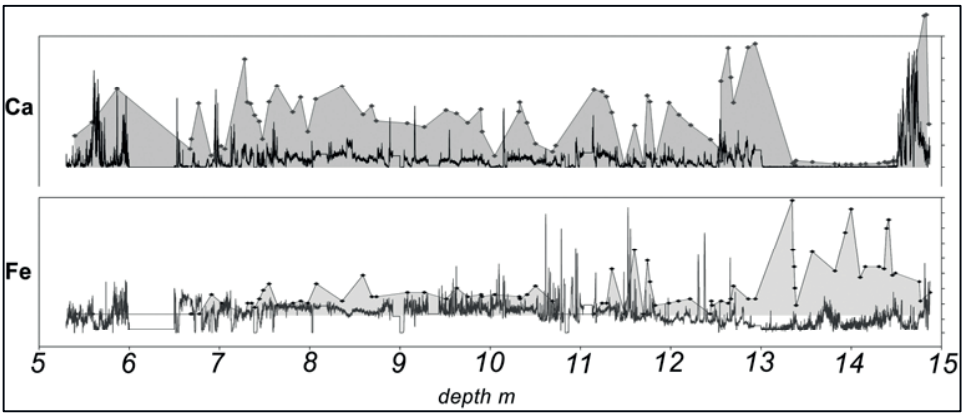

Figure 25 Comparison of point wise (ICP) and total (Geoscanner) chemical analysis

cm. Due to obvious changes in the sedimentary composition (colour, bedding, layer thickness) additional samples were taken in between these intervals, cumulating to 80 subsamples for less than 10 metres. These subsamples were dried and homogenized in a tungsten carbide vibrating cup mill. Small (< 1 cm) variations of the mineralogical and chemical composition cannot be recorded with this method. All results received from this method are considered mean values. In contrast to that, the Geoscanner results show the qualitative distribution of the investigated elements in sub millimetre steps along the whole core. Due to the enormous topographic effects as well as methodical limitations, these values are considered valid only for the particular core section.

Depending on the investigated elements, the results show variations in validity. Some sections show rather good conformities of the methods, e.g. the bottom section of calcium results, others do not show any similar pattern due to the frequency of changing values, e.g. the upper section of Ca-results or several local maxima of iron.

The comparison clearly demonstrates the occurrence of major variations in all geochemical data, the dimension depending on the chosen method. There is yet no way to achieve quantitative results of geochemical and mineralogical measurements with a resolution close to that provided by the so-called Geoscanner. However, as the drawbacks of this method, including the large impact of the sample topography and limited detection range, do not allow quantitative calculations of all main elements, it principally provides useful information in a short time, hardly attainable by “classical” methods.

6.2 Discussion

6.2.1 Age-Depth-Model

Figure 24 shows the distribution of calibrated AMS radiocarbon (^{14}C) dates compared to two conventional uncalibrated dates from the previous coring. The two dates from 6 and 8 metres depth (squares) are uncalibrated conventional radiocarbon dates from a preceded study by Baumhauer (1986).

21 radiocarbon dates were analysed in the Poznan Radiocarbon Laboratory with accelerator mass spectrometry (AMS). The amount of dates was necessary to provide evidence of the complex sedimentation history of the record. For 17 samples, radiocarbon dating was performed on bulk organic matter, revealing a rather chaotic pattern of the upper dates, and interpreted as repeated contamination by translocated organic material.

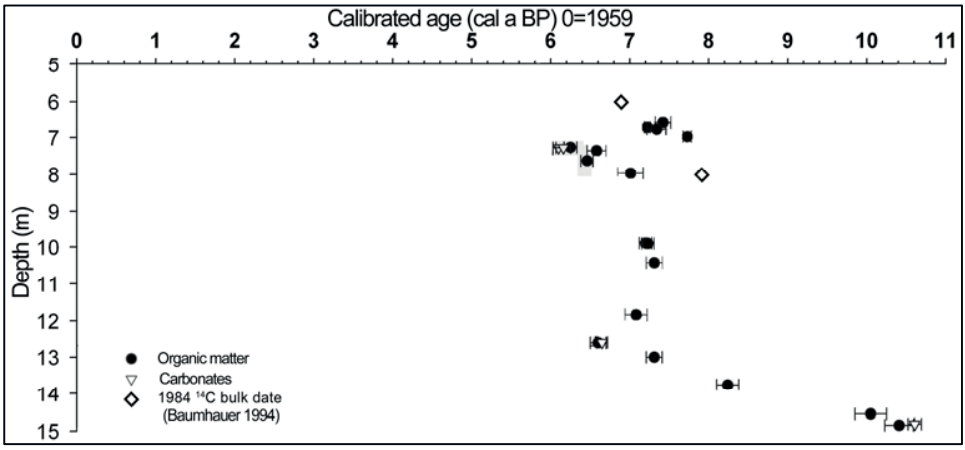

Figure 26 Calibrated radiocarbon dates of the 2005 coring compared to dates from 1984

To receive dates from other sources than organic material, radiocarbon was additionally measured on carbonates. The mineralogical composition revealed singular signals of aragonite at the beginning and the end of the lake phase interpreted as remnants of gastropod shells. Detailed studies on gastropods revealed the reliability of various gastropod taxa for radiocarbon data (Fritz and Poplawski, 1974) especially those of terrestrial snails incorporating aragonite in their shells (Brennan and Quade, 1997, Pigati et al., 2004, Zhou et al. 1999).

When analysing biogenic carbonates by radiocarbon methods, shifts of dates have to be considered, either caused by the contamination of carbon containing groundwater (hardwater effect) or by carbonate bedrock (carbon reservoir effect) (Fontes and Gasse, 1989, Snyder et al., 1994, Zhou et al., 1999). The results show that no nameable hardwater effect contaminated the carbonates. Therefore, it can be assumed that the adjacent radiocarbon dates from the organic material show the true age of the sediment.

The lowermost dated sample was taken from the bottom of the core, close to the bedrock. It places the onset of continuous sedimentation at about 10410 a cal BP ± 180. Radiocarbon dates from within the first stage set the beginnings of the initial lake phase at about 10050 a cal BP ± 200.

Several dates from higher up are evidence of a very low accumulation rate in Unit I. Only about 0.6 mm/a were deposited for over 3000 years, at a very constant rate. Probably this phase has to be extended to cover even more than 4000 years, if the date at 12.61 m depth is included (6.6 ka cal BP). This may be justified by the fact that the accumulation rates of approximately 0.6 mm/a remained the same, even though there had been a change in sedimentary conditions.

The low accumulation rate is evidence of a very low minerogenic input, which might be interpreted as being an indication of very low surface wash in the catchment for several millennia, due to the closed savanna-type vegetation cover inferred from the pollen spectra. The high organic content of the sediment suggests a supporting argument, namely that a closed belt of reed vegetation fringing the lake filtered the surface wash from the adjacent slopes. This could have led to the accumulation of the sediment and the development of sediment banks.

The following sequences (boxed) show rather confusing variations. Starting at 7080 a cal BP ± 140 at 1184 cm depth, all the radiocarbon dates lie within a small range from 7400 a cal BP to 6250 a cal BP and, unlike those from the lower sequence, show no linear distribution. It may be assumed that these variations originate from translocated sediment, originally deposited higher up on the sloping lake bottom during the high-organic sapropel stage. With increasing surface wash and increased sediment input, turbidite movements are likely to have been triggered.

The two dates from 6 and 8 metres depth (squares) are uncalibrated conventional radiocarbon dates from a preceded coring in 1984 by Baumhauer (1986). In a preliminary study of another core from Seggedim (Baumhauer et al., 2004), thin-section analysis revealed the presence of large amounts of charcoal. Such fragments can be preserved unaltered in the sediment, whereas other freshly deposited organic matter will be decomposed almost immediately under oxic conditions. Most likely, such surviving charcoal flakes from burnt grass are the source of the improper dates from 1984 and the 2005 coring. In addition, the time of the frequently discussed fires can be localized in a relatively short period from 7500 to 6200 a cal BP, but can be extended to the beginning of the Initial Phase due to charcoal presence at the lowermost parts of the core.

To construct a simple sedimentation age-depth model it is necessary to ignore changes in bulk density, although they would give information about any postsedimentary compression. Regarding simply the turn points of the sedimentation phases, it is possible to calculate mean accumulation rates that provide an idea of the sedimentation dynamics during that time.

The results presented in Figure 25 evidences that no nameable hardwater effect contaminated the carbonates from the bottom section that were dated. Therefore, it can be assumed that the adjacent radiocarbon dates from the organic material can be considered to show the true age of the sediment. The initial phase shows a continuous mean sedimentation rate of about 0.06 mm/a. It also indicates the stability of this lake stage as the linear accumulation rate shows no significant variation and therefore a continuous sedimentation.

The change from sapropel to lake sedimentation is determined by a massive increase in the mean sedimentation rate from 0.06 mm/a to about 10 mm/a. By the distinctive evidence of huge rock fragments in the upper parts of the lake phase, it can be concluded, that the sedimentation dynamics increased towards the end of the lake phase.

One striking feature is the age of the translocated material (Figure 26). The more sediment is translocated, the older these sediments get (vaguely). This indicates a relatively steady erosion of already deposited material. Consequently, this material may originate in sediment banks marking the maximum lake level. With a decreasing water table, the sediment banks desiccate and the material erodes. In process of time, the more material is excavated, the older the truncated layers (Meyers & Lallier-Vergés, 1999).

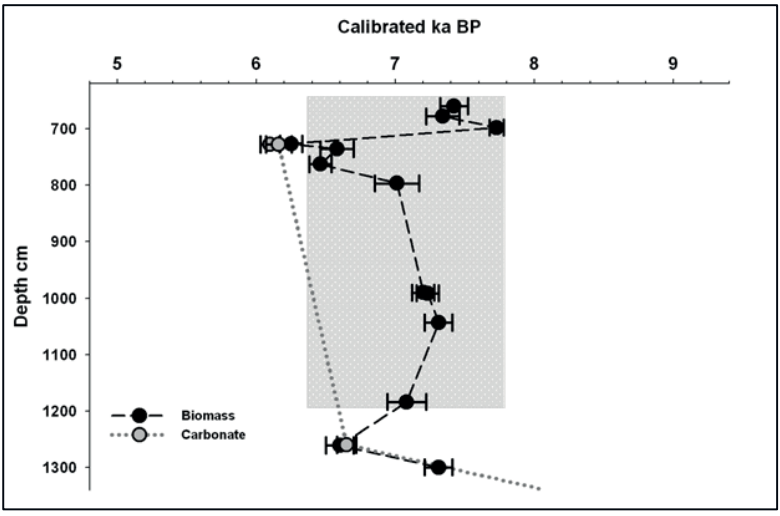

Figure 27 Radiocarbon dates from the bottom core section

The seven dates (carbonate dates included) from the lowermost part of the core appear to be reliable. Those ages from the upper section, as well as the earlier ones published by Baumhauer (1986) and Baumhauer et al. (2004), seem to be the result of intermixture by translocation of sediments of various ages. As the sediment of the sapropel stage contains huge amounts of organic material, it can be concluded, that these deposits in this core section show the true age of the sediment.

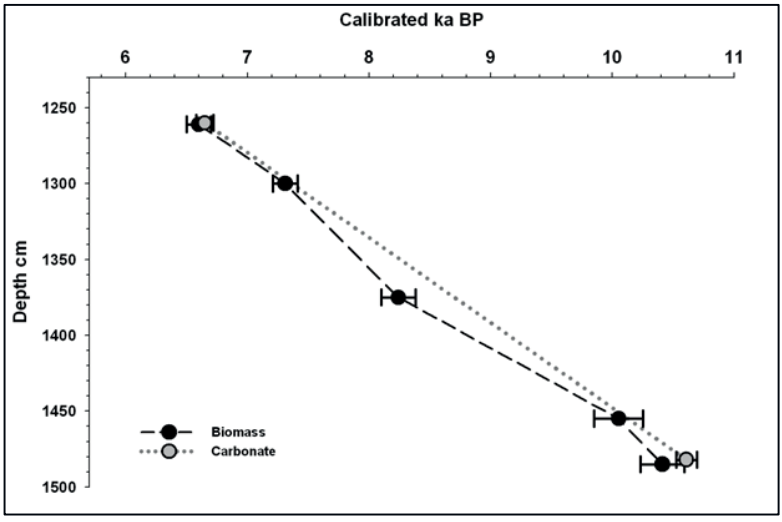

Figure 28 Radiocarbon dates from the mid core section

6.2.2 Conditions of the initial lake phase

The lake phase referred to as initial lake phase, Unit I or swamp is different in many ways from the other ones (cf. Figure 22). It shows high organic carbon content and low pH-values as well as extremely low content of calcium and a total lack of carbonates. The "carbon pump", which has been described by DEAN (1999), is a suitable model for describing the sedimentary conditions during this initial lake phase. The decomposition of a high amount of organic detritus in a hypolimnion will lead to a high oxygen demand and thus to anoxic conditions. CO_2 will be produced in high amounts due to this decomposition, in turn leading to decreasing pH-values. CO_2 production and the decreasing pH-value will cause the destruction of any carbonate remains.

The high values of SiO_2 and the minimum values of Al_2O_3 (clay) in the sapropel stage (Figure 13) originate either in a massive increase in aeolian deposited sand (quartz) or in high populations of diatoms, as indicated by the estimations on biogenic silica (BSi). The texture characteristics of the sediment indicate the latter as well as the initial investigations of the diatom assemblage revealed the presence of large amounts of diatoms that are partly corroded and broken.

The fine, undisturbed laminae in this segment suggest a lifeless lake bottom sealed by a certain depth of water, as the preservation of the organic content can only have been possible under anoxic conditions (SAARNISTO, 1987). This is supported by the high ratio of Fe/Mn, a strong indicator of reducing environments (DAVISON, 1993), which shows several maximum peaks in this segment (Figure 13).

Within this section, XRF images (1401-1409 cm) also indicate a sedimentation mode that differs from the subsequent phases. An apparent alternation of iron bearing layers and layers without any iron is visible. The enhancement of the other element's signals reveals the presence of sulphur within the iron layers and the widespread distribution of silicon. The regularity of the layers implies a reoccurring event of iron deposition, most likely due to pronounced seasonality.

The maximum values of the salinization ratio originate in the unique occurrence of KCl in this segment and the characteristically constant content of halite, which supports the assumption of a strong halocline. As no other evaporitic minerals appear at this depth, sylvine and halite may have originated by solution from the underlying sandstone.

The diatom taxa indicate a shallow, swamp like lake structure, with pronounced and short-term alternations of water chemistry. However, these aquatic regimes do not appear uniform but alternate between Na-carbonate-bicarbonate waters and a palaeomilieu of increased chloride and/or sulphate compartments (BAUDRIMONT, 1974; EHRLICH & DOR, 1985; GASSE, 1986; RICHARDSON et al., 1978). Particularly, the epiphytic and, according to GASSE (GASSE, 1987) explicit euryhaline taxa of *Rhopalodia gibberula* and *Anomoeoneis* as well as *Campylodiscus*, which is presently found inside oligo- to mesohaline shallow and small scale lakes of the Sahara, indicate strong alkaline waters. Euplanktonic diatoms determine the upper core section (1300-1370 cm) of Unit I (Table 8). The absent *Aulacoseira granulata var. angustissima* excluded, the identical taxa appear in this section as in the underlying one (1370-1440 cm). The high amount of *Aulacoseira* as well as *Cyclotella spp.*, the periphytic *Fragilaria ulna*-, *Epithemia adnata*-, *Rhopalodia gibba*- species and a number of freshwater periphytes (*Amphora ovalis*, *Nitzschia amphibia*) indicate a wide spaced but rather shallow water body with numerous makrophytes (GASSE, 1987). This socialisation of species is ubiquitously found in present day shallow lakes and swamps of the African tropics (cf. e.g. BAUDRIMONT, 1974; PATRICK, 1970; TALLING, 1976) and characterizes low alkaline waters with a mean pH value of 7-8.5 within the carbonate-bicarbonate type (GASSE, 1986; GASSE, 1987).

The association of partly very diverse diatom species not only in vertical but also lateral (within a sample) direction is striking, obviously not according to the position within the fringes of a palaeolake. Moreover, it has to be suggested, that the presence of mermomictic lakes is more likely

than presumed before. Subsequently, the inevitable ability of the diverse diatom taxa for the indication of palaeoecological conditions in regards of spatial and temporal oscillations in water charge and water chemistry has to be questioned. The implementation of meromictic conditions is imaginable by the input of freshwater into an alkaline milieu, which would cause stratification within the water body with diverse ecological conditions inside the water column, reflecting in the associated diatom spectrum within the investigated sediment. The plausibility for the development of meromictic lakes is visible in a shallow groundwater lake at the Kaouar area, where a chemocline developed at 23 cm depth within a water column of 40-60 cm deepness. This persistent meromixis is considered to develop by permanent groundwater charge (SCHULTZE et al., 1990). The underlying layer, also referred to as monimolimnion (or monomolimnion), is considered to consist of oligo- to metahaline waters (GASSE, 1987). When considering holomictic lakes, the diverse diatom taxa would indicate enormous instability of the water body in temporal as well as in spatial extend, without any information provided of individual hydrological cycles, i.e. periodicity.

The investigation of the pollen spectrum reveals the presence of remote vegetation units in the bottom section; the evidencing pollen grains followed the predominant wind patterns. The bottom section from 15 to 12.45 metres is dominated by northern vegetation units (*Alnus, Pinus, Olea, Ephedra, Quercus, Betula Artemisia*) also referred to as mediterranean vegetation.

It seems likely that this initial and very stable lake phase was enabled by groundwater discharge from a salt-containing marine aquifer within the Emi Bao formation (BAUMHAUER, 1986) and additional freshwater input by precipitation. The saltworks not far from the coring site and freshwater wells right next to it indicate how complicated - and yet not understood - the hydrogeology in this depression is. There is as yet no way to estimate the share of inflowing salt containing groundwater during the initial lake phase.

6.2.3 Sedimentation and environmental conditions of the subsequent phases

With reference to the age-depth model (Chapter 6.2.1), the subsequent phases appear to have been deposited in a very short time (7500 to 6200 a cal BP). Consequently, the evidences obtained from these sediments are subsumed in this chapter.

Unit II – Transition Phase (1300-1140 cm):

This unit shows rather unstable conditions. Numerous sediment-colour changes and undulated sediment layers support the assumption of dynamically changing lake conditions. Beginning at 12.45 m there is evidence of a balance of the northern and southern (*Securinega, Celtis, Grewia, Combretum Anogeissus)* remote vegetation units. The alternation of the remote vegetation units exists to the present day. A special feature of the vegetation succession in the Kaouar-Djado-Mangueni area is the overall presence of fires. High compartments of charcoal are preserved in the coring of Seggedim; reaching from the bottom section to the freshwater-sebkha transition, mainly consisting of grass taxa (E. Schulz, personal communication, June 2008). A continuous high impact of achab flora (ephemeral vegetation) is evidenced for the area. Some specimen of shrubs and trees (*Ziziphus, Salvadora*, poss. *Grewia* and *Commiphora*) have presumably been preserved being sheltered by rocks, although the environmental setting changed to their disadvantage.

Unit III – Freshwater Lake Phase I (1140-1020 cm):

Compared to the underlying units, this sequence appears to be rather stable, although sedimentation conditions must have changed, as appears from the stratigraphic record. Indicated by

mineralogical and geochemical evidence, there was a time of transition from the stable sapropel stage to a sequence of unstable lake stages showing huge variations in all the attributes investigated. One particular feature of this segment is the occurrence of fish bones at 1032 cm that prove the existence of an ecosystem teeming with life. Referring to the XRF images at 1042-1050 cm, calcium is present in larger amounts in the overall setting, indicated by the brighter background. The obvious correlation of the calcium spots with sulphur in this segment indicates the irregular appearance of gypsum. In contrast, the less intense background signal of calcium indicates a second calcium mineral, most likely calcite. Calcium also appears at 782-790 cm and 1042-1050 cm with an irregular pattern. The brightest spots appear to be debris as they show no regular pattern and build clusters.

The overall magnetic susceptibility maximum values are found in the section between 1000 to 1250 centimetres, where turbulent layers of clay indicate increased seafloor dynamics. These values can be considered to originate in ferrimagnetism originating in secondary minerals (Dearing, 1994). Whether they originate in bacterial activity, traces of nearby fires or developing iron sulphides is a point of discussion.

Unit IV – Freshwater Lake Phase II (1000-750 cm):

Iron oxides found in the section from 750 to 1000 cm are believed to originate in the shore area of the lake (Baumhauer et al., 2009-a), similar to the proposed development of lake ore deposits (Felix-Henningsen, 2004). Subsequently, a dual sedimentary environment is assumed, comprising of the deeper lake area (profundal) and the lake fringes (littoral). The shallow littoral is considered a place of oxic conditions and the formation of iron III oxides. The deeper profundal is dominated by anoxic and acid conditions, where only by coatings of algae or bacteria, the iron oxides were sheltered from reduction.

Unit V – Transition Phase II (750-650 cm):

The sediments of this period represent the transition from a freshwater lake to a sebkha environment. Just like the other transition phase, this is a very unstable sequence, indicating major changes in the environment. No laminations appear throughout this unit, which also shows that there has not been a stable phase of calm and undisturbed sedimentation such as in Unit I.

Unit VI – Sebkha (600–0 cm):

As the sebkha sediments (500-600 cm) and the upper section of the unstratified clay (650-710 cm) show increased susceptibility values above 100 κ, a general high amount of magnetisable material in the catchment area can be considered.

6.2.4 Carbonates – distribution and origin

Figure 16 shows the heterogeneous distribution of carbonates throughout the core. So far it has been assumed that there are no carbonatic rocks in the Seggedim area (FAURE, 1966). Consequently, and due to the different conditions under which aragonite and dolomite would have formed (cf. chapter 3.3), their presence in the sequence may only be explained by aeolian input.

The Mg/Ca mole ratio is a good indicator of changes in carbonate distribution. It shows two large peaks in the deeper parts of the core, but only the one at 12.50 m coincides with aragonite or low-Mg-calcite. Due to the large amounts of calcite in the upper parts of the core, the ratio remains low. The

mole ratio of Sr/Ca is commonly used as an indicator of palaeosalinity (GASSE et al., 1987; GOSCHIN, 1988; HOELZMANN et al., 2000). The authors state that a Sr/Ca mole ratio above 0.003 is indicative of increased salinity. This threshold value is not exceeded throughout the core, although initial investigations on microfossils indicate occasional oligo- to mesohaline conditions, presumably associated with meromixis. Consequently, the ratio of Sr/Ca is not appropriate to indicate palaeosalinity within this sediment archive.

Comparing the amounts of total inorganic carbon (TIC) and calcium, the values are quite constant. Only in the sapropel stage, where the calcium content has decreased due to the low pH value, the mole ratio by far exceeds the stoichiometric ideal of 1. Other fluctuations will be due to changing calcium content throughout the core.

As to the origin and the mineralogical composition of the carbonates (Table 9), several fragments from transition phase II create some problems. The largest one is a massive piece, about 7 cm long and found in 718 cm depth, consisting of dark dolomitic carbonate rock and coated by brighter solid crust of most likely biogenic origin.

This is the first evidence of any carbonate rock in this area, calling for further investigations. FAURE (1966), who studied the geology of the Emi Bao and Seggedim formations, did not report any carbonate strata from the catchment. A second piece (673 cm depth) from the core consists of calcite and aragonite with a calcium content of nearly 30 %, and thus a $CaCO_3$ content of more than 50 %. This material seems to be of biogenic origin, like the coating of the larger piece.

The unusual carbonate composition may best be explained by the transformation of allochthonous carbonate from the catchment area, most probably dolomite, to aragonite by biogenic activity (e.g. terrestrial gastropods) and the regular weathering of primary carbonates to calcite within the water body. Additionally, the analysis of the Geoscanner images reveals the frequent precipitation of calcium as debris at 782-790 cm depth. At 1042-1050 cm depth, the mineralogical composition shows low-Mg-calcite and gypsum both precipitated as debris. This supports the assumption of biogenic calcite precipitati

Table 9 Mineralogical composition of rock fragments

Depth cm	Quartz	Kaolinite	Dolomite	Aragonite	Calcite	Halite	Pyrite	Anhydrite	Gypsum
673	12			28	60				
680	12							25	63
700	9	6	83				3		
718	7		93						
810	16		84						
1380	46					35	19		

Weight Percentages (Semi-Quant.)

6.3 Conclusion

The coring from 2005 has produced some new evidence and has helped to extend understanding of the landscape history of Seggedim. The duration of the lake stages has not yet been determined precisely, because of the irregularities in the sequence of radiocarbon dates. Based on an earlier coring, the transition from freshwater to sebkha conditions had been assumed to be further back in time. The new and more reliable dating, however, now indicates a somewhat longer existence for the Early Holocene freshwater lake, to at least about 5310 ± 40 BP (uncalibrated, 728 cm depth; corr. 6098 cal a BP), rather than 6850 ± 345 BP (600 cm depth; 1984 bulk date). Additional radiocarbon ages from biogenic carbonates have validated some of the dating results obtained from bulk organic matter and have set up a framework for the reconstruction of palaeoenvironmental conditions within the Seggedim basin (Figure 29). This diagram shows the radiocarbon dating results, the corresponding location within the core and the stages of development that have been derived.

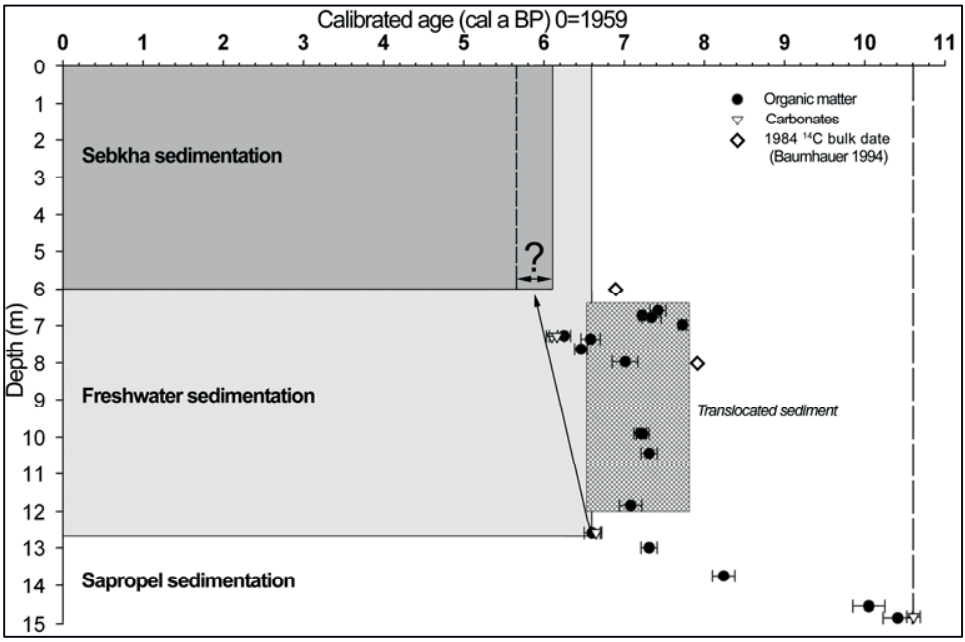

Figure 29 Lake stages and corresponding radiocarbon dating

An initial swamp environment came into existence in the Early Holocene and continued for approximately 4000 years. No evidence has been found of the previously assumed Pleistocene lake stages. A high organic content, with organic fragments partially preserved due to extreme reducing conditions, together with very low accumulation rates within the sediment, are characteristic of the sapropel environment. The investigation of the diatom assemblages indicates a meromictic lake, with an anoxic layer of oligo- to metahaline waters at the bottom (monomolimnion) and significantly less haline waters on top, originating in freshwater inflow. The botanical record reveals the presence of

Saharan savannah vegetation in the area, which may have been the main cause of diminished surface wash, but a belt of reed vegetation may additionally have filtered any surface wash. Radiocarbon dates set the beginning of the stage at about 10.6 ka cal BP, with an exceptionally stable regime until 6.6 ka cal BP (at 12.6 metres depth), when a major change in the sedimentation regime of the basin is recorded in the core. There was a time of transition from the stable sapropel stage to a sequence of freshwater lake stages, indicated by mineralogical and geochemical evidence and showing considerable changes in all the attributes investigated. The distinct increase in Al_2O_3 indicates an increasing input of detritus, due to enhanced surface wash or to a reduction of reed bed vegetation. Variations in the thickness and appearance of layers confirm variations in sedimentation, most likely reflecting changes in precipitation. The occasional occurrence of gypsum suggests phases of desiccation. The discrepancies in the sequence of radiocarbon dates may best be explained by underwater sliding processes within the deposits. Variations between the freshwater lake stages may reflect variations in the amount and seasonality of precipitation. Due to the lack of datable material in the upper core section, the termination of the lake stage and the onset of the subsequent sebkha stage cannot be determined precisely, but can be narrowed to a period around 6 ka BP.

Reducing the palaeoenvironmental information which has been obtained to its major points, as indicated by radiocarbon ages and the corresponding lake stages, the palaeoenvironmental progression within the Seggedim basin can be simplified to the following scheme (Figure 29).

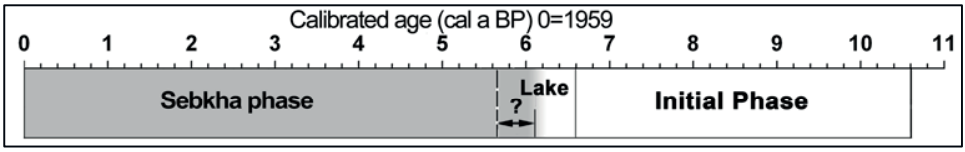

Figure 30 Palaeoenvironmental progression within the Seggedim basin

Evidence of frequent fires raises the question of their cause. Despite the irregularities in the radiocarbon record, the dates from the translocated and redeposited charcoal pieces can be narrowed down to a period of only 1200 cal years, during which regular burnings seem to have occurred. Two models for the causes of the fires have been discussed: natural fires caused by lightning (DOLIDON, 2005, SPONHOLZ 2004), or intentional seasonal burning of the reed beds, which is still a regular procedure among traditional Sahelian herdsmen, to gain access to water for their animals (cf. SCHULZ 2004).

The mineralogical and geochemical study of rock fragments in the core has revealed the presence of carbonatic rocks in the Seggedim area. So far, the nearest known carbonatic outcrops are those of the Carboniferous Dembaba limestone of the Djado basin, at least 100 km northwest and at Ezerza north of Achegour in the southwest.

7 SUPPLEMENTARY STUDY SITES RESULTS

7.1 Fabérgé

7.1.1 Profile 1

Profile 1 is located in the northern tip of a designated palaeolake area within the basin, close to the tamarisk hills and was excavated during the 2005 expedition. It consists of a sediment bank that elevates above the deflated basin floor. The undermost layer of diatomitic silt is present in all lowermost areas within the basin. The profile was sampled stepwise along the slope of the sediment bank. Two basic layers were sampled for radiocarbon dating. At 130-135 centimetres, the dating revealed an age of 5970 ± 50 a BP. The underlying diatomitic layer shows an age of 6690 ± 60 a BP. Both layers contain only very low TOC values, 0.43 mg at 130-135 cm and 0.29 at the 161-171 cm sample. Calibration of these dates revealed ages of 6810 ± 140 (130-135 cm) and 7560 ± 100 cal a BP (161-171 cm). The geochemical distribution of the elements shows a rather smooth pattern (Figure 31). Silicon dominates throughout the whole profile, reaching values between 72.45 and 83.87 weight percentage (Table 10).

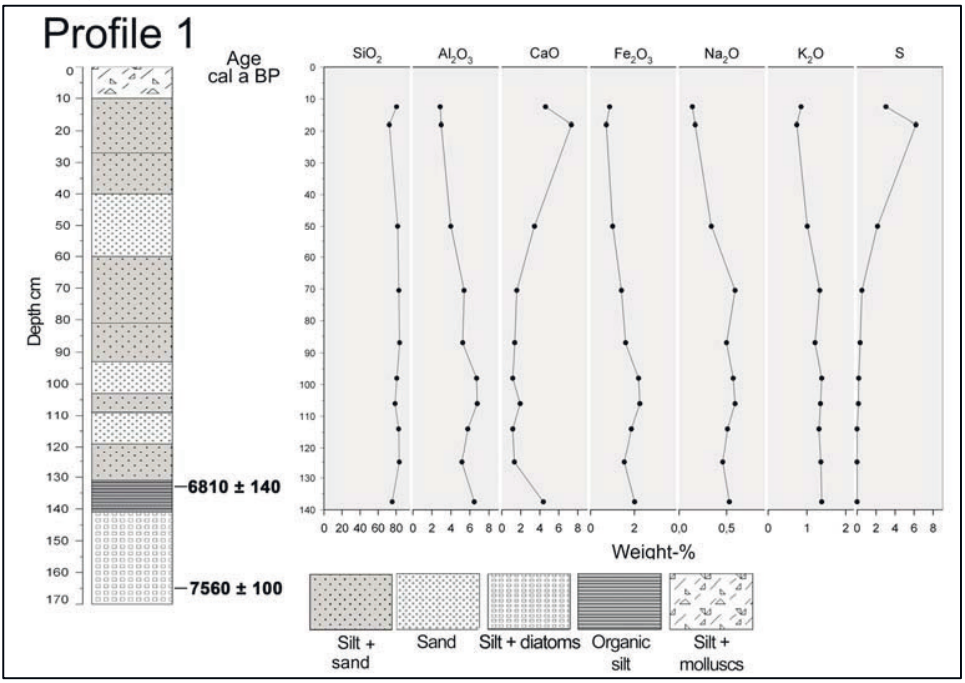

Figure 31 Selected geochemical features of profile 1

Therefore, the mean value of 80.33 % has a standard deviation of only 3.73 (n=10) and a coefficient of variation of 5 %. The amount of aluminium is generally low with values from 2.87 % at the top to 6.77 wt-% at the lower layers. Calcium shows maximum values in the upper (7.33 % at 18 cm) and lowermost (4.38 % at 137 cm) reaches of the profile. The middle layers attain reduced calcium values below 2 % with the minimum of 1.16 weight percentage at 98 centimetres. Calcium and sulphur show distribution patterns contrary to the other elements. Sulphur and calcium reach their maximum values in the second top layer, followed by a steady decrease towards the bottom of the profile. The values of iron, potassium and sodium show distributions similar to silicon with the minimum values at the top and the maximum values in the second half of the profile, starting at 100 centimetres.

Table 10 Main geochemical statistics of profile 1

	SiO_2	TiO_2	Al_2O_3	Fe_2O_3	MgO	CaO	Na_2O	K_2O	P_2O_5	SO_3	MnO
n	10	10	10	10	10	10	10	10	10	10	10
Mean	80.33	0.35	5.14	1.55	0.89	2.83	0.44	1.19	0.07	3.13	0.02
Standard Deviation	3.73	0.07	1.43	0.54	0.54	2.07	0.17	0.24	0.02	5.06	0.02
Minimum	72.45	0.21	2.87	0.72	0.20	1.16	0.14	0.74	0.03	0.00	0.00
Maximum	83.87	0.44	6.77	2.25	1.56	7.33	0.59	1.38	0.10	15.46	0.04
Coefficient of Variation	5%	21%	28%	35%	61%	73%	38%	20%	37%	162%	94%

The correlation matrix of profile 1 (Table 11) shows a strong positive correlation of CaO and SO_3, indicating the presence of gypsum. Contrary to that, the oxides show distinct negative correlation values with other oxides. Working as a counterpart fraction, aluminium, iron, potassium and sodium show

Table 11 Correlation matrix of profile 1

n=10	SiO_2	TiO_2	Al_2O_3	Fe_2O_3	MgO	CaO	Na_2O	K_2O	P_2O_5	SO_3	MnO
SiO2	1.00										
TiO2	0.20	1.00									
Al2O3	0.20	,869(**)	1.00								
Fe2O3	0.18	**,929(**)**	**,979(**)**	1.00							
MgO	0.07	,827(**)	,882(**)	,911(**)	1.00						
CaO	-,844(**)	-0.59	-,677(*)	-,657(*)	-0.53	1.00					
Na2O	0.39	,720(*)	**,943(**)**	,872(**)	,745(*)	-,785(**)	1.00				
K2O	0.44	,801(**)	**,936(**)**	,889(**)	,845(**)	-,803(**)	**,951(**)**	1.00			
P2O5	0.13	,890(**)	,900(**)	,941(**)	,986(**)	-0.57	,762(*)	,851(**)	1.00		
SO3	-0.63	-,807(**)	-,843(**)	-,822(**)	-,750(*)	**,877(**)**	-,872(**)	-,943(**)	-,791(**)	1.00	
MnO	-0.06	,868(**)	,849(**)	,897(**)	,914(**)	-0.38	,662(*)	,742(*)	,917(**)	-,673(*)	1.00

* Statistically significant at the 0.05-level
** Statistically significant at the 0.01-level

The mineralogical composition of profile 1 is presented in Figure 32. Similar to the geochemical distribution, the mineralogical composition shows only minor changes throughout the core. A dominating signal of quartz is ubiquitously present. Medium calcite values only appear in two bottom layers, at 106 and 137.5 centimetres. A weak signal of feldspar is present throughout the core, originating in microcline, orthoclase and albite. Gypsum only appears in the upper reaches where it builds up frequent consolidated layers, which increase towards the top of the profile. Mica shows an

alternating pattern of frequently occurring weak signals. Halite shows merely one weak signal at the topmost layer.

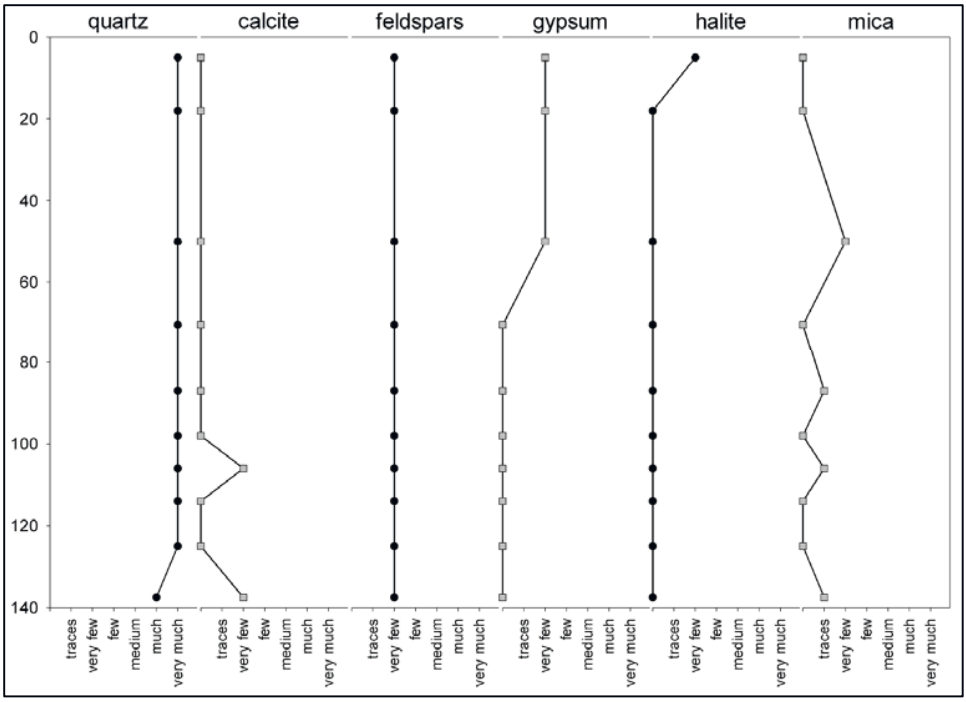

Figure 32 Mineralogical features of profile 1

The ratio of Si/Al shows slightly increasing values towards the top of the profile (Figure 33), reaching 23.93 at the top layer. This increase is due to the decreasing aluminium values towards the top and the rather stable value of silicon (coefficient of variation 5%). The Ca/Si reflects the dominance of silicon throughout the profile, resulting in extremely low values below 0.1. The Al/Ti ratio remains stable at about 23 throughout the profile; only the top layer shows a decreased ratio of 13.64. This value is the lowest of all profiles, indicating a massive weathering of the top layer. The Na+K+Mg/ca ratio shows a twofold profile. The top of the profile is dominated by calcium, indicated by low values, the bottom layers show increased values and therefore a decreasing calcium dominance. The salinization ratio supports the assumption of increased amounts of sodium, potassium and magnesium in the bottom layers. Nevertheless, the ratio of Na+K/Ti evidences the high influence of increased magnesium in the downward section and therefore, the increased salinization ratio does not evidence increased salinity. The CIA ratio remains at medium levels throughout the profile, only reaching low values at the top layers. This pattern is due to the decreased amount of aluminium at the topsoil, associated with less decreased amounts of Na, K and CaO.

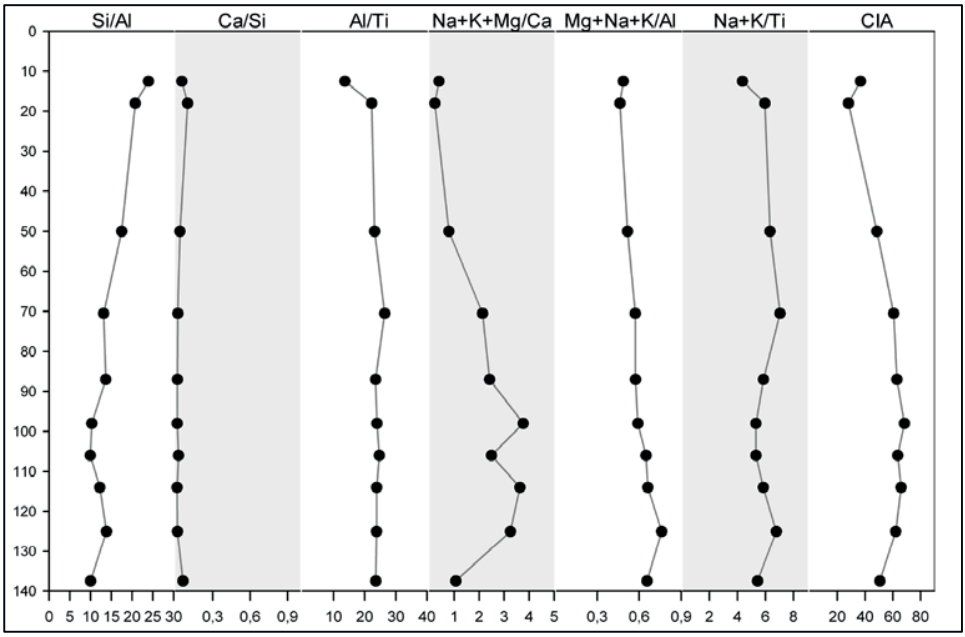

Figure 33 Main mole ratios of profile 1, CIA values derived from oxides

Performing normative balancing on the geochemical results according to the mineralogical composition leads to the results presented in Figure 34. The overall dominance of quartz is obvious, with rather stable values ranging from about 78 % at the bottom layer to 85.59 % in the top layer. Referring to the mineralogical investigations, gypsum is merely present in the three upper layers, reaching a maximum value of 8.65 %. After balancing the gypsum amount using sulphur as the limiting factor, remaining high calcium values led to the proposal of calcite occurrences in the upper reaches of the profile, although not measured by XRD-analysis. Consequently, the three topmost layers of the calcite profile have to be interpreted carefully. Towards the bottom layers, the amounts of K- and Na-feldspars increase, reaching top values of 8.92 % (K) and 5.54 % (Na). Due to the merely low mica amount, this value was not balanced.

7.1.2 Profile 3

Profile 3 is located approximately 200 metres E-NE from profile 1 and was excavated, starting at the deflated basin floor. The top layer consists of a solid diatomitic lining that spreads all over the ground. It is followed by a layer mainly consisting of faunal remnants, probably from gastropods, in combination with presumably organic structures. This layer could be dated to 7270 ± 50 a BP and the calibration led to an age of 8090 ± 120 cal a BP.

Figure 34 summarizes the main geochemical features of profile 3 with the main statistics shown in Table 12. The amount of total organic carbon (TOC) is very low, reaching from 0.17 at the bottom to 0.6 weight percent in the middle and the top of the profile. Total inorganic carbon (TIC) reaches its maximum value at the bottom with 6.02 wt-%, immediately followed by the minimum of 0.44 wt-%

and a slight increase towards the top. Calcium values show a similar pattern with the maximum at the bottom (52.16 wt-%) followed by the minimum (8.35 wt-%) and an increase towards the upper reaches. The mean of calcium is 29.21 % (n=5), which is explicitly higher than the mean values of silicon (25.72 %) and sulphur (22.88 %). The maximum values of sulphur can be found at the top layers of the profile reaching about 34 weight percent, followed by a rapid decrease towards the bottom of the profile.

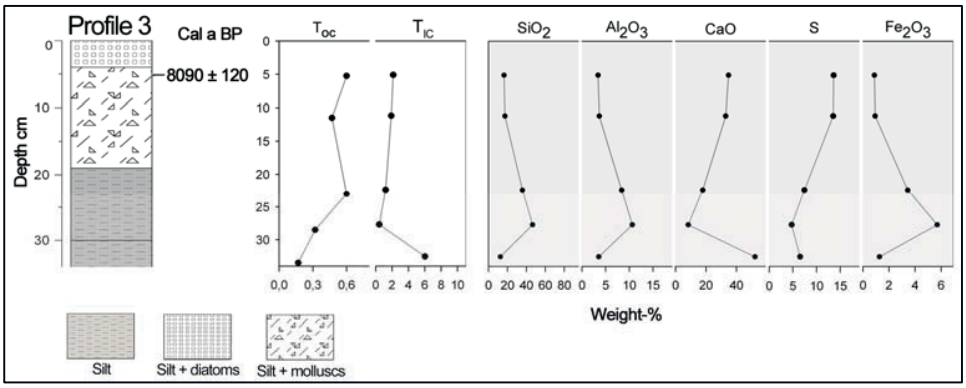

Figure 34 Selected geochemical features of profile 3

Table 12 Main geochemical statistics of profile 3

	SiO_2	TiO_2	Al_2O_3	Fe_2O_3	MgO	CaO	Na_2O	K_2O	P_2O_5	SO_3	MnO
n	5	5	5	5	5	5	5	5	5	5	5
Mean	25.72	0.26	5.92	2.45	1.30	29.21	1.03	1.00	0.19	22.88	0.06
Standard Deviation	14.73	0.14	3.37	2.10	0.61	16.85	0.43	0.50	0.09	10.31	0.05
Minimum	12.52	0.15	3.40	0.88	0.70	8.35	0.39	0.62	0.09	11.84	0.03
Maximum	46.55	0.45	10.64	5.70	2.09	52.16	1.52	1.66	0.28	33.98	0.15
Coefficient of Variation	57%	54%	57%	86%	47%	58%	42%	50%	44%	45%	85%

The correlation matrix of profile 3 is presented in Table 13. It shows the division of the profile with two fractions. On the one hand are calcium and sulphur with strong negative correlations to roughly all major elements. On the other hand, there are numerous elements correlating strongly positive, especially silicon, aluminium iron and titanium.

Five minerals characterize the mineralogical composition (Figure 35). Quartz shows few signals throughout the profile with reduced amounts at the bottom. The maximum signal of calcite is of medium intensity and can be found at the bottom of the profile. The signal of gypsum is rather stable throughout the core showing few signals, the variance of anhydrite appears at the two uppermost layers. Glauberite solitary occurs at the second layer where only traces of it can be found.

Table 13 Correlation matrix of profile 3

n=5	SiO_2	TiO_2	Al_2O_3	Fe_2O_3	MgO	CaO	Na_2O	K_2O	P_2O_5	SO_3	MnO	TC	TIC	TOC
SiO2	1.00													
TiO2	**,993(**)**	1.00												
Al2O3	**,992(**)**	**,997(**)**	1.00											
Fe2O3	**,974(**)**	**,970(**)**	,986(**)	1.00										
MgO	,887(*)	**,918(*)**	,937(*)	,947(*)	1.00									
CaO	**-,942(*)**	**-,913(*)**	**-,895(*)**	**-0.85**	**-0.68**	1.00								
Na2O	0.29	0.20	0.18	0.16	-0.15	-0.55	1.00							
K2O	,993(**)	1,000(**)	,998(**)	,975(**)	,926(*)	-,906(*)	0.19	1.00						
P2O5	-0.60	-0.54	-0.55	-0.59	-0.43	0.63	-0.25	-0.54	1.00					
SO3	-0.63	-0.68	-0.72	-0.76	-,913(*)	0.33	0.46	-0.69	0.19	1.00				
MnO	-0.56	-0.49	-0.45	-0.38	-0.11	0.80	-,882(*)	-0.48	0.44	-0.29	1.00			
TC	-0.77	-0.72	-0.69	-0.63	-0.39	,938(*)	-0.78	-0.70	0.60	-0.01	,956(*)	1.00		
TIC	-0.74	-0.69	-0.65	-0.59	-0.35	,921(*)	-0.78	-0.67	0.59	-0.06	,967(**)	,997(**)	1.00	
TOC	0.09	0.07	0.00	-0.13	-0.26	-0.36	0.45	0.05	-0.23	0.59	-0.69	-0.56	-0.61	1.00

* Statistically significant at the 0.05-level
** Statistically significant at the 0.01-level

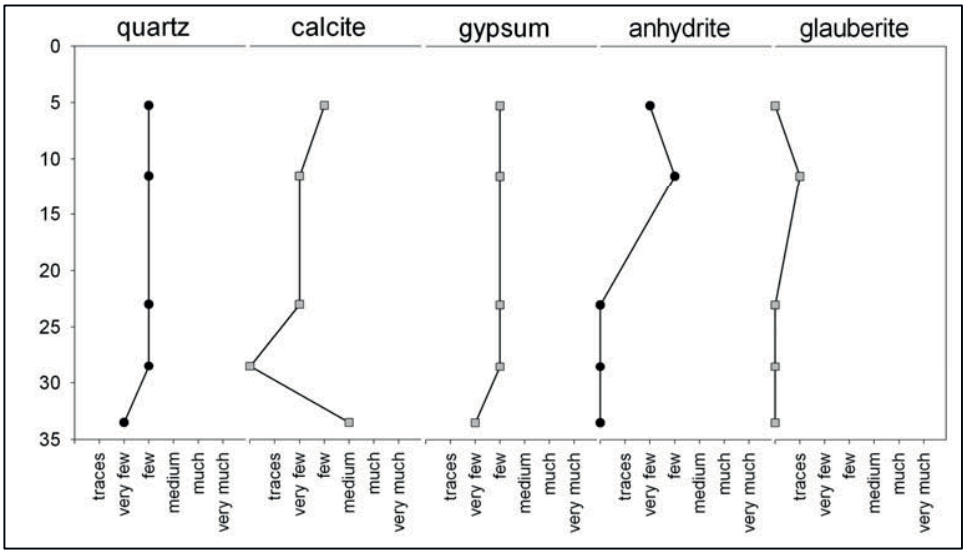

Figure 35 Mineralogical features of profile 3

Grain size

The results for grain sizes from 0 to 150 µm obtained from laser sizer measurements of profile 3 are presented in Figure 36. Due to methodological limitations (cf. chapter 5.2.2), information on grain sizes larger than fine sand (150 µm) are not available.

For the most part reduced on silt and clay sizes, profile 3 shows a rather constant distribution. The proportion of clay sized particles alternates between the minimum value of 24.1 % (19 cm) and a maximum of 32.9 % at the bottommost layer (31 cm). The silt size fraction is dominated by fine silt (2-63 µm) with amounts ranging from 43.6 % (27 cm) to 52.5 % (10 cm), whereas the total silt fraction reaches from 67.10 % (31 cm) to 75.71 % (19 cm).

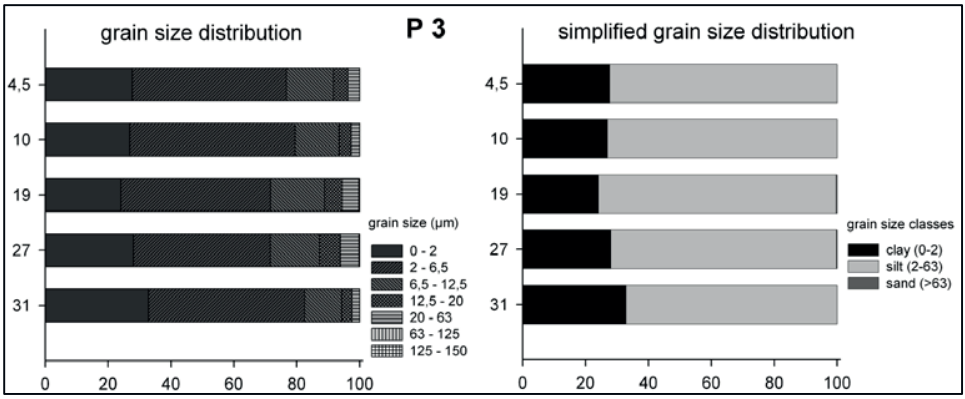

Figure 36 Grain size distribution of profile 3

Geochemical ratios and stoichiometric calculations

The ratio of Si/Al shows gently decreasing values towards the bottom layers (Figure 37). It remains at low levels throughout the profile, indicating a lower quartz amount, compared to the foregoing profile.

The maximum value of the Ca/Si ratio is located in the lowest layer, reaching a medium level at 4.44, immediately followed by the minimum value of 0.19. Towards the top, the ratio shows increasing values reaching 2.26 at the top layer. The Al/Ti ratio generally remains stable at a high level throughout the profile, showing only a minor increase towards the bottom layer.

The ratio of Na+K+Mg/Ca shows very low values, with a maximum of 0.86 at 28.5 centimetres, due to the calcium minimum at this point. The overall low values indicate a dominance of calcium within the profile. The salinization ratio reveals a pattern distinctly increasing towards the top of the profile. This may indicate a top ward movement of the water. However, due to the strong positive correlations of aluminium, magnesium and potassium, the ratio cannot provide evidence of the salinization dynamics of this profile.

The ratio of Na+K/Ti remains rather stable throughout the profile with values between 6.2 and 7. The chemical index of alteration remains at low values, except for one layer at 28.5 centimetres, where the CIA reaches a medium value close to 50. This pattern reflects the overall dominance of calcium. Only where calcium and sulphur show minor values, the CIA may reach a medium level. In order to gain a basic understanding of the quantitative mineralogical composition of the profile, normative balancing was performed combining geochemical results and mineralogical evidence. Quartz is a smaller compartment within the profile, reaching a maximum of 49.43 % at 28.5 centimetres. The maximum amount of calcite is located in the bottom layer and reaches 50.91 %, followed by the minimum amount of 3.90 %. A noticeable increase is visible towards the top layers.

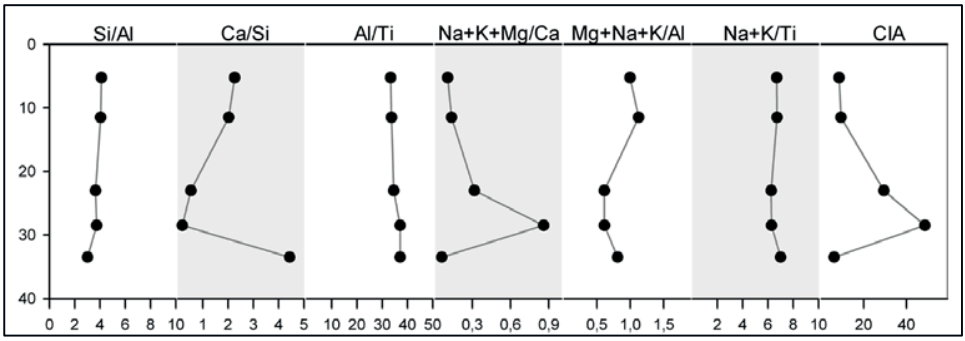

Figure 37 Main mole ratios of profile 3, CIA values derived from oxides

The balancing of gypsum (including anhydrite) reveals a distinct increase towards the top layers (Figure 38). Starting with 28.17 % at the bottom layer, the gypsum amount increases relatively linear, reaching the maximum values of more than 61 % percent in the topmost layers. This evidences the suggested upward water movement within the profile, which must have occurred over a certain time to create the high amounts of gypsum. Additional evidence is the singular appearance of glauberite at 11.5 centimetres; due to the minor value, glauberite was not balanced.

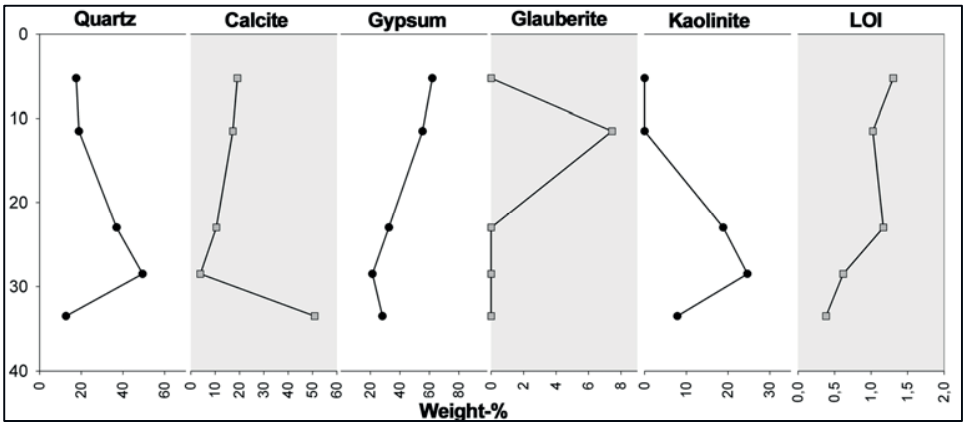

Figure 38 Normative balancing of main minerals in profile 3

The normative balancing referred to the mineralogical evidence obtained from the XRF analysis, when to calculate the weight percentage of the identified minerals. Nevertheless, some layers showed high residual amounts that could not be explained completely by the minerals present. With aluminium providing the highest non-explained values, the additional appearance of alumino-silicates has been suggested. Performing normative balancing of kaolinite (exemplary) on the residual aluminium amounts led to a maximum value of about 24 % at 28.5 centimetres.

7.1.3 Profile 4

Profile 4 is located approximately 300 north eastwards of profile 3. It is situated 30 m away from the beach ridge, near the palaeolake banks. It consists of an excavated, generally two-part profile. The upper part, reaching from 0 to 25 centimetres, consists of hardened sandy-siltic diatomitic material with a varying amount of gypsum crystals. The bottom part consists of gleyic and hardened siltic to sandy material, probably originating from dunes. Two layers were sampled for radiocarbon dating. Although the carbon amount was generally low, AMS dating revealed overlapping ages of 8420 ± 50 (15-19 cm) and 8440 ± 70 a BP (9-15 cm), Calibrating the data led to the concurrent age of 9440 cal a BP with only minor differences in variance of 120 (15-19 cm) and 140 (9-15 cm).

The distribution of the main geochemical features (Figure 39) as well as the geochemical statistics (Table 14) show obviously a two-part profile dominated by the occurrence of quartz. The upper reaches are dominated by high amounts of calcium (max 31.01 %) and very high amounts of sulphur (max 51.35 %). Silicon values of the upper layers do not exceed 13.04 weight percent, aluminium values stay below 3.27 %. In the lowermost layers silicon increases to 64.17 and 70.14 weight percent, whereas calcium values drop to about 2% and sulphur below the detection limit of 0.1 weight percent. Aluminium and iron show a similar pattern to that of silicon and both elements reach their maximum values at the bottom layers. Aluminium reaches 11.92 and 10.53 %, whereas iron values rise to 3.66 and 3.93 %.

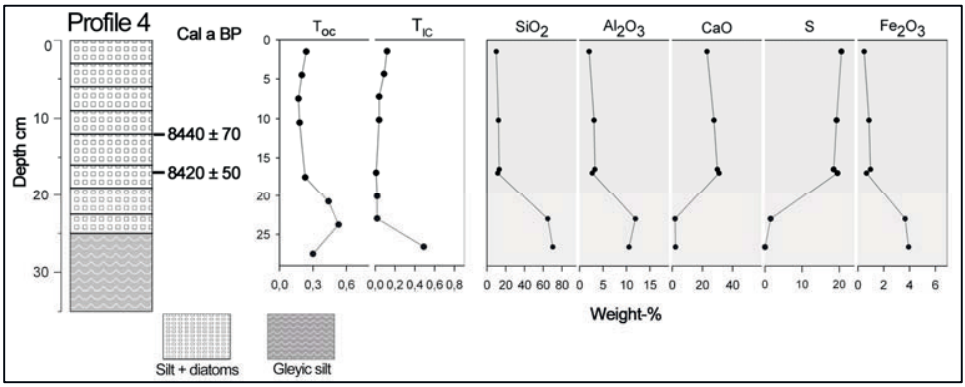

Figure 39 Selected geochemical features of profile 4

The correlation matrix of profile 4 is presented in table 15. It evidences two opposing factions within the profile. Sulphur and calcium show a strong positive correlation of 0.96. The opposing fraction consists of silicon, aluminium, iron, magnesium, titanium and potassium, all showing strong positive correlations with each other. Sodium and phosphorous also show strong positive correlations but no connection towards any other elements.

Table 14 Main geochemical statistics of profile 4

	SiO_2	TiO_2	Al_2O_3	Fe_2O_3	MgO	CaO	Na_2O	K_2O	P_2O_5	SO_3	MnO
n	6	6	6	6	6	6	6	6	6	6	6
Mean	30.25	0.30	5.59	1.77	0.72	19.26	2.93	1.16	0.06	33.01	0.01
Standard Deviation	28.87	0.29	4.41	1.58	0.51	13.62	2.73	1.04	0.06	24.19	0.00
Minimum	9.90	0.09	2.03	0.49	0.25	1.88	0.99	0.42	0.02	0.00	0.01
Maximum	70.14	0.70	11.92	3.93	1.44	31.01	8.25	2.86	0.17	51.35	0.01
Coefficient of Variation	95%	97%	79%	90%	71%	71%	93%	89%	89%	73%	0%

Table 15 Correlation matrix of profile 4

n=6	SiO_2	TiO_2	Al_2O_3	Fe_2O_3	MgO	CaO	Na_2O	K_2O	P_2O_5	SO_3	TC	TIC	TOC
SiO2	1.00												
TiO2	,994(**)	1.00											
Al2O3	,985(**)	,997(**)	1.00										
Fe2O3	,998(**)	,994(**)	,988(**)	1.00									
MgO	,981(**)	,992(**)	,997(**)	,988(**)	1.00								
CaO	**-,971(**)**	**-,971(**)**	**-,956(**)**	**-,959(**)**	**-,936(**)**	1.00							
Na2O	-0.35	-0.35	-0.38	-0.39	-0.44	0.12	1.00						
K2O	,952(**)	,978(**)	,988(**)	,953(**)	,981(**)	-,942(**)	-0.32	1.00					
P2O5	0.00	-0.02	-0.08	-0.05	-0.14	-0.21	,875(*)	-0.06	1.00				
SO3	**-,999(**)**	**-,995(**)**	**-,988(**)**	**-,999(**)**	**-,986(**)**	**,965(**)**	0.38	-,955(**)	0.03	1.00			
TC	,927(**)	,892(*)	,857(*)	,914(*)	,844(*)	-,925(**)	-0.16	0.79	0.27	-,919(**)	1.00		
TIC	0.61	0.53	0.47	0.60	0.47	-0.60	-0.05	0.35	0.35	-0.60	,832(*)	1.00	
TOC	0.73	0.79	,817(*)	0.73	0.81	-0.75	-0.22	,885(*)	-0.05	-0.74	0.53	-0.03	1.00

* Statistically significant at the 0.05-level

** Statistically significant at the 0.01-level

The mineralogical composition of profile 4 is presented in Figure 40. It reveals the accumulation of evaporitic minerals (gypsum, anhydrite and glauberite) at the top of the profiles in combination with a decrease of quartz. Of the evaporitic minerals, gypsum and anhydrite show the strongest impulses. In contrast to that, the signals of calcite show maximum strength in the bottom layer and merely one reappearance in the mid section of the profile. A variety of feldspars is present in the bottom layers, to be more precise albite, orthoclase and microcline (K- and Na-feldspars).

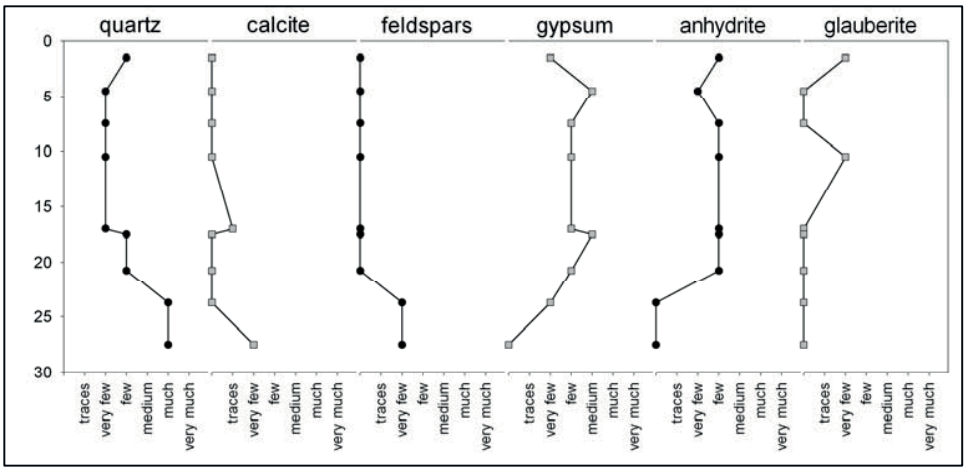

Figure 40 Mineralogical features of profile 4

Grain size

The results for grain sizes from 0 to 150 µm obtained from laser sizer measurements of profile 4 are presented in Figure 42. Due to methodological limitations (cf. chapter 5.2.2), information on grain sizes larger than fine sand (150 µm) are not available.

For the most part reduced on silt and clay sizes, profile 4 shows decreasing values of clay towards the bottom layers. The proportion of clay sized particles alternates between the minimum value of 29.09 % (19 cm) and a maximum of 45.46 % at the topmost layer (0 cm). The silt size fraction is dominated by fine silt (2-63 µm) with amounts ranging from 40.11 % (0 cm) to 54.72 % (0 cm), whereas the total silt fraction reaches from 54.45 % (0 cm) to 70.92 % (19 cm).

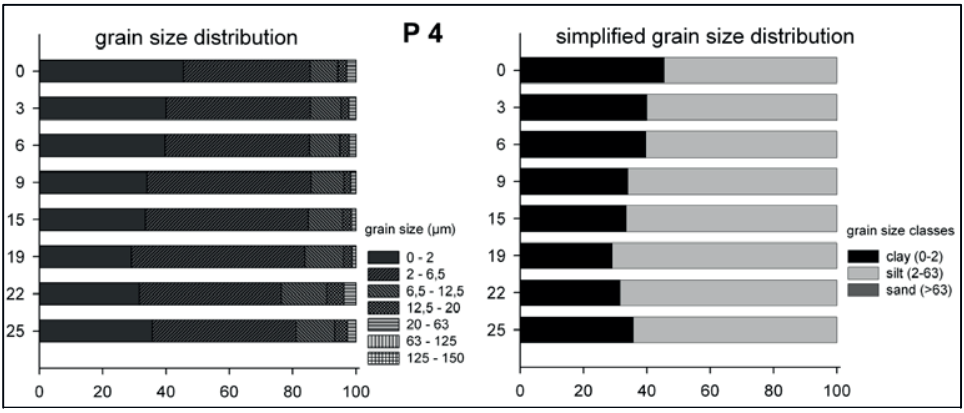

Figure 41 Grain size distribution of profile 4

Geochemical ratios and stoichiometric calculations

Figure 42shows the main mole ratios of profile 4. The low ratio of Si/Al indicates a rather small amount of quartz within the profile, slightly increasing towards the bottom layers. The Ca/Si ratio shows a twofold profile with silicon dominating the bottom layers plus an increased proportion of calcium in the top layers. The ratio of Al/Ti shows a similar distribution, with the overall maximum value of 42.3 at the mid section. The ratio of Na+K+Mg/Ca evidences the twofold profile. While the ratio shows increased values of 3.13 and 4.96 at the two bottom layers, the values decrease to far below 1 at the upper section. This is due to the increasing proportion of calcium at the top. The salinization ratio starts with 0.5 at the bottom but increases clearly towards the top, reaching the overall maximum of 7 at the topmost layer.

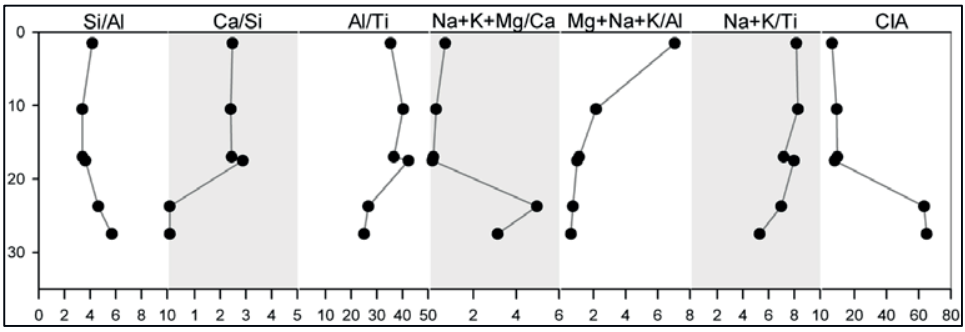

Figure 42 Main mole ratios of profile 4, CIA values derived from oxides

The ratio of Na+K/Ti supports this evidence as it reaches its overall maximum values of more than 8 at the top layers and slightly decreases towards the bottom of the profile. Due to the rather low content of aluminium in the top layers, the CIA shows very low values. Towards the bottom, the chemical index of alteration shows a massive increase, resulting in high values of more than 60. This indicates reduced proportions of the soluble fraction in combination with increasing proportions of the stable/immobile fraction.

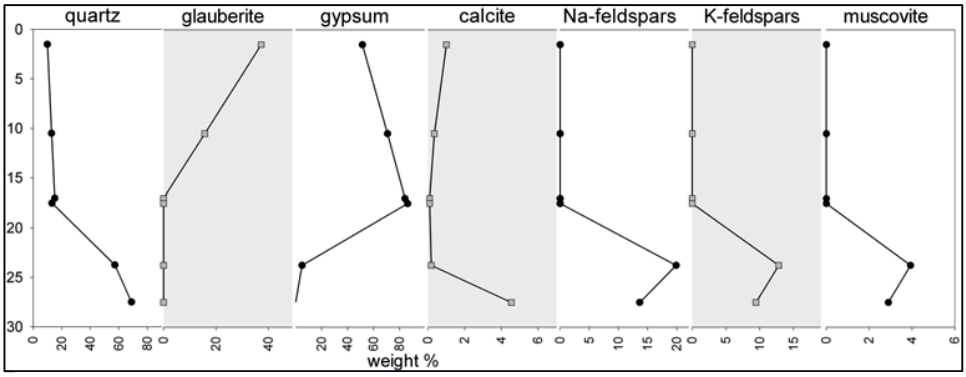

Figure 43 Normative balancing of main minerals in profile 4

Normative balancing of the geochemical results (RFA) of profile 4 considering the mineralogical evidence leads to the results presented in Figure 43. The topmost layer is dominated by the presence of glauberite and gypsum with about 40 w-% that shows decreasing values towards the mid section of the profile. In contrast, gypsum shows increasing values reaching about 80 % at 17 centimetres depth. The bottommost layers are dominated by the presence of quartz (max. 70 %) and feldspars (max. sum about 35 %) as well as calcite and muscovite.

7.1.4 OSL-dating

Two additional sites were sampled for the purpose of OSL-dating by the palaeosoils section within the LIMNOSAHRA project, Prof. Peter FELIX-HENNINGSEN and Peter Kornatz from Gießen University. A ramp of fossil dune sand at the western part of the basin reaching from the designated palaeolake bottom to the upper escarpment level (Position UTM 33Q 0367446 2325911, Lat/Long: 21°01'45,2"N 13°34'27,8"). The ramp shows a declination of 5° with a south-western exposition and a concavity at the mid slope. The OSL dating of the dune sand reveals an age of 6200 ± 400 cal a BP whereas the sand shows signs of soil development (P. Felix Henningsen, personal communication, June 2008).

In addition to that, a dune sand core underneath a tamarisk hill has been excavated and sampled at 50 cm height. The sands reveal a deposition age of 1200 ± 100 cal a BP (P. Felix Henningsen, personal communication, June 2008).

7.1.5 Summary

P1

The strong correlation of aluminium and Na, K and Mg in combination with the overall decrease of these values indicates high weathering intensities at the topmost layers of the profile. The increased amount of gypsum and the solitary occurrence of halite at the top layers evidence a top-headed water movement within the profile. The overall dominance of quartz is most likely a result of dominating aeolian input into the basin. This is supported by the simultaneous and ubiquitous occurrence of albite, orthoclase and microcline, feldspars that are considered to be of detrital origin.

P3

The increased values of anhydrite and gypsum and the singular appearance of glauberite evidences upward water movement within the sediment profile. The radiocarbon dating of the sediment reveals an age of 7270 ± 50 a BP and the calibration led to an age of 8090 ± 120 cal a BP. This indicates the time of deposition, whereas the enrichment of gypsum and especially anhydrite has very likely happened afterwards.

Compared to profile 1, the mineralogical composition of profile 3 appears reduced to five compartments and lacks the feldspar compartments. Normative balancing of the mineralogical composition revealed residual (non-explained) amounts of 8 to more than 24 %. It seems very likely, that a major, undetected part within the profile is of alumino-silicate origin.

P4

The investigations performed on profile 4 reveal a two-fold pattern. Evaporitic minerals (gypsum, anhydrite and glauberite) are predominant at the top but the amounts of quartz and a variety of feldspars increase significantly towards the bottom layers. The bottom layers show a mineralogical composition similar to that o profile 1, as Na- and K-feldspars as well as mica amount to more than

30 weight-percent. Radiocarbon dating indicates an Early Holocene age of the evaporitic sediment (about 8.4 ka BP) that presumably developed on fossil dune sands.

7.2 Enneri Achelouma

7.2.1 Profile 8

Profile 8 mainly consists of silty to sandy sediments with high amounts of mollusc remnants throughout the profile. It elevates 150 cm above the valley ground, whereas the main lacustrine sediments are located between 66 and 136 cm height. The sediment is heavily carved and partially removed. Sand layers on top and underneath frame the lacustrine sediments.

The dark horizons visualized in Figure 44 provided the organic material needed for radiocarbon dating. The (uncalibrated) ages are shown in Figure 46 and Figure 47. They reach from 8450 ± 50 a BP at 68-69 cm, over 8210 ± 50 a BP at 94-97 cm to 8000 ± 50 a BP at 130-136 cm. Calibration of the dates resulted in ages of 9480 ± 80, 9180 ± 180 and 8870 ± 200 cal a BP.

Profile 8 is dominated by the contrarily trending amounts of silica (silicon dioxide, SiO2) and calcium (calcium oxide, CaO) concurrently with total inorganic carbon (TIC). The maximum silicon content of 81.08 weight percent (wt-%) is located at 64 cm above ground attended by the calcium minimum amount of 0.71 weight percent.

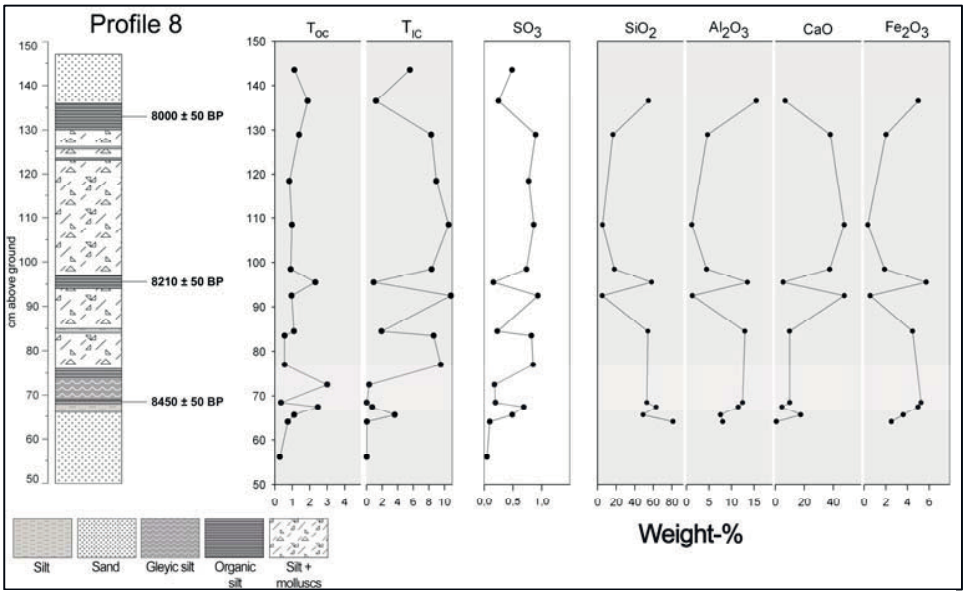

Figure 44 Selected geochemical features of profile 8

Consequently, the maximum calcium amount of 47.58 wt-% at 92 cm is associated with the minimum silica content of 4.96 wt-% (Table 16). Additionally, dark layers with increased total organic carbon (TOC) contents up to 3 % are present at several heights (66-76 cm, 94-97 cm and 130-136 cm). The occurrence of these layers is related to a decrease in TIC and calcium and an increase in silica and aluminium (Al_2O_3), the latter not exceeding 15 wt-%.

Table 16 Main geochemical statistics of profile 8

	SiO_2	TiO_2	Al_2O_3	Fe_2O_3	MgO	CaO	Na_2O	K_2O	P_2O_5	MnO	TC	TIC	TOC
n	10	10	10	10	10	10	10	10	10	10	10	10	10
Mean	40.27	0.45	7.78	3.13	0.85	21.82	0.08	0.46	0.05	0.00	5.75	4.52	1.23
Standard Deviation	26.78	0.28	4.74	1.95	0.22	18.70	0.10	0.28	0.02	0.00	4.38	4.48	0.67
Minimum	4.96	0.06	1.19	0.34	0.58	0.71	0.00	0.08	0.02	0.00	0.36	0.01	0.35
Maximum	81.08	0.79	13.56	5.72	1.21	47.58	0.32	0.76	0.10	0.01	11.79	10.83	2.47
Coefficient of Variation	66%	62%	61%	62%	26%	86%	125%	60%	44%	316%	76%	99%	54%

TiO_2 and Al_2O_3 show a positive high correlation (r) of 0.993 (n=10) in combination with a coefficient of determination (r^2) of 98.61% (Table 17). CaO generally correlates negatively at medium to very strong levels with any other elements but obviously correlates strongly positive with inorganic carbon (r=0.99, r^2= 98.11%, n=10). Aluminium and titanium also show a very strong positive correlation of 0.99, which indicates a chemical connection of the elements.

Table 17 Correlation matrix of profile 8

n=10	SiO_2	TiO_2	Al_2O_3	Fe_2O_3	MgO	CaO	Na_2O	K_2O	P_2O_5	MnO	TC	TIC	TOC
SiO2	1.00												
TiO2	.867(**)	1.00											
Al2O3	.818(**)	**.993(**)**	1.00										
Fe2O3	.755(*)	.952(**)	.975(**)	1.00									
MgO	.647(*)	.770(**)	.814(**)	.876(**)	1.00								
CaO	-.985(**)	-.936(**)	-.903(**)	-.854(**)	-.732(*)	1.00							
Na2O	0.57	.723(*)	.768(**)	.777(**)	.828(**)	-.650(*)	1.00						
K2O	.909(**)	.980(**)	.974(**)	.934(**)	.829(**)	-.962(**)	.790(**)	1.00					
P2O5	0.39	.644(*)	.716(*)	.786(**)	.813(**)	-0.51	.838(**)	.678(*)	1.00				
MnO	0.17	0.28	0.35	0.38	0.51	-0.22	.840(**)	0.38	.733(*)	1.00			
TC	-.954(**)	-.909(**)	-.886(**)	-.834(**)	-.749(*)	.969(**)	-.769(**)	-.962(**)	-0.60	-0.43	1.00		
TIC	-.966(**)	-.941(**)	-.919(**)	-.879(**)	-.781(**)	**.990(**)**	-.742(*)	-.978(**)	-0.60	-0.35	.989(**)	1.00	
TOC	0.22	0.34	0.35	0.42	0.32	-0.29	-0.07	0.24	0.03	-0.46	-0.07	-0.22	1.00

* Statistically significant at the 0.05-level

** Statistically significant at the 0.01-level

An investigation on the mineralogical composition of the profile reveals the dominance of quartz and calcite (Figure 45). Similar to the geochemical results, the amounts of quartz and calcite are running contrarily to each other. The occurrence of the darker, organic enriched layers, concur with an increase of quartz and the decrease of calcite.

Traces of kaolinite are ubiquitously present, whereas feldspars only occur in the lower part of the profile. The course of the kaolinite signals corresponds with the one of the quartz signals and runs contrarily to the calcite impulses.

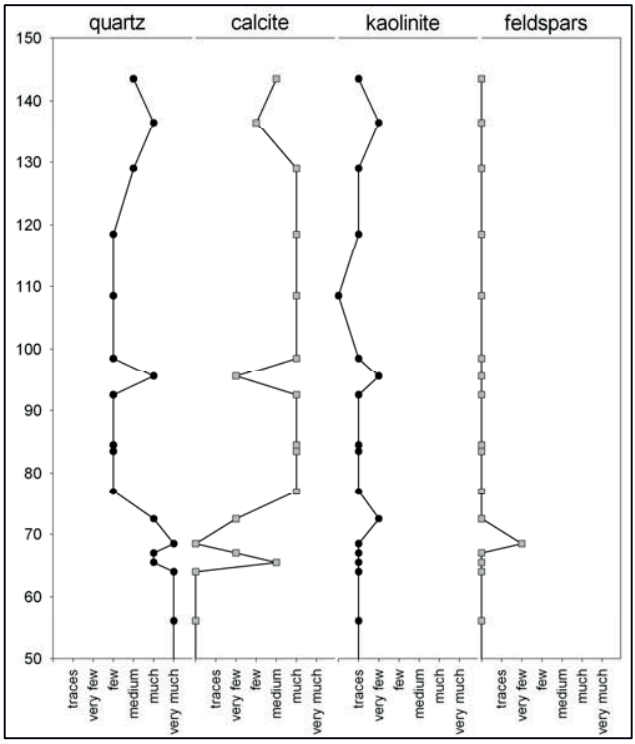

Figure 45 Mineralogical features of profile 8

Grain size

The results for grain sizes from 0 to 150 µm obtained from laser sizer measurements of profile 8 are presented in Figure 46. Due to methodological limitations (cf. chapter 5.2.2), information on grain sizes larger than fine sand (150 µm) are not available.

For the most part reduced on silt and clay sizes, profile 8 shows alternating values with a dominance of silt. The proportion of clay sized particles alternates between the minimum value of 26.52 % (95 cm) and a maximum of 42.91 % at the mid section (84 cm). The silt size fraction is dominated by fine silt (2-63 µm) with amounts ranging from 39.51 % (76 cm) to 52.56 % (18 cm), whereas the total silt fraction reaches contents from 57.10 % (84 cm) to 73.44 % (95 cm).

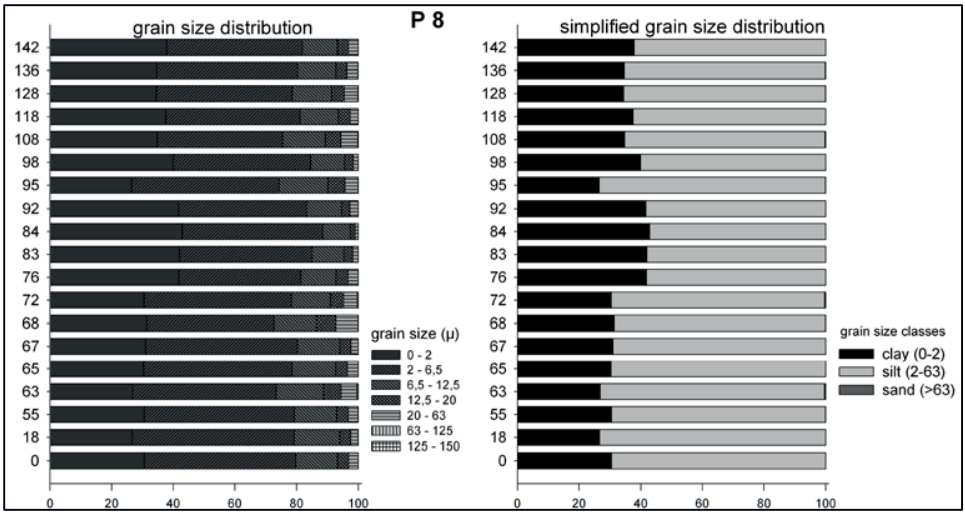

Figure 46 Grain size distribution of profile 8

Geochemical ratios and stoichiometric calculations

The main mole ratios presented in Figure 47 help to differentiate the profile, as they remove any bulk effects. The Si/Al ratio shows a linear distribution at a stable and low level at circa 4, except for the bottom layers, which show increase up to 9. This is due to the underlying sand layers, where quartz dominates and any other minerals only occur in traces. The Ca/Si ratio gives evidence of the major calcite layers, reaching maximum values of about 10. Al/TI ratios provide information about of the detrital input and weathering intensity of clay minerals. Because the ratio remains rather stable, no major change can be derived from that ratio. The ratio of Na+K+Mg/Ca reacts to the dominance of calcium throughout the core. Only in the bottom layer, where the amount of calcium is decreased to a minimum, the ratio shows one maximum value.

The ratio of Mg+Na+K/Al, also referred to as salinization ratio, evidences the accumulation of the soluble fraction (Mg+Na+K) compared to the rather immobile fraction (Al). The ratio shows increasing values according to the ones of the Ca/Si, but remains at small values below 1. Therefore, a small rise of salinity can be considered. The controlling ratio of Na+K/Ti, where potassium and sodium represent the soluble fraction and titanium the immobile fraction, shows only minor increasing values, but at a higher level. This is due to the stable amount of Mg throughout the profile, which is correlating with calcium at a medium negative level. At the calcium maximum layers, the amount of sodium (Na) drops below the detection limit, potassium (K) is only slightly above.

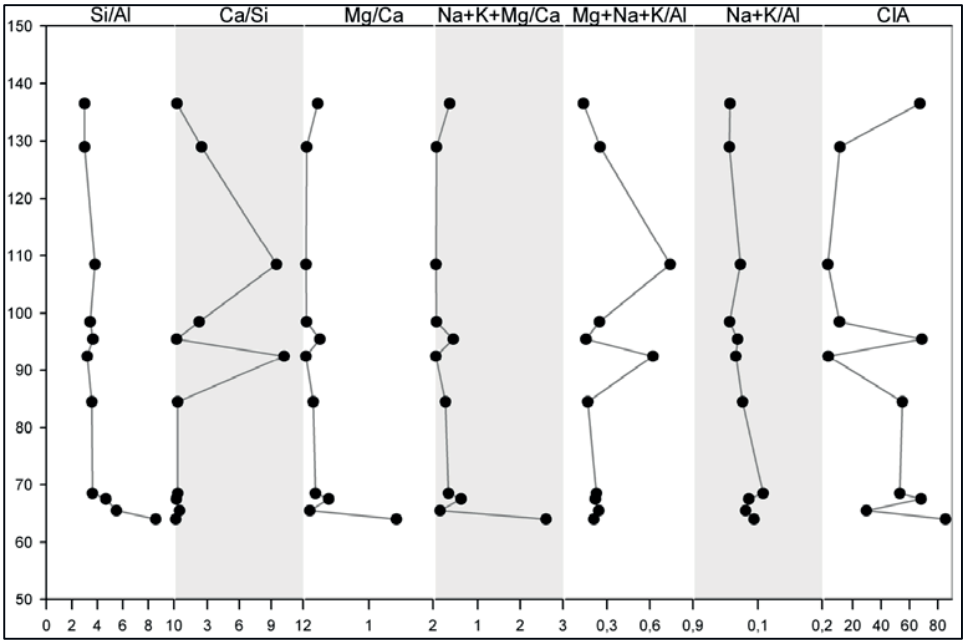

Figure 47 Main mole ratios of profile 8, CIA values derived from oxides

The CIA ratio (chemical index of alteration) is considered to give evidence of the alteration of feldspars, subsequently developing to clay. It indicates the relative enrichment of aluminium (immobile) compared to the main alkali and alkaline earth elements (soluble). High values close to 100 evidence rather pure aluminium occurrences, low levels close to zero show the dominance of the soluble fraction and decreased aluminium values. High values are present at several layers on top, the middle and the bottom of the profile, where the maximum value of about 90 is reached in the lowest layer. This is due to the massively decreased values of calcium and sodium, merely above the detection limit.

When combining the mineralogical evidence with the normative balancing of the geochemical results, the error-prone semi-quantitative results of the XRD analysis can be avoided. The calculated results provide an estimate of the main mineralogical percentages. Figure 48 evidences the dominance of calcite within the profile reaching amounts of more than 90 %. Contrary to that, quartz reaches is maximum value of 79.86 % at the bottom of the profile. Kaolinite shows increased amounts in the lower part of the core, but reaches its maximum of 36.45 % at the topmost investigated layer.

Feldspars only appear, referring to the mineralogical results, in one layer. The normative balancing shows a low amount of sodium feldspar (3.48 %) and a slightly increased value of potassium feldspar (5.77 %). The LOI value is balanced by multiplying the TOC value by 2. It shows accumulations of organic material in the kaolinite enriched and calcite depleted layers. The maximum amount is located at 67.5 centimetres reaching 4.73 %.

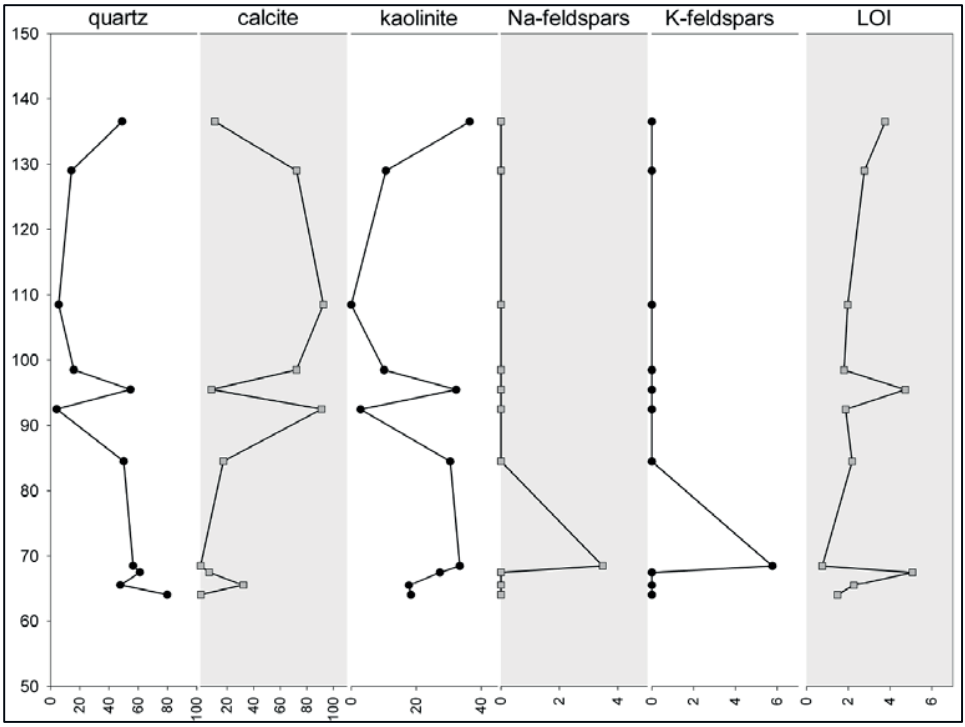

Figure 48 Normative balancing of main minerals in profile 8

7.2.2 Profile 10

Profile 10 consists of deeply incised sediments within the channel bed and is located several hundred meters downstream compared to profile 8. The sediment remnant creates a rock-solid wall of 246 cm above the valley ground. Similar to profile 8, dark and bright layers alternate throughout the profile but colour changes are not that distinct and no mollusc shells are incorporated (Figure 49). The sediment body is composed of mainly silty layers with changing proportions of clay or sand, resulting in different hardness. The top of the profile is coated with a layer of sand and gravel.

Because of the rather low organic content within the profile, only one sample was used for radiocarbon dating. The result shows an uncalibrated age of 8020 ± 50 BP at 211-221 cm. Calibration reveals an age of 8890 ± 200 cal a BP.

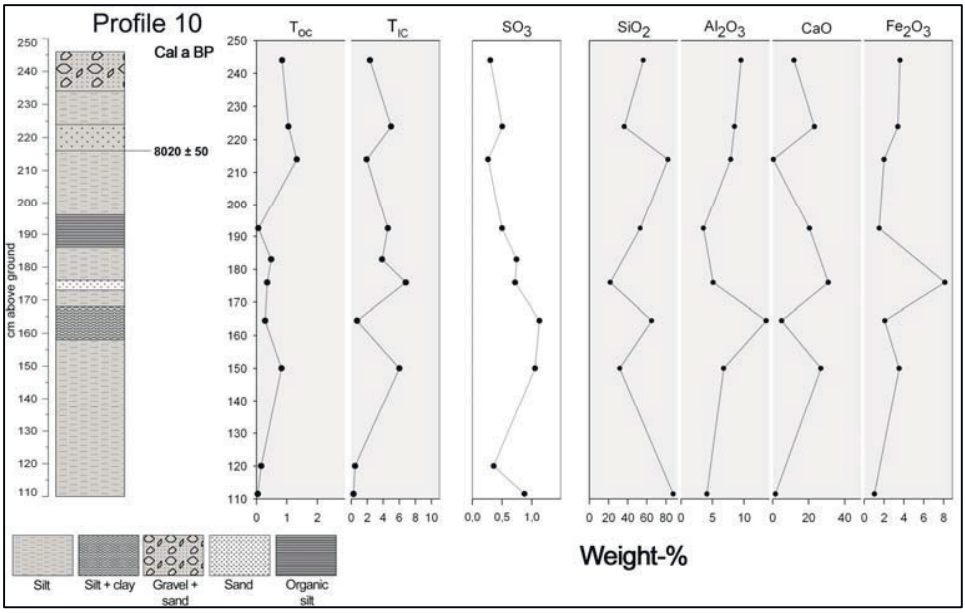

Figure 49 Selected geochemical features of profile 10

The amount of silica reaches a maximum of 87.4 weight percent at 111.5 cm height and the minimum value of 21.8 weight percentage at 176 centimetres (Table 18). Corresponding to that, the calcium values extend from 1.56 wt-% (11.5 cm) to 30.88 wt % (176 cm). Aluminium values lie between 3.55 % and 13.51 wt-%, the maximum iron (iron-III-oxide, Fe_2O_3) of 8.13 wt-% coincides with the calcium maximum. The amount of total organic carbon is generally low and exceeds 1 weight percent only in the upper layers. The maximum amount of total inorganic carbon (TIC) reaches 6.8 % in the calcium rich layers, but is reduced below 1 percent in the silica rich layers. Generally, all values show major variations, referring to the high coefficients of variations, spanning from 41 to 125 % (Table 18).

Table 18 Main geochemical statistics of profile 10

	SiO_2	TiO_2	Al_2O_3	Fe_2O_3	MgO	CaO	Na_2O	K_2O	P_2O_5	SO_3	MnO
n	8	8	8	8	8	8	8	8	8	8	8
Mean	54.17	0.46	7.37	3.15	0.84	15.01	0.25	0.53	0.06	0.33	0.01
Standard Deviation	23.51	0.19	3.27	2.23	0.41	11.90	0.23	0.22	0.04	0.42	0.01
Minimum	21.80	0.22	3.55	1.03	0.27	0.39	0.02	0.31	0.03	0.00	0.00
Maximum	87.40	0.82	13.51	8.13	1.43	30.88	0.76	0.99	0.13	1.05	0.04
Coefficient of Variation	43%	41%	44%	71%	49%	79%	94%	41%	57%	125%	119%

The correlation matrix (Table 19) reveals some information of possible mineralogical coherences. Aluminium and titanium show an exemplary strong positive correlation, typical when clay minerals

are present. The strong positive correlation (0.96) of TIC and CaO, although originating from different analyses, arises due to the occurrence of calcite.

Table 19 Correlation matrix of profile 10

n=8	SiO_2	TiO_2	Al_2O_3	Fe_2O_3	MgO	CaO	Na_2O	K_2O	P_2O_5	SO_3	MnO	TC	TIC	TOC
SiO2	1.00													
TiO2	0.37	1.00												
Al2O3	0.09	**,951(**)**	1.00											
Fe2O3	-,776(*)	-0.27	-0.08	1.00										
MgO	**-,968(**)**	-0.34	-0.07	,846(**)	1.00									
CaO	**-,969(**)**	-0.58	-0.32	0.70	**,917(**)**	1.00								
Na2O	-0.11	,752(*)	**,808(*)**	0.16	0.07	-0.09	1.00							
K2O	0.59	0.58	0.44	-0.35	-0.43	-0.69	0.12	1.00						
P2O5	-0.28	0.69	**,823(*)**	0.24	0.23	0.08	**,824(*)**	-0.08	1.00					
SO3	0.22	0.43	0.31	-0.20	-0.29	-0.28	0.59	-0.14	0.39	1.00				
MnO	-,776(*)	-0.37	-0.13	0.65	,764(*)	,761(*)	-0.16	-0.44	0.26	-0.46	1.00			
TC	-,899(**)	-0.55	-0.30	0.69	,911(**)	,918(**)	-0.15	-0.37	-0.06	-0.48	,737(*)	1.00		
TIC	-,923(**)	-0.62	-0.38	0.70	,903(**)	**,964(**)**	-0.16	-0.52	-0.07	-0.41	,729(*)	,983(**)	1.00	
TOC	-0.07	0.28	0.34	0.09	0.24	-0.03	-0.02	,715(*)	0.00	-0.49	0.21	0.31	0.13	1.00

* Statistically significant at the 0.05-level

** Statistically significant at the 0.01-level

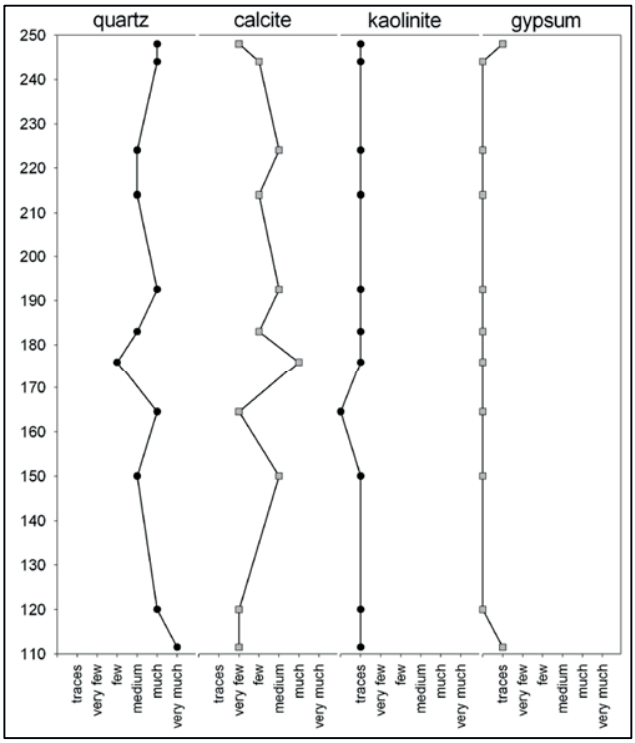

Figure 50 Mineralogical features of profile 10

The strong positive correlation (0.92) of Cao and MgO is also reflected in the correlations of SiO_2 and CaO, as well as of SiO_2 and MgO, which are strong negative (each -0.97). This connection of Cao and MgO is most likely due to the incorporation of magnesium during calcite formation. According to the statistics, magnesium content (max. 1.43 %) is only a fraction of that of calcium (max. 30.88 %). The correlation matrix reveals a trend of alternation of silica on the one hand and inorganic carbon, calcium and magnesium on the other hand.

The mineralogical composition of profile 10 (Figure 50) reveals the dominance of the quartz signal throughout the profile; merely once interrupted by a strong signal of calcite at 176 cm. Calcite shows overall medium values. Traces of kaolinite are roughly ubiquitously present in contrast to the gypsum signals that only occur at the top end and the base of the profile. The overall mineralogical assemblage of the presumably lacustrine sediments indicates high weathering intensities due to the reduced amount of detected compartments.

Grain size

The results for the grain size distribution from 0 to 150 µm obtained from laser sizer measurements of profile 10 are presented in Figure 51. Due to methodological limitations (cf. chapter 5.2.2.1), information on grain sizes larger than fine sand (150 µm) are not available.

Profile 10 shows slightly alternating values with a dominance of silt and increasing amounts of sand towards the bottom layers. The proportion of clay sized particles alternates between a maximum of 39.12 % to the minimum value of 21.43 (162 cm). The silt size fraction is dominated by fine silt (2-63 µm) with amounts ranging from 44.06 % (110 cm) to 50.37 % (191 cm), whereas the total silt fraction reaches contents from 60.89 % (212 cm) to 77.67 % (162 cm). Particles of fine sand size show generally very low amounts below 1 % throughout the profile; only the bottom layer shows a slight increase to 1.76 %.

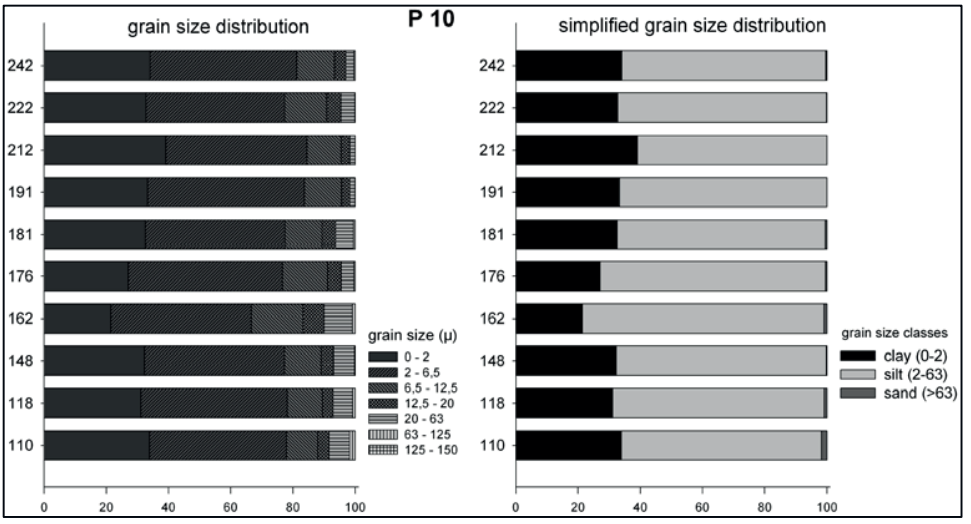

Figure 51 Grain size distribution of profile 10

Geochemical ratios and stoichiometric calculations

The mole ratio of Si/Al reflects the dominance of silica throughout the profile (Figure 52). The generally high values have their maximum of 18.19 in the bottommost layer, not dropping below 3.6 throughout the profile. In other words, the amount of silica is at least 3.6 times higher than that of aluminium and at most 18.19 times higher. The ratio of Ca/Si mainly remains at a low level, only once exceeding 1 at 164.5 centimetres, in accordance with the calcium maximum.

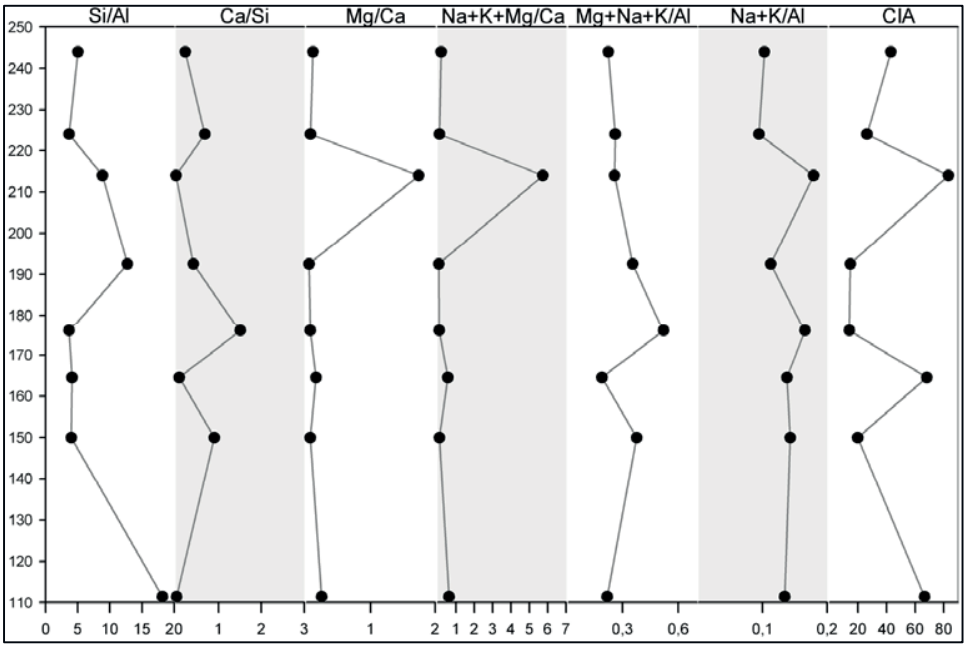

Figure 52 Main mole ratios of profile 10, CIA values derived from oxides

The Ti/Al ratio remains stable throughout the core, with one slightly decreased value in the profile's bottom layer. The singular maximum of the Na+K+Mg/Ca ratio can best be explained by the minimum value of CaO and maximum value of K_2O appearing within this layer.

The salinization ratio (Mg+K+Na/Al) shows no signs of increased salinity throughout the profile and remains at generally low levels. The same applies for the controlling ratio of Na+K/Ti. The chemical index of alteration (CIA) shows major variations throughout the profile, with two local maxima, at 214 and 164.5 centimetres and a minimum reaching from 192.5 to 176 centimetres.

The normative balancing of the main minerals is presented in Figure 53. Quartz alternates between the minimum values of about 20 % to 90.77 weight %. The distribution of calcite shows exactly the contrary pattern, with a minimum value of 2.5 % in the lowest, quartz dominated layer and the maximum of about 64 % at the quartz minimum layer at 176 centimetres. Kaolinite values show an increasing trend toward the top layers, only once interrupted at the quartz maximum, reaching its maximum value of 22.50 % at the topmost layer. The LOI values show roughly a similar increasing trend but with a maximum value at 214 centimetres.

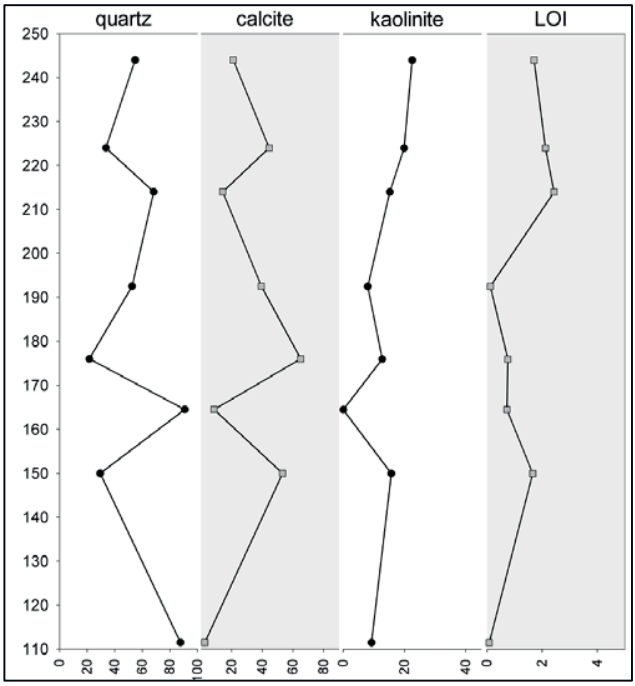

Figure 53 Normative balancing of main minerals in profile 10

7.2.3 Profile 11

Profile 11 is situated some hundreds of meters downstream compared to profile 10. The valley widens and the lacustrine sediments are more dismantled. The profile consists of a vertical wall of about 2 metres height with alternating layers of darker organic and brighter carbonate layers in the middle. The lacustrine layers can be found between 120 and 50 centimetres and are framed by massive layers of gravel on top and underneath (Figure 54).

Three layers were found suitable for radiocarbon dating. The results show ages reaching from 8430 ± 50 (55-61 cm) and 8010 ± 50 (85-93 cm) to 7910 ± 50 a BP (118-120 cm). The calibration of these dates shifts the results to 9460 ± 100, 8880 ± 200 and 8780 ± 260 cal a BP.

The distribution of organic and inorganic carbon (TOC + TIC) shows an alternating pattern throughout the core. The amount of organic carbon reaches medium values with a maximum of 2.09 weight percent at 106 centimetres and a minimum of 0.19 weight percent at 124 and 36 centimetres. Total inorganic carbon shows high values up to 9.98 weight percent at 82 centimetres and minima values at the top and base of the profile. The amount of sulphur is generally low and reaches a maximum of about 1 percent at 70 to 80 centimetres.

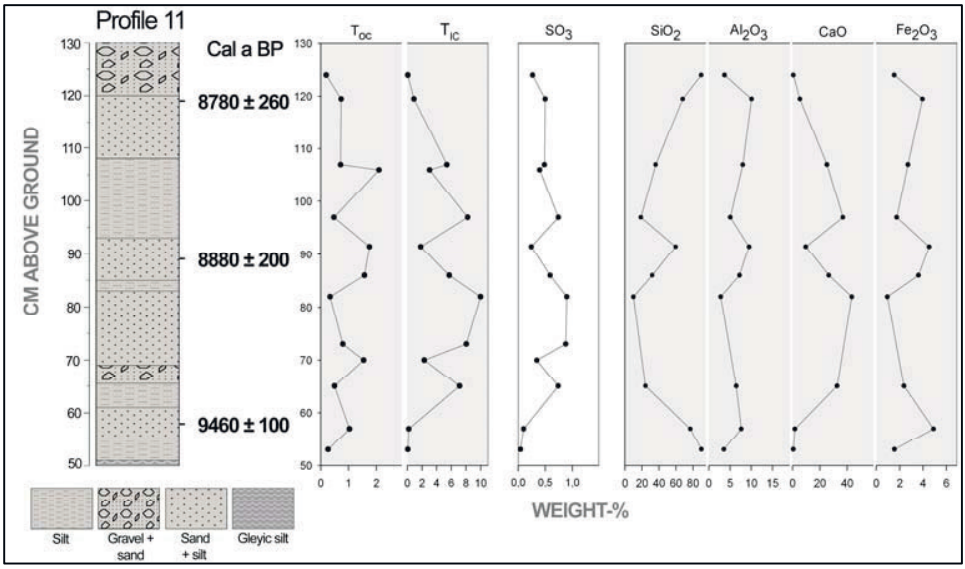

Figure 54 Selected geochemical features of profile 11

Silicon shows maximum values on top and base of the profile of about 90 percent and minimum values of 10 percent at the TIC maximum (82 cm). Aluminium shows an unsteady distribution and reaches from 2.81 to 10.08 weight percent (Table 20), the minimum values can be found at the top and base of the lacustrine segment. The values of Fe_2O_3 show a similar course to that of aluminium. The maximum lies at 57 centimetres and reaches 4.90 percent, the minimum of 0.94 at 82 centimetres. The distribution of calcium runs contrary to that of silicon. The minimum values of about 0.5 percent can be found at the top and base of the lacustrine sediments, the maximum value of 43.41 weight percent is located at 82 centimetres and coincides with the TIC maximum.

Table 20 Main geochemical statistics of profile 11

	SiO_2	TiO_2	Al_2O_3	Fe_2O_3	MgO	CaO	Na_2O	K_2O	P_2O_5	SO_3	MnO
n	10.00	10.00	10.00	10.00	10.00	10.00	10.00	10.00	10.00	10.00	10.00
Mean	50.50	0.40	6.41	2.78	0.67	18.23	0.04	0.40	0.07	0.00	0.01
Standard Deviation	29.98	0.16	2.54	1.39	0.26	16.47	0.05	0.16	0.03	0.00	0.01
Minimum	9.84	0.14	2.81	0.94	0.15	0.55	0.00	0.16	0.03	0.00	0.00
Maximum	89.97	0.69	10.08	4.90	0.89	43.41	0.12	0.67	0.11	0.00	0.02
Coefficient of Variation	0.59	0.41	0.40	0.50	0.39	0.90	1.19	0.40	0.37		1.70

The correlation matrix of profile 11, presented in Table 21, as well reveals contrary distributions of calcium and silicon with strong negative correlations of SiO_2 and CaO of -0.985. Calcium is essentially appearing in carbonates, referring to the extremely strong positive correlation of CaO and inorganic carbon (TIC) of 0.999. This association results the high negative yet strong correlation of SiO_2 and TIC of -0.98.

Table 21 Correlation matrix of profile 11

n=20	SiO_2	TiO_2	Al_2O_3	Fe_2O_3	MgO	CaO	Na_2O	K_2O	P_2O_5	MnO	TC	TIC	TOC
SiO2	1.00												
TiO2	0.32	1.00											
Al2O3	0.08	**,958(**)**	1.00										
Fe2O3	0.27	,843(**)	,877(**)	1.00									
MgO	-,727(*)	0.35	0.59	0.44	1.00								
CaO	**-,985(**)**	-0.47	-0.25	-0.42	0.60	1.00							
Na2O	0.23	,799(**)	,791(**)	,813(**)	0.42	-0.36							
K2O	0.40	**,978(**)**	**,909(**)**	,836(**)	0.26	-0.54	,806(**)	1.00					
P2O5	-0.50	0.52	,694(*)	0.47	,800(**)	0.37	0.25	0.44	1.00				
MnO	-,655(*)	-0.48	-0.36	-0.29	0.29	,679(*)	-0.38	-0.47	0.10	1.00			
TC	**-,992(**)**	-0.42	-0.18	-0.33	,657(*)	,993(**)	-0.31	-0.48	0.44	,712(*)	1.00		
TIC	**-,978(**)**	-0.50	-0.28	-0.45	0.57	**,999(**)**	-0.38	-0.57	0.34	,689(*)	,990(**)	1.00	
TOC	-0.05	0.60	,709(*)	,811(**)	0.54	-0.09	0.51	0.62	,661(*)	0.12	0.02	-0.12	1.00

* Statistically significant at the 0.05-level
** Statistically significant at the 0.01-level

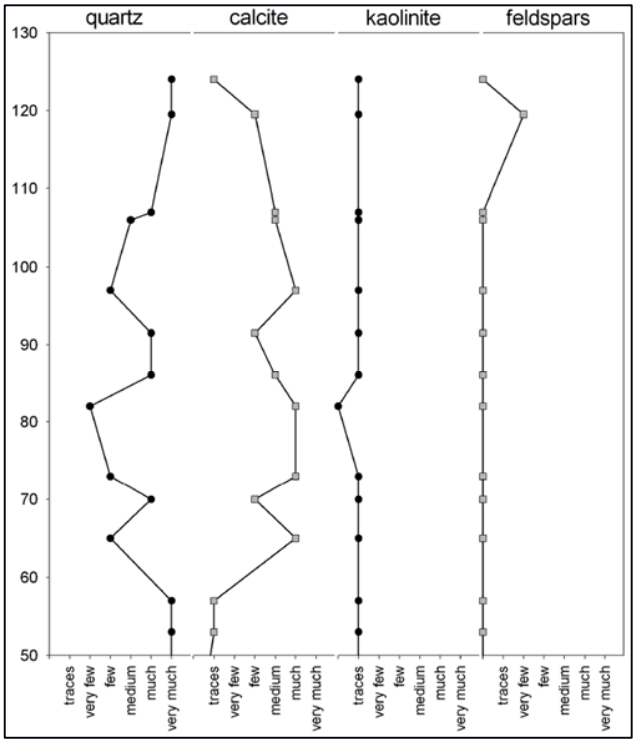

Figure 55 Mineralogical features of profile 11

Identical to the geochemical results, the mineralogical distribution profile (Figure 55) is dominated by the alternation of two compartments, in this case calcite and quartz. These two minerals show generally high signals but quartz shows slightly higher impulses at the top and base of the investigated profile. Traces of kaolinite are almost ubiquitously present, whereas feldspars (K-feldspar, albite) only appear at the top of the profile, where the quartz signal is dominating.

Grain size

The results for grain sizes from 0 to 150 µm obtained from laser sizer measurements of profile 11 are presented in Figure 56. Due to methodological limitations (cf. chapter 5.2.2.1), information on grain sizes larger than fine sand (150 µm) are not available.

Profile 11 shows slightly alternating values with an overall dominance of silt. The proportion of clay sized particles alternates between a solitary maximum of 49.08 % at 96 cm to the minimum value of 26.07 % at the bottommost layer. The silt size fraction is dominated by fine silt (2-63 µm) with amounts ranging from 35.99 % (96 cm) to 50.69 % (35 cm), whereas the total silt fraction reaches contents from 50.92 % at the clay maximum (96 cm) to 73.79 % (35 cm). Particles of fine sand size show generally very low amounts below 1 % throughout the profile.

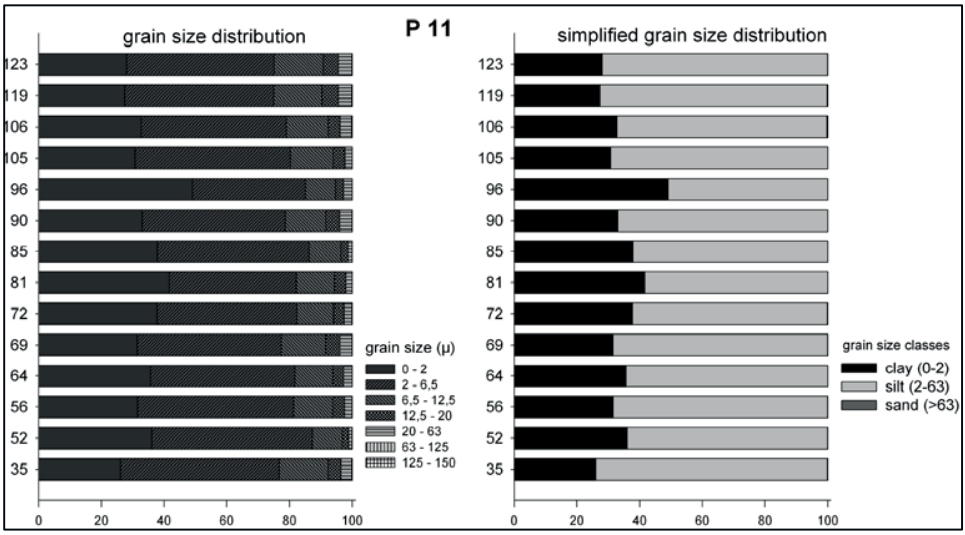

Figure 56 Grain size distribution of profile 11

Geochemical ratios and stoichiometric calculations

Figure 57 shows the main mole ratios of profile 11. The ratio of Si/Al indicates the occurrence of sand layers on top and at the bottom of the profile, as the maximum values (>20) are located there. The ratio of Ca/Si locates the calcium/calcite maximum at 82 centimetres with a quite high ratio of 4.7. The ratio of Al/Ti gives slight hints of quartz maxima as the top and bottom layers show decreased values. The Na+K+Mg/Ca ratio reflects the dominating presence of calcium with values way below 1 throughout the profile, the top and bottom layers excluded. The salinization ratio shows no specifics and remains at a low level as well as the ratio of Na+K/Ti, which shows a rather linear

pattern. A striking feature of the CIA ratio is the similarity of the pattern compared to the SiO_2 results of Figure 54 respectively the quartz distribution of Figure 58. This is due to the dominance of quartz in the top and bottom layers, indicating an aeolian setting with major input of quartz sands. Since the CIA ratio is derived from the differing amounts of Al on one hand and Ca, K and Na on the other hand, depleted amounts of the soluble fraction results in increased CIA results. In this case, calcium and sodium concentrations are reduced to 0 at the bottom and top layers.

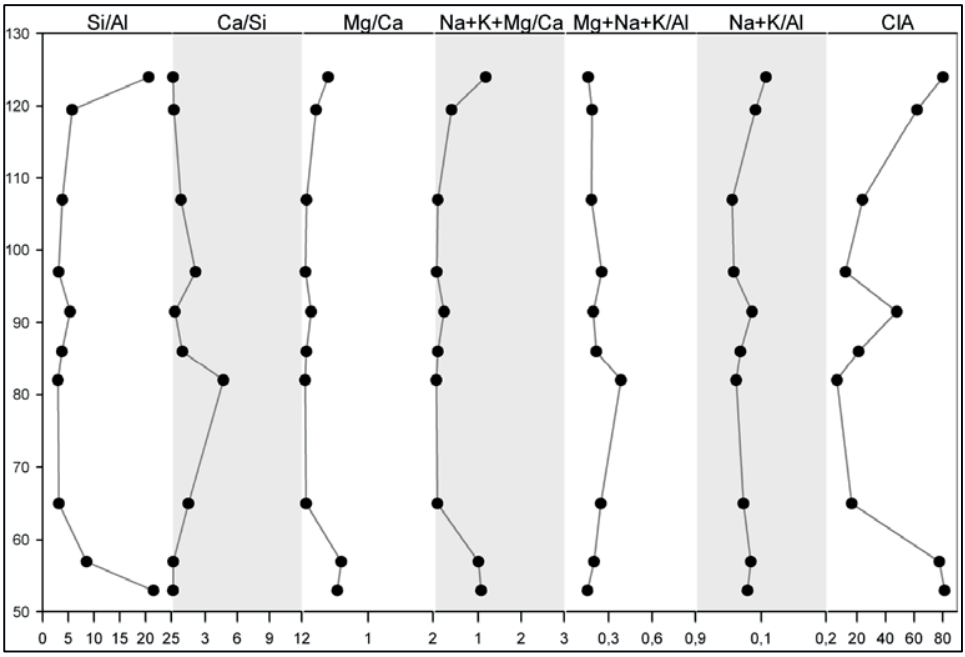

Figure 57 Main mole ratios of profile 11, CIA values derived from oxides

Normative balancing of the minerals is presented in Figure 58. There, the maximum values of calcite and quartz show similar extends as both reach up to about 90 percent at different heights. The minimum values show slightly differences, while calcium decreases down to 0.5 % at the top and bottom, the proportion of quartz does not fall below 10 % (at 82 cm). The kaolinite distribution shows depleted values at the calcite maxima, with maximum values of more than 20 % at 91.5 (22.23 %) and 119.5 (23.13 %) centimetres. The kaolinite maximum is in accordance with the singular appearance of feldspar. This could be evidencing the origin of the kaolinite as to the weathering of feldspars. The LOI shows a distribution similar to that of kaolinite, with its maximum values (>3 %) located in the middle of the investigated section (86-91.5 cm).

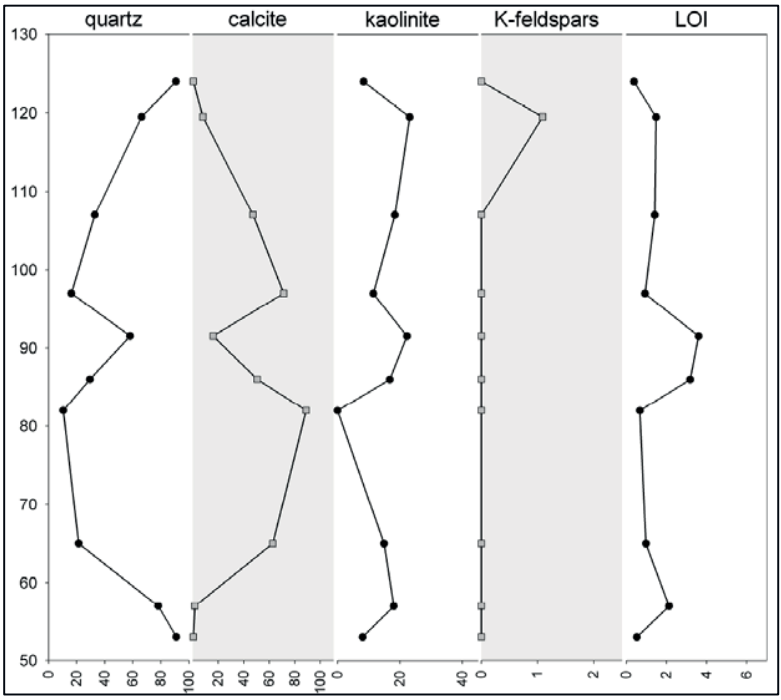

Figure 58 Normative balancing of main minerals in profile 11

7.2.4 Summary

Profile 8

The alternation of calcite and quartz shows a multi phased development of lacustrine sediments, dominated by the development of calcite. Variations of quartz and kaolinite occur simultaneously; therefore, the generally stable ratio of Si/Al can be used to estimate the detrital input. The ratio of Si/Al shows stable values at about 4 except for the lowest layers, where the amount of silicon doubles to a maximum value of about 9. The constant values evidence a stable input primarily from the surrounding catchment. Rising values towards the bottom layer indicate a transition from an environment mainly determined by aeolian dynamics and high quartz amounts, towards the lacustrine setting recorded in the upper layers. The rather low contents of potassium and sodium indicates an environment of low salinity but could also be considered an indicator of a highly weathered or leached profile. The ratio of Ca/Si mainly corresponds to the calcium maxima and silicon minima, its maximum values providing information about the main periods of lacustrine sedimentation/accumulation, which lie between 8000 and 8450 a BP, or 9480 ± 80 and 8870 ± 200 cal a BP.

Profile 10

Similar to profile 8, calcite and quartz show alternating values throughout the profile, indicating multiple phases of sedimentation. The lowest layer indicates an aeolian phase with only minor kaolinite occurrences. Then, involving a massive decrease of quartz and a significant increase of calcite, aquatic, most likely lacustrine sedimentation set in. The local quartz maximum is probably of detrital origin, whereas the Si/Al ratio points to an increase of diatomitic silica between 192.5 and 214 centimetres. As the TI/Al ratio usually shows a similar pattern as the Si/Al ratio (cf. profile 8) this differing patterns may indicate increasing diatom populations.

The rather low amount of minerals present within the profile indicates high weathering intensities. The radiocarbon dating result originating in the upper section of the profile is coincidental with the topmost dating of profile 8.

Profile 11

Just like the other lacustrine sediment profiles at this study site, profile 11 shows contrary running distributions of calcite and quartz. Due to the distinct dominance of quartz in the profile's upper and lower reaches a clear distinction of the aeolian and lacustrine stages can be made.

The three results of the radiocarbon dating are located within the lacustrine section. They show ages spanning from 8430 ± 50 (55-61 cm) and 8010 ± 50 (85-93 cm) to 7910 ± 50 a BP (118-120 cm). The calibration of these dates shifts the beginning of the lacustrine sedimentation to about 9460 ± 100 and the termination to approximately 8780 ± 260 cal a BP.

7.3 Yoo Ango

7.3.1 Profile 12

Profile 12 is located in the south-eastern area of the basin, in between numerous NE-SW moving barchans. In this area, lacustrine sediments mainly appear in small depressions. The profile was excavated stepwise along the slope of a small sediment bank that elevates about 1.5 metres above the basin floor. The base layers consist of cemented sands that show gleyic features of alternating proportions (Figure 59). Three layers were found suitable for radiocarbon dating at 50-58, 79-80 and 106-108 centimetres. They show a non-linear age distribution reaching from 17560 ± 130, and 23300 ± 300 to 11530 ± 70 a BP. Calibration of the dating results in ages from 21080 ± 320 and 28090 ± 520 to 13430 ± 180 cal a BP.

The main geochemical features of profile 12 are presented in Figure 62. The distribution of silicon and aluminium shows overall small variations as indicated by the coefficients of correlation in table 22, but silicon amounts show a distinct decrease towards the upper section of the profile, reaching the minimum value of 37.28 % at the top layer. Calcium remains at very low amounts in the lower parts of the profile but steadily increases at the top section to a maximum value of 21.42 weight-percent.

Iron shows a similar pattern with a distinct increase towards the top. Sodium amounts remain at a very low level with a mean of 2.93 %, but reach a maximum of 7.52 % at 79 centimetres. Potassium shows only minor variations with a mean of 24 % and high values between 0.8 and 1.73 %. Sulphur values alternate between a minimum of 0 to a maximum value of 11.48 %. Similar to the sodium values, sulphur amounts increase in a section below the top layers.

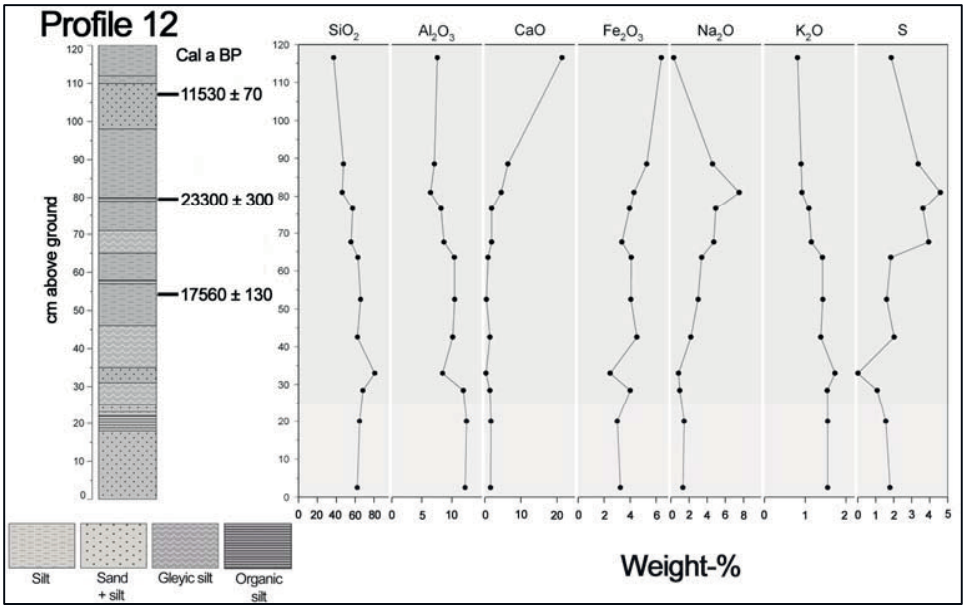

Figure 59 Selected geochemical features of profile 12

The correlation matrix of profile 12 is presented in Table 23. It shows only a few strong positive correlations. The strong positive correlation of SiO_2 and K_2O may indicate the occurrence of aeolian deposits (quartz and feldspars) in some layers. The obligatory strong positive correlation of titanium and aluminium supports the presence of alumino-silicates (feldspars).

The high number of medium to strong negative correlations, especially concerning silicon, reflects the opposing chemical distributions in the upper section of the profile. Strong positive correlations of sodium and sulphur, excluding calcium with weak correlations, point to the appearance of sodium sulphate (glauberite).

Table 22 Main geochemical statistics of profile 12

	SiO_2	TiO_2	Al_2O_3	Fe_2O_3	MgO	CaO	Na_2O	K_2O	P_2O_5	SO_3	MnO
n	12	12	12	12	12	12	12	12	12	12	12
Mean	59.28	0.51	9.49	4.06	2.64	3.62	2.93	1.29	0.11	5.67	0.17
Standard Deviation	11.49	0.11	2.04	1.05	1.39	5.87	2.17	0.30	0.22	3.32	0.27
Minimum	37.28	0.37	6.45	2.46	0.46	0.28	0.29	0.81	0.03	0.00	0.01
Maximum	80.76	0.66	12.42	6.40	5.44	21.42	7.52	1.73	0.81	11.48	0.81
Coefficient of Variation	19%	21%	22%	26%	52%	162%	74%	24%	206%	59%	153%

Table 23 Correlation matrix of profile 12

n=12	SiO_2	TiO_2	Al_2O_3	Fe_2O_3	MgO	CaO	Na_2O	K_2O	P_2O_5	SO_3	MnO
SiO2	1.00										
TiO2	0.36	1.00									
Al2O3	,580(*)	**,958(**)**	1.00								
Fe2O3	-,814(**)	-0.22	-0.46	1.00							
MgO	-,853(**)	-0.53	-,683(*)	,655(*)	1.00						
CaO	-,772(**)	-0.26	-0.45	,810(**)	0.44	1.00					
Na2O	-0.39	-0.56	-,577(*)	0.06	,664(*)	-0.19	1.00				
K2O	**,948(**)**	,594(*)	,772(**)	**-**,779(**)	**-**,898(**)	**-**,685(*)	**-**0.54	1.00			
P2O5	-,609(*)	-0.11	-0.28	,707(*)	0.19	**,957(**)**	-0.39	-0.50	1.00		
SO3	-,679(*)	-0.50	-0.57	0.28	,815(**)	0.10	**,887(**)**	-,760(**)	-0.10	1.00	
MnO	-,827(**)	-0.44	-,650(*)	,807(**)	,628(*)	,876(**)	0.16	-,794(**)	,749(**)	0.32	1.00

* Statistically significant at the 0.05-level

** Statistically significant at the 0.01-level

The mineralogical composition of profile 12 is presented in Figure 60. It shows a multitude of minerals, most of them are only present in the upper section of the profile. The quartz signal shows overall very strong signals, merely reduced in the upper layers. The feldspars signals are exclusively present in the mid and bottom section with rather weak signals.

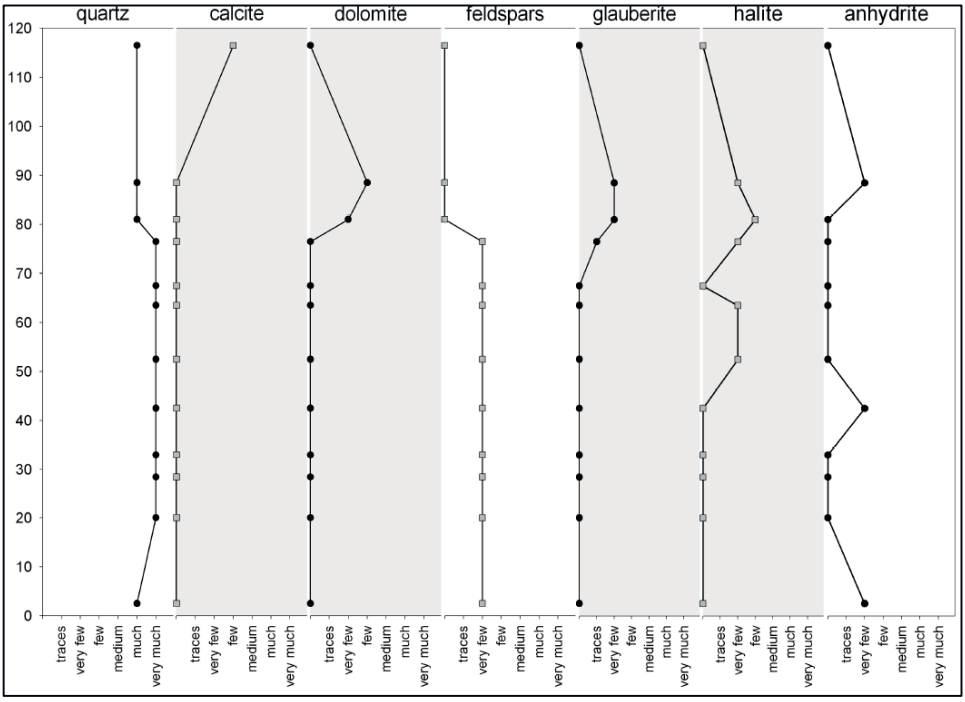

Figure 60 Mineralogical features of profile 12

Carbonates are present as calcite and dolomite, which is a unique appearance in all measured profiles. Both carbonates appear with few-medium signals in the upper section, calcite only in the topmost layer, dolomite in the two underlying layers. Additional evaporites of higher solubility are as well present in the profile. Glauberite and halite show few signals in the upper section, where halite appears additionally in the mid section (55-65 cm). Anhydrite, which also shows a few signals, even appears in the bottom layer of the profile. The multiple occurrences of evaporites throughout the profile indicate a multi-phased development of the basin, with several distinct evaporative sequences.

The mineralogical composition itself indicates a rather low chemical weathering intensity as a multitude of minerals is present within the profile. The presence of the highly soluble evaporitic minerals (halite + glauberite) at the top layers indicates an upward movement of water within the sediment profile. The presence of feldspars in the bottom sections point out to increased detrital input as feldspars, as well as mica, are exclusively considered to be of allogenic origin.

Grain size

The results for grain sizes from 0 to 150 µm obtained from laser sizer measurements of profile 12 are presented in Figure 61. Due to methodological limitations (cf. chapter 5.2.2.1), information on grain sizes larger than fine sand (150 µm) are not available. Profile 12 shows strongly alternating values with a dominance of silt and frequent presence of sand. The proportion of clay sized particles spans from very little amounts below 5 % at 0 and 40 cm to maximum values above 30 % at 27 and 31 cm. The silt size fraction is dominated by fine silt (2-63 µm) with amounts ranging from the minimum value of 25.61 % (40 cm) to the adjacent maximum of 52.63 % (50 cm), whereas the total silt fraction reaches very high contents from 68.36 % (31 cm) to above 90 % at several layers (0, 40, 62 and 65 cm). Particles of fine sand size show alternating amounts with their maximum values of above 3 % coinciding with the overall silt maxima (0 and 40 cm).

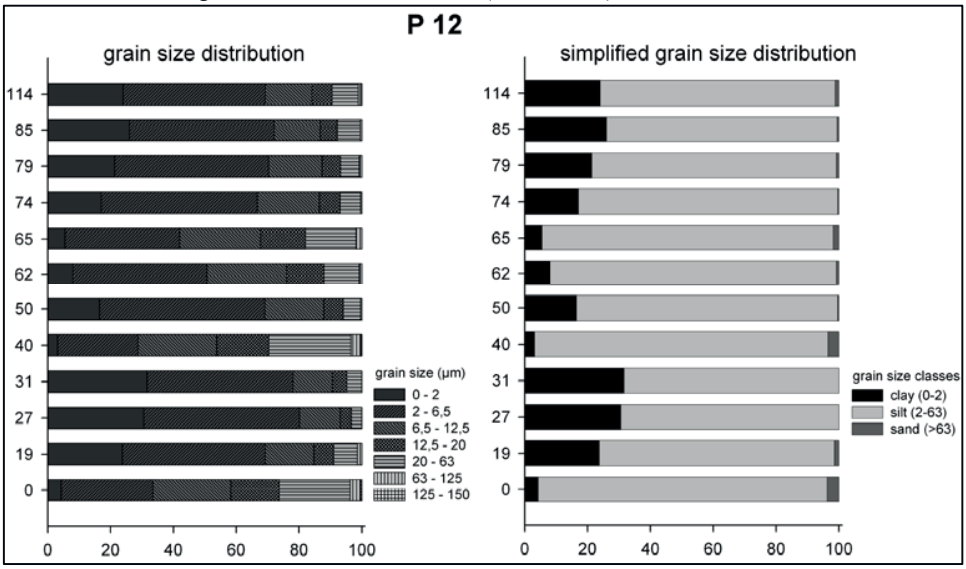

Figure 61 Grain size distribution of profile 12

Geochemical ratios and stoichiometric calculations

The main mole ratios of profile 12 are presented in Figure 65. The Si/Al remains rather stable throughout the profile, with slightly decreasing values towards the top and one exceptional maximum value (>8) at 31 centimetres. The solitary maximum points out to a solitary event of either quartz input or a rise of diatom populations. The Ca/Si ratio shows increased values in the topmost layers, the values of the bottom layers remain at very low levels, just above zero. The Al/Ti ratio shows only minor fluctuations, with values ranging from 25 to approximately 34.

The ratio of the main alkaline and earth alkaline metals indicates an enrichment of sodium, potassium and magnesium compared to calcium in the mid section. Referring to the geochemical and mineralogical results, this rise originates in the reduced amounts of calcium and the appearance of Na- and K-feldspars in this section.

The salinization ratio (Na+K+Mg/Al) reveals a distinct increase of the soluble fraction towards the top layers but the topmost layer shows a massively decreased value. The maximum value at 79 centimetres originates in the presence of dolomite at the upper reaches as well as in the presence of halite (NaCl) and glauberite ($Na_2Ca(SO_4)_2$) and therefore reflects indeed a higher salinity in this section.

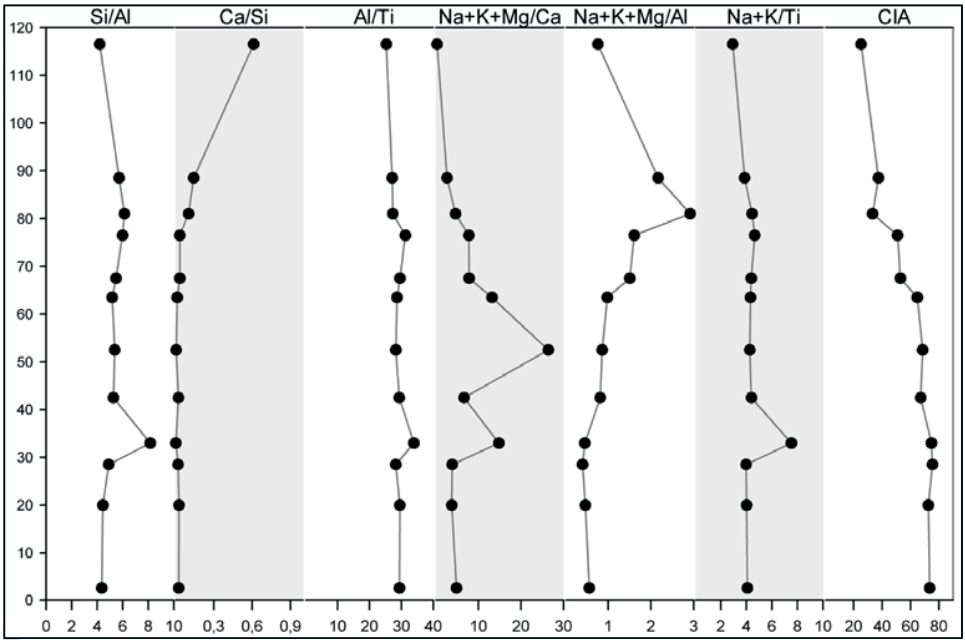

Figure 62 Main mole ratios of profile 12, CIA values derived from oxides

The ratio of Na+K/Ti shows overall high values with a maximum value in the silicon maximum layer (31 cm). The chemical index of alteration (CIA) reflects the general decrease of aluminium towards the top as well as the presence of evaporites at the upper section. It decreases from more than 70 in the bottom layers to 25 at the top layer.

Normative balancing of the mineralogical components led to the results presented in Figure 66. The proportions of the eleven detected minerals allow the separation of the profile in at least two segments. The top section shows high amounts of carbonates (calcite 40 %, dolomite 29.4 %) and high soluble evaporites like halite (8.4 %) and glauberite (12.9 %). The presence of these minerals indicates an extreme brine environment (saltwater) which actually enabled the formation of dolomite as a secondary carbonate.

The mid and bottom section show a rather chaotic pattern of mineralogical proportions. Feldspars show medium to low values (Na-feldspars 7.5 to 44 %, K-feldspars 5.3 to 11 %). Calcite merely randomly appears with amounts from 0.5 to 4.4 %. The unique appearance of a kaolinite signal could point out to increased weathering as the feldspars show local minima in this layer.

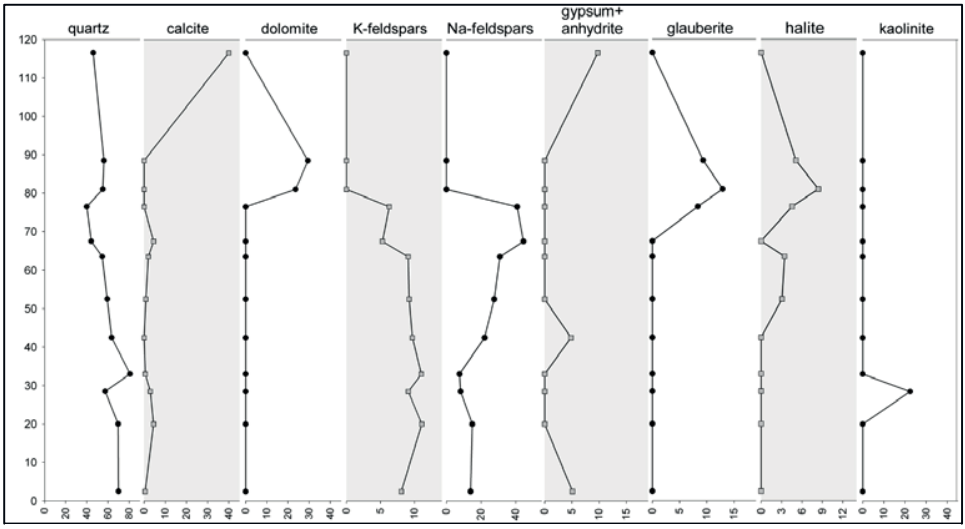

Figure 63 Normative balancing of main minerals in profile 12

7.3.2 Profile 13

Profile 13 is located only a few metres southwest of profile 12 and was excavated in a similar way. Due to overall low carbon content, only one layer was analysed for radiocarbon dating. With a total of organic carbon of merely 0.31 mg/g the layer was dated to 10890 ± 90 a BP. The calibration of the date revealed an age of 12850 ± 160 cal a BP.

The main geochemical features of profile 13 are presented in Figure 64 and Table 24. The main elements show a rather linear distribution throughout the core. Silicon dioxide proportions dominate the profile with amounts ranging from 50.8 % at the top layer to 83.92 % at the bottom layer of the profile. The greatest decrease is visible at the top, from 71.46 % at the second down to 80.8 % at the top layer; a drop of 20 %. Aluminium shows quite the opposite tendency, with lowest amounts at the bottom section (5.38 % at 8 cm) and maximum values at the top (14.75 %); the biggest increase located between the second and the first layer. CaO, SO_3 and Fe_2O_3 show a similar pattern as they show minimum values at the bottom and maximum amounts at the top layer. Potassium and sodium oxides show compared to CaO a linear distribution with very low amounts.

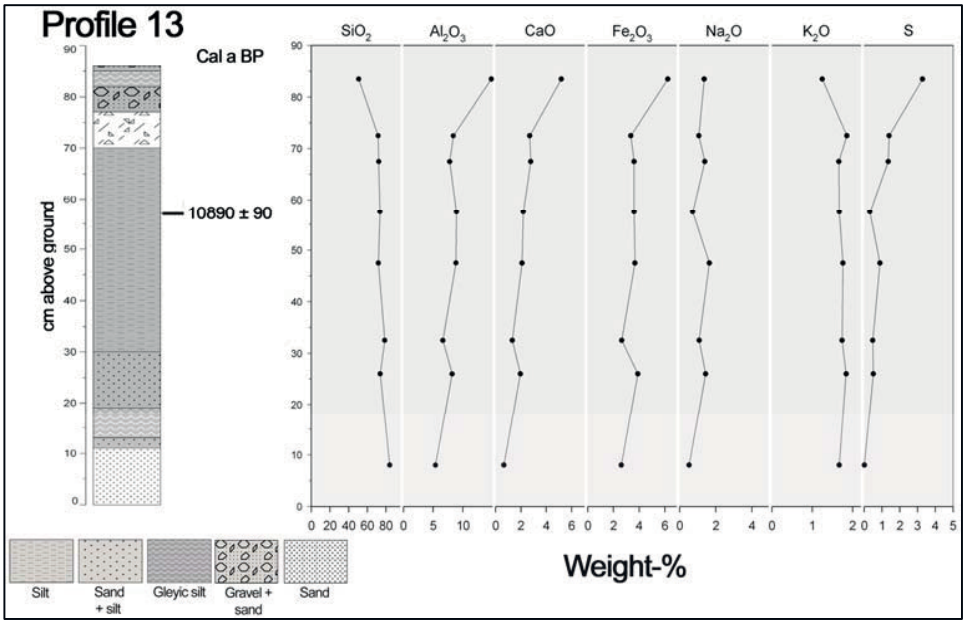

Figure 64 Selected geochemical features of profile 13

Table 24 Main geochemical statistics of profile 13

	SiO_2	TiO_2	Al_2O_3	Fe_2O_3	MgO	CaO	Na_2O	K_2O	P_2O_5	SO_3	MnO
n	8	8	8	8	8	8	8	8	8	8	8
Mean	72.02	0.48	8.60	3.70	1.05	2.35	1.15	1.68	0.12	2.56	0.03
Standard Deviation	9.57	0.12	2.76	1.13	0.38	1.34	0.38	0.19	0.06	2.58	0.02
Minimum	50.81	0.33	5.38	2.61	0.53	0.64	0.53	1.25	0.07	0.00	0.00
Maximum	83.92	0.73	14.75	6.23	1.78	5.19	1.64	1.86	0.25	8.19	0.07
Coefficient of Variation	13%	24%	32%	30%	36%	57%	33%	11%	48%	101%	83%

The correlation matrix of profile 13 (Table 25) evidences the exceptional position of silicon oxide within the profile as it shows strong negative correlations to virtually all the other compartments, potassium and sodium excluded. In contrast to that, the other main compartments show very strong positive correlations (cf. aluminium or iron). Sodium and potassium show only weak to medium correlations, indicating the presence of soluble salts, feldspars and mica. The increased correlation of potassium and silicon dioxide indicates the presence of mica or K-feldspars, an obvious suggestion as both mineral groups are present in profile 12.

Table 25 Correlation matrix of profile 13

n=8	SiO_2	TiO_2	Al_2O_3	Fe_2O_3	MgO	CaO	Na_2O	K_2O	P_2O_5	SO_3	MnO
SiO2	1.00										
TiO2	**-,948(**)**	1.00									
Al2O3	**-,986(**)**	,976(**)	1.00								
Fe2O3	**-,971(**)**	,923(**)	,975(**)	1.00							
MgO	**-,953(**)**	,884(**)	,938(**)	,896(**)	1.00						
CaO	**-,984(**)**	,912(**)	,951(**)	,937(**)	,959(**)	1.00					
Na2O	-0.49	0.35	0.42	0.46	0.43	0.46	1.00				
K2O	,748(*)	-,780(*)	-,765(*)	-,782(*)	-0.58	-,726(*)	-0.04	1.00			
P2O5	-,938(**)	,921(**)	,951(**)	,983(**)	,846(**)	,913(**)	0.35	-,830(*)	1.00		
SO3	-,951(**)	,839(**)	,896(**)	,886(**)	,903(**)	,964(**)	0.47	-,741(*)	,841(**)	1.00	
MnO	-,987(**)	,909(**)	,954(**)	,945(**)	,954(**)	,998(**)	0.45	-,738(*)	,919(**)	,973(**)	1.00

* Statistically significant at the 0.05-level

** Statistically significant at the 0.01-level

The mineralogical composition of profile 13 is presented in Figure 65. It emphasizes the proposed dominance of silicon within the profile as quartz shows very high amounts throughout the profile. Only in the top layer, a slight decrease is visible which conforms to the geochemical results.

Besides quartz, a variety of minerals is present throughout the profile, which is comparable to the composition of profile 12. Some minerals solely appear at the top layer, in detail kaolinite, anhydrite and sylvite also referred to as sylvine. They all show few to very few signals, indicating rather low compartments.

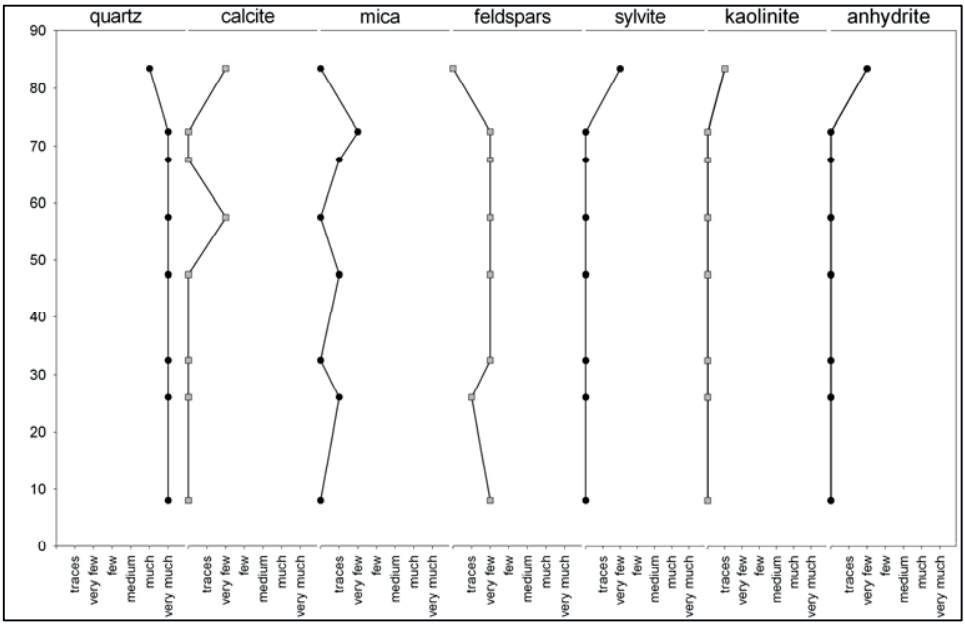

Figure 65 Mineralogical features of profile 13

Calcite is also present at the top layer but also appears at 67.5 centimetres, with low counts in both cases. Mica and feldspars do not appear at the top layer but show several low to very low counts throughout the profile. The measured feldspars are albite (Na) orthoclase and microcline (K), the majority of counts originating in K-feldspars. The mica group is represented by muscovite.

Grain size

The results for grain sizes from 0 to 150 µm obtained from laser sizer measurements of profile 13 are presented in Figure 66. Due to methodological limitations (cf. chapter 5.2.2.1), information on grain sizes larger than fine sand (150 µm) are not available.

Profile 13 shows a generally linear distribution of grain size classes with a definite dominance of silt and increasing amounts of sand towards the bottom layers. The proportion of clay sized particles alternates between a maximum of 35.47 % at the topmost layer to the minimum value of 24.76 % at the bottommost layer (6 cm).

The silt size fraction is dominated by fine silt (2-63 µm) with amounts ranging from 29.69 % at the bottom (6 cm) to 46.18 % at the top (82 cm), whereas the total silt fraction slightly alternates between 64.52 % (82 cm) and 73.68 % (70 cm). Particles of fine sand size show relatively high

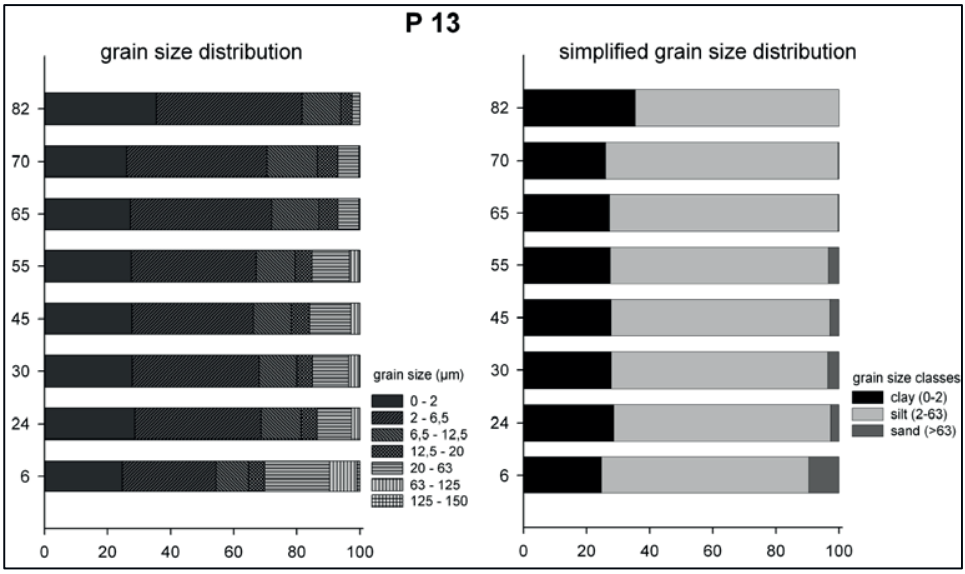

Figure 66 Grain size distribution of profile 13

amounts up to 9.52 % at the bottommost layer, followed by a distinct decrease towards the top.

Geochemical ratios and stoichiometric calculations

The main mole ratios of profile 13 are presented in Figure 67. The ratio of Si/Al actually reflects the distribution of silicon within the profile as it shows maximum values in the bottom section and decreases towards the top layer, resulting in a very low value of 2.9. The ratio of Ca/Si indicates the low proportion of calcium in the profile, with values far below 1 and a relatively linear course. The ratio of Al/Ti also shows a linear distribution with slightly increasing values towards the top.

The ratio of Na+K+Mg/Ca indicates a linear distribution with increasing values towards the bottom section due to decreasing values of sodium, magnesium and calcium and a constant presence of potassium throughout the profile. The salinization ratio shows low values below 1, with a minimum value of about 0.4 due to high aluminium amount in the top layer.

The exceptional conditions within the upper section are reflected in the Na+K/Ti ratio as it also shows its minimum in the top layer, indicating the removal of the soluble fraction (Na, K, Mg) and the passive accumulation of aluminium. This situation does not affect the chemical index of alteration as the high compartment of calcium, which is included in the CIA, blankets the accumulation of aluminium in the top layer. Consequently, the CIA shows a linear course with medium values ranging from 57 to 65.4.

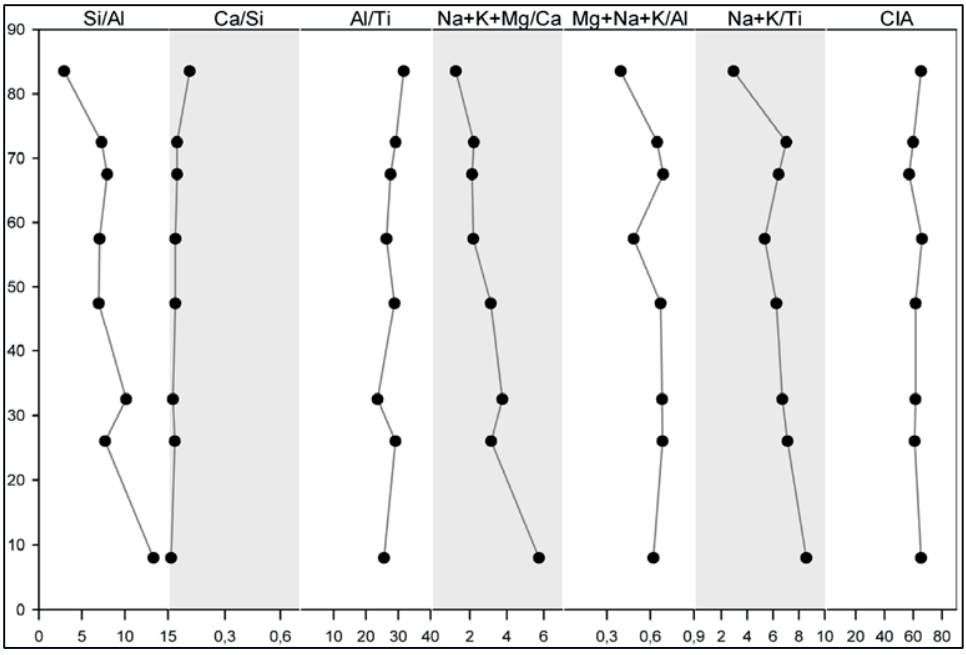

Figure 67 Main mole ratios of profile 13, CIA values derived from oxides

The normative balancing of the geochemical results considering the mineralogical evidence led to the results presented in Figure 68. The overall dominance of quartz within the profile leads to amounts ranging from more than 83 % at several layers to 48.95 % at the topmost layer. There, the singular appearance of kaolinite was calculated to 37.40 % and anhydrite present at the top layer, shows a percentage of 6.49.

The presence of calcite was evidenced for merely two layers by the mineralogical investigation. Nevertheless, the amount of residual calcium content compared to the confirmed minerals led to the conclusion of additional calcite in the profile. Balancing of the residual calcium content led to low amounts ranging from 1.2 % to 6 % in the topmost layer.

Orthoclase and microcline amounts were calculated as K-Feldspars, resulting in amounts ranging from 8 to 11.74 %, the top layer excluded as it showed no signal of feldspars. Due to the decreased amount of potassium in the top layer, the balancing of sylvine led to an amount of 1.15 (not displayed). The calculation of sodium feldspar (in this case albite) resulted in alternating values from 4.74 % at the bottom layer to a maximum of 15.29 % in the mid section. Muscovite shows a similar alternating distribution. There, all amounts show a rather small range, reaching from 2.46 to 2.80 %.

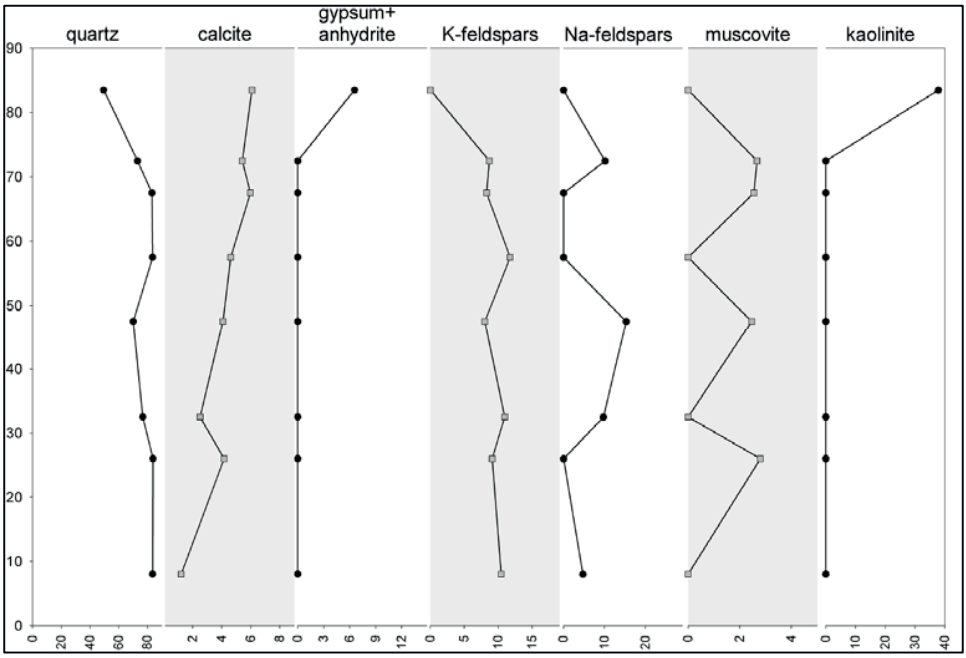

Figure 68 Normative balancing of main minerals in profile 13

P14 - Radiocarbon dating of a fireplace

Charcoals from a fireplace only a few metres away from profile 13 were dated to estimate the time of human settlement. The result shows an age of 5070 ± 40 a BP, the calibration led to a Neolithic age of 5820 ± 120 cal a BP.

7.3.3 Summary

Profile 12

A multi-phased development of the basin with several distinct evaporative sequences is indicated by the multiple occurrences of evaporites with diverse solubilities (glauberite, halite and anhydrite) throughout the profile. The exclusive evidence of dolomite in the upper section coincides with the presence of the highly soluble evaporitic minerals (halite + glauberite) and the maximum of the salinization ratio, indicating an upward movement of water within the sediment profile and highly saline conditions. The multitude of minerals verified within the profile indicates rather low chemical weathering intensity. The general mineralogical composition of the bottom sections point out to increased detrital input as feldspars, as well as mica, are exclusively considered to be of allogenic origin. The results obtained from radiocarbon dating show a non-linear age distribution reaching from 17560 ± 130, and 23300 ± 300 to 11530 ± 70 a BP (calibrated to 21080 ± 320, 28090 ± 520 and 13430 ± 180 cal a BP).

Profile 13

Profile 13 shows a distinct twofold distribution. The deposited feldspars and mica are partly weathered. The weathering results in the single occurrence of kaolinite in the topmost layer as it is considered a product of the chemical weathering of feldspars and mica.

The presence of gypsum and anhydrite has also to be considered of post sedimentary origin as it only appears at the top most layers. A supporting argument is the additional appearance of sylvite (KCl) in this layer. The intense chemical weathering of the feldspars first led to the downward removal of the soluble fractions (Ca, Mg, K, Na), presuming sufficient amount of precipitation. A subsequent upward movement of water within the sediment profile, caused by high aridity, would lead to the efflorescence of gypsum and subsequent alteration to anhydrite, and to the accumulation of soluble salts at the sediments surface. As potassium feldspars show higher amounts than Na-feldspars resulting in higher amounts of potassium, the development of sylvite (KCl) is more likely than that of halite (NaCl).

7.4 Discussion

As the investigated sites show large variations in their composition, the key points of discussion are derived from the environmental setting. But the overall data quality must first be validated before drawing any conclusions. The next step is to deduce the past environmental settings, as indicated by the investigations.

7.4.1 Evaluation of the supplementary study sites and data quality

As the sediment profiles originate in different environmental settings, some problems in their interpretation arise. The various accumulation settings lead to the variable reliability of the palaeoenvironmental statements derived from the profiles.

The Seeterrassental at Enneri Achelouma is a site of limited temporal existence as the natural dams and the associated lacustrine sedimentation show ages ranging from 9480 ± 80 to 8780 ± 260 cal a BP, and 7804 ± 110 cal a BP (GRUNERT, 1983). The profiles provide information about a very small catchment, because of their position in the upper reaches of the valley. It can be considered as a short-term archive, which responded rapidly to local climate-induced changes in precipitation. The number of biological proxies is limited, as the complete profile shows intense weathering, which led to the destruction of the majority of the pollen, while only a few diatoms have remained intact. The remnants of the lacustrine accumulations show distinct changes in environmental conditions, indicated by the alternating geochemical values and the mineralogical composition, although the profiles are highly weathered.

The sites of Yoo Ango and Fabérgé show a completely different sedimentation milieu, as they consist of basins within the foothills of the Tchigai, which are, at least in some areas, traversed by remnants of palaeodrainage systems. Additionally, an unknown amount of groundwater is thought to influence the Fabérgé basin, as currently active tamarisk plants indicate the presence of water. The regular appearance of evaporitic minerals such as gypsum, anhydrite, glauberite and halite within the sediment bodies gives proof of an environment of elevated evaporation.

The study sites show increased catchment sizes, probably extending towards the Tchigai massif. Radiocarbon dates indicate the existence of Yoo Ango as a sedimentation area since the Late Pleistocene (pre-LGM). The Fabérgé depression shows a limited temporal extent, from 6810 to 9440 cal a BP. The widespread occurrence of wind-shaped relicts and the limited amount of lacustrine remnants indicate generally high aeolian activity in both areas. Only in sheltered locations were parts of the lacustrine sequences preserved. The investigation of the local topography leads to the conclusion that there was probably orographic rainfall, assuming a prevailing monsoonal influence in the area (ZUPPI & SACCHI, 2004). Given the right circumstances, the Tibesti Mountains may have acted as “water towers”.

The mineralogical composition and the geochemical values of all the study sites are problematic in respect of their interpretation and reliability. According to SMYKATZ-KLOSS et al. (2004), carbonate-containing profiles have only restricted validity in geochemical analysis. Weathering processes involving micas and feldspars are often underrated, due to a high content of elements in the form of carbonates (mainly Ca, Mg and Sr). This restriction can be extended to the general dominance of evaporitic minerals.

As carbonates only contain a limited number of elements (Ca, Mg, Sr, C) but evaporites generally increase the range (Na, K, SO_4, and HCO_3-CO_3) (EUGSTER, 1980), the true intensity of weathering

and alteration may be hard to determine with respect to other minerals. In particular the profiles of Yoo Ango and Fabérgé show very large amounts of evaporites, of different solubility and composition, causing problems with regard to a correct geochemical and mineralogical interpretation. The massive appearance of evaporites leads additionally to the conclusion of either poor drainage conditions in the investigated material, or an environment of elevated evaporation associated with the presence of water (DONER & GROSSL, 2002).

The widespread occurrence of evaporites raises the question of their source. A continuous supply of soluble minerals is a prerequisite for the development of an evaporitic basin. One source of the soluble minerals is aeolian input, but as the depressions of Fabérgé and Yoo Ango are located in the foothills of the Plateau de Tchigai, frequent fluvial supply is also very likely. The additional investigation of palaeosoils in both basins has revealed the impact of groundwater, as the deeper sections show very large amounts of gypsum and salts. Furthermore, the bottom layers of some Yoo Ango profiles show gleyic characteristics, with accumulations of carbonates and salts (P. FELIX-HENNINGSEN, personal communication, June 2008).

The most challenging task when investigating palaeoenvironmental deposits is accurate dating. The profiles from the Seeterrassental at Enneri Achelouma and from the Fabérgé depression show a continuous sequence of sedimentation over a relative narrow period. Thus the datings can be considered correct and without further contamination.

In contrast, profile 12 from Yoo Ango reveals time confusion, as the oldest dating is located between two younger layers. Figure 69 shows one possible explanation of the problematic radiocarbon dates of profile 12. The most likely source of error originates in the method of sampling the sediment bank. Multiple inclined layers suggested that a stepwise sampling could successively cut layers of different temporal origin, depending on the stratigraphy. Consequently, this would have led to mixed dating results such as occurred in profile 12.

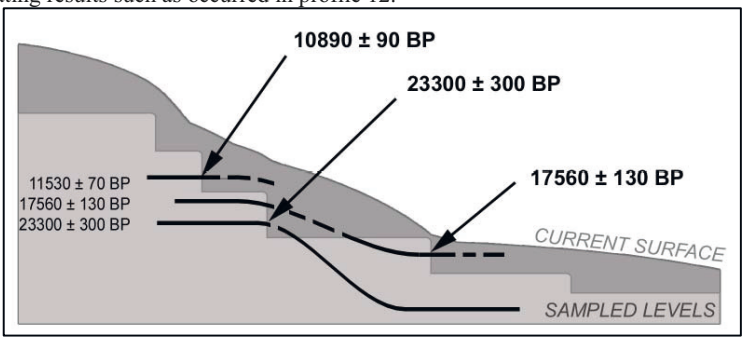

Figure 69 Potential source of error for alternating radiocarbon dates of profile 12

An additional explanation is the redistribution and relocation of the sediments by increased fluvial activity. The radiocarbon dates themselves show very large temporal distances compared to the distances within the sediment. It seems very likely that the material of at least one layer has been redeposited. Investigation of pollen has revealed the presence of charcoal within the profile. As the amount of organic matter is very low, this charcoal must be the source of the radiocarbon dates. As was seen in the Seggedim coring, such charcoal remnants can easily be relocated and subsequently give rise to interrupted chronologies. Consequently, the ages derived from profile 12 cannot be used to determine the lacustrine periods in the depression, but rather indicate periods with fires.

Referring to the Seggedim coring, such redistribution of sediments is very common, especially in areas with rapidly changing environments. However, this process can also lead to an interrupted chronology. Thus, the vertical distribution of the minerals and elements of profile 12 cannot be used to conclude anything about post-depositional redistribution and dynamics.

Due to massive deflation and relocation of the sediments, only the sediment profiles located in the Seeterrassental in Enneri Achelouma and the Fabérgé depression can be considered to provide valuable information on the timing and the development of the environmental conditions.

7.4.2 Environmental settings

FABÉRGÉ

The site referred to as Fabérgé shows a unique assemblage of evaporitic minerals. All three profiles show at least a minimal increase in the salinization ratio in their upper layers, in combination with clearly increased values for gypsum and anhydrite. Calcite always shows its maximum values in the bottom layers. Consequently, an upward-tending water movement due to evaporation can be assumed. The time of redistribution cannot be determined, but is obviously after the deposition of the lacustrine sediments.

The joint appearance of calcite and gypsum is common in soils, but the increased solubility of gypsum compared to calcite may lead to its solution within the soil and to reprecipitation following the water movement. In arid areas, where groundwater or near-surface water tends to ascend through a sediment body, gypsum is typically redeposited by capillary rise, also referred to as *per ascensum* (DONER & GROSSL, 2002). Thus, above-average accumulations of gypsum or anhydrite in the upper layers of a sediment body originate in upward-tending water movement due to increased evaporation. The formation of anhydrite requires high soil surface temperatures and extremely low humidity (DONER & GROSSL, 2002); both conditions are complied with in the central Sahara. In normal conditions, in soils with at least a minimum input of rainfall, anhydrite will be transformed to gypsum by the incorporation of H_2O.

At this site, a groundwater body appears to be the major influence on the development of the basin. Active, i.e. living, tamarisk hills and a large number of burial mounds lead to the conclusion that there have been long-lasting freshwater or slightly saline to brackish ponds. Radiocarbon and OSL dating have revealed the occurrence of massive lacustrine sediments during the Middle Holocene. The increased accumulation of these sediments during that period is believed to be of climatic origin: increased precipitation led to an enhancement of fluvial input into the basin and therefore to rising lake levels.

Massive deflation has removed large parts of the sediments, but some have remained intact under a sheltering crust of gypsum/calcite/dolomite. These sediments show postsedimentary relocation of evaporites due to upward-directed water movement and accumulations of the most soluble salts in the upper layers. Some sandy layers show gleyic features, due to changing water tables. These changes must have occurred with high frequency over a long period, as they are widespread and regularly present.

The radiocarbon dating reveals the presence of lacustrine environments between 5970 ± 50 and 8440 ± 50 a BP; calibration leads to an age-range from 6810 ± 140 a BP to 9440 ± 140 a BP. It cannot be determined whether there was one long-lasting lake phase or several short intervals with pools due to precipitation, as the geomorphological position and the habitus of the sediments is quite diverse. The saline character of the minerals found suggests a highly saline environment, but accumulation effects are very likely to have happened postsedimentary, when the lake or pools were drying out.

In addition, it is not really clear whether the basin filled only as a result of increased precipitation or whether this occurred because of increased surcharge by groundwater. The numerous spring mounds within the depression support the latter hypothesis, but there is no reliable way of estimating the amount of water supplied. The tamarisks in the basin give a general proof of the presence of groundwater but not of the probable depth, since some tamarisk species are known to have roots of up to 20 metres in length (CANADELL et al., 1996).

The presence of a large number of burial mounds, also referred to as tumuli, and of Neolithic artefacts, gives evidence for the presence of prehistoric settlers during various periods. The very large number of archaeological finds suggests a highly-frequented settlement site, most likely due to the presence of water. In addition, bone remnants were found when excavating a profile. The bones were transferred to the Université Abdou Moumouni de Niamey, but have not yet been identified or dated. The size of the skeletal remains, probably a femur of more than 30 centimetres length and parts of a pelvis, indicate a very large mammal, certainly not human.

The hypothesis of a multi-phased development of the basin is supported by the presence of dune sands below the tamarisk hills. These sands show gleyic features, as seen in the bottom parts of profile 4, such as strain-hardening (i.e. solidification) in combination with accumulations of iron oxides, and rusty stains visible to the naked eye. It appears that these dune sands have undergone reducing conditions, as a result of hydric fluctuations after their deposition. It is very likely that the subsequent shell-like growth of the tamarisks on top of the dunes prevented the removal of these sands during humid conditions. OSL-dating of a dune core within a tamarisk hill reveals an age of 1200 ± 100 ka BP (P. FELIX-HENNINGSEN, personal communication, June 2008).

A ramp of fossil dune sand was investigated and revealed an age of 6200 ± 400 ka BP. This age indicates the time of deposition of the dune sands after the Early Holocene humid period. Weak signs of soil development give evidence for the occurrence of at least random precipitation after the time of deposition (P. FELIX-HENNINGSEN, personal communication, June 2008).

ACHELOUMA

The Seeterrassental at Enneri Achelouma is a unique place as it shows lacustrine accumulations in a rather unexpected position. Due to massive landslides, several dams blocked the valley at several positions simultaneously, leading to the development of lacustrine ponds. The profiles investigated show continuous sedimentation records, but only for a short period between the Early and the Mid-Holocene. It is possible to gain indirect evidence of the impact in the Middle Holocene, as the sediment deposits have been dissected and partly removed (KRAUSE & SCHUETT, 2009).

The sequential stratification in all the profiles gives evidence of a multi-phased development of these sediments. Variations in rainfall are very likely to have occurred. The transitions from aeolian to lacustrine and back to aeolian-dominated sedimentation presumably occurred over a short period, as there are distinct differences in the stratification. The mineralogical composition shows a reduced range of minerals, indicating high weathering intensity after the time of deposition.

The stratification shows a distinct maximum of lacustrine sedimentation from 9480 ± 80 cal a BP to 8780 ± 260 a BP. Profile 8 and profile 11 both yielded three radiocarbon dating results giving evidence of the time of lacustrine accumulation. An age depth/height model indicates comparable accumulation rates, of about 61 to 65 centimetres in both profiles, over a period of 610 to 680 years. The radiocarbon dating of profile 10 can be assigned to the final stage of lacustrine sedimentation, because of its position in the upper parts of the profile. Consequently, this date reveals a similar extent of accumulation, of approximately 60 centimetres, starting at the first calcite layer at 150 centimetres.

GRUNERT (1983) has dated organic components of the sediments between 8165 ± 200 a BP (Calendric Age calBP: 9074 ± 276) and 6960± 120 a BP (Calendric Age calBP: 7804 ± 110), and assumes the end of the lacustrine sedimentation about 6 ka BP. Investigations of pollen and ostracods have indicated a cooler climate than at present with evidently greater humidity. The author states that the increased precipitation is of mediterranean origin, because of the southward migration of the ITCZ (GRUNERT, 1983).

The landslides which causing the damming must therefore have occurred earlier than the oldest dating from the lacustrine sediments, which is 9480 cal a BP. BUSCHE (2001) suggests that the landslides took place in the Early Pleistocene. The presence of these landslides in the present arid environment has led to an estimation of the amount of rainfall required to set the bedrock in motion. Rock slides may occur when the shear strength of the bottom material is exceeded, either through the swelling of clay minerals by water saturation or by sodium substitution in their octahedral layer (PACHUR & ALTMANN, 2006). GRUNERT (1983) estimates that a minimum annual precipitation of 300 mm in the northern hemisphere winter would be required to produce these landslides, due to the reduced evaporation. In contrast, BUSCHE (2001) disputes this figure and proposes a considerably higher amount, without any restrictions on the prevailing climate.

In addition, the date of the increased fluvial dynamics which caused the incision of the lacustrine deposits can be established as Middle Holocene, since the dating shows ages younger than 8780 cal a BP. With reference to the dating obtained from GRUNERT (1983), fluvial erosion must have happened later than 7804 cal a BP.

Because of the geographic setting, any significant influence of ground water can be excluded, as can any appreciable increase in orographic precipitation. The radiocarbon dating has yielded Early to Middle Holocene ages for the sediments, leading to the conclusion that a climate-driven increase in precipitation was the origin of the sediments. Subsequent variations in precipitation in the Middle Holocene (possibly due to enhanced seasonality) and the resulting surface wash must have led to the removal of the dams as well as of the deposited sediments. In addition, the generally intense weathering of the sediment profiles indicates the prevailing presence of moisture after their deposition.

Balancing of the palaeodischarge based on the palaeochannel morphology of three terrace levels (KRAUSE & SCHUETT, 2009) has revealed some general aspects of the Holocene fluvial dynamics in the Seeterrassental:

- there is a downstream decrease in discharge, due to increasing infiltration occurring in all channel generations;
- the oldest channel shows the highest discharge values, and the youngest shows the lowest values, indicating a decrease of discharge (and consequently precipitation) throughout the Holocene;
- there is an increasing extent of both deviations of flood events and bank-full discharge (maximum velocity within banks) from the past to the present, indicating/caused by Middle Holocene aridisation – increasingly erratic rainfall and increasing variability in daily rainfall.

Estimates of precipitation vary in extent and amplitude, according to the kind of investigation performed (model-based or based on palaeoenvironmental records). Using meteorological hindcast, RENSSEN et al. (2006) estimate a mean annual precipitation of about 290 mm for 9-7.5 ka cal BP, in combination with high summer temperatures and increased precipitation in the Western Sahara and the Sahel. The authors reveal a key precipitation anomaly at 9 ka cal BP, restricted to the northern hemisphere summer months (June to August). The greatest effect of the anomaly is apparently located at 20° N with a maximum increase of precipitation in August of 110 mm. Most importantly,

increasing rainfall variability, associated with higher amplitudes, is considered to have developed at a later date.

DeMENOCAL et al. (2006) have derived data from a deep-sea coring and have concluded that the maximum of the so-called African Humid Period was at approximately 10.6 ka BP, and involved an increase in annual precipitation of 40% compared to the present. According to the authors, the AHP developed because of changes in the earth's orbital setting, resulting in increased summer insolation with a subsequent increase in monsoon intensity. Reconstruction of summer insolation values has indicated that the beginning of the AHP was at about 14.5 ka BP and the end at about 5.5 ka BP.

NICHOLSON & FLOHN (1980) have investigated and compared lacustrine records from northern Africa and propose a three-phased climatic development, starting in the Pleistocene. They assume two humid periods in the Holocene, from 10 to 8 ka BP and from 6.5 to 4.5 ka BP. During these humid phases, new lakes developed and existing lake levels rose, as a result of an increase in annual precipitation of approximately 400 mm.

When estimating the extent of present-day discharge a rare rainfall event, recorded at the Madama station in the vicinity of the Enneri Achelouma, must be mentioned. It brought 41.1 mm rain during one day in May 1941 (GRUNERT, 1983). According to DUBIEF (1971), rainfall amounts in northern Africa originate in singular events lasting between 45 minutes (in northern hemisphere summer) and 6 hours (in the northern hemisphere winter) (KRAUSE & SCHUETT, 2009).

Combining the distinct increase of precipitation reported by many authors for the time around 10 ka BP with an estimated discharge rate of 80 % at the upper reaches of the Seeterrassental (KRAUSE & SCHUETT, 2009), it is conceivable that the fluvial dynamics were sufficient to cause the removal of the valley dams and lacustrine deposits in the middle of the Holocene.

YOO ANGO

The frequent appearance of evaporites in soil environments leads to the conclusion of either poor drainage conditions in the investigated area or an environment of elevated evaporation (DONER & GROSSL, 2002). The analyses of profiles 12 and 13 indicate a multi-phased development of these sediments. The main components are quartz, with mica and feldspars, all of them considered to be of detrital origin.

Regarding the data quality, the radiocarbon dates show very large temporal distances, compared to the overall accumulation thickness of the sediment. The radiocarbon ages obtained from the sediment profiles range from 12850 ± 160 cal a BP to 21080 ± 320 cal a BP to 28090 ± 520 cal a BP. The very low amount of carbon in these profiles (e.g. profile 13 at 55-60 cm depth contained as little as 0.31 mg of carbon), in combination with the large amounts of calcite in both the sampled and the adjacent layers, indicate increased accessibility of carbon, which may produce misleading age-values (hardwater effect).

The non-linear chronology of profile 12 indicates either a relocation of the sediment or an error, which may have been produced by the sampling technique (Figure 72). As the organic carbon contained in the profiles most likely originates from charcoal, relocation of the sediments seems very likely. As a result, the vertical distribution of the minerals and elements of profile 12 cannot be used to deduce any depositional dynamics. However, the results of the radiocarbon dating give evidence for the timing of fires. Whether the fires originated in manmade fire or in lightning cannot be determined. A fireplace near profiles 12 and 13 has been dated to 5820 ± 120 cal a BP and can be excluded as the source of disordered chronology. However, if the ages and derived accumulation rates can be considered reliable, they would indicate the removal of extensive sequences from the profile, which would lower the reliability of any derived information about landscape succession.

The study sites of Fabérgé and Yoo Ango are located in the current of the Harmattan, a NE-SW running North African wind system of the northern hemisphere winter. The Harmattan is one component (the ground) of the African continental trade wind system and is considered to be the driving force of aeolian dust export from the Bodelé depression to southern West Africa. The southward migration of the ITCZ during the LGM, and the associated shift of the rain-bearing monsoon, caused the expansion of desert conditions. This also intensified the aeolian impact of the Harmattan on the landscape, causing massive deflation in Late Pleistocene (SCHWANGHART & SCHUETT, 2008). The extremely low accumulation rate at Yoo Ango indicates massive deflation and removal of deposited material as soon as the basin fell dry. However, post-depositional processes, such as the upward relocation of evaporites, can be assumed, as gypsum and other highly soluble minerals accumulated in the upper layers.

Yoo Ango is most likely influenced by an increased water supply, because of orographic rainfall in the Tibesti foothills and/or the subterranean groundwater charge in the area (PIRARD, 1962). According to PACHUR et al. (2006), the increased precipitation at the southwestern and western fringes of the Tibesti Mountains induced river systems with many incorporated lacustrine basins in the Early Holocene. This is why the sediment records show a rather irregular occurrence of lacustrine sediments reaching back to the Pleistocene. The lacustrine records from the northern tip of the Tibesti foothills have revealed a similar unusual/unexpected pattern, which does not fit the overall climate evolution theory (JAEKEL, 1979). The geoecological scenario of the Tibesti Mountains during the Early and Mid-Holocene as concluded by PACHUR et al. (2006) is as follows:

- precipitation at 2000 m asl were 4-5 times greater than at present;
- there was episodic drainage of the valleys;
- torrential discharge was absorbed by vegetation or increased retention.

7.5 Conclusion

The supplementary study sites give a glimpse of the variety of palaeoenvironmental records in the Central Sahara. The profiles investigated show a variety of properties, not all necessarily suitable for the derivation of palaeoclimatic information, as they are to a certain extent determined by regional factors. The groundwater supply in the Yoo Ango and Fabérgé depressions, and the associated development of evaporites in the upper layers of the profiles investigated, overlay most of the synsedimentary signals. Furthermore, the high weathering intensity has led to the destruction of biological indicators as well as of most index minerals. The Seeterrassental at Enneri Achelouma is thought to provide palaeoenvironmental information which is mainly determined by the regional climate, as local modifying factors can be neglected.

In the plateau landscapes of Djado, Mangueni and Tchigai, two depressions and a valley consisting of lacustrine terraces were investigated for palaeoenvironmental reconstruction. These sediment archives indicate a relatively short existence, of a few hundred years, but reveal additional information about the landscape dynamics from the Early to the Middle Holocene. Depending on local modifying factors, these archives show temporal variations in the extent of the lacustrine phases as well as in their termination dates.

During the Early Holocene, the lacustrine pools became established in the Achelouma area (Seeterrassental), initiated by fossil landslides, which had produced natural dams in the valley. At the same time there were pools or ponds in Fabérgé, probably of fresh water and with frequent nomadic settlements adjacent to them. Alternating values in the profiles indicate climatic fluctuations, but with generally wetter conditions than now, from about 9.5 to 6.8 ka BP at Faberge and from 9.5 to 8.8 at the Seeterrassental.

In the Middle Holocene, the environmental situation changed. In the Enneri Achelouma, the increased surface flow led to the erosion of the natural dams and to the dismantling and incising of the deposited sediments. At Fabérgé, the water pools must have developed into evaporitic ponds and subsequently into desiccating pools. The explicit evaporitic environment became established after 5970 ± 50 a BP (or 6810 ± 140 cal a BP), since the remnants of a lacustrine environment were dated to this point in time. The tendency for aeolian activity to occur in the foothills of the Tchigai plateau led in the Middle Holocene to the onset of dune activity in the depression of Fabérgé, with signs of subsequent precipitation.

The site of Yoo Ango shows a rather irregular pattern of lacustrine deposition. It is very likely to have developed as a result of massive deflation and fluvial relocation of lacustrine sediments. The very large number of fireplaces in this area indicates a considerable human population in the Middle Holocene. The dating of a fireplace revealed an age of 5070 ± 40 a BP, calibration gave an age of 5820 ± 120 cal a BP. Presumably there was accessible freshwater at least up to that point of time,, but because of the scanty evidence, no additional information can be obtained from that site.

No indications of separate Early and Middle Holocene wet periods were found in the investigated profiles, as they show relatively short, but nevertheless significant and continuous accumulation of lacustrine sediments from the Early to the Middle Holocene. However, substantial variations in the precipitation regime are evident, indicated by alternating values in the profiles of Achelouma and their subsequent removal by temporarily increased fluvial dynamics. The profiles of Yoo Ango indicate multiple lacustrine phases, from the Pleistocene to the Holocene, or at least show indices of fires, but due to confusing radiocarbon dating and probable relocation of the sediment, these hypotheses cannot be verified.

8 SYNTHESIS

As this work comprises several elements, this final chapter makes a synthesis of the interconnected evidence and the insights of the preceding chapters. A comparative summary of the literature on palaeoenvironmental archives provides the basis for the derivation of those geographical factors which have affected landscape development at the study sites and have modified the results obtained. A model of climate-driven landscape progression is then constructed, interconnecting the results inferred from the diverse study sites as well as evidence from other studies in palaeoenvironmental reconstruction in northern Africa.

8.1 Synopsis of palaeoenvironmental reconstruction

The information that lacustrine sediments provide is considered to be mainly of the synsedimentary type and may only explain the environmental conditions within the lake drainage basin being investigated (SCHUETT & KRAUSE, 2009) and thus only be applicable on a regional scale. In addition, lacustrine proxies may show non-linear reactions to climate variations, and the coherence of climatic proxies at a single stage is modified by changing environmental conditions (FRITZ, 2008). In particular, palaeoenvironmental reconstructions from lakes with small catchment areas are highly susceptible to error. In such cases, a regional comparison of several multiproxy records may provide reliable data, but individual variations can occur even in adjacent areas (BAUMHAUER, 1991; FRITZ, 2008).

When deriving palaeoclimate information from palaeoenvironmental proxies, it is essential to know whether an investigated site is controlled primarily by local factors or climatic forcing. The examination of the existing literature on Holocene palaeoenvironmental studies in the Sahara (SCHUETT & KRAUSE, 2009) confirms that there is general agreement on at least one humid period in the Early Holocene, but important differences are to be found in the diverse time extents proposed by different authors (Figure 73). These extend from just a few hundred years (BUSCHE, 1979; GRUNERT, 1983; GRUNERT et al., 1991) to almost 10 ka (GASSE & van CAMPO, 1994; JAEKEL, 1979), barely interrupted by a small number of arid intervals. These inconsistencies are essentially caused by the regional factors influencing the environmental record of a study site, especially those of lakes in the Sahara. Consequently, the different environmental succession of palaeolakes within the Sahara, indicated by palaeoenvironmental proxies, is not the result of small-scale, regional climatic differences, but is an expression of the diversity in the geographical setting of the sites (BAUMHAUER, 1991).

A major source of erroneous interpretation is the unmeasurable and unpredictable inflow of groundwater into a drainage basin. Especially in arid areas, groundwater surcharge can overlay climatic forcing and lead to substantial dissimilarities even among contiguous drainage basins. GRUNERT et al. (1991) and BAUMHAUER (1991) have emphasized the dissimilar response of palaeolakes in the central Sahara to climate forcing. For instance, there are large aquifers in the Kaouar area which have a major influence on the recharge and water levels of the water bodies in this region (BAUMHAUER, 1986; BAUMHAUER, 1988; BAUMHAUER, 1991; BAUMHAUER, 2004; BAUMHAUER et al., 1989; BAUMHAUER & SCHULZ, 1984; BAUMHAUER et al., 2004).

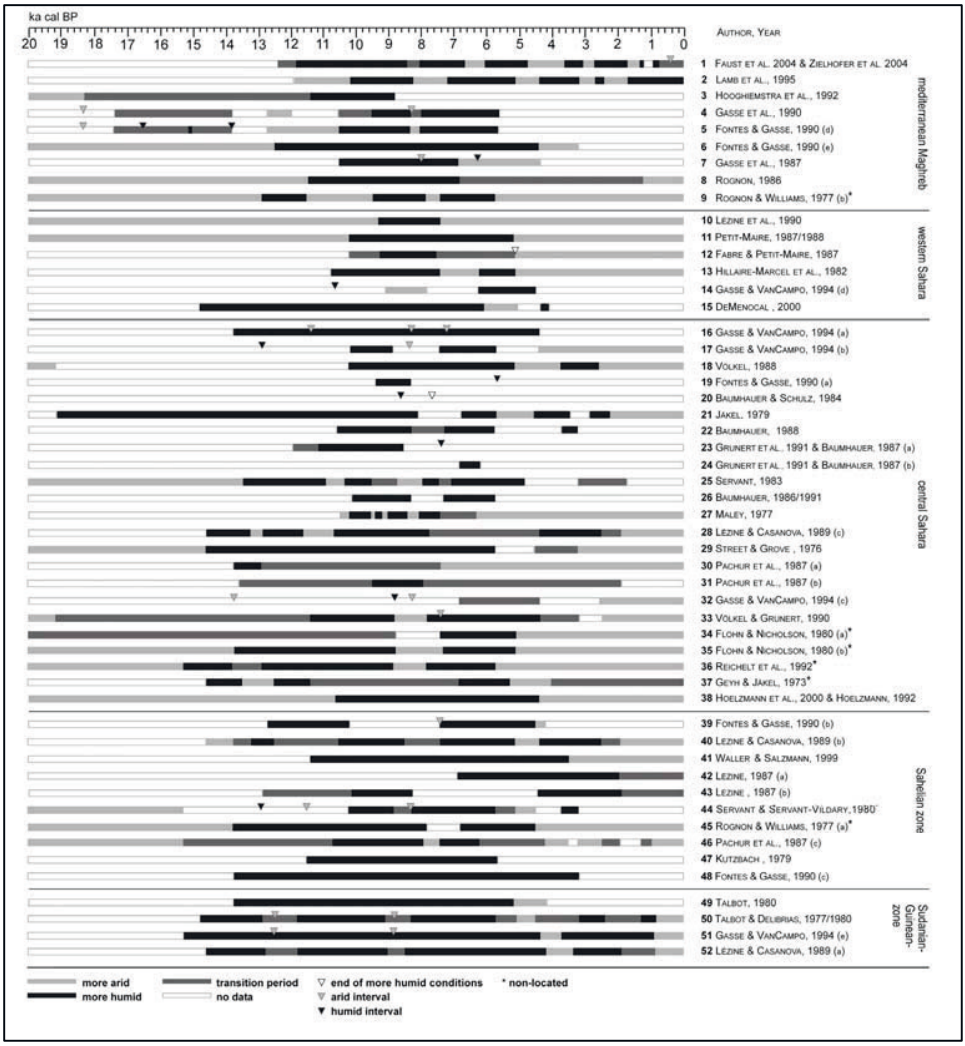

Figure 70 Literature analysis of Holocene palaeoenvironmental research in the Central Sahara (modified from SCHUETT & KRAUSE, 2009)

Large aquifers in Northern Africa have the proven potential to unlink the development of water bodies from climate forcing. Hypersaline lakes in the Eyeden Murzuk (Pachur and Altmann, 2006) and in the Northern Chad still exist, actually not fed primarily by precipitation but by large aquifers within the sandstone underlying huge areas in the Sahara. An investigation of lacustrine sediments obtained from Lake Yoa (19.03° N, 20.31° E, 380 m asl) in Northern Chad revealed a continuous sedimentation record for at least the last 6000 years (Kröpelin, et al., 2008). The lake was preserved throughout the Late Holocene because of the groundwater charge from the Nubian Sandstone aquifer although the overall climatic situation was tending towards arid conditions. As the total surface area of the lake remained quite stable, a very large amount of remote pollen was blown into the lake and thus archived, creating a continuous pollen record.

Lake Yoa is situated merely about 800 km east of Seggedim, and the geographical setting is quite similar to the Seggedim depression, but clearly differs in the amount of groundwater inflow and the aquifer size. Most likely, the different environmental successions of these lakes are not results of small scale, regional climatic differences but expressions of the diversity in the geographical setting of the sites. As a consequence, the information inferred from lakes fed by aquifers within a fully arid area may be misleading regarding the climatological signal. Depending on the buffering capacity of the water body, alterations in precipitation are for the most part not immediately recorded in the sediment archive because the lakes are mainly fed by groundwater charge. Furthermore, as the palaeoenvironmental information obtained is primarily of the synsedimentary type and will merely reflect the environmental conditions within the respective drainage basin (Krause and Schütt, 2009) it is also only applicable on the regional scale.

The topography of mountainous areas such as the Tibesti and Air Massifs operates additively "as water towers" (GASSE, 2000) for the surrounding lowlands and therefore increases the regional water supply. The present mean annual rainfall in the Air massif shows variations from only 100 mm at the SW to 170 mm in elevated regions and down to less than 5 mm in the mountain's rain shadow, at the north-eastern fringes (GALLAIRE, 1995). ZUPPI and SACCHI (2004) refer to the massifs of the central Sahara as a "topographic barrier", which prevents the movement of air masses to the north or south and leads to orographic (relief) precipitation on the windward side of mountainous areas. Orographic precipitation increases the probability of the development of lacustrine sediments. The Tibesti and Air Massifs give proof of increased rainfall at times when no other regions of the central Sahara were receiving appreciable amounts of rain. Even under the recent hyper-arid conditions, the Air Mountains receive an annual rainfall of 1400 mm (PACHUR & ALTMANN, 2006).

A comparative study of radiocarbon dates from Chinese and north African water bodies has shown that the majority of recorded sites in the Sahara, between 25° to 29° N, are situated either in mountainous areas such as the Hoggar or the Tibesti Massif or along wadis originating in the highland areas (GUO et al., 2000). Furthermore, a decline in palaeoenvironmental data between 24°N to 30°N is visible, compared with the regions to the north and south.

The study sites show a variety of properties, of which some are determined by local factors. For instance, the sites at Yoo Ango and Fabérgé were most likely influenced by local groundwater or aquifer charge. However, the general geological situation is not well documented, and only the hydrogeological investigation of PIRARD (1962) indicates potential groundwater charge in the area. Nevertheless, due to the topography, increased precipitation at the western flanks of the Tibesti would automatically lead to increased surface runoff and temporary rivers, draining towards the Tchigai foothills. In combination with the proposed groundwater table, long lasting ponds are imaginable for the Early to Middle Holocene, and would be frequently visited by nomads, as indicated by the numerous fireplaces and tumuli.

The depression of Seggedim shows little topography capable of enhancing precipitation, but outcrops of the Bilma aquifer ensure the freshwater supply to the adjacent oasis up to the present day.

Moreover, the presence of groundwater, as well as the intense evaporation, has led to the development of a sebkha, due to the upward movement of groundwater within the deposited sediment (per ascensum). As the presence of the aquifer did not prevent the siltation of the lake, the contribution of groundwater to its total water budget can be considered steady, but not predominant, in the lake's succession throughout the Holocene. The outstanding linearity of the radiocarbon dates, from the Early to the Middle Holocene, indicates a stable climate without major long-term droughts, as is also shown by the West Nubian Paleaolake in the eastern Sahara (HOELZMANN et al., 2000).

The Seeterrassental in the Enneri Achelouma provides information about a temporary lacustrine period of only a few centuries. Environmental changes, probably increased precipitation, led to the accumulation of lacustrine sediments, due to natural dams in the valley in the Early Holocene, and to the subsequent removal of the dams, probably as a result of increasing variability in precipitation. The investigated profiles only provide information about a very small catchment, due to their position in the upper reaches of the valley. This can be regarded as a short-term archive, which responded rapidly to local climate-induced changes in precipitation. The remnants of the lacustrine accumulations show distinct changes in environmental conditions, indicated by the alternating geochemical values and the mineralogical composition, even though the profiles are highly weathered. The environmental setting of the Seeterrassental is comparable to the blocking of Wadi Bakht in Egypt by a sand dune barrier, which developed under earlier arid conditions (LINSTAEDTER & KROEPELIN, 2004). The formation of this natural dam also led to the development of lacustrine sedimentation during Early and Mid Holocene. The authors also emphasize that the palaeoenvironmental information obtained from their project is restricted to the unique environmental setting of their study site.

The question arises if the temporal offset between the start of lacustrine phases in Seggedim, Fabergé and Seeterrassental solitarily emerged due to the respective longitudinal position of the sites. The onset of lacustrine sedimentation at the northern study sites, Seeterrassental and Fabergé, is recorded at similar times around 9.5 ka cal BP, although the longitudinal distance between both points amounts to 140 km. Fabergé and Seggedim show a longitudinal distance of only 70 km but, referring to the onset of lacustrine sedimentation, a temporal offset of about 1000 years.

An explanation for this offset may be found in the undermost parts of the Seggedim core. There, the preliminary investigation of the diatom assemblages combined with the geochemical results indicates a meromictic lake, with an anoxic layer of oligo- to metahaline waters at the monomolimnion (GASSE, 1987) and significantly less haline waters on top, apparently originating from freshwater inflow. The implementation of meromictic conditions would cause stratification within the water body with diverse ecological conditions inside the water column, reflecting in the associated diatom spectrum within the investigated sediment. The plausibility for the development of meromictic lakes is visible in a shallow groundwater-fed lake at the Kaouar area, where a chemocline developed at 23 cm depth within a water column of 40-60 cm deepness. This persistent meromixis is considered to develop by permanent groundwater charge (SCHULTZE et al., 1990). Most probably the initial and very stable lake phase at Seggedim was enabled by groundwater discharge from a salt-containing marine-sediment aquifer within the Emi Bao formation (BAUMHAUER, 1986). The saltworks not far from the coring site and freshwater wells right next to it indicate how complicated - and not yet understood - the hydrogeology of the area is. There is as yet no way to estimate the share of inflowing groundwater during the initial lake phase but inflow may have created not only an early onset of a lake environment but also a temporal offset concerning the end of the lake phase.

However, in a landscape with limited palaeoenvironmental evidence, where information is only conserved under favourable conditions, the combination of evidence from different locations may provide useful information about overall climatic development. To achieve this, the local properties of the individual archives (Table 26) must be investigated and their influence on the palaeoenvironmental information taken into consideration.

Table 26 Contrasting properties of palaeoenvironmental archives

Small Catchment Size	↔	Large Catchment Size
Short Existence	↔	Long Existence
Short-Term Archive	↔	Long-Term Archive
Immediate Response (e.g. Lake Levels)	↔	Slow Response/Time Lag
No/Local Aquifer System	↔	Large Aquifer
No/Little Topography	↔	Mountainous Areas
Limited Biological Proxies	↔	Plenty Biological Proxies
Annual Resolution	↔	Decadal, Millennial
Regional Response	↔	Supra-Regional Response

8.2 Model of Late Quaternary environmental progression in NE Niger

The coring of 2005 yielded some new evidence and has helped to consolidate information about the landscape history of Seggedim, since modern radiocarbon AMS dates both provide new information and help to complete the succession model of the central Sahara. Additionally, the supplementary sites in the north have provided detailed information about local environmental changes. The comprehensive picture is shown in Figure 71, in which the most reliable information about major palaeoenvironmental changes, obtained from the sediment profiles and the Seggedim core, is visualized on a time scale. To explain the regional environmental progression as well as its primary/principle causes throughout the Late Pleistocene, three time-slices will be investigated and described.

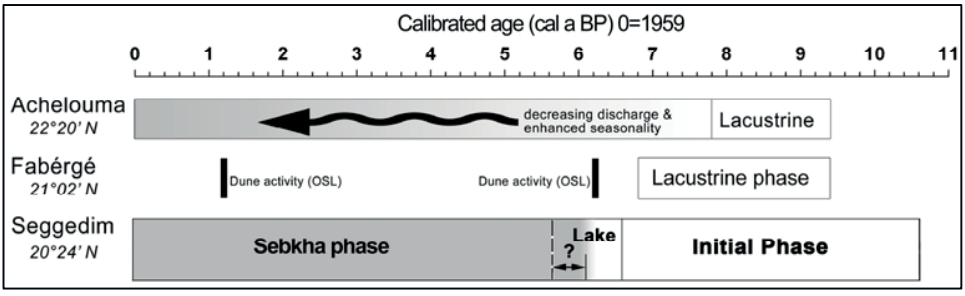

Figure 71 Regional palaeoenvironmental progression throughout the Holocene

Late Pleistocene (LGM/18 ka to 12 ka)

Palaeoenvironmental results for the Late Pleistocene have not been found at the three main study sites. Only the OSL dating of a sand ramp at Seggedim has revealed an age of 11660 ±1100 cal a BP (P. FELIX-HENNINGSEN, personal communication, June 2008). This indicates arid conditions at that time. In addition, the bottommost dating obtained from the coring shows an age of 10410 ± 180 cal a BP. No signs of previous lacustrine sedimentation have been found. This indicates increased aeolian activity and the removal of any deposited material (whether deposited by fluvial or aeolian activity) before the onset of the recorded sedimentation.

The Seeterrassental at Enneri Achelouma showed no signs of noteworthy sedimentation, although the valley-blocking landslides must have taken place in the Late Pleistocene (BUSCHE, 2001). Due to the exceptional environmental setting, dry conditions can be assumed for the period before lacustrine sedimentation set in (Early Holocene).

The Fabérgé depression contains no signs of older lacustrine accumulations, as massive deflation has degraded and reshaped the residual sediments. Radiocarbon dating shows maximum ages of 9440 ± 140 cal a BP, indicating an earlier high-intensity aeolian phase.

Radiocarbon dating from the Yoo Ango site show Pleistocene ages, although these are not reliable as the carbon content is generally low and contamination cannot be excluded. Furthermore, these dates presumably originate from charcoals, as any organic matter has usually been reworked and destroyed. The relocation of charcoal fragments is a common occurrence and must be taken into account, especially in landscapes with high dynamics.

Comparing these results to the general view of climatic development, they confirm largely dry conditions for the central Sahara during the last part of the Pleistocene. Concerning the regional climatic differences, ROGNON and WILLIAMS (1977) have proposed a southward shift of the global pressure belts due to the massive continental ice shield in Central Europe. As indicated by lake sediments and pollen investigation, as well as aeolian deposits, a southward migration of the ITCZ (4-5°), in combination with intensifying trade winds (Harmattan), is considered to have caused a cooler but dry climate during that time (GASSE & ROBERTS, 2004).

The general southward migration of the atmospheric circulation also caused a shift of the Westerlies to the south. As a result, the mountainous areas in the Sahara received precipitation in the northern hemisphere winter (GEB, 2000; NICHOLSON & FLOHN, 1980), although the surrounding lowlands received no rainfall. Because of increased trade wind activity, as indicated by the massive deflation at the study sites, high wind velocities must have been common/frequent. The proven increase of evaporation would have prevented the detection of any increase in precipitation in lower areas (MALEY, 2000).

This fundamental change originated in cooler sea surface temperatures in the subtropical Atlantic (deMENOCAL et al., 2000) and an intensified Hadley cell, in combination with the southward shift of the subtropical high (GASSE & ROBERTS, 2004; NICHOLSON & FLOHN, 1980). These substantial modifications of the atmospheric circulation resulted in generally lower precipitation in northern Africa and a southward retreat of the monsoonal migration (BRACONNOT et al., 2000), as indicated by active dunes in the Sahel during the LGM (MICHEL, 1973; SERVANT, 1973/1983; VOELKEL, 1988). The consequent weakened monsoon activity caused the southward extension of the Sahara margin. Depending on local environmental settings, the recorded shift lies between 200 and 500 km (NICHOLSON & FLOHN, 1980).

Early Holocene (11 to 8 ka BP)

During the Early Holocene, an initial lake environment came into existence in the Seggedim depression and continued to exist for the following 4000 years. Radiocarbon dates set the beginning of this stage at about 10.6 ka cal BP. The botanical record has revealed the presence of Saharan savannah vegetation in the area, most likely resulting in closed vegetation cover, as the sediment record indicates diminished input into the lake. Around 9400 cal a BP the establishment of lacustrine pools in the Achelouma valley (Seeterrassental) took place, initiated by fossil landslides that had produced natural dams within the valley. In addition, freshwater pools with frequent adjacent settlements existed at the same time in the Fabérgé basin.

Numerous authors propose humid conditions from about 11 to 6.5 ka cal BP in the Central Sahara, as described in the literature analysis by SCHUETT and KRAUSE (2009). According to NICHOLSON & FLOHN (1980), this change was initiated by the increased thermal contrast of the hemispheres, due to changing insolation values, and the decreasing internal contrast in the northern hemisphere, as large parts of the American ice shield remained intact while the European ice shield disintegrated.

In consequence, the northern Hadley cell (the north Atlantic subtropical high) weakened and shifted northwards (NICHOLSON & FLOHN, 1980). In the same way/at the same time the African monsoon moved northward and rainfall increased again, involving a northward retreat of the Atlantic westerlies (EDMUNDS et al., 2004). In the Early to Middle Holocene humid phase the position of the southern Sahara border is thought to have migrated almost 1000 km to the North, compared to the last position in the LGM (LIOUBIMTSEVA et al., 1998). For the eastern Sahara, KUPER & KROEPELIN (2006) have reconstructed, from palaeoecological data, a northward migration of the Sahara-Sahel border of about 600 km.

The major factor for increasing monsoon activity is thought to be the warming of the Atlantic, especially near the equator, and the subsequent elevated humidity due to increased evaporation (NICHOLSON & FLOHN, 1980). In addition, feedback processes between the atmosphere, ocean and vegetation have very probably participated in the enhancement of the monsoon activity and intensity (BRACONNOT et al., 2000; BRACONNOT et al., 1999; NICHOLSON & FLOHN, 1980). A major source of summer precipitation is the interaction of moist air south of the ITCZ with upper-level westerly troughs (NICHOLSON & FLOHN, 1980). The establishment of a more-or-less permanent trough over east Central Europe (NICHOLSON & FLOHN, 1980) during the Early Holocene set up an undulated weather system over Northern Africa, initiating increased winter rains down to approx. 20° N (GEB, 2000), especially in the eastern Sahara.

Regarding the presumed feedback processes which enhanced local precipitation, a region of enhanced humidity with a minimum of 100.000 km² is a prerequisite for initiating the creation, intensification and stabilization of specific troughs and cyclones with recycled local moisture (GEB, 2000). It is open to discussion whether the numerous lakes and ponds within the Ténéré and Central Sahara could have provided sufficient local humidity for increased convective precipitation to initiate an additional northward migration and enhancement of monsoon activity.

The temporal course of these profound events is a key point of debate and reveals major differences, because of the environmental settings and positions of the sites investigated (cf. preceding chapter). However, the majority of authors describe changes in zonal palaeoclimatic patterns associated with the displacement of landscape belts, as indicated by numerous pollen studies and by computer modelling.

For example, the gradient of humidity which is recorded in palaeosoils on fossil dunes in Niger most likely developed through a decline in precipitation (FELIX-HENNINGSEN, 2000). This may be the ground-level manifestation of the monsoon track, as it generally follows the typical SW-NE

direction. Another study from the eastern Sahara indicates an Early Holocene precipitation gradient, of decreasing rainfall, running south to north, with the rainfall considered to be of seasonal character (summer precipitation) (ABELL & HOELZMANN, 2000). Aquifers were recharged by increased monsoonal precipitation between 9000 and 6000 a BP. Lakes situated further to the north (slightly above 20°N) received less precipitation and evaporation was present over extended periods.

Estimations of precipitation vary in extent and amplitude, according to the kind of investigation carried out (model-based, or based on palaeoenvironmental records). Using meteorological hindcast, RENSSEN et al. (2006) estimate a mean annual precipitation of about 290 mm for 9 to 7.5 cal ka BP, in combination with high summer temperatures and increased precipitation at the western Sahara and Sahel. The authors show a key precipitation anomaly, with a maximum at about 9000 cal BP, restricted to the northern hemisphere summer months (June to August). The greatest effect of the anomaly is apparently located at 20° N with a maximum increase of precipitation in August of 110 mm. Most importantly, increasing rainfall variability and higher amplitudes are thought to have developed subsequently.

Evidence of frequent fires raises the question of their cause. Despite the irregularities in the radiocarbon record, the dates from the translocated and redeposited charcoal pieces at Seggedim can be narrowed down to a tight time span of 1200 cal years, during which the regular burnings appear to have occurred. In respect of the radiocarbon ages obtained from the sediment profiles of Yoo Ango, which originate most likely in charcoal remnants, the presence of fires can be deduced/assumed at 12850 ± 160 cal a BP, 21080 ± 320 cal a BP and 28090 ± 520 cal a BP. Investigations of fulgurite (remnants of lightning strikes on sandy grounds) distribution in the southern areas of the central Sahara have revealed a northward decrease in frequency, and consequently a decreasing gradient of thunderstorm activity, running S-N. Although accurate/adequate dating remains problematic for fulgurites, they are most likely the result of increased monsoonal activity during the Middle Holocene (SPONHOLZ, 2004; SPONHOLZ et al., 1993). Corresponding evidence comes from north-western Sudan, where intense monsoonal precipitation in combination with thunderstorms is assumed to have prevailed from approx. 9.5 to 4 ka BP (HOELZMANN et al., 2000). Beside the theory of natural fires caused by lightning (DOLIDON, 2005, SPONHOLZ 2004), the intentional burning of reed beds may be an alternative explanation, at least for the Seggedim depression. This method is still a regular procedure among traditional Sahelian herdsmen, in order to provide access to water for their animals when the pond is enclosed by vegetation (cf. SCHULZ 2004).

Considering the palaeoenvironmental evidence of this work as mainly climate-induced, a slight temporal delay/divergence in the onset of the lacustrine stages is visible in Figure 74. The beginning of lacustrine sedimentation in Seggedim can be determined at 10.6 ka cal BP. The radiocarbon results which determine the onset of lacustrine sedimentation in the Achelouma valley and the Fabérgé depression show similar ages, at around 9400 cal BP. Whether this was due to an increase in local precipitation or the rise of a replenished aquifer is still open to discussion, as the role of groundwater recharge in the hydrological balance of the depression is still unknown. In addition, variations in the mineralogical and geochemical composition of the profiles from the Seeterrassental indicate small-scale changes in the environmental setting between 8780 and 9460 a cal BP. The alternations of calcite and quartz, Fe_2O_3 and CaO, and TOC and TIC maxima indicate varying moisture supply and/or temperature changes, lasting at least several decades. The information obtained from the profiles indicates an increase of aeolian activity between 8 and 8.2 ka cal BP. Whether the results were a reaction to the 8.2 ka cooling event cannot be determined, but it at least shows a contemporaneous timing, since the whole 8.2 ka event lasted from about 8247 to 8086 a BP (THOMAS et al., 2007).

The results obtained from the Seggedim coring show no variations in this period: on the contrary they indicate exceptionally stable conditions. However, it can be concluded that the Bilma aquifer

was very probably a vital influence on the establishment of the lake, as the high water table is still the foundation of the Seggedim oasis in the present day. The extraordinary stability of the geochemical and mineralogical results from the Early to the Middle Holocene is most likely a result of small but steady groundwater inflow from the Bilma aquifer.

Mid Holocene 6.5 to 4.5 ka BP

Around 6.6 ka cal BP, a major change in the sedimentation regime of the Seggedim basin is indicated by the mineralogical and geochemical evidence. Variations in the thickness and appearance of the layers confirm variations in sedimentation, most likely reflecting changes in precipitation and clastic input. The occasional occurrence of gypsum suggests phases of desiccation. Variations in the freshwater lake stages may reflect variations in the amount and seasonality of precipitation. The siltation most probably occurred as a result of reduced vegetation cover and increased surface wash into the depression. Sedimentation rates show a very large increase of sediment input in the middle of the Holocene. Because of a lack of dateable material in the upper core section, the termination of the lake stage and the onset of the subsequent sebkha stage cannot be precisely determined, but they can be narrowed down to a period around 6 to 5.8 ka BP. In addition, it is probable that the closed vegetation cover fringing the lake and the corresponding aquifer are jointly responsible for its long existence, as they prevented the lake from siltation, although the surrounding landscape was determined by aeolian activity and increased aridity.

At the Fabérgé depression, the pools must have developed into evaporitic ponds and subsequently to desiccating pools. The explicitly evaporitic environment must have become established after 6810 ± 140 a cal BP, as the remnants of a lacustrine environment have been dated to this point. The additional OSL dating of a fossil dune has shown the age of dune activity as 6200 ± 400 cal a BP, whereas the sand shows signs of soil development, which must have occurred after its deposition. This indicates increasing aeolian activity in the area, while precipitation occurred only occasionally.

The site of Yoo Ango shows a rather irregular pattern of lacustrine deposition and because of the shortage of evidence no additional information can be obtained from that site. The large number of fireplaces in this area indicates at least a temporarily increased human population in the Middle Holocene. The dating of a fireplace gives an age of 5820 ± 120 cal a BP. It can be assumed that accessible fresh water must have existed at least up to that point in time. However, a direct proof of freshwater conditions cannot be obtained from the sediment records.

According to NICHOLSON & FLOHN (1980) a thermal maximum for the European part of the northern hemisphere is recorded at about 6 ka BP. As a result of this warming, the northern hemisphere temperature gradient decreased, causing a weakening and a northward expansion of the subtropical high over the Atlantic. At the same time, a cooling trend is recorded for the southern hemisphere, in response to the enhancement of the hemisphere's thermal contrast, and a northward migration of the meteorological equator (the ITCZ) set in. The onset of desiccation in the Sahara is assumed to have begun around the middle of the Holocene, when the Saharan disturbances occurred less frequently and were limited to the summer season (NICHOLSON & FLOHN, 1980). As a result, the precipitation regime within the central Sahara presumably changed from a moderate bi-phased rainy season to a distinct seasonality in the highlands, as recorded in the mountainous areas of the central and eastern Sahara (MALEY, 2000). A Middle Holocene erosive phase is thought to have occurred at about 6 to 6.5 ka BP, because of the dominant monsoonal precipitation, which is considered to be more dynamic. In general, this hypothesis is in accord with the results from the Seeterrassental at Enneri Achelouma, where increased surface flow led to the erosion of the natural dams and to the dismantling and incising of the deposited sediments. According to KRAUSE and

SCHUETT (2009), the maximum erosion intensity must have occurred around the Middle Holocene, as the calculated palaeodischarge has decreased towards the present day.

The dating of the termination of the humid period in the middle of the/in the Middle Holocene is a major point of discussion, as it shows considerable variation, depending on the site investigated (Figure 70, cf. chapter 4). Figure 75 illustrates the regional palaeoenvironmental information from this work, compared with summer insolation values (BERGER & LOUTRE, 1991) and a terrigenous dust export record from an offshore coring (deMENOCAL et al., 2000). The information obtained from the Fabérgé depression indicates an onset of dune activity at about 6200 cal a BP, although the dune sands show signs of soil development. Consequently, this is an indicator of frequent precipitation after the deposition of the dune and therefore of short-term climatic variations. The onset of major dust export from Northern Africa, as indicated by the offshore coring (deMENOCAL et al., 2000), is dated to about 5.5 cal ka BP. This evidence leads to the assumption of rapid environmental changes occurring in a short period, presumably over decades or a few centuries.

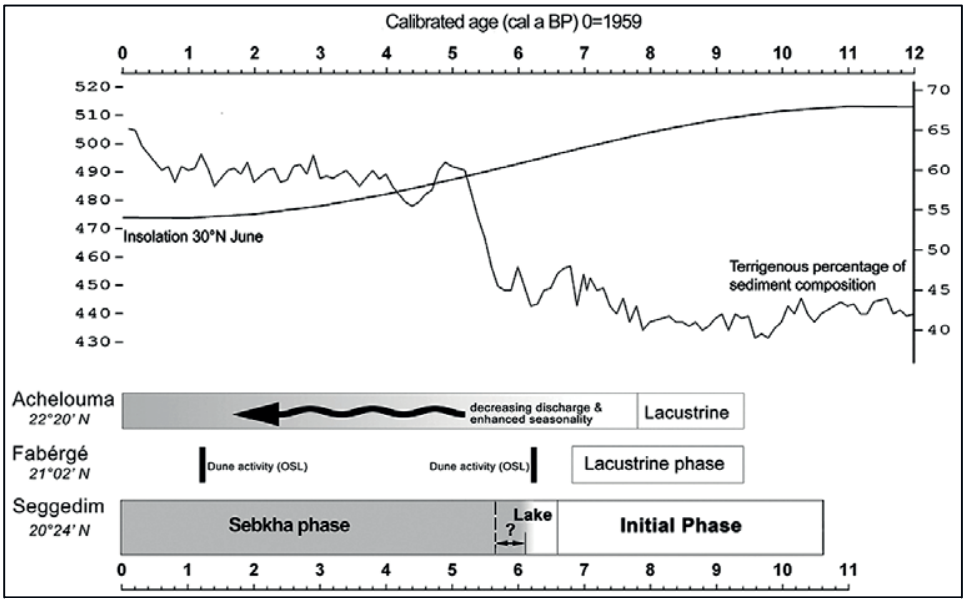

Figure 72 Comparison of local results with insolation values (30°N) and terrigenous dust records from a deep sea coring. Original dust record (deMENOCAL et al., 2000), Insolation values (BERGER & LOUTRE, 1991)

A large number of palaeoenvironmental records from the Central and Western Sahara (Figure 70) indicate sudden changes in conditions between 6 and 5 cal ka BP. Nevertheless, an equal number of investigations show transitional periods over an extended period, as is also shown by the investigations in this work.

The combined characteristics indicate high climatic variability during the Middle Holocene, although the overall trend was indisputably towards more arid conditions. Depending on the controlling regional factors, the majority of lacustrine archives terminate between 7 and 5 ka BP (cf. chapter 4.2), whereas some have continued to the present day as a result of aquifer recharge and established permanent vegetation cover, both features stabilizing the landscape.

8.3 Conclusion

The compilation of palaeoenvironmental records (Figure 70) and the information obtained from the records investigated in this work confirm the heterogeneity of the reconstructed environmental succession in the central Sahara. The Early Holocene can be considered a period of wetter conditions, although the different study sites show major variations in the timing and extent of lacustrine and aeolian periods, depending on modifying local factors.

An initial lake environment came into existence in the Seggedim depression at about 10.6 ka cal BP. The botanical record reveals the presence of Saharan savannah vegetation in the area, most likely resulting in a closed vegetation cover, as the sediment record indicates diminished detrital input into the lake. In the Achelouma valley (Seeterrassental), lacustrine pools developed around 9400 cal a BP, initiated by fossil landslides that had produced natural dams within the valley. At the same time, freshwater pools with frequent adjacent settlements existed in the Fabérgé basin.

The rapid (within decades) and particular uniform development in the Middle Holocene, from more humid to extremely arid environmental conditions, as indicated by several studies (cf. chapter 4), cannot be confirmed for the central Sahara. Additionally, a separation between Early and Middle Holocene wet periods cannot be confirmed either, as the results from multiple sites indicate alternating but generally wetter conditions from about 10 to about 7 ka cal BP. Evidently, a transitional period, when alternating influences prevailed, occurred between 7 and 5 ka BP. This is indicated by the varying sedimentation conditions in the Seggedim depression, as well as the evidence of soil properties in a fossil dune, with a time of deposition dated to 6200 ± 400 cal a BP, and the removal of lacustrine sediments in the Seeterrassental at the Middle Holocene.

The migration of the atmospheric circulation components, especially the frequency and extent of the monsoon, was initiated by global factors (cf. chapter 4.4), which are the framework for climatic alterations (GEB, 2000) and characterize continental and long-term development. In contrast, regional factors, determined by a particular environmental setting, provided the basis for a series of feedback processes and controlled the individual timing of lacustrine and arid phases. Depending on the archive investigated, climatic information can be overlaid by local properties (e.g. aquifer inflow); thus, time lags (non-linear behaviour) arise in the overall environmental progression. For instance, a constant vegetation cover, fed by an aquifer system or even by local rainfall alone, increases the soil's absorption of precipitation and the water storage capacity of the top layers. In contrast, bare soil surfaces, lacking vegetation cover, are likely to be eroded and altered, causing an overall deterioration of soil conditions (SCHEFFER et al., 2001), as indicated in the Seggedim coring. This view is confirmed by numerous computer-based climate investigations, which emphasize the essential function of vegetation-atmosphere feedbacks, whether in influencing albedo values or air humidity (cf. chapter 4).

A sufficient number of palaeoenvironmental archives is a prerequisite, both for the reconstruction of palaeoclimatic dynamics for a wider region and in determining whether changes in separate archives occurred because of spatial and temporal climatic variations or local factors (FRITZ, 2008). Conversely, only the investigation of several dissimilar locations within a designated study area has the potential to provide a complete picture of landscape succession. This is especially true in a landscape which has yielded limited palaeoenvironmental archives, where information has only been conserved under favourable conditions. The few perennial lacustrine climate archives in the Sahara still active to the present day,, such as Bilma or Lake Yao/Chad (KROEPELIN et al., 2008), reveal apparently unique characteristics, as the local conditions that led to their existence are indeed exceptional. The interpretation of such a unique location must be performed with caution, as it provides several sources of error.

As shown in this work (cf. chapter 6), the Seggedim depression can be considered as such a unique location, at least during a limited period. The information obtained from the initial and freshwater lake sediments showed no noticeable signs of climatic alterations until the Middle Holocene. Nevertheless, the supplementary sediment archives (cf. chapter 7) give evidence of the previous onset of aeolian activity and the simultaneous presence of alternating levels of precipitation, as well as the previous removal of several metres of sediment in the Seeterrassental at Enneri Achelouma. These processes were most likely initiated by increasing seasonality of precipitation, an incidence that was not recorded in the Seggedim core. In addition, the cautious interpretation of biological indicators is a prerequisite for these exceptional sites. It is well known that pollen records can provide excellent evidence of changing environmental conditions. However, the fringes of lakes tend to maintain more or less constant vegetation taxa if the lake level remains stable (cf. chapter 6). Changing climatic conditions would only be reflected in distant areas, where the influence of the open water body is diminished. Thus the information inferred from such an isolated lake, fed by an aquifer but inside a fully arid area, may be misleading with respect to climatological signals. Depending on the buffering capacity of the water body, alterations in precipitation would for the most part not be recorded in the sediment archive.

The buffering capacity of an investigated area with respect to climatic changes is a vital factor in the interpretation of palaeoenvironmental archives. On a larger scale, this capacity may be expressed as positive or negative feedbacks, in fact as local conditions, which tend to create non-linear behaviour in subsystems. To obtain a complete picture of landscape progression over an extended period such as the Holocene, the aim of further environmental reconstruction is to provide not only a multi-proxy but also a multi-habitat approach. As the sources of palaeoenvironmental information are limited in highly dynamic landscapes such as the Sahara, completing the task remains problematic.

9 REFERENCES

ABELL, P.I. and HOELZMANN, P., 2000. Holocene palaeoclimates in northwestern Sudan: Stable isotope studies on molluscs. *Global and Planetary Change*, 26(1-3): 1-12.

ADAMS, J.M. and FAURE, H., 1997. Preliminary Vegetation Maps of the World since the Last Glacial Maximum: An Aid to Archaeological Understanding. *Journal of Archaeological Science*, 24(7): 623-647.

ADAMS, L. and TETZLAFF, G., 1984. Did Lake Chad exist around 18,000 yr BP? *Meteorology and Atmospheric Physics*, 34(3): 299-308.

ADAMS, L.J. and TETZLAFF, G., 1989. Annual precipitation values at 20° N/0° E in the Early Holocene. *Theoretical and Applied Climatology*, 39(4): 205-212.

ALLEY, R.B. et al., 2003. Abrupt Climate Change. *Science*, 299(5615): 2005-2010.

BATTERBEE, R.W. et al., 2001. Diatoms. In: W.M. Last, H.J.B. Birks and J.P. Smol (Editors), *Tracking Environmental Change Using Lake Sediments: Terrestrial, Algal, and Siliceous Indicators*. Developments in Paleoenvironmental Research. Kluwer Academic Publishers, Dordrecht, pp. 155-202.

BAUDRIMONT, R., 1974. Recherches sur les diatomées des eaux continentales de l'Algerie: écologie et paléoécologie. Memoires de la Societe d'Histoire Naturelle de l'Afrique du Nord. Nouvelle Serie (Algeria), 12. Societe d'Histoire Naturelle de l'Afrique du Nord, Algiers, 249 pp.

BAUMHAUER, R., 1986. Zur jungquartaeren Seenentwicklung im Bereich der Stufe von Bilma (NE-Niger). Upper Pleistocene and Holocene evolution of lakes in the Bilma region, northeastern Niger. Wuerzburger Geographische Arbeiten, vol.65. Bayerische Julius-Maximilians Universitaet Wuerzburg, Wuerzburg, Federal Republic of Germany (DEU), 235 pp.

BAUMHAUER, R., 1988. The Kawar - Holocene lakes in the foreland of a scarp area. In: H. Becker and W.D. Hutterot (Editors), *Tagungsbericht und wissenschaftliche Abhandlungen 46 Deutscher Geographentag, Munchen, 1987*. Steiner; Verhandlungen 46, pp. 332-341.

BAUMHAUER, R., 1991. Palaeolakes of the south central Sahara - problems of palaeoclimatological interpretation. *Hydrobiologia*, 214: 347-357.

BAUMHAUER, R., 2004. Late Pleistocene and Holocene palaeolakes in the central Sahara - New results from Tenere, Erg of Tenere and Erg of Fachi-Bilma, NE Niger. *Erde*, 135(3-4): 289-313.

BAUMHAUER, R., BUSCHE, D. and SPONHOLZ, B., 1989. Relief history and palaeoclimate of the Saharan East Niger. *Geographische Rundschau*, 41(9): 493-499.

BAUMHAUER, R. and SCHULZ, E., 1984. The Holocene lake of Seguedine, Kaouar, NE Niger. In: J.A. Coetzee and E.M. van-Zinderen-Bakker-Sr (Editors), *Palaeoecology of Africa*. Balkema, pp. 283-290, 3 figs, 5 refs.

BAUMHAUER, R., SCHULZ, E. and POMEL, S., 2004. Environmental changes in the Central Sahara during the Holocene - The Mid-Holocene transition from freshwater lake into sebkha in the Segedim depression, NE Niger. In: W. SMYKATZ-KLOSS and P. FELIX-HENNINGSEN (Editors), *Paleoecology of Quaternary Drylands*. Lecture notes in earth sciences. Springer, Berlin, pp. 31-45.

BAUMHAUER, R., SCHUETT, B. and FELIX-HENNINGSEN, P., 2009a. Geomorphological Research in the South-Central Sahara in Review, *Holocene Palaeoenvironmental History of the Central Sahara*. Palaeoecology of Africa.

BAUMHAUER, R. et al., 2009b. Holocene palaeoenvironmental changes in Central Sahara inferred from Seggedim scarpfoot depression (NE-Niger), *Holocene Palaeoenvironmental History of the Central Sahara*. Palaeoecology of Africa.

BENNET, K.D. and WILLIS, K.J., 2001. Pollen. In: W.M. Last, H.J.B. Birks and J.P. Smol (Editors), *Tracking Environmental Change Using Lake Sediments: Terrestrial, Algal, and Siliceous*

Indicators. Developments in Paleoenvironmental Research. Kluwer Academic Publishers, Dordrecht, pp. 5-32.

BERGER, A. and LOUTRE, M.F., 1991. Insolation values for the climate of the last 10 million years. *Quaternary Science Reviews*, 10(4): 297-317.

BIGHAM, J.M., FITZPATRICK, R.W. and SCHULZE, D.G., 2002. Iron Oxides. In: J.B. Dixon and D.G. SCHULZE (Editors), *Soil Mineralogy with Environmental Applications, no. 7*. SOIL SCIENCE SOCIETY OF AMERICA BOOK SERIES, pp. 323-367.

BLACKWELL, P.G., Buck, C.E. and Reimer, P.J., 2006. Important features of the new radiocarbon calibration curves. *Quaternary Science Reviews*, 25(5-6): 408-413.

BOYLE, J., 2002. Inorganic Geochemical Methods in Palaeolimnology, *Tracking Environmental Change Using Lake Sediments*, pp. 83-141.

BOYLE, J.F., 2000. Rapid elemental analysis of sediment samples by isotope source XRF. *Journal of Paleolimnology*, 23(2): 213-221.

BOYLE, J.F., 2001. Inorganic geochemical methods in paleolimnology. In: W.M. Last and J.P. Smol (Editors), *Tracking Environmental Change Using Lake Sediments: Physical and Geochemical Methods*. Developments in Paleoenvironmental Research. Kluwer Academic Publishers, Dordrecht, pp. 83-141.

BRACONNOT, P., JOUSSAUME, S., de NOBLET, N. and RAMSTEIN, G., 2000. Mid-Holocene and Last Glacial Maximum African monsoon changes as simulated within the Paleoclimate Modelling Intercomparison Project. *Global and Planetary Change*, 26(1-3): 51-66.

BRACONNOT, P., JOUSSAUME, S., MARTI, O. and de NOBLET, N., 1999. Synergistic feedbacks from ocean and vegetation on the African monsoon response to mid-Holocene insolation. *Geophysical Research Letters*, 26(16): 2481-2484.

BRENNAN, R. and QUADE, J., 1997. Reliable Late-Pleistocene Stratigraphic Ages and Shorter Groundwater Travel Times from14C in Fossil Snails from the Southern Great Basin. *Quaternary Research*, 47(3): 329-336.

BRISTOW, C.S., DRAKE, N. and ARMITAGE, S., 2009. Deflation in the dustiest place on Earth: The Bodélé Depression, Chad. *Geomorphology* 105: 50−58.

BUBENZER, O., BESLER, H. and HILGERS, A., 2007a. Filling the gap: OSL data expanding 14C chronologies of Late Quaternary environmental change in the Libyan Desert. *Quaternary International*, 175(1): 41-52.

BUBENZER, O., HILGERS, A. and RIEMER, H., 2007b. Luminescence dating and archaeology of Holocene fluvio-lacustrine sediments of Abu Tartur, Eastern Sahara. *Quaternary Geochronology*, 2(1-4): 314-321.

BURPEE, R.W., 1972. The Origin and Structure of Easterly Waves in the Lower Troposphere of North Africa. *Journal of the Atmospheric Sciences*, 29(1): 77-90.

BUSCHE, D., 1979. Die geomorphologische Entwicklung des westlichen Murzuk-Beckens, des Djado-Plateaus und des nördlichen Kaouar. Habilitation Thesis, Universität Würzburg, Würzburg.

BUSCHE, D., 1998. Die zentrale Sahara - Oberflächenformen im Wandel. Perthes Geographie im Bild. Perthes, Gotha, 248 pp.

BUSCHE, D., 2001. Early Quaternary landslides of the Sahara and their significance for geomorphic and climatic history. *Journal of Arid Environments*, 49(3): 429-448.

CADET, D.L. and NNOLI, N.O., 1987. Water Vapour Transport Over Africa and the Atlantic Ocean During Summer 1979. *Quarterly Journal of the Royal Meteorological Society*, 113(476): 581-602.

CANADELL, J. et al., 1996. Maximum rooting depth of vegetation types at the global scale. *Oecologia*, 108(4): 583-595.

CHALIE, F. and GASSE, F., 2002. Late Glacial-Holocene diatom record of water chemistry and lake level change from the tropical East African Rift Lake Abiyata (Ethiopia). *Palaeogeography, Palaeoclimatology, Palaeoecology*, 187(3-4): 259-283.

CHEDDADI, R., LAMB, H.F., GUIOT, J. and VAN DER KAARS, S., 1998. Holocene climatic change in Morocco: a quantitative reconstruction from pollen data. *Climate Dynamics*, 14(12): 883-890.

CLAUSSEN, M., BROVKIN, V., GANOPOLSKI, A., KUBATZKI, C. and PETOUKHOV, V., 2003. Climate Change in Northern Africa: The Past is Not the Future. *Climatic Change*, 57(1): 99-118.

CLAUSSEN, M. et al., 1999. Simulation of an abrupt change in Saharan vegetation in the mid-Holocene. *Geophysical Research Letters*, 26(14): 2037-2040.

COHMAP_MEMBERS, 1988. Climatic Changes of the Last 18,000 Years: Observations and Model Simulations. *Science*, 241(4869): 1043-1052.

COLLINSON, J.D., 1982. Lakes. In: H.G. Reading (Editor), *Sedimentary environments and Facies*. BLACKWELL Scientific, Oxford, pp. 61-79.

CUBASCH, U., VOSS, R., HEGERL, G.C., WASZKEWITZ, J. and CROWLEY, T.J., 1997. Simulation of the influence of solar radiation variations on the global climate with an ocean-atmosphere general circulation model. *Climate Dynamics*, 13(11): 757-767.

DAMNATI, B., 2000a. Holocene lake records in the Northern Hemisphere of Africa. *Journal of African Earth Sciences*, 31(2): 253-262.

DAMNATI, B., 2000b. Holocene lake records in the Northern Hemisphere of Africa. *Journal of African Earth Sciences*, 31: 253-262.

DAVISON, W., 1993. Iron and manganese in lakes. *Earth-Science Reviews*, 34(2): 119-163.

DEAN, W.E., 1999. The carbon cycle and biogeochemical dynamics in lake sediments. *Journal of Paleolimnology*, 21(4): 375-393.

DEARING, J., 1994. Environmental Magnetic Susceptibility, Using the Bartington MS2 System, Bartington Handbook, 2nd edition 1999. Chi Publishing, pp. 54 p.

deMENOCAL, P. et al., 2000. Abrupt onset and termination of the African Humid Period:: rapid climate responses to gradual insolation forcing. *Quaternary Science Reviews*, 19(1-5): 347-361.

deMENOCAL, P.B., 2001. Cultural Responses to Climate Change During the Late Holocene. *Science*, 292(5517): 667-673.

DONER, H.E. and GROSSL, P.R., 2002. Carbonates and Evaporites. In: J.B. Dixon and D.G. SCHULZE (Editors), *Soil Mineralogy with Environmental Applications, no. 7*. SOIL SCIENCE SOCIETY OF AMERICA BOOK SERIES, pp. 199-228.

DULLER, G.A.T., BØTTER-JENSEN, L. and MURRAY, A.S., 2003. Combining infrared- and green-laser stimulation sources in single-grain luminescence measurements of feldspar and quartz. *Radiation Measurements*, 37(4-5): 543-550.

ECKARDT, F.D., DRAKE, N., GOUDIE, A.S., WHITE, K. and VILES, H., 2001. The role of playas in pedogenic gypsum crust formation in the Central Namib Desert: a theoretical model. *Earth Surface Processes and Landforms*, 26: 1177-1193.

EDMUNDS, W.M. et al., 2004. Groundwater as an archive of climatic and environmental change: Europe to Africa. In: R.W. Battarbee, F. GASSE and C.E. Stickley (Editors), *Past Climate Variability through Europe and Africa*. Developments in Paleoenvironmental Research. Springer Netherlands, pp. 279-306.

EHRLICH, A. and DOR, I., 1985. Photosynthetic microorganisms of the Gavish Sabkha. In: G.M. Friedman and W.E. Krumbein (Editors), *Hypersaline Ecosystems, the Gavish Sabkha*. Springer, Berlin, pp. 256-299.

ELTAHIR, E.A.B. and GONG, C., 1996. Dynamics of Wet and Dry Years in West Africa. *Journal of Climate*, 9(5): 1030-1042.

EUGSTER, H.P., 1980. Geochemistry of Evaporitic Lacustrine Deposits. *Annual Review of Earth and Planetary Sciences*, 8: 35-63.

FAURE, H., 1966. Reconnaissance geologique des formations sedimentaires post-paleozoiques du Niger Oriental. ÉDITIONS DU BUREAU DE RECHERCHES GÉOLOGIQUES ET MINIÈRES, 1. Direction des Mines et de la Géologie, Paris, 587 pp.

FELIX-HENNINGSEN, P., 2000. Paleosols on Pleistocene dunes as indicators of paleo-monsoon events in the Sahara of East Niger. *Catena*, 41(1-3): 43-60.

FELIX-HENNINGSEN, P., 2004. Genesis and Paleo-ecological Interpretation of Swamp Ore Deposits at Sahara Paleo-lakes of East Niger, *Paleoecology of Quaternary Drylands*, pp. 47-72.

FICKEN, K.J. et al., 1998. Glacial/interglacial variations in carbon cycling revealed by molecular and isotope stratigraphy of Lake Nkunga, Mt. Kenya, East Africa. *Organic Geochemistry*, 29(5-7): 1701-1719.

FLEMMING, B.W., 2000. A revised textural classification of gravel-free muddy sediments on the basis of ternary diagrams. *Continental Shelf Research*, 20(10-11): 1125-1137.

FOLEY, J.A., Coe, M.T., SCHEFFER, M. and WANG, G., 2003. Regime Shifts in the Sahara and Sahel: Interactions between Ecological and Climatic Systems in Northern Africa. *Ecosystems*, 6(6): 524-532.

FONTES, J.C. and GASSE, F., 1989. On the ages of humid Holocene and Late Pleistocene phases in North Africa -- Remarks on "Late Quaternary climatic reconstruction for the Maghreb (North Africa)" by P. ROGNON. *Palaeogeography, Palaeoclimatology, Palaeoecology*, 70(4): 393-398.

FONTES, J.C. and GASSE, F., 1991. PALHYDAF (Palaeohydrology in Africa) program: objectives, methods, major results. *Paleoenvironments of Salt Lakes*, 84(1-4): 191-215.

FRITZ, P. and POPLAWSKI, S., 1974. 18O and 13C in the shells of freshwater molluscs and their environments. *Earth and Planetary Science Letters*, 24(1): 91-98.

FRITZ, S., 2008. Deciphering climatic history from lake sediments. *Journal of Paleolimnology*, 39(1): 5-16.

GALLAIRE, R., 1995. Hydrologie en milieu subdésertique d'altitude: Le cas de l'AÏR (Niger) = Hydrology in altitud subdesertic environment: case of Aïr (Niger), Université de Paris, Paris, 388 pp.

GALLAIRE, R., FONTES, J.C. and ZUPPI, G.M., 1995. Isotopic characterization and origin of rainwater on the Air massif (Niger) *International Association of Hydrological Sciences*, 232: 293-302.

GANOPOLSKI, A., KUBATZKI, C., CLAUSSEN, M., BROVKIN, V. and PETOUKHOV, V., 1998. The Influence of Vegetation-Atmosphere-Ocean Interaction on Climate During the Mid-Holocene. *Science*, 280(5371): 1916-1919.

GARCIN, Y., VINCENS, A., WILLIAMSON, D., BUCHET, G. and GUIOT, J., 2007. Abrupt resumption of the African Monsoon at the Younger Dryas--Holocene climatic transition. *Quaternary Science Reviews*, 26(5-6): 690-704.

GASSE, F., 1986. East African diatoms. Taxonomy, ecological distribution. *Bibliotheca Diatomologica*, 11: 201 pp.

GASSE, F., 1987. Diatoms for reconstructing palaeoenvironments and paleohydrology in tropical semi-arid zones. *Hydrobiologia*, 154(1): 127-163.

GASSE, F., 2000. Hydrological changes in the African tropics since the Last Glacial Maximum. *Quaternary Science Reviews*, 19(1-5): 189-211.

GASSE, F., 2002. Diatom-inferred salinity and carbonate oxygen isotopes in Holocene waterbodies of the western Sahara and Sahel (Africa). *Quaternary Science Reviews*, 21(7): 737-767.

GASSE, F., BARKER, P., GELL, P.A., FRITZ, S.C. and CHALIE, F., 1997. Diatom-inferred salinity in palaeolakes: An indirect tracer of climate change. *Quaternary Science Reviews*, 16(6): 547-563.

GASSE, F. et al., 1987. Biological remains, geochemistry and stable isotopes for the reconstruction of environmental and hydrological changes in the Holocene lakes from North Sahara. *Palaeogeography, Palaeoclimatology, Palaeoecology*, 60(1-2): 1-46.

GASSE, F. and ROBERTS, C., 2004. Late Quaternary Hydrologic Changes in the Arid and Semiarid Belt of Northern Africa: Implications for Past Atmospheric Circulation, *The Hadley Circulation: Present, Past, and Future*, pp. 313-345.

GASSE, F. and STREET, F.A., 1978. Late Quaternary lake-level fluctuations and environments of the northern rift valley and Afar region (Ethiopia and Djibouti). *Palaeogeography, Palaeoclimatology, Palaeoecology*, 25: 145-150.

GASSE, F., TEHET, R., DURAND, A., GIBERT, E. and FONTES, J.-C., 1990. The arid–humid transition in the Sahara and the Sahel during the last deglaciation. *nature*, 346(6280): 141-146.

GASSE, F. and van CAMPO, E., 1994. Abrupt post-glacial climate events in West Asia and North Africa monsoon domains. *Earth and Planetary Science Letters*, 126(4): 435-456.

GEB, M., 2000. Factors favouring precipitation in North Africa: seen from the viewpoint of present-day climatology. *Global and Planetary Change*, 26(1-3): 85-96.

GOSCHIN, M., 1988. El Atrun (Nubien) - Ein frühholozänzeitlicher See. Thesis Thesis, 221 pp pp.

GRUNERT, J., 1983. Geomorphologie der Schichtstufen am Westrand des Murzuk-Beckens (zentrale Sahara), Bornträger/Schweizerbart, Berlin/Stuttgart, 271 S pp.

GRUNERT, J., BAUMHAUER, R. and VOELKEL, J., 1991. Lacustrine sediments and Holocene climates in the southern Sahara: the example of paleolakes in the Grand Erg of Bilma (Zoo Baba and Dibella, eastern Niger). *Journal of African Earth Sciences*, 12(1-2): 133-146.

GUETTER, P.J. and KUTZBACH, J.E., 1990. A modified Köppen classification applied to model simulations of glacial and interglacial climates. *Climatic Change*, 16(2): 193-215.

GUO, Z., PETIT-MAIRE, N. and KROEPELIN, S., 2000. Holocene non-orbital climatic events in present-day arid areas of northern Africa and China. *Global and Planetary Change*, 26(1-3): 97-103.

HOELZMANN, P., et al. 2004. Palaeoenvironmental changes in the arid and sub arid belt (Sahara-Sahel-Arabian Peninsula) from 150 kyr to present, *Past Climate Variability through Europe and Africa*, pp. 219-256.

HOELZMANN, P., et al.,1998. Mid-Holocene land-surface conditions in northern Africa and the Arabian peninsula: a data set for the analysis of biogeophysical feedbacks in the climate system. *Global Biogeochemical Cycles*, 12(1): 35-51.

HOELZMANN, P., KRUSE, H.J. and ROTTINGER, F., 2000. Precipitation estimates for the eastern Saharan palaeomonsoon based on a water balance model of the West Nubian Palaeolake Basin. *Global and Planetary Change*, 26(1-3): 105-120.

HOLZ, C., STUUT, J.-B.W., HENRICH, R. and MEGGERS, H., 2007. Variability in terrigenous sedimentation processes off northwest Africa and its relation to climate changes: Inferences from grain-size distributions of a Holocene marine sediment record. *Sedimentary Geology*, 202(3): 499-508.

HORNBURG, V. and LUEER, B., 2000. Vergleich zwischen Total- und königswasserextrahierbaren Elementgehalten in natürlichen Böden und Sedimenten. *Journal of Plant Nutrition and Soil Science*, 162(2): 131-137.

JAEKEL, D., 1979. Run-off and fluvial formation processes in the Tibesti mountains as indicators of climatic history in the central Sahara during the Late Pleistocene and Holocene. *Palaeoecology of Africa*, 11: 13-44.

JOLLY, D., HARRISON, S.P., DAMNATI, B. and BONNEFILLE, R., 1998a. Simulated climate and biomes of Africa during the late quaternary: comparison with pollen and lake status data. *Quaternary Science Reviews*, 17(6-7): 629-657.

JOLLY, D. et al., 1998b. Biome reconstruction from pollen and plant macrofossil data for Africa and the Arabian peninsula at 0 and 6000 years. *Journal of Biogeography*, 25(6): 1007-1027.

JONES, B.F. and BOWSER, C.J., 1978. The mineralogy and related chemistry of lake sediments. In: A. Lerman (Editor), *Lakes: Chemistry, Geology, Physics*. Springer Verlag, New York, pp. 179-235.

KALLENBACH, H., 1972. Beiträge zur Sedimentologie des kontinentalen Mesozoikums am Westrand des Murzukbeckens (Libyen). *International Journal of Earth Sciences*, 61(1): 302-322.

KELTS, K. and K.J.HSUE, 1978. Freshwater carbonate sedimentation. In: A. Lerman (Editor), *Lakes: Chemistry, Geology, Physics*. Springer-Verlag, New York, pp. pp. 295–323.

KEMP, A.E.S., DEAN, J., PEARCE, R.B. and PIKE, J., 2001. Recognition and analysis of bedding and sediment fabric features. In: W.M. Last and J.P. Smol (Editors), *Tracking Environmental Change Using Lake Sediments: Physical and Geochemical Methods*. Developments in Paleoenvironmental Research. Kluwer Academic Publishers, Dordrecht, pp. 7-22.

KLITZSCH, E., SONNTAG, C., WEISTROFFER, K. and SHAZLY, E.M.E., 1976. Grundwasser der Zentralsahara: Fossile Vorräte. *International Journal of Earth Sciences*, 65(1): 264-287.

KNOTT, J.R. and OWEN, L.A., 2007. Dating Quaternary sediments and landforms in Drylands. *Quaternary International*, 166(1): 1-3.

KRAUSE, J. and SCHUETT, B., 2009. Fluvial geomorphology of the Achelouma valley, NE Niger, *Holocene Palaeoenvironmental History of the Central Sahara*. Palaeoecology of Africa

KRAUSKOPF, K.B. and BIRD, D.K., 1995. Introduction to Geochemistry. McGraw-Hill, New York.

KROEPELIN, S. and PETIT-MAIRE, N., 2000. Paleomonsoon variations and terrestrial environmental change during the late Quaternary. *Global and Planetary Change*, 26(1-3): vii-viii.

KROEPELIN, S. et al., 2008. Climate-Driven Ecosystem Succession in the Sahara: The Past 6000 Years. *Science*, 320(5877): 765-768.

KUPER, R. and KROEPELIN, S., 2006. Climate-Controlled Holocene Occupation in the Sahara: Motor of Africa's Evolution. *Science*, 313(5788): 803-807.

KUTZBACH, J.E. and GUETTER, P.J., 1986. The Influence of Changing Orbital Parameters and Surface Boundary Conditions on Climate Simulations for the Past 18 000 Years. *Journal of the Atmospheric Sciences*, 43(16): 1726-1759.

KUTZBACH, J.E. and LIU, Z., 1997. Response of the African Monsoon to Orbital Forcing and Ocean Feedbacks in the Middle Holocene. *Science*, 278(5337): 440-443.

KUTZBACH, J.E. and STREET-PERROTT, F.A., 1985. Milankovitch forcing of fluctuations in the level of tropical lakes from 18 to 0 kyr BP. *Nature*, 317(6033): 130-134.

LARRASOANA, J.C., ROBERTS, A.P., STONER, J.S., RICHTER, C. and WEHAUSEN, R., 2003. A new proxy for bottom-water ventilation in the eastern Mediterranean based on diagenetically controlled magnetic properties of sapropel-bearing sediments. *Palaeogeography, Palaeoclimatology, Palaeoecology*, 190: 221-242.

LAST, W.M., 2001a. Mineralogical analysis of lake sediments. In: W.M. Last and J.P. Smol (Editors), *Tracking Environmental Change Using Lake Sediments: Physical and Geochemical Methods*. Developments in Paleoenvironmental Research. Kluwer Academic Publishers, Dordrecht, pp. 143-187.

LAST, W.M., 2001b. Textural analysis of lake sediments. In: W.M. Last and J.P. Smol (Editors), *Tracking Environmental Change Using Lake Sediments: Physical and Geochemical Methods*. Developments in Paleoenvironmental Research. Kluwer Academic Publishers, Dordrecht, pp. 41-81.

LEFRANC, J.P. and GUIRAUD, R., 1990. The continental intercalaire of northwestern Sahara and its equivalents in the neighbouring regions. *Journal of African Earth Sciences*, 10(1-2): 27-77.

LEZINE, A.-M., DUPLESSY, J.-C. and CAZET, J.-P., 2005. West African monsoon variability during the last deglaciation and the Holocene: Evidence from fresh water algae, pollen and isotope data from core KW31, Gulf of Guinea. *Palaeogeography, Palaeoclimatology, Palaeoecology*, 219(3-4): 225-237.

LIAN, O.B. and ROBERTS, R.G., 2006. Dating the Quaternary: progress in luminescence dating of sediments. *Quaternary Science Reviews*, 25(19-20): 2449-2468.

LINSTAEDTER, J. and KROEPELIN, S., 2004. Wadi Bakht revisited: Holocene climate change and prehistoric occupation in the Gilf Kebir region of the Eastern Sahara, SW Egypt. *Geoarchaeology*, 19(8): 753 - 778.

LIOUBIMTSEVA, E., SIMON, B., FAURE, H., FAURE-DENARD, L. and ADAMS, J.M., 1998. Impacts of climatic change on carbon storage in the Sahara-Gobi desert belt since the Last Glacial Maximum. *Global and Planetary Change*, 16-17: 95-105.

LIU, Z. et al., 2007. Simulating the transient evolution and abrupt change of Northern Africa atmosphere-ocean-terrestrial ecosystem in the Holocene. *Quaternary Science Reviews*, 26(13-14): 1818-1837.

MALEY, J., 2000. Last Glacial Maximum lacustrine and fluviatile Formations in the Tibesti and other Saharan mountains, and large-scale climatic teleconnections linked to the activity of the Subtropical Jet Stream. *Global and Planetary Change*, 26(1-3): 121-136.

MASSUEL, S. et al., 2006. Deep infiltration through a sandy alluvial fan in semiarid Niger inferred from electrical conductivity survey, vadose zone chemistry and hydrological modelling. *CATENA*, 67(2): 105-118.

MAYEWSKI, P.A. et al., 2004. Holocene climate variability. *Quaternary Research*, 62(3): 243-255.

MCGREGOR, G. and NIEUWOLT, S., 1998. Tropical Climatology. John Wiley & Sons, Chichester, 339 pp.

MEYERS, P.A. and LALLIER-VERGÉS, E., 1999. Lacustrine Sedimentary Organic Matter Records of Late Quaternary Paleoclimates. *Journal of Paleolimnology*, 21(3): 345-372.

MEYERS, P.A. and TERANES, J.L., 2001. Sediment organic matter. In: W.M. Last and J.P. Smol (Editors), *Tracking Environmental Change Using Lake Sediments: Physical and Geochemical Methods*. Developments in Paleoenvironmental Research. Kluwer Academic Publishers, Dordrecht, pp. 239-269.

MICHEL, P., 1973. Les bassins des fleuves Sénégal et Gambie, 63. Études géomorphologiques. Mémoires de l'ORSTOM, Paris, 752 pp.

MONTOYA, M., VON STORCH, H. and CROWLEY, T.J., 2000. Climate Simulation for 125 kyr BP with a Coupled Ocean & Atmosphere General Circulation Model. *Journal of Climate*, 13(6): 1057-1072.

MUELLER, G., IRION, G. and FÖRSTNER, U., 1972. Formation and diagenesis of inorganic Ca−Mg carbonates in the lacustrine environment. *Naturwissenschaften*, 59(4): 158-164.

NEUMANN, K., 1989. Holocene vegetation of the Eastern Sahara: charcoal from prehistoric sites. *African Archaeological Review*, 7(1): 97-116.

NICHOLSON, S.E., 2001. Climatic and environmental change in Africa during the last two centuries. *Climate Research*, 17(2): 123-144.

NICHOLSON, S.E., submitted 2007. A revised picture of the structure of the "monsoon" and land ITCZ over West Africa. *Bulletin of the American Meteorological Society*: 53.

NICHOLSON, S.E. and FLOHN, H., 1980. African environmental and climatic changes and the general atmospheric circulation in late pleistocene and holocene. *Climatic Change*, 2(4): 313-348.

NICOLL, K., 2001. Radiocarbon chronologies for prehistoric human occupation and hydroclimatic change in Egypt and Northern Sudan. *Geoarchaeology*, 16.

NOËL, D., 1986. Les diatomées de deux marais salants méditar-ranéens: Salin-de-Giraud (S-E de la France) et Santa Pola (Levant Espagnol). Similitudes et différences. In: M. Ricard (Editor), 8th International Symposium on Diatoms, Paris. Koeltz, Koenigstein, pp. 655–665.

OKRUSCH, M. u. M., SIEGFRIED, 2005. Mineralogie. Springer, Berlin.

PACHUR, H.-J. and ALTMANN, N., 2006. Die Ostsahara im Spätquatär. Springer, Berlin, 662 p. pp.

PACHUR, H.-J. and HOELZMANN, P., 2000. Late Quaternary palaeoecology and palaeoclimates of the eastern Sahara. *Journal of African Earth Sciences*, 30(4): 10.

PAQUET, H., 1987. Composition minéralogique de la fraction argileuse des sondages de Bogoria, *Bulletin des Centres de Recherche et d'Exploration-Production Elf-Aquitaine*. SNEA, Boussens.

PATRICK, R., 1970. The diatoms. Ianula: An account of the history and development of the Lago di Monterosi, Latium, Italy,. *Transactions of the American Philosophical Society New Series*, 60(4): 112-120.

PEINERUD, E.K., INGRI, J. and PONTER, C., 2001. Non-detrital Si concentrations as an estimate of diatom concentrations in lake sediments and suspended material. *Chemical Geology*, 177(3-4): 229-239.

PETERS, M. and TETZLAFF, G., 1988. The structure of West African Squall Lines and their environmental moisture budget. *Meteorology and Atmospheric Physics*, 39(2): 74-84.

PETIT-MAIRE, N. and RISER, J., 1981. Holocene lake deposits and palaeoenvironments in Central Sahara, Northeastern Mali. *Palaeogeography, Palaeoclimatology, Palaeoecology*, 35: 45-61.

PIGATI, J.S., QUADE, J., SHAHANAN, T.M. and HAYNES, C.V., 2004. Radiocarbon dating of minute gastropods and new constraints on the timing of late Quaternary spring-discharge deposits in southern Arizona, USA. *Palaeogeography, Palaeoclimatology, Palaeoecology*, 204(1-2): 33-45.

PIRARD, F., 1962. Hydrogéologie du Niger oriental. Bureau de Recherche Geologique et Minière, Dakar.

PRENTICE, I.C. and JOLLY, D., 2000. Mid-Holocene and glacial-maximum vegetation geography of the northern continents and Africa. *Journal of Biogeography*, 27(3): 507-519.

RENSSEN, H., BROVKIN, V., FICHEFET, T. and GOOSSE, H., 2003. Holocene climate instability during the termination of the African Humid Period. *Geophysical Research Letters*, 30(4): 33 1-4.

RENSSEN, H., BROVKIN, V., FICHEFET, T. and GOOSSE, H., 2006. Simulation of the Holocene climate evolution in Northern Africa: The termination of the African Humid Period. *Impact of rapid environmental changes on humans and ecosystems*, 150(1): 95-102.

RIAL, J.A. et al., 2004. Nonlinearities, Feedbacks and Critical Thresholds within the Earth's Climate System. *Climatic Change*, 65(1): 11-38.

RICHARDSON, J.L., HARVEY, T.J. and HOLDSHIP, S.A., 1978. Diatoms in the history of shallow East African lakes. *Polskie Archiwum Hydrobiologii*, 25: 341-353.

RITCHIE, J.C., EYLES, C.H. and HAYNES, C.V., 1985. Sediment and pollen evidence for an early to mid-Holocene humid period in the eastern Sahara. *nature*, 314(6009): 352-355.

RITCHIE, J.C. and HAYNES, C.V., 1987. Holocene vegetation zonation in the eastern Sahara. *nature*, 330(6149): 645-647.

RODRIGUES, D., ABELL, P.I. and KROEPELIN, S., 2000. Seasonality in the early Holocene climate of Northwest Sudan: interpretation of Etheria elliptica shell isotopic data. *Global and Planetary Change*, 26(1-3): 181-187.

ROGNON, P. and COUDÉ-GAUSSEN, G., 1996. Paleoclimates Off Northwest Africa (28°-35°N) about 18,000 yr B.P. Based on Continental Eolian Deposits. *Quaternary Research*, 46(2): 118-126.

ROGNON, P. and WILLIAMS, M.A.J., 1977. Late quaternary climatic changes in Australia and North Africa: A preliminary interpretation. *Palaeogeography, Palaeoclimatology, Palaeoecology*, 21(4): 285-327.

ROWELL, D.P. and MILFORD, J.R., 1993. On the Generation of African Squall Lines. *Journal of Climate*, 6(6): 1181-1193.

RYNER, M., GASSE, F., RUMES, B. and VERSCHUREN, D., 2007. Climatic and hydrological instability in semi-arid equatorial East Africa during the late Glacial to Holocene transition: A multi-proxy reconstruction of aquatic ecosystem response in northern Tanzania. *Palaeogeography, Palaeoclimatology, Palaeoecology*, 248(3-4): 440-458.

SAARNISTO, M., 1987 Annually laminated lake sediments. In: B.E. Berglund (Editor), *Handbook of holocene palaeoecology and palaeohydrology*. John Wiley and Sons Inc., New York, NY, pp. 343–370.

SCHEFFER, M., CARPENTER, S., FOLEY, J.A., FOLKE, C. and WALKER, B., 2001. Catastrophic shifts in ecosystems. *nature*, 413(6856): 591-596.

SCHNURRENBERGER, D., RUSSELL, J. and KELTS, K., 2003. Classification of lacustrine sediments based on sedimentary components. *Journal of Paleolimnology*, 29(2): 141-154.

SCHULTZE, E., BAUMHAUER, R., SCHULZ, E., SPONHOLZ, B. and TICHY, G., 1990. Primary production in dependence on climatic history in central Saharian lakes and lake deposits, Bulletin de la Societe Geologique de France.

SCHULZ, E., 1991. Holocene environments in the central Sahara. *Hydrobiologia*, 214: 359-365.

SCHULZ, E., 1994. The southern limit of the Mediterranean vegetation in the Sahara during the Holocene. *Historical Biology*, 9(1-2): 137-156.

SCHULZ, E. et al., 2000. The Holocene landscape and vegetation history of northern and western Africa. A palaeoecological atlas.

SCHUETT, B., 1998a. Reconstruction of Holocene paleoenvironments in the endorheic basin of Laguna de Gallocanta, Central Spain by investigation of mineralogical and geochemical characters from lacustrine sediments. *Journal of Paleolimnology*, 20(3): 217-234.

SCHUETT, B., 1998b. Reconstruction of palaeoenvironmental conditions by investigation of Holocene playa sediments in the Ebro Basin, Spain: preliminary results. *Geomorphology*, 23(2-4): 273-283.

SCHUETT, B., 2004. The chemistry of playa-lake-sediments as a tool for the reconstruction of Holocene environmental conditions - a case study from the central Ebro basin, *Paleoecology of Quaternary Drylands*, pp. 5-30.

SCHUETT, B. and BAUMHAUER, R., 1999. Holocene climatic change in the basin of Laguna de Gallocanta (Iberian Chain) by investigation of mineralogical and geochemical characters from lacustrine sediments. *Erdkunde*, 53(1): 48-64.

SCHUETT, B. and KRAUSE, J., 2009. A literature analysis of Holocene palaeoenvironmental research in the Central Sahara, *Holocene Palaeoenvironmental History of the Central Sahara*. Palaeoecology of Africa.

SCHWANGHART, W. and SCHUETT, B., 2008. Meteorological causes of Harmattan dust in West Africa. *Geomorphology*, 95(3-4): 412-428.

SERVANT-VILDARY, S., 1977. Étude des Diatomées et paléolimnologie du Bassin tchadien au Cénozoïque supérieur. Travaux et documents de l'ORSTOM (Office de la recherche scientifique et technique outre-mer), 84. Institut français de recherche scientifique pour le développement en coopération. ORSTOM, Paris, 346 pp.

SERVANT, M., 1973/1983. Séquences continentales et variations climatiques: évolution du bassin du Tchad au Cénozoïque Supérieur. Travaux et documents de l'ORSTOM, 159. Institut français de recherche scientifique pour le développement en coopération. ORSTOM, Paris, 573 pp.

SERVANT, M., 1983. Séquences continentales et variations climatiques: évolution du bassin du Tchad au Cénozoïque Supérieur. Travaux et documents de l'ORSTOM, 159

Institut français de recherche scientifique pour le développement en coopération. ORSTOM, Paris, 573 p: tab., ill., graph., carte, bibliogr. p. 517-559 pp.

SMYKATZ-KLOSS, W., SMYKATZ-KLOSS, B., NAGUIB, N. and ZOELLER, L., 2004. The reconstruction of palaeoclimatological changes from mineralogical and geochemical compositions of loess and alluvial loess profiles, *Paleoecology of Quaternary Drylands*, pp. 101-118.

SNYDER, J.A., MILLER, G.H., WERNER, A., JULL, A.J.T. and STAFFORD, T.W., Jr., 1994. AMS-radiocarbon dating of organic-poor lake sediment, an example from Linnevatnet, Spitsbergen, Svalbard. *The Holocene*, 4(4): 413-421.

SONNENFELD, P., 1984. Brines and Evaporites. Academic Press, London, 613 pp pp.

SOULIÉ-MÄRSCHE, I., 1991. Charophytes as lacustrine biomarkers during the quaternary in North Africa. *Journal of African Earth Sciences*, 12(1-2): 341-351.

SPONHOLZ, B., 2004. Fulgurites as palaeoclimatic indicators - the proof of fulgurite fragments in sand samples, *Paleoecology of Quaternary Drylands*, pp. 73-78.

SPONHOLZ, B., BAUMHAUER, R. and FELIX-HENNINGSEN, P., 1993. Fulgurites in the southern central Sahara, Republic of Niger and their palaeoenvironmental significance. *Holocene*, 3(2): 97-104.

SPOSITO, G., 1998. Bodenchemie. Ferdinand Enke Verlag, Stuttgart.

STAGER, J.C., MAYEWSKI, P.A. and MEEKER, L.D., 2002. Cooling cycles, Heinrich event 1, and the desiccation of Lake Victoria. 183(1-2): 169-178.

SWEZEY, C., 2001. Eolian sediment responses to late Quaternary climate changes: temporal and spatial patterns in the Sahara. *Palaeogeography, Palaeoclimatology, Palaeoecology*, 167(1-2): 119-155.

SZABO, B.J., HAYNES, C.V. and MAXWELL, T.A., 1995. Ages of Quaternary pluvial episodes determined by uranium-series and radiocarbon dating of lacustrine deposits of Eastern Sahara. *Palaeogeography, Palaeoclimatology, Palaeoecology*, 113(2-4): 227-242.

TALLING, J.F., 1976. The Depletion of Carbon Dioxide from Lake Water by Phytoplankton. *The Journal of Ecology*, 64(1): 79-121.

THIEMEYER, H., 2000. From Megachad to Microchad : environmental changes during the holocene, *Berichte des Sonderforschungsbereiches 268*, Frankfurt am Main, pp. 11-19.

THOMAS, E.R. et al., 2007. The 8.2 ka event from Greenland ice cores. *Quaternary Science Reviews*, 26(1-2): 70-81.

THOMPSON, L.G. et al., 2002. Kilimanjaro Ice Core Records: Evidence of Holocene Climate Change in Tropical Africa. *Science*, 298(5593): 589-593.

TILLET, T., 1985. The Palaeolithic and its environment in the northern part of the Chad basin. *African Archaeological Review*, 3(1): 163-177.

U.S.G.S., 2001. Piston core - Coring, http://esp.cr.usgs.gov/info/lacs/piston.htm. ESP Web Team, U.S. Department of the Interior.

UDELHOVEN, T., 1992. Das computergestützte Partikelanalysesystem GALAI CIS-1 und seine Eignung für die Untersuchung von Schwebstoffen Diploma thesis, Department of Geography, Trier University 78 pp.

VIZY, E.K. and COOK, K.H., 2001. Mechanisms by Which Gulf of Guinea and Eastern North Atlantic Sea Surface Temperature Anomalies Can Influence African Rainfall. *Journal of Climate*, 14(5): 795-821.

VOELKEL, J., 1988. Zum jungquartären Klimawechsel im saharischen und sahelischen Ost-Niger aus bodenkundlicher Sicht. *Würzburger Geographische Arbeiten*, 69: 255-276.

WANG, Y. et al., 2007. Detecting vegetation-precipitation feedbacks in mid-Holocene North Africa from two climate models. *Clim. Past Discuss.*, 3(4): 961-975.

WEBER, H. and HERZIGER, G., 1972. Laser, Grundlagen und Anwendungen. Physik Verlag, Weinheim.

WENINGER, B. and JOERIS, O., in press. Towards an Absolute Chronology at the Middle to Upper Palaeolithic Transition in Western Eurasia: A New GreenlandHulu Time-scale based on U/Th Ages. *Journal of Human Evolution*.

WENINGER, B., JOERIS, O. and DANZEGLOCKE, U., 2007. CalPal-2007 Cologne Radiocarbon Calibration & Palaeoclimate Research Package.

WILLIAMS, M.A.J., ABELL, P.I. and SPARKS, B.W., 1987. Quaternary landforms, sediments, depositional environments and gastropod isotope ratios at Adrar Bous, Tenere Desert of Niger, south-central Sahara. *Geological Society, London, Special Publications*, 35(1): 105-125.

WINTLE, A.G., 1997. Luminescence dating: laboratory procedures and protocols. *Radiation Measurements*, 27(5-6): 769-817.

WINTLE, A.G. and MURRAY, A.S., 1997. The relationship between quartz thermoluminescence, photo-transferred thermoluminescence, and optically stimulated luminescence. *Radiation Measurements*, 27(4): 611-624.

WRIGHT, H.E., 1991. Coring tips. *Journal of Paleolimnology*, 6(1): 37-49.

ZHOU, W., HEAD, M., WANG, F., DONAHUE, D. and A. JULL, 1999. The reliability of AMS radiocarbon dating of shells from China. *Radiocarbon* 41(1): 17-24.

ZUPPI, G.M. and SACCHI, E., 2004. Hydrogeology as a climate recorder: Sahara-Sahel (North Africa) and the Po Plain (Northern Italy). *Global Climate Changes during the Late Quaternary*, 40(1-2): 79-91.

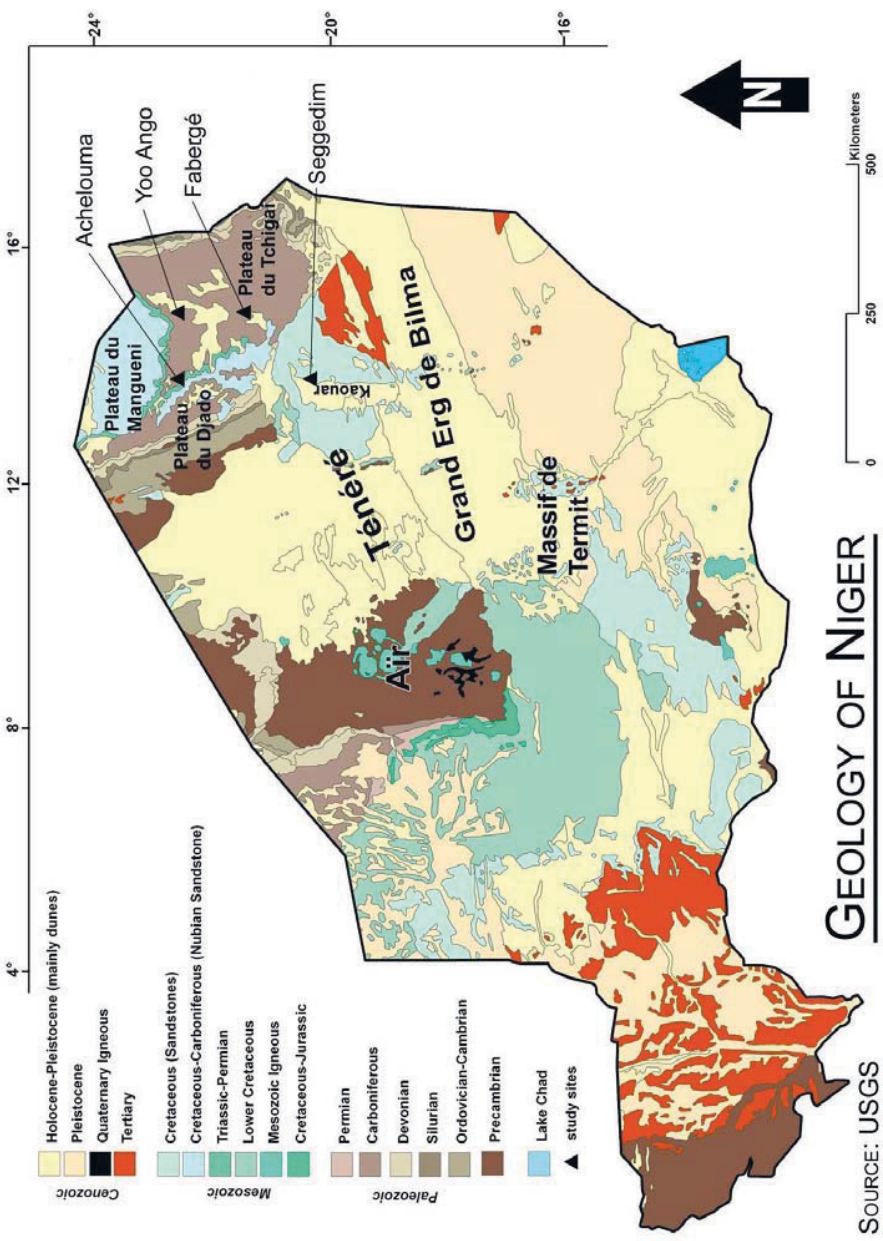

Appendix Figure I Generalized geological map of Niger (based on USGS data)

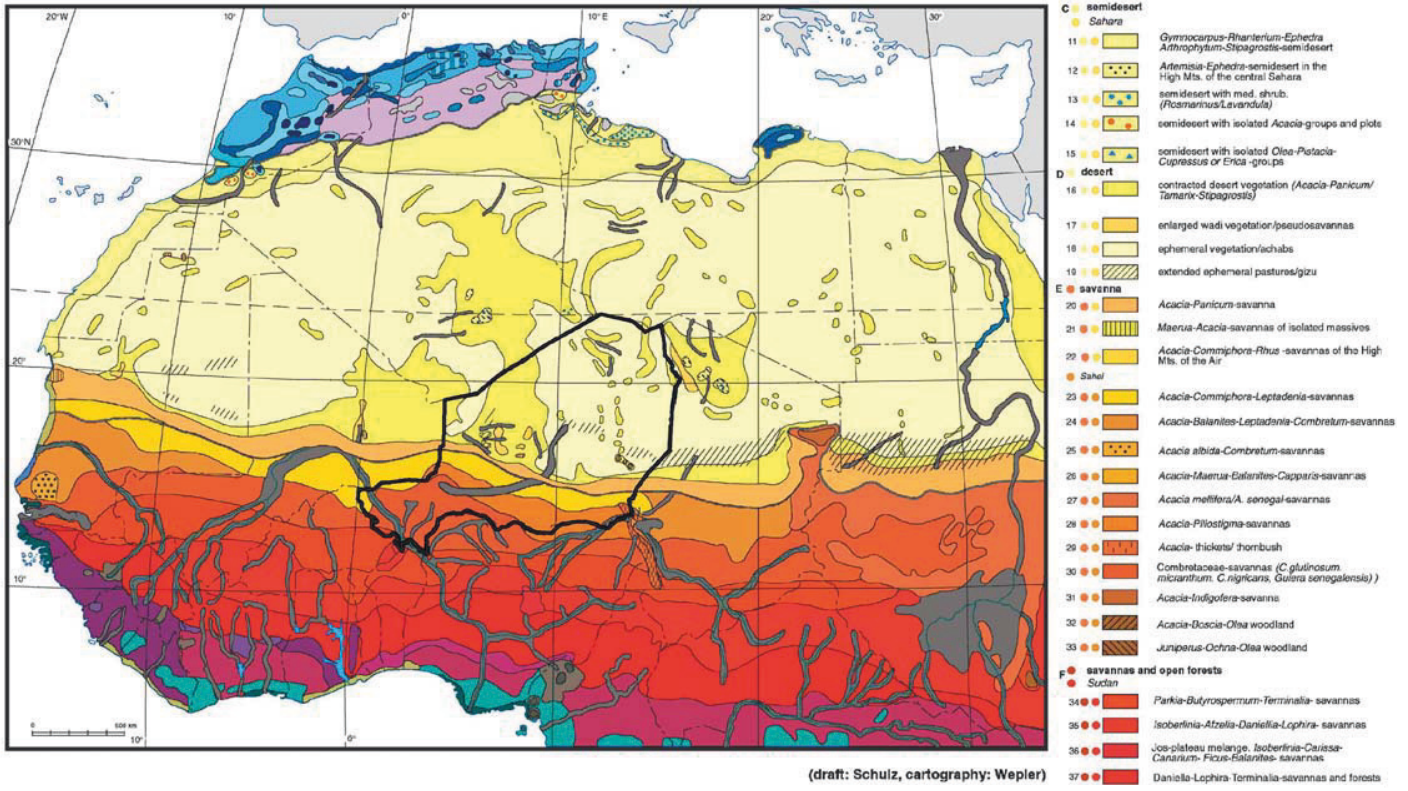

Appendix Figure II Schematic vegetation map of Northern and Western Africa (SCHULZ et al. 2000) - extract

Appendix Tables

Appendix Table 1 Mineralogical composition of bedrock samples (semi quantitative)

		Quartz	Hematite	Goethite	Kaolinite
Swamp iron ore	LiSa 2	91		9	
Emi Bao	LiSa 1	98			2
	LiSa 3a	99	1		
	LiSa 3b	100			
	LiSa 3c	72	28		
	LiSa 5a	98	2		
	LiSa 5b	85		15	
	LiSa 5c	100			
	LiSa 5d	100			
Pic Zoumri	LiSa I	100			
	LiSa II	100			
	LiSa III	100			
	LiSa IV	95			5
	LiSa V	100			
	LiSa 4a	94	6		
	LiSa 4b	97	3		
	LiSa 4c	100			

Appendix Table 2 List of performed analyses, methods and participating labs

Analysis	Method/device	Laboratory
Chemical Parameters		
Elemental analysis	Segment scan - EDXRF-Geoscanner	BGR Hannover
Elemental analysis	Aqua regia - ICP-OES	FU Berlin
Carbon analysis (T_{OC}, T_{IC})	Woesthoff-Carmhograph, LECO	FU Berlin
Elemental analysis (1 cm)	X-ray fluorescence (XRF) fused tablets	University Wuerzburg
pH-values	pH-meter	University Wuerzburg
Mineralogical Analysis	Powder diffraction (XRD)	FU Berlin
Physical Parameters		
Grain size	Galai CIS-1 Analyzer	University Trier
Magnetic susceptibility	Bartington MS2E	University Jena
Stratigraphy	Thin sections (still under preparation)	Gent
Dating	Radiocarbon dating (C14)	Poznan Radiocarbon Laboratory
Biological Parameters		
Diatoms	Microscope	University Wuerzburg
Pollen	Hydroflouric acid (HF)-solution	University Wuerzburg

Appendix Table 3 Lower limits of detection for the XRF analysis of fuse tablets

Weight-%	**Elements**			
0.1	Na2O	S		
0.01	Al2O3	Fe2O3	K2O	MnO
	MgO	SiO2	TiO2	
0.005	CaO			
0.02	P2O5			
ppm	**Elements**			
10 ppm	Zr	Ba		
5 ppm	Sr			

Appendix Table 4 Core segments and features

Core segments		Main colour(s)	Lamination thickness	Texture	Contacts	Additional features
0	600		x	sand	x	Sebkha material, gypsum etc.
600	*650*	*x*	*x*	*x*	*x*	*gap*
650	668	7.5 YR 5/8	homogenous	clay + sand	diffuse	debris
668	685	10 YR 6/2	homogenous	clay + sand	sharp	distinct colur change, fragments
685	713	10 Y 6/1	homogenous	clay	sharp	distinct colour change, fragments
713	738	7.5 Y 4/2	homogenous	clay	x	turbidite (?), large dolomitic rock
738	*752*	*x*	*x*	*x*	*x*	*disturbance/gap*
752	770	5 6 Y 2/1	laminated	clay	sharp	set of laminations
770	*778*	*x*	*x*	*x*	*x*	*disturbance/gap*
778	923	2.5 GY 4/1	laminated	clay	sharp	regular
923	995	7.5 Y 4/1	homogenous	clay	x	sandstone fragments; turbidite (?)
995	1019	numerous	very thin bedded	clay	sharp	distinct change, inclinated beds
1019	1055	7.5 Y 4/1-3/1	laminated	clay	sharp	set of fine laminations, fishbones at 1032 cm
1055	1083	7.5 Y 4/1-5/1	very thin bedded	clay	sharp	undulated, irregular set of beds, ferric lenses
1083	*1099*	*x*	*x*	*x*	*x*	*disturbances*
1099	1139	10 6 Y 3/1	laminated	clay	sharp	rarely disturbed by single cm-thick white bands
1139	1253	10 B 3/1 - 7.5 Y 5/1	thin bedded	clay	diffuse	distinct change, undulated, disturbances
1253	1270	5 GY 2/1	very thin bedded	clay	sharp	shell fragments, irregular thickness
1270	1300	7.5 Y 3/2 - 7.5 Y 5/1	thin bedded	clay-silt	sharp-diffuse	irregular sequence, more frequent white layers
1300	1470	7.5 Y 2/2 - 7.5 Y 4/3	laminated	organic clay	sharp	sapropel, rarely disturbed by white bands
1470	1500	7.5 Y 5/1	(very) thin bedded	clay-silt	diffuse	bedrock/sandstone, shell fragments